DOTTORATO DI RICERCA IN CHIMICA

Convenzione tra
UNIVERSITÀ DEGLI STUDI DI TRIESTE
e
UNIVERSITÀ CA' FOSCARI DI VENEZIA

CICLO XXXVII

INNOVATIVE MORTARS FOR MOSAIC CONSERVATION: ANCIENT ROMAN TECHNIQUES MEET MODERN RESTORATION NEEDS

Settore scientifico-disciplinare: **CHIM/12**

DOTTORANDA
NEVA M. E. STUCCHI

COORDINATORE
PROF. ENZO ALESSIO

SUPERVISORE DI TESI
PROF. ANDREA VAVASORI

CO-SUPERVISORE DI TESI
DR. ARIANNA TRAVIGLIA

CO-SUPERVISORE DI TESI
DR. CRISTINA DE NARDI

ANNO ACCADEMICO 2023/2024

Ad Anna.

Nell'augurio che nella vita tu possa raggiungere qualsiasi obiettivo.

La zia sarà sempre al tuo fianco per supportarti in ogni tua decisione.

Abstract

The primary goal of this research is to develop mortars for the conservation of ancient Roman mosaics, with a focus on creating sustainable and compatible restoration materials. This study analyzes the composition of archaeological samples from the ancient city of Aquileia, examining both *tesserae* and mortars to understand their original makeup and guide the development of innovative mortar formulations.

Traditional restoration methods often used cement pastes that were incompatible with the original substrates, leading to degradation and instability. In light of the green revolution, there is a pressing need for eco-friendly restoration materials that minimize environmental impact and ensure operator safety. To address this, the research aims to develop innovative mortars that not only match the original Roman mixtures but also promote sustainability.

Two primary formulations were created, using slaked lime and Natural Hydraulic Lime 3.5 as binders, to replicate the original Roman mortar. Additionally, the study explored the use of a natural gel derived from the *Opuntia ficus-indica* plant added in the mortar formulations. This resulted in two additional mortar types that showed promise in enhancing compatibility and sustainability. The research also tested self-healing properties by incorporating a polymeric capsule with a reactive core into two more mortar formulations, making a total of six different mortars produced.

These mortars were analyzed for their physicochemical and rheological properties, as well as their chemical composition. The findings suggest that the inclusion of natural gel, significantly enhances the mechanical characteristics of the mortars, making them closely resemble the Roman formulations. This innovation ensures long-term durability for both the conservation intervention and the original substrates, demonstrating the potential for improved, sustainable restoration techniques in mosaic conservation.

Contents

1 Introduction

This research aims to develop innovative mortar formulations for the conservation of ancient mosaics. The mortar design process is guided by two core principles: compatibility with the ancient substrate, and the sustainability of the designed compound. To this end, the historical characteristics of the original substrates were carefully examined through the analysis of Roman material compositions and production methods. This understanding, combined with the specific requirements of modern restoration, led to the development of six distinct mortars. Testing and analysis of these formulations identified the optimal mortar, which best aligned with the guiding principles and demonstrated superior performance in compatibility and sustainability. Mosaic production experienced its peak from the 4th c. BCE to the 14th c. CE. From the 15th till 19th c., however, mosaic production nearly ceased, with efforts focused solely on the conservation of existing works. A revival of mosaic artistry began anew in the 20th century CE. The cycles of growth, decline, and resurgence in mosaic art have been shaped by a complex interplay of artistic, religious, political, technical, and economic factors [1].

Mosaics production: an overview

Mosaics are composed of several layers and different materials, but two main elements can be identified: *tesserae* (in Latin, also known as *tessellae,* translated in English as tiles) and mortar stratifications. The word *tesserae* comes from the Greek word τεσσαράγωνος (tr. square) that indicates a quadrangular tablet, referring to their typical shape. They can be produced by the cutting of mainly glass or stone with variable sizes and geometries depending on the needs of the composition. Mortars are the pastes that compose the stratification below the *tesserae* and are responsible of their adhesion. The change in the technical approach used for mosaic composition over time is only limited to the use of different materials, but the process of production is also nowadays similar to the one used by the Romans: over a prepared ground, layers of mortars (that can change in number depending from the historical period) are settled, the last mortar *stratum* is laid gradually to maintain its freshness, allowing the *tesserae* to be set into it. This system makes mosaics excellent subjects for examining diverse mortar compositions. In recent decades, numerous investigations have concentrated on examining the composition and structure of ancient Roman mortars. The interrogation about the phenomenon of carbonation and its connection to mortar strength has long captivated researchers, and in recent years, some insights have been uncovered [2,3]. The detailed characterisation of individual archaeological artefacts has significantly deepened our understanding of the technological practices employed by Roman

builders at specific sites. The durability of Roman mortar is acknowledged to be intricately linked to the chemical processes involved in its curing, which predominantly hinge on its composition and the conditions under which hardening occurs [4,5]. However, the complexity of the technology related to the materials used by Romans for composition remains uncertain, given their propensity to incorporate easily accessible organic or inorganic materials into the mortar mixture [6]. Furthermore, the multifaceted composition inherent in each *stratum* presents a myriad of challenges for conservators working in the preservation of mosaics [7]. Interactions with the environment cause a spectrum of deterioration manifestations, encompassing mortar fractures and swelling, which in turn expose to risk the *tesserae*'s stability, thereby jeopardizing the overall integrity of the mosaic. The maintenance of the original position of the *tesserae*, and of the dimension and shapes of the joints, is essential since they were originally designed to create a specific three or two dimensionality and a defined chromatism to the composition. Thus, mosaic conservation processes are imperative in order to maintain the artworks allowing them to continue to live with their original purpose, to decorate architecture and express history and thought.

Traditional conservation approaches

The changing role of mosaic in the decorative artworks across time brought also to a change in the applied methods of restoration. In the past, the prevailing approach to mosaic conservation involved applying restoration procedures designed for other types of artworks (mainly frescoes) to this unique system, an approach ruled by the lack of importance of mosaic technique [8,9]. Moreover, the inorganic nature and the apparent hardness and strength of the materials that compose mosaics, have led to the idea that they were not subjected to deterioration, a theory that has limited the study of ad hoc restoration approaches. However, in recent decades, this trend has shifted, allowing for the development of methods of conservation specifically tailored to mosaics. Mosaics are situated on floors, walls, and ceilings, requiring them to deal with the structural role of the surfaces they are applied to. The preservation of mosaics is widely recognised to be contingent upon the stability of their supporting structure, a critical factor heavily influenced by the composition and quality of the underlying *strata* [10]. Consequently, the majority of interventions focus on consolidation processes not only for the surface layer but also for the layers beneath the *tesserae*.

Two main approaches can be identified in the conservation of mosaics over the centuries. The first is related to filling *lacunae*, conserving the mosaic *in situ*, sometimes using materials that are not compatible with the original substrate, or applying a mimetic approach that makes restoration intervention difficult to be distinguished from the original work. The second one, is the removal of mosaic from its original location by completely detaching it and relocating it to a museum. These conservation processes include the use of pastes to fill cracks, repointing lost *tesserae*,

consolidating mortar layers through grouting process, and creating new substrates for detached mosaics [11,12].

Over the last century, concrete and Portland cement have been predominantly used for restoring lime-based materials. The widespread adoption of these materials in the 20th c. has been extended to conservation practices. Particularly for mosaics, commonly it was believed that these materials could enhance the longevity of mosaics while upholding the idea of the "eternal painting" described by Vasari [9]. However, these interventions often lack compatibility with the original materials and only after decades the chemical-physical incompatibility showed up. Other alternative methods included the use of acrylic, vinyl and epoxy resins, commercial products in use also nowadays [10,13], nevertheless they showed many drawbacks in the application on lithic substrates [14]. These interventions showed a deficiency in resistance, speeding up the process of degradation, thus making necessary to intervene again on the restored surface. Sometimes acrylic compounds has been added to hydraulic lime or non-hydraulic mortar in order to enhance its properties, producing injection pastes [15]. Nevertheless, the evaluation of restoration techniques applied to mosaics using these pastes has highlighted the occurrence of harmful effects on the restored archaeological artefacts [16].

More recently, lime-based mortars have been favoured for mosaic restoration due to their flexibility, which allows them to accommodate structural movements and maintain their plasticity over time, even under mechanical stress [17,18]. However, hydraulic lime can sometimes compromise the integrity of mosaics by introducing rigidity to restored areas, leading to potential structural inconsistencies [8]. Therefore, it is essential to move beyond traditional practices and focus on the specific needs of each restoration project by selecting or designing materials that are chemically, mechanically, and physically compatible with the original substrate. Furthermore, the principles of "green" and "sustainable" materials have become increasingly important in materials science. A material is considered sustainable when its composition is derived from renewable or sustainable resources, such as the reuse of waste of production. Additionally, it qualifies as sustainable when production methods minimise waste end involved non-toxic materials that are safe for both the environment and the operators. To be sustainable, a material should have a low environmental impact throughout its entire life cycle, from sourcing to disposal or recycling.

In this context, research must integrate modern technology with traditional practices to develop restoration materials that effectively protect and maintain historical structures, ensuring the longevity and integrity of heritage sites.

Rationale for research

The primary aim of this research is to design innovative mortars specifically tailored for mosaic conservation, ensuring chemical compatibility with the original ancient substrate and the

sustainability of the product. The products must not only match the composition of ancient substrates but also incorporate modern improvements, such as enhanced durability and workability. Furthermore, the designed mortar must align with today's demand for sustainable materials. The overarching question guiding this research is: Can a mortar be successfully produced that balances compatibility with ancient substrates, enhanced performance through additives, and adherence to contemporary sustainability standards?

To answer this question, in the present research ancient materials were examined to inspire ideas adapting them for the modern contexts, considering the necessities of restoration products sector. This process is based on the concept of "paleo inspiration" [19], which is also related to the "reverse engineering" theory. Reverse engineering involves studying a material to understand its original fabrication process, allowing for its replication. These methods ensure that restoration materials closely match the original substrate composition, preserving authenticity and structural stability. As a result, this approach leads to more durable restoration outcomes and extends the integrity of the restored object [20].

Sustainability of the designed mortars has been assessed through the selection of additives that extend the durability of the material in which they are included. Also in this case, ancient material production came to our aid, suggesting the use of natural compound. Indeed, the practice of using plant-based materials is not only a modern tendency, but it is a practice in use since ancient times. Indeed, historical evidence shows that natural organic compounds, were traditionally added to mortar mixtures to enhance their mechanical and physical properties [6]. For example, the Mesoamerican population used to add gel from *Opuntia ficus indica* in building materials assessing the enhancement of their mechanical strength. This early understanding of the benefits of natural additives is being revisited today, with recent research exploring the use of plant-based products, such as gels and fibres, to improve the characteristics of mortars and cements. These studies show promising results, indicating that natural elements can effectively replace synthetic, less environmentally friendly materials, thereby improving the mechanical properties [21,22] and workability of mortars and reducing the need for frequent interventions, thus being sustainable.

In addition to using natural gels, this research tested a new additive which aligns with the sustainable demands of modern times, called "self-healing material". These innovative materials were particularly used in cement-based applications, because they can autonomously repair cracks and fissures in structures, restoring integrity without external intervention. Recently, there has been a growing interest in adapting self-healing materials for the restoration and preservation of cultural heritage [23]. Indeed, the technology of this material reduces the need for maintenance, extends the material's lifespan, leading to significant cost savings and minimising waste, enhancing sustainability, all of which are desirable characteristics for a restoration material [24–26].

Taking into account insights into sustainable and historically inspired materials, and aligning with the primary aim of the research, the work was structured into three main sections: i) the characterisation of mosaic specimens, including the analysis of their structure and composition; ii) the formulation of mortars and production of additives; and iii) the assessment of the properties of these formulated mortars, followed by their testing within the restoration process.

Characterisation of mosaics

To develop restoration materials a paleo-inspired approach was used to design six different mortars compatible with ancient mosaics. Thus, an initial characterisation phase was conducted to determine the nature of Roman mosaic fragments from Aquileia (Italy), acquiring detailed information about the composition of both the *tesserae* and the mortars.

The Aquileian Roman mosaics were selected as a reference case study in this process, a choice motivated by the recognition of the city's profound historical significance. Indeed, due to its central role in commercial routes, the city was a flourishing centre of craftsmanship's that provided the production of marvellous mosaics created between the 1st c. BCE and the 4th c. CE.

To conduct an in-depth analysis of the materials composing these mosaics, an extensive sampling campaign was necessary. Thus, sacrificial' archaeological materials was used i.e. decontextualized remnants of ancient mosaics. These samples were collected during archaeological surveys of the surface in the suburban areas of the ancient city. A key limitation of these materials is their lack of contextualisation with the original substrates, making it challenging to make definitive conjectures. However, their unsuitability for specific site placements makes them ideal for irreversible sampling processes. A total of 153 specimens of ancient mosaics, including both *tesserae* and mortars, were analysed through microscopic investigation and chemical analysis to fully understand their composition.

The information gathered was then used to accurately reproduce the composition of the mosaics by creating mock-ups, following the Roman recipes of mosaic production. These mock-ups were analysed using, for the first time ever on mosaic fragment, Synchrotron Radiation Tomography. This non-destructive technique allows to assess the feasibility of this new type of analysis on mosaic fragments without the need for destructive sampling, thereby preserving the integrity of the fragments. The analysis provides information about the internal micro-cracks and pores, without sampling the specimen, thus overcoming the limitations of classical characterisation methods. Moreover, being this samples replica of real mosaic, the results acquired improve the knowledge about the underlying structure of mosaic, enhancing the knowledge needed to produce a suitable mortar for mosaic restoration.

Production of new mortars

Based on the results of the mosaic characterisation and employing the principles of "reverse engineering," two mortar mixtures were designed using modern materials to replicate ancient compositions. These mortars were developed from ancient recipes, specifically focusing on the archaeological materials from Aquileia. The resulting composition shares similar properties with mortars found at other archaeological sites, demonstrating a strong connection to historical techniques. For example, the use of *cocciopesto* as a substitute for the pozzolanic materials typically used by the Romans in southern Italy highlights this versatility. Therefore, although the mortar is specifically inspired by the Aquileian case study, its composition allows for broader applicationS without significant limitations.

In addition to mimicking ancient techniques, the research emphasizes sustainability by incorporating natural gels and self-healing materials into the mortar mix.

A significant part of the study focuses on producing and analysing a natural gel derived from the treatment of *Opuntia ficus-indica* (prickly pear cactus). The use of this gel is intended to improve the mechanical characteristics and workability of the mortars. This gel was used as replacement of water in mortar mixtures, designed with the inspiration of ancient material, thus producing two additional mortars.

Furthermore, to meet modern restoration interests, the research explores the production of a self-healing material composed of a calcium and silica active binding core encapsulated in a polymeric shell. The goal is to create an additive that can react to fragmentation by filling cracks and repairing the mortar. This self-healing ability is based on carbonation reactions, which are crucial for mortar hardening. This additive was incorporated in the designed mortars formulating 2 mortars.

In totality six different mortars were designed based on the knowledge of sustainable and historically inspired materials.

Evaluation of mortar properties

All the designed mortars were tested and analysed in order to assess the performances of the mortars and the effects of additives in enhancing them, identifying the mixture with the best quality. The workability of the fresh paste was tested during the production phase of the mortars. Along the hardening phase of the mortars, they were subjected to flexural and compressive tests to evaluate their mechanical properties. Water absorption tests were also conducted to determine imbibition properties. The results of these tests were correlated with analyses of micro-, meso-, and macro-pores. These findings, along with the results from chemical analyses conducted on all the prepared mortars, allowed for a correlation between chemical composition and the properties of the mortars. Thus, the results help to determine which of the six formulated mortars is the most

suitable in terms of compatibility, durability, and sustainability, effectively addressing the needs of mosaic restoration.

The research also aims to test the chemical and mechanical compatibility of the six newly formulated mortars with the ancient one. Therefore, both ancient and new mortars were characterised through chemical analysis, micro-compression tests, and evaluation of surface hardness, and the results were compared, determining which of the designed mortars is characterised by parameters of strength and composition more similar to the ancient one.

Since the mortar is designed to reattach *tesserae* and fill fractured points, another objective is to develop a method for assessing the adhesive properties of the mortar on *tesserae*, especially in light of the lack of existing literature that considers the specific sizes of *tesserae*. Additionally, the best mortar formulation was tested in a simulated restoration intervention on mock-ups. These test were conducted under stable laboratory conditions and may not fully reflect in-situ conservation challenges. However, these tests offer valuable insights, indeed they were applied on degraded fragments of mosaic, thus replicating the actual condition of real case study, thus assessing mortar restoration effectiveness on realistic sample.

Significance of the study

The research has shown strengths and some weaknesses in each of its parts.
The results achieved from the characterisation of original samples of Aquileia Roman mosaic, serving as starting point of the research and source of inspiration for the design of innovative mortars Moreover, the results achieved contribute to the improvement of archaeological knowledge about mosaic composition.

Application of Synchrotron Radiation Tomography opened new horizons for the heritage science community. Indeed thanks to its application it was possible to achieve information about the porosity and internal structure of each mortar layers that compose mosaic. The study on mosaic deterioration through mock-up degradation offers insights into conservation treatments and enhances our understanding of real-case reactions.

By applying “reverse engineering” principles, the research demonstrates how paleo-inspiration can guide the design of restoration materials that respect the original’s chemical, mechanical, and physical properties. The study highlights the benefits of using *Opuntia ficus indica* gel for mortar preparation for the improvement of workability and strength.

Tests involving the addition of a self-healing compound revealed some limitations related to its ability to remain inactive during the hardening phase. Despite this, the compound has shown an improvement in enhancing mechanical properties when activated in the environment. Therefore,

further consideration is needed regarding its potential effectiveness as a slow-release element to improve strength.

The primary limitation in evaluating the mortar's restoration properties lies in assessing its long-term effectiveness over several years and in actual in-situ restorations. Acknowledging the limitations of this research could drive further development in this field.

Structure of the thesis

The thesis is organised as follows.

Chapter 2 covers all the aspects related to mosaic systems: history, production technology, characterisation processes, conservation techniques, and materials production. It provides a comprehensive overview of Roman mosaic systems, describing the technology used for their production and focusing on the composition of Aquileian mosaics. The chapter also discusses classical methods for characterising archaeological materials and introduces a new method for analysis of entire mosaic fragments, highlighting its feasibility. Finally, the chapter presents an overview of current conservation practices, emphasising innovations in mortar paste design for restoration.

Chapter 3 details the results of the analysis of Roman mosaic samples, including method and results of the analysis conducted with SXCT for the characterisation of mosaic mock-ups using.

Chapter 4 is dedicated to the core of this research: the methodology, development, testing, and analysis of the designed mortars for restoration. It begins with the rationale behind the mortar design and details the methodologies for producing additives and mortars. The chapter also presents the results of analyses and tests conducted on the produced compounds. The results presented in the chapter allow the individuation of the best mortar produced in terms of compatibility with the ancient material and properties, which performances are deeply analysed in the following chapter.

Chapter 5 focuses on the efficiency of the best produced mortar as restoration products. It provides a detailed account of the steps leading to the design and production of the pull-off test system, for the analysis of the adhesiveness, discussing also the results achieved. In this chapter process and results of simulation of restoration intervention on mock-ups of mosaic are presented.

The findings of the research are summarised in Chapter 6, which concludes the study and offers suggestions for future research directions.

2 The mosaic system. History, composition, restoration approach and new materials

2.1 The Roman Mosaic. Story and composition

This chapter explores the evolution of mosaic art, focusing on the historical developments of mosaics, including those from Greek, Roman, and Byzantine periods. It presents the various types of mosaics produced from the Roman era to the present day, with a particular emphasis on Roman techniques. Special attention is given to mosaic production in Aquileia, covering the period from the 2nd c. BCE to the 4th c. CE.

2.1.1 Evolution of the mosaic technique

Mosaic artistic production flourished particularly in Rome in the 1st c. BCE, where it was mainly used for floors covering. Along the period that elapsed between the 1st c. BCE and the 3rd c. CE, several types of mosaic were produced and the technique of floor decoration evolved achieving the production of complex decorative pattern.

The earliest type of floor covering was the mosaic made of pebbles (developed in Greece since the 5th c. BCE). This technique consists of the application of black and white pebbles to create decorative motifs, thus it can be considered the ancient form of mosaic.

Production of *tesserae*, which are squared cut pieces of material, primarily made of stone and coloured marble, began in the Hellenistic period. In this period several type of *Opus* (the Latin name that indicates a type of construction) were developed: *Opus Tesssellatum*, the finest *Emblemata* and *Opus Vermiculatum*. Additionally, *Opus Sectile* technique was used in Rome since the 1st c. BCE, this kind of composition can be associated to mosaic because of the use of big slabs of marbles and stones cut and laid in order to create regular geometric pattern.

During the Republican and Imperial period simpler types of composition were produced by nesting more or less regular pieces of marbles and stone inside a cement (e.g. *Opus Scutulatum, Opus Segmentatum, Concrete Pavement)* [27]. Under Emperor Augustus, materials trade was driven by merchant interests, and the Empire's control of quarries from the 1st c. CE led to regulation of sales, utilising river and sea trade routes. Materials used for the production of the majority of the *tesserae* were sourced locally, but from the 2nd-3rd c. CE, various white and coloured marbles and

stones spread across the Roman Empire. Despite the flourishing of *marmora* trade, smaller, remote cities used local materials. Specialised technicians managed quarries, marking blocks with material and origin details. This regulated stone trade flourished until the 3rd c. CE. The stockpiles in Roman harbours were able to satisfy the necessities of materials even during trade disruptions [28].

Floor mosaic production was prevalent until the 3rd c. CE, when the production of walls mosaic (*Opus Musivum*) overcame the floor making mosaic. At the same time, the scarcity of stones and marbles in Rome, due to a decay of the commerce, led to campaign of expoliation of the monuments in order to compensate the absence of materials. This scarcity led to a simplification of decorative composition in terms of colour and accuracy in the cutting of the material. The finest mosaic became more rare being destined only to wealth committance and public and religious buildings. The loss of finesse of mosaic production also led to a reduction of the role of *lapidaries*, the artisans producer of stone mosaic, in favour of *musivarius* (the artisans who produced glazed *tesserae*). Upon the production of new stone mosaics tendency to restore the already produced mosaic became the commonest approach in parallel with the growing application of *Opus Musivum*, bringing to the complete disappearance of the finest floor mosaic artworks [8,9]. This decorative expression reached its apex in early Christian era for the decoration of ecclesiastic buildings. The most flourishing moment of this artistic technique was the period of the reign of Constantine who founded, in the 3rd c. CE, the school of musive art for the production of glass *tesserae* [9]. Starting in the 4th c. CE, mosaics became popular across the Byzantine Empire, with artisans moving from Constantinople to Ravenna to create beautiful works. Mosaic technique evolved in response to changes in artistic taste, socio-economic factors, and historical events.

The rise of iconoclasm in the 8th c. led to increased mosaic production and technological advancements, such as using *tesserae* at different angles for visual effects and gold backgrounds to highlight central figures. Artisans aimed to make saints and divine figures appear as lifelike as possible. However, the end of iconoclasm led to a decline in mosaic production, as the Church restricted divine representations, prompting a shift towards simpler designs and a focus on technique. In the 9th c. CE, there was a change in mosaic production. While in Rome mosaic production flourished, with the development of intricate geometric patterns using coloured marble and stone in the "*alla cosmatesca*" style, Ravenna's mosaic production faced significant decline and exploitation [9]. Since the Early Middle Ages, the Byzantine technique for mosaic production was revived through the dissemination of knowledge by Byzantine artisans. In the 11th c., Venice saw the creation of some of the city's earliest mosaics and by the 12th c., Venetians had mastered the production of glass *tesserae*. Since the time of Giotto, the popularity of mosaics began to decline in favour of frescoes. From then on, mosaics were regarded as a subset of painting techniques, a notion that persisted for 500 years. During this period, the revival of mosaic techniques or artistic floor-making was limited to a few instances, and it wasn't until the 20th century that a thorough revitalisation occurred. Mosaics started to be seen as a bridge between

architecture and painting, transcending artistic hierarchies and leading to a unification of art forms [29]. Throughout the 20th c., mosaics remerged as an independent art form, integrating into architecture as decorative elements and gaining recognition from designers and architects. This resurgence also influenced conservation practices, enhancing awareness about methods and materials used[1]. Additionally, the study of mosaic techniques from both historical and artistic perspectives has advanced, providing greater clarity on the various types of mosaics produced. A classification of these mosaic types has been identified based on their composition and underlying structure [30]. Moreover, thanks to the type of materials shapes and colours of *tesserae* it is possible to differentiate the type of mosaic [8,9,27,31].

On the bases of the bibliographic research conducted, a description of all the types of mosaics present in the Roman period is presented. For each typology of mosaic, the material of production, the period of application, the birthplace of the technique and one example of well-known mosaic are reported.

Mosaic with pebbles

Materials and methods: the decoration is made of pebbles, with round shape, different sizes and varying colour (primarily black and white). This type of decoration was used particularly for the production of floors, using pebbles of big dimensions. Small pebbles were used to outline draws, enhancing the clarity of the designs, sometimes they were contoured with lead sheets to improve the mark of the draw.

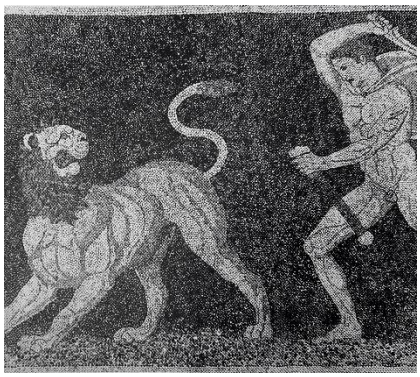

Figure 1 “Lion hunt”, Gnosis, IV c. BCE, Archaeological Museum Pella, Macedonia. Photo credits to Dunbabin K. “Mosaics of the Greek and Roman world”.

Period and place of production: the production of this type of mosaic began in the Hellenistic era (323 c. BCE- 31 c. BCE) till 1st c. BCE. This type of mosaic were produced mainly in Greece and Asia Minor.

Example: in Figure 1 is reported a detail of the mosaic “Lion hunt”, produced in the 4th c. BCE, in Pella, Macedonia, from the house of Dionysus, now conserved at Archaeological Museum of Pella [27]. For the first time for a mosaic is reported the name of the author: Gnosis.

[1] For more information about the technique of conservation please look at §2.3 Introduction to the Conservation of mosaics.

Opus Sectile

Materials and methods: this type of composition was prepared using marble inserts with geometric shape. Different type of material were used for the production, as soft limestone and sandstones, but also coloured marbles.

Figure 2 Detail of the floor of room D of "House of the Nymphaeum", Ostia antique, Italy, 4th c. CE. Photo credits to Jan Theo Bakker.

Period and place of production: this type of pavements were produced firstly in Greece, from the first simple type of pavements the technique evolved and was imported in Rome where more complex decoration has been created since the 1st c. BCE [8]. As for *Opus tessellatum*, also this technique was reused during the 12th c. CE and the 14th c. CE.

Example: in Figure 2 is reported the image of a portion of the floor of the House of the Nymphaeum, a Roman Villa located in Ostia antique [32]. The sectile pavements was produced in the 4th c. CE.

Opus Tessellatum

Materials and methods: the name of this type of decoration come from the Latin word *tessella* (*tesserae*, small cube). The material used can be stone, marble or cotto. The composition can be monochromatic, dichromatic and polychrome. Medium-sized *tesserae*, featuring irregular profiles and approximately 10 mm in size, were prevalent during the Hellenistic era, though their distribution was limited. Large regular *tesserae*, exceeding 15 mm in size, were systematically arranged to form homogeneous monochrome fillings or designs characterised by large modules. These mosaics, typically employed in open or utilitarian spaces, were considered of lesser artistic value. Minute *tesserae* (smaller than 10 mm) with a smooth surfaces, were employed to craft intricate compositions, and often used to delineate *emblemata*. These *tesserae* possess an irregular polygonal profile and offer the potential for further artistic elaboration. Mosaic panels incorporating minute *tesserae* are typically constructed on frames or supported by stone or clay substrates. A technical characteristics of this type of production underscored the application of a meticulous execution, particularly in the creation of the preparatory layer to counteract moisture issues and groundwater seepage. Monochrome

Figure 3 Detail of the mosaic floor "*Asàrotos òikos"*, Heraklitos, Vatican Museum, Rome, 2nd c. CE. Photo credits to Musei Vaticani.

installations with white backgrounds are typical, reflecting influences from central Italian culture. Stripes and regular dotting are some of the predominantly utilised decorative patterns.

Period and place of production: this artistic style has some relevance dating back the 3rd c. BCE, and then it continued to be produced throughout the Hellenistic period. Despite its diffusion in different countries it is still unknown the first place of production of masterpieces made with this technique. Its use is also documented during the 12th c. CE and the 14th c. CE, a period of renovation of the Roman stylistic style.

Example: in Figure 3 is reported the image of a portion of mosaic of *Asàrotos òikos* ("the unswept floor") signed by Heraklitos. The mosaic was produced in the 2nd c. CE for a villa on the Aventine Hill in Rome and today is conserved at Vatican Museums in Rome [33].

Opus Vermiculatum

Materials and methods: this artistic technique is one of finest mosaic production for naturalistic and figurative draws. The technique includes the use of *tesserae* with small size from 1 to 4 mm with irregular shape, placed in order to create sinuous structure (that resemble small worms, in Latin *vermicus*). *Tesserae* are made of various materials such as marble, brick, or glass of various colours. Compositions exhibit diverse characteristics and are often integrated with larger module of lithic or lithoid inserts, marble fragments, or a combination thereof. This technique is also employed for the production of *emblemata*.

Figure 4 "The battle of Alexander the Great over Darius III", 2nd c. BCE, Museo Archeologico Nazionale di Napoli (MANN), 5.8 m x 3.13 m. Photo credits to MANN.

Period and place of production: this technique was the most used during the Hellenistic period. It was developed in the Hellenic area and then it was exploited also in the Italic Peninsula. The most outstanding masterpieces has been produced in the 2nd-1st c. BCE.

Example: the mosaic (Figure 4) "The battle of Alexander the Great over Darius III" also known as "Battle of Isso", 2nd c. BCE, the original location was the exedra of House of the Faun in Pompei, today conserved at Museo Archeologico Nazionale di Napoli (MANN) [34]. It is composed of a million of small pieces of marbles and stones and represents one of the greatest example of *Opus Vermiculatum* mosaic. 2nd -1st c. BCE, Archaeological museum of Naples.

Emblemata

Materials and methods: bibliographic research highlights that sometimes there is a convergence in the use of the definition of *emblemata*, *Opus Alessandrino* and *Opus Vermiculatum*. Indeed, these techniques involved the use of small pieces of stone, placed along thin lines creating sinuous design in order to achieve a realistic representation. Differently from *Opus vermiculatum*, *emblemata* are single decoration positioned in the centre of a floor, often decorated with a dichromatic *tessellatum* that became the frame of the *emblemata* positioned in the centre. This decoration were produced on movable panels, in laboratories, allowing to produce them with extreme care, and inserting them in a second moment in the location of interest. Because of their intrinsic movable nature, these artworks were often reused and placed in different sites respect to the original.

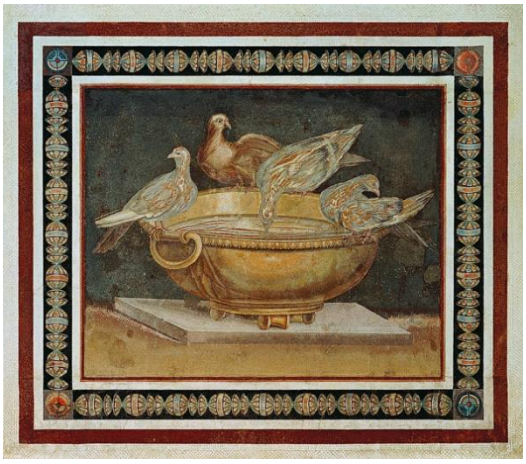

Figure 5 "Mosaic of the Doves", Sosus of Pergamon, 2nd c. BCE, Musei Capitolini, Rome, Italy. Photo credits to Musei Capitolini.

Period and place of production: the technique has been developed during the 3rd-2nd c. BCE in Alessandria of Egypt. In this city were formed the majority of most skilled artisans of the period. Once formed in Alessandria artisans expatriate in other location of the Empire spreading the artistic manner. Numerous signatures were recorded on *emblemata*, being evidence of the importance given to the artisans that produced these artworks. Pliny the Elder remembered the Greek artist Sosus of Pergamon, which signature appears in different mosaics. Signatures along with inscription, iconography and style are other proof of the provenience of artworks [35].

Example: "Mosaic of the Doves" (Figure 5) is an *emblemata* produced in the 2nd c. BCE for the decoration of Hadrian's Villa in Tivoli, today the mosaic is conserved at Musei Capitolini in Rome [36].

Opus Scutulatum

Materials and methods: floors are decorated with irregular coloured stone and marble fragments called s*cutule* or *crustae*. The *scutule* are nested inside the preparatory layer made of compacted ground or inside a *tessellatum* floor, fragments are arranged without meticulous care.

Figure 6 *Opus Scutul*atum floor mosaic present in room 47 of Villa of Mysteries in Pompei, 1st c. BCE. Photo credits to Annette Haug, ERC Grant 681269 DÉCOR.

Period and place of production: this technique was developed since the second half of the 2nd c. BCE and for all the 1st c. CE in the Italic Peninsula, particularly in Rome.

Example: in Figure 6 is reported an image of the floor mosaic present in room 47 of Villa of Mysteries in Pompei [37]. Multi-coloured *scutulae* are nested inside a white and black *tessellatum* pavement.

Opus Segmentatum

Materials and methods: this composition is made of stone and marble fragments nested inside compacted ground, covering the entire space, leaving thin joints. Sometimes it is used also as synonym or confused with *Opus Scutulatum and Signinum*.

Figure 7 *Opus Segmentatum* floor of Central Bath, Herculaneum, Italy, 1st c. CE. Photo credits to Robert Hanson.

Period and place of production: the production of this type of decorative pattern appeared around 2nd - 1st c. BCE in Greece, particularly in Delos area.

Example: in Figure 7 is reported the image of a floor in *Opus Segmentatum* made with segmented black, grey and white marble. This floor is part of Central Bath building of Herculaneum constructed in the 1st c. BCE the decoration of the Villa were made possibly in the 1st c. CE [38].

Concrete pavements

Materials and methods: this composition is primarily made of cements or clay poured on the ground, indeed it is indicated with the term "decorated cement" [30]. This layer is enriched with lithic insertion or *tesserae* that create simple geometric pattern ("*Cementizio a Base Fittile*" or "*Cementizio a Base Litica*"). Three different type of coloured *Concrete pavements* can be individuated depending on the colour imparted by the components of the cement: black (lime mixed with *pozzolana*), white (lime with travertine powder and or fragments of flint) and red (mortar with addition of *cocciopesto*, term used also as synonym to indicate this kind of *Opus*) [39]. Sometimes it is used also as synonym or confused with *Opus Segmentatum*.

Figure 8 *Concrete pavement* floor, *Domus Aurea*, Rome, Republican Period. Photo credits to M.L. Morricone Matini.

Period and place of production: this decorative manner is one of the primary type of floor decoration being developed between 5th-4th c. BCE. It has been employed till the 1st c. CE mainly in the Mediterranean area.

Example: in Figure 8 is reported an example of *Concrete pavement* floor discovered in the buildings below the Domus Aurea in Rome [40]. The periodization of the mosaic is probably the same of the building constructed in the Republican era.

2.1.2 Technology of Roman Mosaic

The artisanal techniques in mosaic craftsmanship evolved over time[2]. Our understanding of the composition of Roman buildings materials is primarily derived from three foundational ancient sources which, together, give us all the information about the technology used for the production of mosaics as well as mortars. Cato the Elder (2nd c. BCE) in his work *Liber De Agri Cultura* described the inorganic binder used for the production of mortar [41]. Also the ancient author Pliny the Elder in the work *Naturalis Historia* (1st c. CE) described the recipes used for the production of the mortar [6]. Despite the importance of the aforementioned Roman sources, only the Roman architect Vitruvius in its work *De Architectura* (1st c. BCE) described the complete composition of the stratification of mosaics [42], becoming a pillar of reference material for the study of mosaics.

Mosaics are complex systems composed of different layers, which were delineated by Vitruvius. In Figure 9 is illustrated a schematic depiction of the five-*stratum* system that composes Roman mosaics, according to the roman architect description.

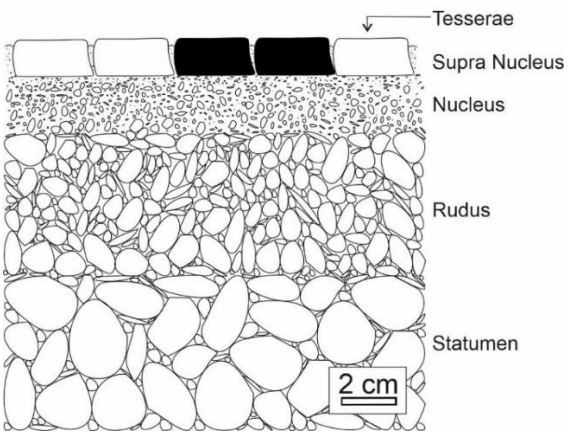

Figure 9 Stratification of mosaic as detailed by Vitruvius.

[2] For more information please look at §2.1.1 Evolution of the mosaic technique.

Starting from the bottom and moving to the top, the foundational layer, known as *Statumen*, comprises large rough stones and bricks compacted onto the ground. The subsequent *Rudus* layer, approximately 20 mm thick, consists of a coarser mortar blend featuring sizable aggregates of either *cocciopesto*, stones, sand and gravel or a combination thereof, with variable size, mixed with lime. Overlying the *Rudus* layer there are one or two *strata* of finely compacted mortar. The first is *Nucleus*, ranging from 10 to 20 mm in thickness, consisting of lime mixed with aggregates at a binder-to-aggregate ratio of 1:3. The aggregate fraction comprising sand and/or *cocciopesto* bonded with lime and water as necessary. As articulated by *Vitruvius*, some mosaic which required meticulous attention, the joints between *tesserae* are filled with a finishing layer known also as *Supra Nucleus* that was used as a *tesserae* setting bed [43]. This layer consisting of slaked lime sometimes also tempered with oil was applied also to prevent liquid penetration, serving as a finishing coat. *Tesserae*, can be made of stone, marble, or glass, occasionally incorporating pebbles and shells. Positioned within the superficial mortar layer, *tesserae* varies in shape and size according to decorative requirements. The materials used for *tesserae* production depend on the availability of raw materials, highlighting how a population's trade connections were closely tied to its artistic production. Generally, Roman mosaics were produced by using stone (in some cases also semi-precious) and marble *tesserae* of various colours. Moreover, within the different discoveries, terracotta *tesserae*, tiles with coloured patina to enhance the colour, and tiles made of Egyptian *fritta* and faience were also recorded, along with pebbles, shells, pearls and *madreperla*. As today, in ancient times, mosaic makers preferred to use sedimentary and metamorphic rocks, primarily limestone. The technology used to cut and shape these materials was also a crucial factor in the final execution of the mosaic. Therefore, it can be inferred that the choice of material was influenced not only by availability but also by how easily it could be cut, as in the case of limestone.

As presented, each layer of the mosaic is composed of heterogeneous materials depending on the availability of local and imported resources at the time and place of production. Furthermore, variations in composition are due to the techniques applied during the mosaic's creation and may be influenced by different environmental conditions, which could affect the overall structure [44]. Indeed, it is well known that Romans were able to adapt to environmental conditions by selecting one type of material over another, also by specifically designing them if necessary. For example, *cocciopesto* was utilised as a substitute for *pozzolan* when the latter was unavailable, providing hydraulic properties to the mortar [45,46]. This composition enables mortar hardening underwater as well as in humid conditions, making them similar to modern-day mortars. The preparation of the mortars is only one of the passages of production of mosaic, it is possible to individuate 4 different phases [47]:

- The conception of the mosaic
- The production of the subfloor

- The production of the mortars for each layer, and their laying
- The cutting and nesting of the *tesserae*

Although the Vitruvian stratification system is the most widespread [48] and frequently used in all the studied floor, in her work Pasqualucci (2004) [7] underlined the frequent presence of two more layers not cited by the historical material. Indeed, in her studies she individuates the presence of one mortar layer with drawings, used as matrix to compose the decoration with *tesserae*, and a bedding layer for *tesserae* not corresponding to the one described by Vitruvius. Thus, one additional phase of production could be present sometimes: the engraving in the mortar, using a needle, to draw the mosaic composition. By placing screws and lead sheet the artisans used to create guidelines for the production of the decoration [8]. Placement of the *tesserae* in ancient time follows the so called "direct method", thus small portion of mosaic were placed nesting them in still fresh mortar. In this way, the artisan was able to observe the product of its work, having the possibility to enhance the artistic effect as the *chiaroscuro* (lights and shadows) [49].

Besides the information of the technology used, the individuation of the number of layers, particularly the finishing ones, serves as an indicator of mosaic quality and also of possible periodization. Indeed, as noted by Dilaria et al. (2019) [50], mosaics from the Proto-Republican to Late Antique periods differ in the number of layers present, with earlier mosaics typically featuring more layers, while later ones often consist of just a single layer. Through rigorous analyses conducted over the years, scholars have advanced a nuanced comprehension of the compositional intricacies of Roman mortars and of the skills exhibited by Roman craftsmen in formulating these blends [5,51–53]. Various factors such as the dimensions of *tesserae*, the material used and its availability, the presence of finishing layers, layer thickness, the composition of the mortars utilised are elements that allow to assess the care put to produce each phase of pavement layering [54]. Thus, considerations about the stratification can be valuable also for identifying the possible period of production as well as the quality of mosaics and the technological prowess of artisans.

2.1.3 Aquileian mosaics

900 mosaic floors have been discovered in Aquileia nowadays. This massive production of mosaic is the result of the wealth of this flourishing city. Aquileia was the capital of the 10th region of the Roman Empire. Located in the north-east of Italy a few kilometres from the Adriatic coast it was in a strategic geographical position within the network of trade routes, assuming a pivotal role as a commercial hub linking the Mediterranean Sea, the Padania flatland, and the transalpine regions. Moreover, the city's significance was augmented by historical events and Roman expansion endeavours [55]. Renowned as one of the nine most significant cities of the ancient world, Aquileia flourished in antiquity. However, during the medieval and Renaissance periods, the city was

systematically ruined, causing damages to the preservation of its ancient structures [56]. Aquileia became a cultural melting pot, attracting diverse populations, thus gaining access to different raw materials, which boosted its wealth and craftsmanship, particularly between the 2nd c. BCE and 4th c. CE [55].

Different works in literature contain information regarding the building materials used in Aquileia [57,58]. However a scarce number of studies are specifically dedicated to Aquileian mosaic analysis [55,59]. Nonetheless, a conspicuous lacuna persists within extant scholarship concerning the examination of materials employed in the north-eastern precincts of the Roman Empire, with particular emphasis on Aquileia [3].

In Aquileia, artworks feature the typical mosaic stratification reported by Vitruvius[3] [42]. Floor production was made considering both the decorative function of the composition and the functional purpose of the spaces, demonstrating artisans' awareness of production methods [60].

Bueno et al. (2011) [61] identified four main types of floor coverings in Aquileia, which were the most common flooring systems [31]: 2% cements coverings, 70% *opus tessellatum*, 4% *opus sectile*, and 20% brickwork. Rinaldi's chronotypological seriation [31], supported by Bueno et al. [61] and Salvadori [31] researches, exemplified the flooring evolution over time in Aquileia. Moving from cementitious layers (1st c. BCE), artisanal production evolved to create two-dimensional dichromatic decorative patterns (from the 2nd c. till the 1st c. BCE) and then involving the use of coloured three-dimensional geometric schemes [60]. The construction methods and mosaic decoration in Aquileia were influenced also by the proximity of the Slovenian area [62], leading to more complex decorative solutions [60]. In the same period, customisation of pre-existing mosaics began, with the insertion of new patterns and figures inside the already present black and white decoration [61]. This practice, repeated over the centuries was also shaped by the influence of various stylistic trends coming from different places. This tendency demonstrates the complexity in the evaluation of the identification of the original mosaic and of the chronological seriation of the mosaic composition, a practice that can be considered a first application of restoration of the pre-existing. By the 4th c. CE, mosaics reached their peak, symbolising the patron's status and the structure's function [60]. This historical expression of the lifespan of mosaic in Aquileia highlights the continuous presence in the art history of the city of mosaic as the main decorative elements.

The investigations on Aquileian mosaics have expounded upon the materials and characteristics of mortars employed within the historical context of Aquileia [50]. Researches shade lights into the construction methodologies used in the ancient city, affording valuable insights about the

[3] For more information please look at §2.1.2 Evolution of the mosaic technique.

exceptional quality of mortars employed [63], underscoring their significance within Roman architectural traditions in Northern Italy. Moreover, the wealth of the population and their skills in refining raw resources are evident in the myriad of artefacts unearthed by archaeologists and the impressive buildings still adorning Aquileia today. As underscored by Previato (2015) [57], the utilisation of various materials during the Roman era signifies artisans' discerning selection of specific lithotypes, based on the requirements of the construction and the specific characteristics of the material [64]. Additionally, composition of the *tesserae* provides insights into the availability and variety of materials at the time, offering clues about ancient trade routes. Aquileia is an interesting example of a site where different types of materials came from nearby location as well as foreign countries. Indeed, white limestone was likely sourced from nearby quarry because of the presence of one of the most exploited quarries in the vicinity named *Cava Romana* (namely Roman Quarry) [65,66]. A study by Boschetti et al. [59] confirms its use, as well as the employment of white material coming from other Italian region as Carrara marble, of pink and red hues sourced from the Veneto pre-Alps and black materials originating from central Italy. Observations within the mosaics have also revealed the use of exotic marble coming from Africa. The diverse range of lithic materials documented in existing literature complicates the characterisation process, highlighting the necessity for in-depth analysis for their characterisation. In this framework, Aquileia emerges as a pivotal example for delineating technological advancements and the application of construction materials for mosaic production in the Roman times.

2.2 Methods of characterisation of archaeological material

Determining the origin, dating, artisans, and production sites of mosaics is complicated because of the widespread practice of reuse of materials from other buildings, started along the 3rd c. CE [31,64]. For example e*mblemata*, thanks to their movable nature and their dimensions, have been widely employed in different sites compared to the original one. Moreover, identifying a mosaic's original state is further hindered by restoration efforts that began as early as the Roman era [9]. The complexity deepens when considering that craftsmen and materials frequently moved throughout the Empire. Consequently, reconstructing trade routes and accurately evaluating these factors is difficult using bibliographic research alone.

Scientific analysis, therefore, becomes a valuable tool to complement and enhance the information gathered from historical and artistic sources. By integrating scientific methods, we can obtain a more comprehensive understanding, leading to more definitive and well-rounded conclusions about the quarries from which the raw materials originated historical trade routes, the relationships between different populations, and the technological skills of the artisans. This approach allows us to provide more accurate answers and fill gaps in our knowledge with greater certainty. Moreover, interest in analysing the materials used in mosaic composition stems from the understanding that such analysis can reveal crucial information about the materials' composition and degradation state.

Information of the composition are essential for selecting the best restoration methods, the most compatible materials and additionally to take inspiration from the ancient technology that allowed to maintain cultural heritage to this day. Thus, a comprehensive examination of mosaic structures is fundamental not only for restoration but also for uncovering the historical knowledge encapsulated within mosaics. In literature, only a limited number of studies are dedicated specifically to mosaic analysis, as exemplified by Ion's work [67]. The complex and heterogeneous composition of layered mosaic systems necessitates the use of specialised investigative processes tailored to mosaics and if necessary to each individual layer. Each layer boasts a distinct composition, resulting in varying levels of porosity and microstructure, which has direct impact on the attachment, integrity, and interaction of layers. Although the complexity of the mosaic system, the predominantly inorganic and lithic nature of these layers includes investigative efforts under petrographic analysis. Indeed, both *tesserae* and mortars can be examined using similar methodologies. However, the process of sampling differs significantly between these two materials. Despite the archaeological significance of the materials, it is sometimes possible to remove small fragments of mortar for analysis without causing significant damage to the overall structure. This procedure, however, is not feasible for *tesserae*, as their removal would compromise the integrity of the mosaic. As a result, *tesserae* often remain in situ during analysis,

necessitating non-invasive techniques and only in reduced cases they are removed and analyse completely using sometimes destructive technique.

While the analysis of individual layers and materials within mosaics has advanced significantly, and nowadays is a well-established practice, the non-destructive examination of entire fragments remains an underdeveloped area of study. Currently, there is a notable deficiency in the capability to analyse whole fragments without causing disruption or damage. This limitation highlights a critical area for further research and development in the field, emphasising the need for innovative methods that can provide comprehensive analysis while preserving the integrity of these invaluable archaeological artefacts.

2.2.1 Analysis of the *tesserae* and characterisation of their lithotypes

The focus of this research is the analysis of stone and marble *tesserae* used in the production of Roman mosaics, thus the research excludes the investigation and conservation processes related to mosaics produced with glass *tesserae*. However, it is possible to state that the majority of the techniques used for stone *tesserae* characterisation are suitable also for the investigation of glass ones [68,69].

When it is possible to gain single *tesserae* from a mosaic or small fragments it is necessary to perform firstly a macroscopic investigation of the specimens and then move to microscopic investigation, making description of the material at both levels [70]. The process begins with the assessment of the colour, dimensions, and shapes, alongside a photographic campaign applied to document their features. When the dimensions of the tiles are too small or when it is necessary to visualise fine details, an Optical Microscope (OM) is employed to magnify the surface and evaluate the material's characteristics. In addition colorimetric measurement of the *tesserae* can be performed using a CIELab colorimetric measurements for the evaluation of colorimetric parameters [67] or with the application of Fiber Optics Reflectance Spectra (FORS) in order to acquire the reflectance spectrum of the recorded colour.

To characterise the material from its petrographic nature, *tesserae* are prepared as cross section and thin sections and analysed using Polarized Light Microscopy (PLM). This analysis is the prior one performed and it is also ruled by norm [71], indeed it allows to gain a comprehensive examination of the material making this solo analysis enough for the characterisation of the specimens. Indeed, it allows the investigation of the geological features of the materials, allowing the evaluation of the grain size, the structures and typology of minerals, the presence and type of bioclasts such as the fossils contents as well as the visualisation of veins and porosity in the matrix [59,70,72]. The microscope is coupled with a camera that allows the acquisition of the images of

the materials analysed, in order to have images to use for the comparison and the evaluation of the found elements. This information is often sufficient to identify the nature of the material, especially when compared with reference materials. However, even the most experienced geologists sometimes require additional support to define the nature of inclusions, necessitating chemical analysis.

To avoid further sampling of the material, the same thin section used for PLM investigation can be re-utilised for Scanning Electron Microscopy (SEM) coupled with Energy Dispersive X-ray Spectroscopy (EDX). This combined analysis allows for greater magnification of the matrix and facilitates its chemical investigation, providing a comprehensive understanding of the material's composition. Specifically, the analysis can be used to determine the presence of plagioclase and zeolite that can give information of the geological environment of the formation [72].

The presented pathway of analysis is the one used for the evaluation of the *tesserae* included in this research being enough in order to answer to the purpose of research. However, other analyses could be applied to deepen in the composition of *tesserae*. For example, X-ray Fluorescence (XRF) is an advantageous technique because being non-invasive it offers a semi-quantitative analysis of the material's constituents [67,72]. In addition, other techniques could be applied for the investigation of the composition of the material that composes the *tesserae* for example X-ray microanalysis, to evaluate the constituent elements of the stone or X-ray Diffraction (XRD) to characterise the crystalline minerals in the sample. These techniques are all complementary and together allows to complete the information regarding the nature of the analysed lithotypes that compose *tesserae* [73].

2.2.2 Analysis of ancient mortar

Mortar are from definition "materials traditionally composed of one or more binders, aggregates, water, possible additives and admixtures combined to form a paste used in masonry for bedding, jointing and bonding, and for surface finishing (plastering and rendering) of masonry units, which subsequently sets to form a stiff material" [74]. Besides this definition along centuries different kind of mortars and more generally cement pastes has been prepared [5] for the production of domestic buildings, infrastructures and formulated specifically for each necessary part of the construction and the environmental conditions of the site. The Romans distinguished themselves by constructing enormous structures that still stand today, sparking significant scientific interest in understanding the technology behind Roman cement. Numerous studies have focused on evaluating the composition of Roman mortars, with some specifically examining mortar production in the Aquileian area [50,57,63]. As a result, the analysis of ancient mortars has become common practice, and the investigative methods are now well established. Furthermore,

considering the study of ancient mosaics, the cohesion of layers is intricately tied to the compaction process, mortar consistency, and the microstructure of the solidified paste [54]. Enhanced layer cohesion fosters stability, mitigating the occurrence of fractures and material loss, thereby facilitating the preservation of the mosaic artworks. In addition, different works have focused on how the composition of mortars was specifically selected by Romans in order to achieve different effect. For example, Stefanidou et al. (2014) [75] observed that the addition of brick powder to lime was used to enhance the paste's resistance to humidity in the joints between *tesserae*. Additionally, the inclusion of sand in the lime was recorded as a method to reduce the volumetric contraction of the finishing layer [76]. This framework highlights how, while the identification of mortar composition and structural characteristics poses challenges, it remains pivotal for a comprehensive understanding of the technological methodologies employed by the Romans.

Since mortar is a lithic material and contains stone in its composition, the approaches and techniques used for its analysis are similar to those used for the characterisation of stone[4] (thus of *tesserae*). A standard procedure specifically addressed to the investigation of archaeological mortars has been published [77]. Along with the majority of the publications, it indicates as fundamental prior step: the initial survey and its documentation. The report must include information about colour, function, texture and visible characteristic aspects of the material. On the bases of the documentation and for the behalf of knowledge, if necessary, the material must be sampled following norm EN16085 [78]. The analytical strategy begins with macroscopic evaluation, also performed during the preliminary investigation, in order to assess the texture of the mortar, the presence of any decay form or particular aspect, and all the visible features, also colour measurement is included in this phase (following EN15886 [79]). In order to dive deeper inside the composition of mortars, allowing a complete characterisation of aggregates and binder is necessary to enlarge their visualisation. Thus, samples of mortar are prepared in form of cross section or thin section and subjected to microscopic investigation with Optical Microscopy (OM) using transmitted polarised light microscopy (PLM) or reflected light. This technique is quick and costless, thus is the most used for mortar characterisation. Indeed, through the comparison of images acquired and bibliographic material it is possible to achieve simply the great majority of the information [77,80,81] such as the definition of the binder and aggregate nature and ratio, the presence of lumps and or possible of additives, porosity, processes of decay, minerals inclusions, individuation of mosaic stratigraphy, etc.. The investigation of the matrix of mortars, extends far beyond understanding their composition; it can provide a wealth of information. For instance, the individuation of composition of mortar and the presence of layers in a mosaic can indicate the period of its creation [50]. If the elements in the mortar are too small for the solo visualisation with

[4] For more information please look at §2.2.1 Analysis of the *tesserae* and characterisation of lithotypes.

OM, the Scanning Electron Microscopy (SEM) can be applied for the analysis of thin sections, allowing the greater visualisation of elements such as micro cracks of smaller elements in the mortars [63,82]. This analytical technique if coupled with Energy Dispersive Spectroscopy (EDS) can give back also chemical information of the composition and being a supplementary analysis to the other applicable [83]. Indeed, elemental and mineral composition of the material can be defined through the application of X-ray Diffraction (XRD). Before the application of these techniques, for a better comprehension of the composition respectively of binder and aggregate, a process of separation is advised. However, sometimes for the lack in quantity of archaeological sample this process is not possible. XRD is one of the most used techniques indeed it allows the individuation of the mineral phase through the acquisition of a diffractogram achieved after the interaction of the ray with the analysed matter [50,84]. Along with XRD also Thermal Gravimetric Analysis (TGA) is applied [52,85,86], allowing the individuation of materials trough the individuation of signals of interaction of the matter at different rate of heat.

In addition to chemical composition, porosity is an important parameter strictly related to intrinsic lithotypes properties and can be correlated to elemental analysis allowing the definition of the correlation of chemical and structural features. Indeed, porosity of a material and specific dimensions of the pores are correlated with the specific properties of mortar to resist to degradation. The various textural and structural characteristics of stones or mortars with the same chemical composition, but different mineral-petrographic compositions, can lead to the development of different forms of alteration in the materials. This is due to the relationship between porosity and fluid dynamics, specifically the movement of water and other liquids within the material [52,87]. This information allows a possible prediction of the resistance of the material, sheds light on the mechanism of process of deterioration, providing valuable information for the development of materials for conservation purposes. Thus, evaluation of the size, density and distribution of the pores (indicating with this term also voids and crack within the material) must be conducted by using Mercury Intrusion Porosimetry (MIP) [46,52,86].

The information acquired can contribute to expand the knowledge about the efficiency of the mortar, for example the effectiveness of carbonation reaction of the aerial or hydraulic nature of the mortar, information directly related to the technology of production and the consciousness of builders in the process of composition.

2.2.3 Micro-CT: an effective non-destructing technique for mosaic 3D analysis

As already presented, investigations of mosaic fragments are largely confined to the superficial analysis of specimens through optical microscopic examination. But, it is important to analyse the complete structure of the mosaic in order to understand the technology used for its preparation [88] and the best conservation approach to apply. The commonest approach applied for the petrographic analysis and for the evaluation of the internal structure, involves a sampling (or sectioning) procedure, thus the disruption of the specimen. These techniques can give 2-dimensional (2D) images with high resolution, but do not allow the analysis of the entire specimen, since sample preparation involves the cutting of the specimen in small slices and their preparation in form of thin sections. Consequently, these results might not allow for a comprehensive investigation of the microstructure of all layers, their structural interactions, or the adhesiveness at the interface of the stratification, suggesting that traditional approaches are inadequate for a thorough analysis. This limitation highlights the need for more suitable investigative techniques, to develop methods that can effectively analyse entire mosaic fragments being non-invasive. Addressing this gap will not only enhance our understanding of these complex structures but also ensure their preservation.

The utilisation of tomography analysis in the examination of in-situ mosaics primarily pertains to the scrutiny of the structural elements within walls or floors [89]. Existing literature underscores that tomography employed for mosaic analysis is primarily associated with the deployment of sensors on the mosaic's surface to reconstruct the underlying structure through the use of direct current electrical resistivity tomography (ERT). Nonetheless, even this method remains relatively infrequent and offers insights on a large scale (centimetre or meter-scale) being unsuitable for small fragments. In literature, the application of X-ray Computed Tomography (XCT) has historically been focused on assessing cracking and pore structure of cement and mortars [90]. This has facilitated considerations related to bond strength characteristics and the identification of cracks in mortar structures, enabling the monitoring of mortar reactions to specific climatic conditions. The mosaic system presents a distinctive and intriguing case study for tomographic analysis, owing to multiple mortar-based stratifications and *tesserae*. Thanks to the application of Computerized X-ray microtomography (XmCT) it is possible to analyse the microstructure of entire 3D specimen, both inner and outer side [91]. As for SEM and PLM, XCT analysis can be used for the evaluation of internal fractures or voids inside cements, allowing the individuation of their propagation [92], but without the needs of sampling the material. The technique is based on the acquisition of 2D X-ray radiographs from different angles, which are collected and reconstructed in form of 3D image [92]. Nonetheless, obtaining 3D visualisations of the internal microstructure of mortar layers, under the *tesserae* of the mosaic, presents significant challenges

when utilising laboratory-scale XmCT sources. This is primarily due to the effect of beam-hardening, and to the limited coherence of laboratory X-ray sources. Notably, the accurate quantification of micro cracks in mortars and the interfaces of stratification necessitate high-resolution, and phase-contrast enhancement which are only attainable with Synchrotron X-ray Computed Tomography (SXCT). Compared to its laboratory counterpart, SXCT can provide greater contrast and high resolution in a fraction of the time, enabling unmatched 3D microscopic visualisation and quantification of porosity and cracks, and an in depth analysis of these features at the micrometre scale. In addition, SXCT in phase-contrast mode achieves greater sensitivity to elements and contrast enhancement up to 3 orders of magnitude compared to conventional, absorption-contrast XCT [93,94]. Some studies underlined its feasibility for the analysis of stone and building materials [95–97] proving to be useful for microscale information acquisition, enhancing the resolution of reconstructed data and enabling phase contrast analysis [96]. In this framework, SXCT can be considered feasible also for the analyses of layered mosaics system. Utilising phase-contrast imaging, the analysis allows the visualisation of internal characteristics of mosaic with great visibility. When this is applied, as an example, for the analysis of the 3D distribution of cracks within the bulk and the surface of mosaic samples, it can provide a better understanding of the mechanisms behind cracks formation and morphology of the voids. Moreover, the analysis can allow to visualise the interaction of the *strata* and the examination of the interface, providing valuable data on the thickness and density of individual layers on the samples. Different works [96,97] have presented the potentiality of this instrument for the evaluation of treatment applied in building materials. The positive results achieved from this analysis could serve as a starting point for further research, for example using SXCT for the evaluation of the consolidation process applied to the analyse specimens. In this way it will be possible to assess the effectiveness of the restoration intervention.

2.3 Introduction to the Conservation of mosaics

Understanding the processes of degradation is crucial to achieve a better comprehension of how time and external factors, such as climate, humidity, and pollution, affect materials and historical structures, all essential information for the development of effective conservation strategies.
Additionally, knowledge about the restoration methods used to date provides insight into techniques that have been successful and those that may have caused further damages. This type of knowledge is vital for avoiding past mistakes and for innovating in the field of conservation, promoting more sustainable and respectful restoration practices that ensure long lasting processes while preserving the historical value and material integrity of artworks and monuments.

2.3.1 Degradation of mosaic

Individuation of the degradation on artworks is a prior step to conduct in order to define the restoration intervention to apply. Thus, it is necessary to perform an accurate examination in order to acknowledge the decay and trying to trace the source that cause the deterioration. Evaluation of the degradation state can be made during the characterisation phase of the material[5], also considering that characteristic composition of the subject and deterioration are strictly related.

As already presented, mosaics are composed of several type of lithic materials each subjected to different type of degradation. For the purpose of research, degradation phenomena that occurs on mosaic made with stone or marble *tesserae* and on mortars will be considered.

Degradation of *tesserae* follows the same processes of decay of natural stone, the majority of which happen for the formation of deposits on the surface of the material or at the interface between the tiles [8,98]. Accumulation of materials on the surface can bring to the chemical alteration of stones, depending on their composition and texture of the outer layer (i.e. roughness). This secondary degradation phenomena can change the matter of the *tesserae* forming argillaceous minerals, saline solutions and insoluble minerals. Formation of black crust are the commonest form of aggressive patina on stone surfaces and their formation can occurs also on mosaic. This crust are the combination of the deposition of carbonaceous substance, gypsum, soil dust, microorganism and halite [8]. Generally, processes of degradation (for mosaics conserved both in situ and in museum) depend on environmental factors, as the thermal variation that occurs in seasonal cycle. But the main degradation effect are due to wet/dry climatic cycle which brings to the crystallisation of soluble salt, forming efflorescence and sub florescence inside the pores of the materials which

[5] For more information please look at § 2.2 Methods of characterisation of archeological materials.

induce an internal pressure that brings to mechanical degradation. Under this phenomena the *tesserae* can be fractured and exfoliated by the salts crystallised, while mortars can suffer a complete disaggregation, depending strictly on the porosity of the material. Similarly, the same degradation effect is caused by frost/thaw cycle of the fluids that pass through the material [99]. Also in this case porosity along with degree of saturation of the pores and mechanical characteristics of the material, are leading factors of the effect induced by this degradation phenomenon [100].

Biological and microbiological growth are also source of deterioration of archaeological surfaces in particular the one conserved in situ [101]. Indeed, bio elements find nutrient in the soil, in the moisture and even in the minerals that compose the substrate, resources that allow their growth. On the surface, they form a patina that induces colorimetric alteration, moreover, the inorganic and organic acids, products of their metabolic activity, induce a chemical alteration. In addition, their growth cause physical alteration inducing pressure in the porosity, which create more space for the colonisation, thus inducing a chain reaction [102].

It is widely recognised that the preservation of mosaics integrity hinges upon the stability of their supporting structure, a critical element that depends heavily on the composition and quality of the *strata* and the technique applied for the production of the layers (as for example the given degree of compactness) [10]. However also external factors can be responsible for the instability of the mosaic system. For example, presence of plant nearby the archaeological site can be problematic [103], indeed the roots can grow below the mosaic causing the physical disruption of the floor, the cracks of the mortar, producing a subsequent detachment of the *tesserae*.

The effect of these degradation agents can be controlled by the application of regular monitoring of the state of conservation of the surface. Indeed, lack of control or absence of adequate roofs are others primary cause of deterioration along with incorrect conservation processes (for example the use of incompatible materials[6]). The degradation caused by human action can be also related to over tourism that can be present in the archaeological site and museums. For example, one of the primary cause of deterioration is due to the walking on mosaics, that cause wear of the floor and the detachment of *tessera* [104]. The overview about degradation phenomena highlighted the wide variety of deterioration that can occur in mosaic, and the importance of the application of the best restoration practices. Thus, in the following paragraphs is presented the evolution of the conservation processes and the practices in use nowadays.

[6] For more information please look at §2.3.3 Restoration methods and type of pastes used in recent time.

2.3.2 Conservation procedures for mosaics

It can be said that the restoration of mosaics is as old as their production. Indeed, the first recorded restoration of a mosaic dates back to 79 CE on a mosaic floor in Pompeii [105]. Since that time, conservation methods have evolved alongside changing perceptions of mosaics as artworks and the development of conservation theory. The fluctuating importance placed on mosaics as artworks has led to varying levels of care in their restoration. Indeed, restoration techniques originally developed for frescoes were applied to mosaics, leading to deterioration due to the different material compositions.

In recent decades, the significance of mosaic artworks has increased, leading to ad hoc processes of conservation that involve the use of new materials and the application of preventive approach, reducing the impact of massive restoration processes [106]. Considerations regarding the placement of mosaics and their relationship with their surroundings have also been taken into account. Mosaics must be considered site-specific artworks, which, if decontextualized, partially lose their meaning. Viewing a mosaic that has been detached and relocated to a museum creates a bias in the observer, who cannot fully appreciate its original context [8]. As a result, restoration techniques have adapted to reflect this heightened awareness, shifting towards preserving mosaics in situ, without detachment or replacement of the underlying support structures [107]. In situ conservation allows for the preservation of the entire stratification of mosaics, as different layers can provide important information about production techniques and artisanal skills. Moreover, the integrity of the superficial layer is closely tied to breaks induced by mechanical stress, which can occur during detachment. Therefore, restoration processes that avoid detachment are now preferred, with consolidation seen as the most important phase in mosaic conservation.

The evolution of conservation methods has led to the contemporary approach. Whether mosaics are preserved in situ or relocated to museums, the general restoration process typically involves the following steps:

1. Documentation
2. Cleaning
3. Pre consolidation or consolidation
4. Edge restrain and filling of lacunae
5. Protection

The practice of documentation appeared only in the 17th c., and restoration interventions began to be meticulously recorded. Through documentation, it is possible to trace the conservation history

of a site from its discovery through to its current state, providing a record of its condition over time.

Historically, cleaning methods include the use of aggressive procedures aimed at restoring the substrate's original colour. For example, a common practice in use in the 19th century was to clean mosaic surfaces using nitric acid [9]. Nowadays more respectful practices are applied, considering the composition of the material to clean. The first cleaning process after discovery involves gentle cleaning with a brush to remove dust and soil. From this initial step, various cleaning methods may be employed, including mechanical cleaning with scalpels or more complex tools like drills. Cleaning with water involves the use of controlled systems to manage water pressure and application. Despite the presence of a lot of type of cleaning methods also by the application of lasers or ultrasound, the most used cleaning methods involved the application of chemicals. Cleaning solutions are applied to the surface by using compresses, their composition depend on the bases of the nature of the material that compose the surface and the type of residue to remove [8]. It is important to remember Cesare Brandi's idea: an understanding of the specific composition of a mosaic is fundamental in defining the most appropriate restoration interventions [7]. This theory complements another approach developed in the last century, which emphasizes preventive restoration applying environmental control and protection measures for mosaics. These concepts are governed by scientific knowledge of material composition and reactions, which are essential for making informed restoration choices. These new ideas have shaped modern restoration techniques and the production of conservation materials used today.

The pre-consolidation and consolidation phases primarily involve the use of pastes, which will be further analysed in the following paragraphs, along with the use of reinforcing metallic elements. For example, in the 19th c., consolidation processes also included the use of T-shaped or cross-shaped iron clamps to strengthen structures. The general trend governing restoration before the 20th c. was to preserve only the *tessellatum* (the layer of *tesserae*), while abandoning the underlying *strata*, due to the mistaken belief that the mosaic was merely an image composed of *tesserae* [9]. This often led to the detachment of the superficial layers (made of *tesserae* and the first mortar *stratum*), and in some cases, the disassembly of individual *tesserae*, which were then reassembled on new substrates [108]. Only in Aquileia, already starting from the first decade of the 20th century, the preservation of mosaics in situ, on their original substrates, became the preferred approach whenever possible [109]. Contemporary, in Venice, a new restoration method was developed to avoid detaching mosaics from their original site, known as "*restauro dal dietro*" [7]. This technique involved reinforcing structural elements without working directly on the mosaic surface. These

[7] Translate in English "restoration from the back".

innovations in the 20th c. marked the beginning of more innovative conservation processes, sparking scientific debate and leading to the development of new materials and methods.

The process of filling lacunae also involved the use of pastes. This practice has been used in mosaic restoration since the 3rd c. CE, when the scarcity of lithic material led to a tendency to reuse existing artworks through renovation, a practice that continued through the Renaissance [9]. This phase is fundamental to give back integrity to the mosaic without replacing original *tesserae* and allowing also the consolidation of the substrate.

The detachment of a mosaic should always be considered a last resort for preserving its integrity [8]. The fragility of archaeological contexts is often influenced by the structures covering the mosaics. For the protection of in situ mosaics, it is crucial to renew the architectural, designing ad hoc roofing systems. If restoration is not feasible, it is preferable to bury the mosaics to conserve the cultural patrimony. This process, known as "interro" (burial), can be done in various ways. The primary method involves covering the mosaic without creating a waterproof barrier, which could cause water stagnation and deterioration. For long-term burial, an inert, durable covering is placed directly on the substrate, followed by layers of expanded clay, sand, and soil where grass can grow. Temporary burial may also be necessary, which involves systems that are easily removable [8].

2.3.3 Mortars and pastes used for restoration

The primary focus of the present research is the development of a mortar to be employed for the consolidation of mosaics, aimed at mitigating damage within mosaic systems. Various approaches exist, including: (i) incorporating consolidants during the grouting process; (ii) using injection mortars to fill cracks; (iii) reinstating lost *tesserae* with pastes [11,12]; (iv) filling complete lacunae; and (v) detaching and relocating mosaics onto new supports [110]. Operations described in (i)-(iv) typically involve the use of cements, pastes, or mortars.

In the 20th century, the discovery of cement pastes became a dominant factor in conservation processes. Cement's ability to harden while providing adhesive properties and enhancing structural resistance was considered highly beneficial for mosaic conservation. As a result, cement was widely used in techniques like the tearing method and in the production of new substrates. The discovery of concrete and cement pastes in the 20th century led to their application in various restoration interventions. The relocation process often involved using cement pastes to create new supports for mosaics [48,111], such as pastes made from cement blended with marble powder. The process also included the use of cement mixed with fine pebbles to increase porosity [112]. In later decades, the reapplication of mosaics involved placing them on substrates made of reinforced concrete. Additionally, the substitution of original lime-based mortars with Portland cement during

restoration became widespread in building restoration [113]. Initially, the success of these interventions led to further adoption of these materials. However, after some years, the adverse effects on pre-existing structures became evident, revealing the detrimental impact on restored archaeological artefacts [16,113].

Cementitious mortars contain soluble salts and have low porosity, which leads to the build-up of water and subsequent salt crystallization. This, in turn, generates internal pressures that cause mortar detachment and rapid deterioration. The unsuitability of cementitious mortars for restoration interventions arises from their inability to accommodate underlying movements and their failure to comply with the critical principle of compatibility [17,114]. The use of cement in mosaic restoration has been largely replaced by modern resins (epoxy, vinyl, and acrylic), applied on new types of substrates using reinforced stainless steel or aluminium panels [35].

In contrast to cement pastes, lime-based mortars, especially those made with air lime, offer greater flexibility to accommodate structural movements. They also undergo a slow carbonation process, which helps maintain the mortar's plasticity over time, even under mechanical stress [17,18]. Sometimes, either hydraulic or non-hydraulic lime mortars are blended with acrylic emulsions [15,115]. However, despite being more compatible with the substrate than concrete, these materials can still introduce a different level of rigidity to restored sections compared to the rest of the mosaic, potentially leading to structural disruptions [8].

To address the lack of suitable materials for restoration, recent studies have focused on the analysis of air lime mortars and their potential re-application in conservation processes. The findings suggest that these pastes are highly compatible with older substrates, making them effective for restoration. However, their application remains rare due to a lack of theoretical and practical training for technicians, as well as difficulties in controlling reaction times and environmental conditions during their use [114].

2.4 Advancements in restoration: innovation in mortar paste design

Before investigating new methods for the production of innovative mortars for the restoration, it is necessary to make a review of the technology behind mortar hardening, which strictly depends to their composition.

Mortar is a composite material made from a mixture of binder, aggregates (such as sand), water, and sometimes additives. According to the UNI 10924 standard (2001) [116], mortar is defined as a "mixture of inorganic and organic binders, fine aggregates, water, and optional additives, combined in proportions that ensure workability when fresh and provide adequate physical and mechanical properties once hardened". Aggregates are added to confer durability and stability to the mortar, acting as filler of the volume, thus contrasting mortar shrinkage in phase of hardening [117]. They can be inert or reactive, the most used inert are sand or gravel, which classification depends to the size. While, one of the most famous reactive aggregate, used since Roman times, is *cocciopesto*, which derived from the fragmentation of bricks. This aggregate is reactive because it participates directly in hardening process forming calcium silicate hydrate crystals (C-S-H), exhibiting mechanical properties [118] conferring hydraulic properties to the mortar. Binders are categorised based on their setting and hardening capabilities in different environments:

Air-setting (aerial) binders: these lose their initial fluidity when exposed to air and do not function in the presence of water (e.g. gypsum and aerial lime);

Hydraulic binders: can harden even in the presence of water, developing mechanical strength that increases over time (e.g. cement and hydraulic lime).

Once prepared mortar is a fluid, an easily mouldable mass, then it is applied to a substrate and left exposed to air. From this moment two processes occurs involving different phenomena:

1. Setting: it occurs when the mixture loses workability after being applied, becoming plastic, losing the water used in phase of preparation.
2. Hardening: refer to the final stage, it involves a chemical process known as carbonation, where the air binder reacts with atmospheric carbon dioxide, developing the mechanical strength necessary to provide stability and hardness to the system.

Non-hydraulic mortars, which develop mechanical strength only when exposed to air (and not in water), undergo initial hardening due to the evaporation of water from the mix. This is followed by the carbonation process. In this final stage, portlandite, reacts in solution with atmospheric carbon dioxide to form calcite, which is significantly stronger, harder, and much less soluble than portlandite, which it replaces. Portlandite, absorb atmospheric carbon dioxide, which diffused in

the pores of the mortars, leading to formation of calcite crystals, which precipitate in the pores [18], by the following reaction:

(1) $Ca(OH)_2 + CO_2 \rightarrow CaCO_3 + H_2O$

In this process the presence of water in the mix is essential to allows the dissolution of CO_2, a reactant in the carbonation reaction [18], following the reported reaction (2).

(2) $CO_2 + H_2O \rightarrow HCO^{3-}$

Thus, it is possible to rewrite reaction 1 combining with 2, having the following exothermic reaction [119]:

(3) $Ca(OH)_2 + CO_2 + H_2O \rightarrow CaCO_3 + 2H_2O$

The process of hardening of pozzolanic lime mortar is different. Indeed, presence of *cocciopesto* in the mixture, also with aerial binder, imparted hydraulic performances leading to the formation of CSH [2,120]. The process begin with the reaction of lime with water:

(4) $CaO + H_2O \rightarrow Ca(OH)_2$

Then, calcium hydroxide react with pozzolan (can be *cocciopesto*) which is made of reactive silica and aluminosilicates, and water, forming calcium silicate hydrate or calcium silicate aluminium hydrate. Indeed, *cocciopesto* became centre of reaction, and in the reaction rim is formed the CSH gel, by the following reaction:

(5) $Ca(OH)_2$ + pozzolan + $H_2O \rightarrow$ C-S-H ± C-A-S-H

Excess of $Ca(OH)_2$ is carbonated, forming calcite (following reaction 3), a process that can be also due or enhanced to degradation of C-S-H and C-A-S-H, after time [3,120].

Carbonation in mortar is influenced by both external and internal factors. High carbon dioxide concentration and moderate temperatures promote calcite formation, while extreme humidity levels, either too low or too high, can hinder the process by affecting pore structure and water or gas diffusion [121,119]. The type of binder and its composition are crucial, as they determine how the material reacts with CO_2. There is also a close correlation between carbonation and porosity, which are inversely proportional, indeed, as the degree of carbonation increases, the porosity of the system decreases [121]. The carbonation product has a higher molar volume than the initial hydrate, reducing porosity and gradually blocking carbon dioxide entry, which slows carbonation and maturation [122]. This slow process allows for a steady increase in mechanical strength over time, as calcite crystals continuously form and enhance the material's durability.

As presented in the previews chapter[8], restoration method for mosaic conservation primary involves the use of mortars for the consolidation of the mortar layers. The "historic mortars" or "ancient mortars" that compose the archaeological substrate are defined as intricate composite materials comprising a vast array of primary constituents, including a wide variety of binders, aggregates, and additives [123]. These elements participate directly to reaction of hardening and curing phases of the mortars defining the physical and mechanical characteristics [20]. Historical mortars undergo continuous evolution over time due to environmental factors[9] (e.g., frost and thaw), resulting in ongoing adjustments to masonry and a natural aging of the material. Therefore, meticulous consideration is essential in selecting appropriate new formulations for restoration endeavours to prevent further deterioration induced by the utilisation of incompatible materials that can react differently, bringing to the early fail of the restoration intervention. In order to enhance the quality of the conservation process, it is fundamental to employ mortars that are carefully crafted to harmonize with the original materials of the specific subject of the restoration intervention. Mortars used for restoration purposes, must to possess a range of general/architectural and chemical/physical characteristics, that can effectively address decay and deterioration in vulnerable areas [124]. They should have an aesthetic visual appearance that align with the original historical context, maintaining authenticity. The mortars need to be reversible or retractable, allowing for future interventions without compromising the structure. Controlling shrinkage is crucial, as the mortar must behave mechanically similarly to the substrate, avoiding disparities between layers. Additionally, the mortars should enhance both the aesthetic appearance and structural durability of the restored areas. From a chemical perspective, the formulation's composition must to consider the type of binder and the binder-to-aggregate ratio, the mineralogical composition used in the original substrate. The design restoration mortar should be characterised in its physical characteristics, including frost resistance, porosity, and particle size distribution, essential factors for ensuring the mortar's longevity and performances. Lastly, mechanical properties, such as compressive strength and stiffness, are critical for the mortar's ability to withstand physical stresses.

Incompatibility of materials used in restoration processes, is an unsustainable choice that can provoke an earlier necessities to intervene by replying restoration process [113,125] involving the use of other materials, economical resources and being time consuming. Consequently, it becomes imperative that substances utilised in preservation efforts conform to the principles of compatibility and align with conservation needs. Necessitating meticulous attention to achieve physical, chemical, and mechanical compatibility with the substrate [126]. The continuous use of not suitable materials for the restoration is a clear sign that there is a distance between what is

[8] For more information please look at §2.3.3 Restoration methods and type of pastes in use in recent time.
[9] For more information please look at §2.3.1 Degradation of mosaic.

available and what is effectively necessary for restoration process, highlighting the needs in the design of new suitable material and their application [125].

2.4.1 Application of Reverse Engineering Theory for the production of tailored restoration paste

As already presented it is fundamental to know the composition of the material used for mosaic production in order to develop compatible material. To achieve an accurate formulation of repair mortar suitable for application on a damaged historical substrate, it is possible to apply reverse engineering. This method involves determining the composition of a material in order to replicate it. The implementation of reverse engineering technique entails a meticulous approach, encompassing specific steps [124]:

1. Conducting on-site investigations involving the sampling of original, historical mortar.
2. Identifying the mortar within its historical context.
3. Analysing the present damage to discern the causes of deterioration necessitating the application of restoration mortar.
4. Formulating restoration mortar with an optimal composition.
5. Executing on-site application of the restoration mortar.

Through this process, the optimal formulation for restoration interventions can be determined and designed, thereby upholding the fundamental principle of restoration: ensuring compatibility between the new and the ancient materials [20,127]. It is imperative to conduct a historical-analytical study of the original materials before initiating any interventions, as incorrect actions may exacerbate their deterioration. The analytical techniques used for evaluating ancient works are categorised based on the nature of the analysis required[10]: whether it is solely qualitative or involves also quantitative aspects. The mortars produced following the conducted analyses must provide effective protection to the substrate to which they are applied, ensuring they do not adversely interact with the original materials. This is essential to prevent the initiation of processes that may lead to further degradation of the underlying structure [128].

As exemplified by the research of Moropoulou [10], favourable outcomes have been attained through the utilisation of mortar mixtures meticulously selected based mirroring those of the original materials. The concept of “paleo inspiration” encapsulates the practice of drawing inspiration or ideas from ancient or prehistoric sources, commonly observed across diverse domains including art, design, architecture, and technology. It involves a deliberate exploration of

[10] For more information please look at §2.2 Methods of characterisation of archaeological material.

historical contexts to derive creative concepts or solutions applicable in contemporary settings. This term unifies “paleo”, signifying ancient or prehistoric, with “inspiration”, denoting the process of stimulating creative impulses or insights [129].

Driven by both “reverse engineering” and “paleo inspiration”, information acquired from analysis can be used to produce new compound, supported by the modern consciousness of the chemistry behind the reaction of each material. Today, there is a wealth of information available on how to properly prepare lime based mortars that has been used for centuries in historic monuments and masonry constructions. Binder-to-aggregate ratio significantly influences mortar performance. While literature suggests ratios ranging from 1:1 to 1:4, a 1:3 binder/aggregate volume ratio is considered optimal for achieving good compaction and is recommended for the restoration and rehabilitation of ancient structural works. Other key considerations include adding just enough water to achieve good workability without excess, ensuring a well-graded distribution of aggregate sizes, thoroughly mixing the ingredients until a uniform consistency is reached [114]. As exemplified previously there are two different type of binder, depending to the environment of reaction, air lime or hydraulic lime binder. Thus, the choice of binder must to be taken in consideration the type of environment were the designed mortar will be applied and the desired properties, playing a crucial role in restoration applications [117]. The knowledge in our possess nowadays is fundamental to drive the production of new solutions, also by the addition to ancient mortars formulations of new type of additives that can enhance their intrinsic performances.

2.4.2 The use of natural additives in mortar pastes

Evidence from ancient literature indicates a long-standing historical practice, dating back already to the Roman time, wherein craftsmen incorporated natural organic compounds. The deliberated addition of organic elements was intended to improve the structural integrity and impart unique characteristics to the mortar.

The ancient architect Pliny the Elder, lived in the 1st c. CE, in his wok *Naturalis Historia* reported this word [6]:

"*Maltha e calce fit recenti. Glaeba vino restinguitur, mox tunditur cum adipe suillo et fico, duplici lenimento. Quae res omnium tenacissima et duritiam lapidis antecedens"* [11].

Pliny the Elder, Naturalis Historia, 1st c. CE

The empirical observation of the properties of the *maltha* (mortars) obtained by the described process, by adding smashed figs and fat let him to assess the increment in workability. Moreover, the addition of this natural elements improved mortar strength which he said "result stronger than the stone". This early recognition underscores the profound impact that natural materials can have on the performances and durability of building materials.

The modern emphasis on sustainability has catalysed renewed interest in the use of plant products, reflecting a broader commitment to environmental care and the advancement of sustainable construction practices. Tendency in the use of natural additives increased particularly in the last decades, leading to a resurgence in the utilisation of plant-based products as additives in building admixtures. In literature, several typology of natural additives were used for the production of mortar and cements pastes [130,131]. For example in their work Alisi et al. (2021) tested the effect of *Aloe vera*, *Cylindropuntia californica*, *Opuntia engelmanii*, *Opuntia ficus-indica*, *Salvia hispanica* mucilage as additives for mortars for restoration [132]. While, León-Martínez tested the effect induced by the addition of *Opuntia ficus-indica* and of brown algae [133]. Among the natural additives, tested for the production of mortars and cements, mucilage of *Opuntia ficus-indica (OFI)* gave positive results [22,132,134,135] for the effect of increment in durability, viscosity of the pastes that exhibit the lowest bio receptivity. Investigating the composition of *Opuntia ficus-indica* mucilage provides valuable insights into the mechanism, behind the enhancement of mortars and cements strength [21] allowing to understand the multiple properties of this material. The plant is also known with the Mexican name *Nopal*, it is a cactacea that can grow in arid and semi-arid places thanks to its Crassulacean acid metabolism of storying water [136]. Cladodes (flattened stems) that compose the plant are made of *clorenchyma* (the external part) and *parenchyma* (the inner side of cladodes) where water is stored [137] (Figure 10).

[11] English version: *"Mortar is made from fresh lime. A lump is quenched with wine, and then pounded with pork fat and fig with double softening. This substance is the most tenacious of all and precedes the hardness of stone. What is coated with mortar is first rubbed with oil"*.

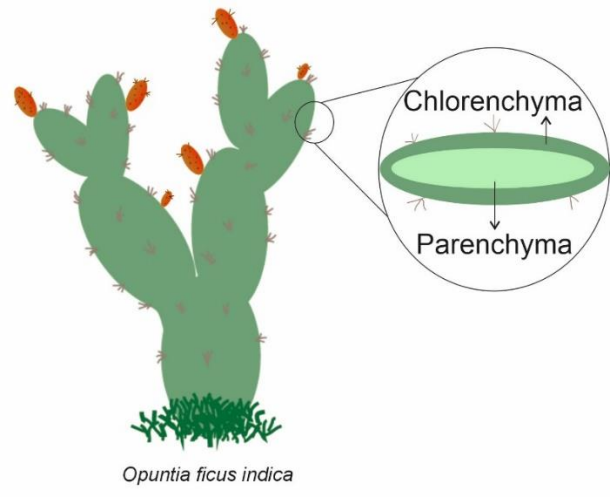

Figure 10 Schematic representation of *Opuntia ficus indica* plant.

Inspiration for the use products of these cactacea for production of materials for restoration comes from the Mexican culture. Indeed, gum of *Opuntia* mucilage has been utilised as an additive in Mexican frescoes (Figure 11A) [138] already by Maya population [139,140], and in more recent times in the work of the famous Mexican muralist Diego Rivera who worked as muralist painter during the first half of the 20th c. CE (Figure 11B) [141–143]. The use of mucilage of *Opuntia ficus indica* has found for centuries wide employment in the production of mortar for the construction of buildings in the Mexican culture, a tradition that continuous to this day [52,63,64,65]. This long-standing practice highlights the enduring significance of this natural material in enhancing the properties of construction mixtures and the results of research present in literature give promising results. The persistent use of *Opuntia* mucilage underscores its effectiveness and the cultural importance placed on sustainable building techniques throughout Mexican history.

Figure 11 Mexican frescoes: A) Los Murales de la Batalla y del Pórtico "A", Cacaxtla, Tlaxcala (Photo credits to Mediateca Inah); B) Murals of The Market, Diego Rivera, 1923–24,Court of Fiestas, north wall, first floor, Secretaría de Educación Pública, Mexico City (Photo credits to, Lauren Kilroy-Ewbank, CC BY-NC-SA 4.0).

The content of sugars, ash, fat, fibres, protein and moisture in the plant depends to several factors such as the maturity stage and the harvest season, and by the environmental characteristic of the cultivation as temperature, light irradiance and soil [147,148]. The composition of mucilage from *Opuntia ficus indica* is highly complex, thus multiples studies have focused on investigating its makeup. Here, are reported the components identified through different research efforts [21,147,149–152]:

- Polysaccharide as galactose, arabinose (that are the main neutral sugars), rhamnose and xylose
- Uronic acids (as glucuronic acid and galatturonic acid)Proteins
- Polyphenols
- Microcrystalline structures, such as calcium carbonate, calcium magnesium bicarbonate, magnesium oxide, calcium oxalate monohydrate, potassium peroxydiphosphate, potassium chloride

First of all production of gel is possible through extraction in water, the easiest practice used also in ancient time. Gel formation is allowed thanks to the presence of sugars and uronic acids in mucilage [137] (Figure 12). Moreover, the long polysaccharide chains (with hydroxyl functional groups) that form the mucilage are crucial for its ability to bind with water molecules and inorganic elements, thereby inducing water retention within cellular structure [21,137,153]. The mucilage has the characteristic to act a sponge like structure that trap water and chloride motion, allowing the enhancement of electrical resistivity, porosity and rapid chloride permeability [22]. The water retention capability of this substance improves the hydration of the mortar inhibiting rapid drying, preventing cracks formation [154], inducing the improvement of mechanical properties, thus of durability [21,22,134]. Recorded enhancement in mechanical properties can be related to the content of calcium and potassium ions which promote the crystallisation process [134] and also to the adhesive property of the mucilage [135]. Pozzolanic reaction of hydraulic mortar is based on the interaction between silica and calcium in the presence of water, leading to the formation of calcium silicate hydrate (CSH) phases. This mineral phase is fundamental in determining the hardening time of mortar and in providing its compressive and flexural strength. Thus, the over mentioned increment in mechanical strength can be related to the gel which being rich in calcium ions can enhance the pozzolanic reaction [131,155]. Furthermore, this addition promotes the packing of portlandite crystals, resulting in a more homogeneous microstructure [131], indeed it allows the formation of Calcium Hydroxide crystals emphasizing the growth mechanism of crystals during lime slaking, influenced by Nopal, reaching good shape and size and their colloidal stability and acting as a drying retardant [156]. By acting as a retardant of drying, it reduces the production of cracks during the hardening phase [157]. As reported by Ventolà et al (2011) [158], the incorporation of Nopal mucilage improves the carbonation process without inducing significant mineralogical variation. This improvement is attributed to the mucilage’s ability to

facilitate a more efficient pozzolanic reaction and create a more uniform distribution of crystalline structures within the mortar matrix. Indeed, during the carbonation process high quantity of small crystal of calcite crystals are formed due to the interaction of mucilage in the CSH formation phase (Figure 13), inducing formation of more sites for the nucleation [155]. Recent discoveries have highlighted other several important properties that addition of *Opuntia ficus indica* mucilage imparted to mortar. Proteins in mucilage, with their hydrophobic chains, render the mortar water-repellent, thereby increasing its resistance to water absorption [135]. Additionally, the presence of polyphenols in mucilage contributes to reducing the bio-receptivity of the mortar, which helps in minimizing biological growth [132]. Furthermore, mucilage derived from Nopal cacti imparts high viscosity to the mortar, ensuring stability and a solid-like behaviour even in its fresh state [22,133]. Finally, *Opuntia ficus-indica* mucilage showed to prove comparable compactness in mortar mixtures addittivated with Primal 33, thus serving as an effective substitute for chemical additives [132].

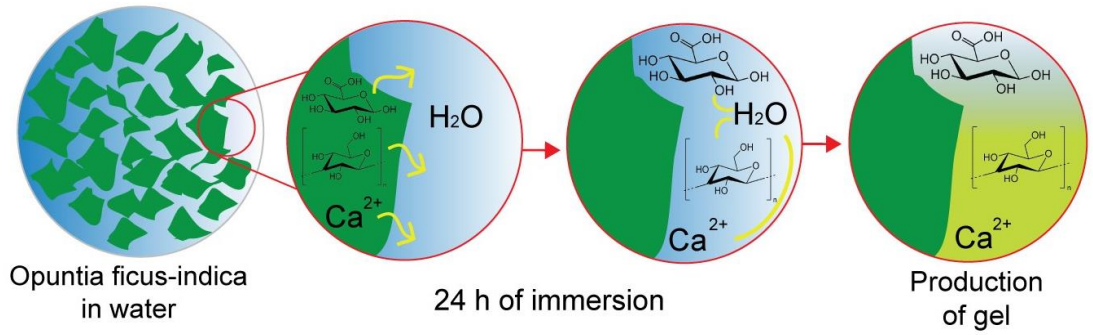

Figure 12 Reaction of production of gel.

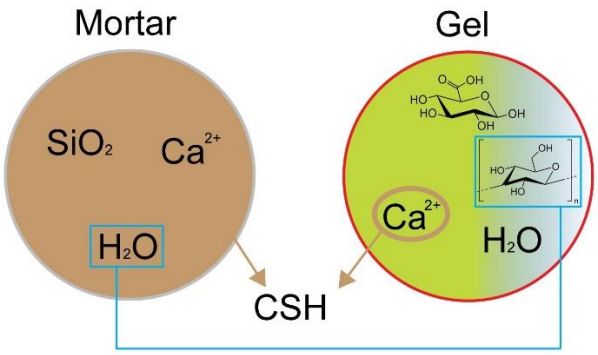

Figure 13 Scheme of reaction between mortar and gel, improvement of CSH formation in pozzolanic reaction.

Despite the fact that the plant is cultivated primarily for the fruits that produced, these findings collectively underscore the multifaceted benefits of incorporating *Opuntia* products in mortar mixtures, contributing to improved structural integrity and longevity. Its products can satisfy the request of different sectors for example production of forage for animals, production of bio energy,

for biotechnological application (as in dietary treatment) and also for water depuration [145,159]. The aforementioned research highlights the versatility of this plant, demonstrating its applications beyond the food industry to include its products into the construction materials industry. The cultivation of prickly pear is prevalent in Mexico (world leader of this cultivation) [160] and southern Italy, where Sicily cover the 90% of the European production [161]. The use of products produced by the treatment of cladodes that can be effectively repurposed for the production of gels, mucilage or fibres for other employment of Opuntia ficus d'indica can be considered sustainable. Indeed, seasonal pruning, which is necessary for robust plant growth, generates significant biomass waste (6-10 tons for each hectare) [162,137]. Moreover, the production of Nopal gel itself is environmentally sustainable, owing to its minimal environmental impact and efficient production methodology. The use of this mucilage for the production of mortar can be considered sustainable because of the presented researches proved the improvement of the characteristic of lime mortar, making it more durable, allowing the production of eco-friendly intervention in buildings [131]. This sustainable approach not only mitigate waste but also leverages the beneficial properties of Nopal gel, reinforcing its viability as a green additive in construction materials. This trend highlights the potential of integrating historical techniques within contemporary frameworks to enhance the sustainability of building materials.

2.4.3 Addition of self-healing materials

The increasing demand for innovative and sustainable materials in restoration and construction has inspired extensive research and development. This effort aims to create materials that offer enhanced safety, durability, and reduced repair costs. Among these, "self-healing materials" are particularly appealing due to their remarkable ability to autonomously repair cracks or fissures in structures. This inherent self-repairing behaviour occurs automatically and independently, without the need for external intervention, either during or after the occurrence of damage, eliminating the need for additional interventions and thereby reducing expenses [24–26]. In recent years, the use of self-healing materials has expanded across various fields within material science, notably in cement-based materials [163–166], lime mortars [167–169], and more recently, in the development of materials for heritage restoration [23]. This paradigm shift presents a compelling alternative to conventional methods, highlighting its potential for proactive damage prevention [169,170]. There are two distinct types of self-repair processes [24,26,171]:

Autogenous: This process relies solely on the original constituents of the material, which, under specific environmental conditions, facilitate crack repair due to their unique chemical composition.

Self-contained: through the incorporation of additional external components into the formulation [26].

In the context of the first self-repair process mentioned in point 1, examples of material exhibiting autogenous self-repair capability are cements [165] and lime-based mortar. Supposition about the capabilities of Roman concrete and mortar to repair themselves along time has been made and they were demonstrated in recent research [3]. This type of mortar achieves self-repair through the dissolution, transportation, recrystallization, and precipitation of calcium salts within cracks and fissures. As a result, of this mechanism, small cracks can be precisely repaired by the recrystallization of calcium compounds. However, it is crucial to distinguish between the processes of dissolving and re-precipitating calcium crystals and those of soluble salts. Soluble salts, for instance, can undergo solubilisation and transportation even under low humidity conditions, leading to internal and external efflorescence that can cause cracks and aesthetic alteration [167].

The self-repairing properties inherent in the binder of the mortar can be integrated into the mortar by incorporating external components into the formulation [171], presented in point 2. Three different type of system can impart autonomous self-healing properties, which include vascular systems [26], microbial healing agents [25] and microcapsules containing monomers or binders.

The vascular repair method consists of a network of capillaries within the mortar matrix, which are connected to external reservoirs containing repair agents. These systems are categorised based on the number of reservoirs and types of repair agents they use. Single-channel vascular system is employed when there is only one component in the repair agent, while a multi-channel vascular system is used when the repair agent consists of multiple components (Figure 14) [172,173]. These system can be useful when applied to new buildings, however they are impractical for restoration intervention, because they can results invasive necessitating of external reservoirs.

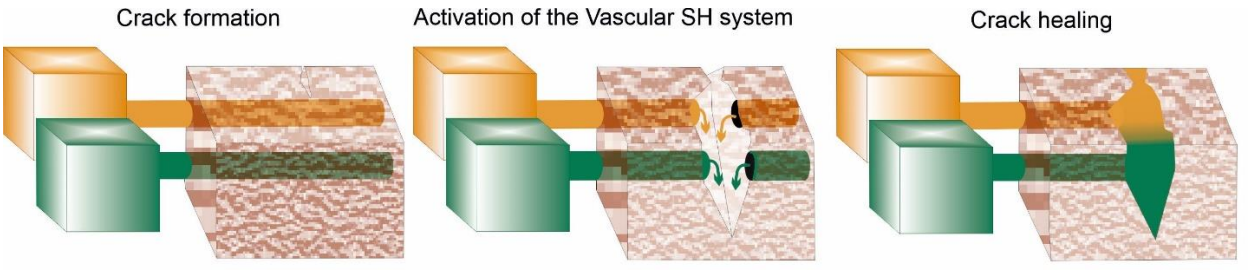

Figure 14 Process of self-repairing thanks to vascular system.

Self-healing based on bacterial reactions relies on the ability of bacteria to produce and respond by absorbing elements and converting them into different substances, for example converting urea into ammonium and carbonate [25]. The production of calcium carbonate, by precipitating in fractures, repairs the damaged system [174]. The bacteria are able to resist to the extreme pH conditions present in concrete and mortars, leaving inside it and staying silent. Bacteria can be

incorporated in the mortar or dispersed (through spray and injection) in an existing one. Additionally, they can be also encapsulated in gel or polymers and then added in the pastes [175]. The research conducted employing this method of healing has demonstrated good results [25,174], however, further research are necessary for a better control of the system. Indeed, environmental factors for the conservation of the bacteria are difficult to be controlled and along with food availability affect their longevity and their efficiency [175].

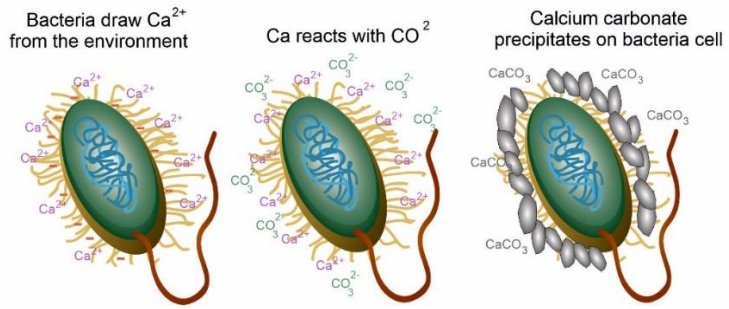

Figure 15 Process of self-repairing thanks to microbial action.

Polymeric microcapsule can be filled with a restorative agent (such as a monomer) with a catalyst, and then embedded in a mortar matrix [26,173]. The steps of activation of this self-repair mechanism are as follows (Figure 16):

1. Formation of cracks that propagate to the polymer capsules;
2. Rupture of the capsules, resulting in the release of their contents;
3. Polymerisation reaction of the released content (monomer). This reaction can be triggered by various factors, such as contact with the matrix, reaction with a catalyst, hydration, or heating.

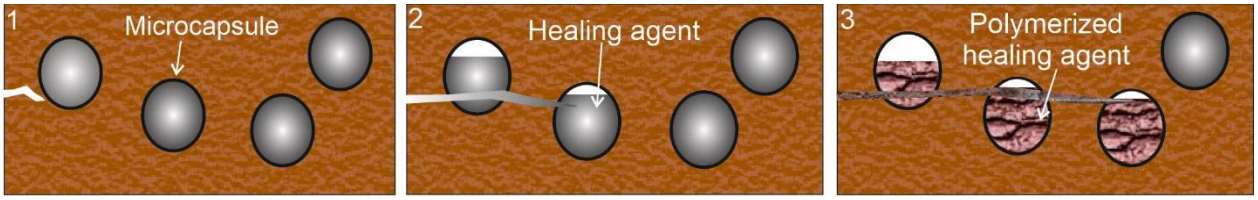

Figure 16 Process of self-repairing thanks to polymeric microcapsule.

The polymer thus formed fills the crack through capillary action, achieving the self-repair effect, however can results distant in composition and in compatibility from an ancient substrate. Following similar process of polymeric capsule, encapsulate binder can be considered more indicated for restoration material. Indeed, while the mortar possesses inherent self-healing capabilities, they can be enhanced and augmented by incorporating encapsulated binder agents in polymeric capsules [176]. The operational mechanism, exemplified in Figure 17, of this method involves two main steps:

1. Binder is encapsulated in a polymer capsules, and subsequently are introduced into the mortar as an additive, keeping them inert and inactive during the mortar-curing phase.
2. Damage to the mortar provoke cracking or breakage, the reaction happens when the polymer capsule is exposed to air or water through the fracture. This binder is released and then activated provoking a delayed hardening process [170,171].

This advanced approach overcomes the limitations of autogenous processes, which typically address only minor cracks. By significantly enhancing the overall durability of materials, this innovation represents a major leap forward in concrete and cement paste technology in the 21st c. The emergence of self-healing materials marks a cutting-edge advancement in this field [170].

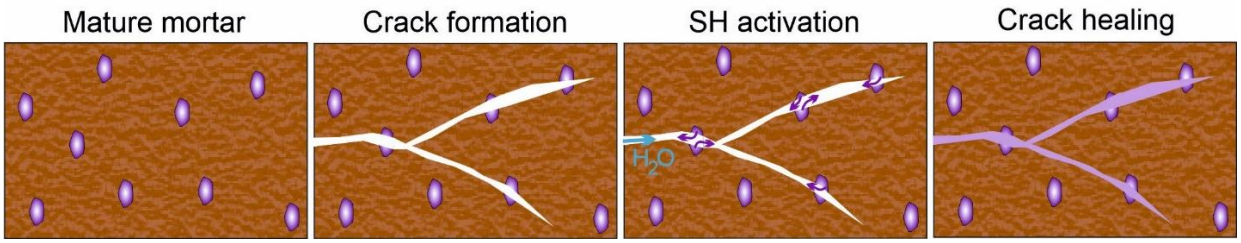

Figure 17 Process of self-repairing thanks to encapsulate binders.

3 Composition of mosaics under study from Aquileia

When dealing with the production and use of restoration products, it is fundamental to consider the composition of the original substrates to be restored. Compatibility is crucial to ensure the durability of the restoration and minimise the need for future interventions. Therefore, understanding the composition of the original ancient materials is essential for developing a suitable mortar for mosaic restoration. Additionally, analysing the composition of each layer of the mosaic (from the *tesserae* to the *Rudus* layer) enables the creation of accurate mock-ups that closely replicate the ancient materials, which can be use as surface for restoration simulation. For these reasons, analyses has been conducted on archaeological samples collected in Aquileia.

The around 2000 pieces used as study material in this thesis were collected by archaeologists during field walking survey campaigns held between 2011 and 2017. The specimens were meticulously organised based on their recovery area. Each individual piece underwent a thorough cleaning procedure, wherein the surface was delicately brushed to eliminate any traces of ash and dust. The surveyed region was systematically divided into 4 distinct subfields (North West, North East, South West, and South East) as visible in Figure 18, highlighted by the yellow lines. In supplementary material (Figure 1S) is reported the image of the detailed map illustrating the distribution of *tesserae* across various geographical areas. Criteria employed for the selection encompassed the hue of the upper external surface, the presence of adhered mortar, and the existence of secondary crusts and deposits. This methodological approach facilitated the attainment of a comprehensive representation of specimen diversity within each area and their dispersion throughout the surveyed territory. In sum, a total of 153 pieces comprising black, white, and coloured *tesserae* were subjected to petrographic analysis in order to assess the nature of lithic material. 29 samples of the 153 selected presented mortars, some of them are fragments with mortar interwoven within the *tesserae*, while other display pieces of mortars still adhered to the surface of the tiles.

Figure 18 Map of the area of the provenance of the material.

Detailed information about the nature of each of the 153 analysed samples can be found in Table 1S[12]. The investigation presented in this chapter pertains to the analysis of mosaic fragments both in their mortars and *tesserae* composition, employing a diverse array of analytical techniques. In Figure 19 is reported a diagram of the analysis applied for the investigation of *tesserae* and or mortar, which results are respectively presented in §3.1 and §3.2.

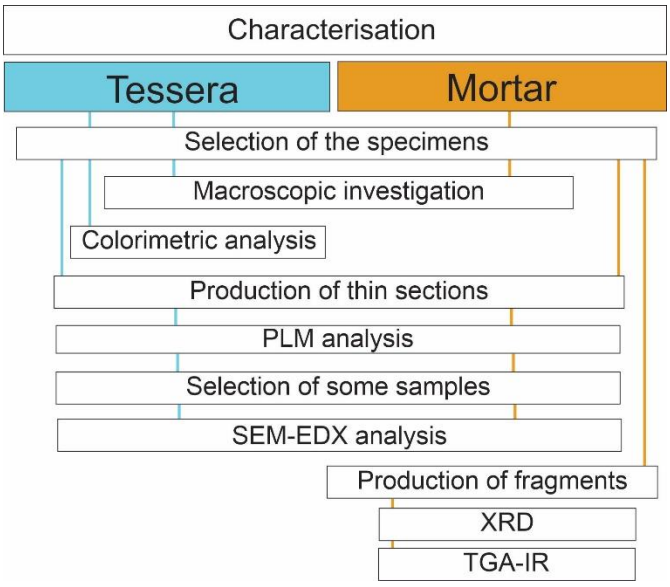

Figure 19 Diagram of the analysis applied for the characterisation.

[12] For more information please look at Annex_A, Table 1S Summary of the information acquired for each specimen.

The analysis of archaeological samples involved a sampling procedure that led to the partial loss of material. To address this issue, a new method was tested to analyse entire mosaic fragments without sampling, aiming to surpass traditional characterisation methods. This trial involved the use of Synchrotron X-ray Computed Tomography (SXCT) to explore its potential as an alternative investigative technique. The rationale behind this approach is that detailed information about the microstructure of mosaic fragments can reveal production deficiencies and structural failures, thereby advancing our understanding of degradation phenomena. This information is crucial for preparing mortar suitable for restoring the internal microstructures investigated. As this is the first time such an analysis has been conducted on mosaic fragment, the samples analysed were mock-up replicas of archaeological materials, with compositions was based on the results of prior characterisation analyses. The mock-ups were subjected to SXCT, and the results, discussed in this chapter, demonstrate that SXCT is effective for obtaining 3D images of both the internal and external features of mosaic specimens, highlighting its feasibility for comprehensive microstructural analysis.

3.1 Petrographic nature of *tesserae*

The samples underwent comprehensive characterisation based on macroscopic features, including the colour of the upper external surface and a freshly cut surface, as well as petrographic characterisation. This comprehensive approach enabled the determination of the petrographic composition of the *tesserae*[13]. In mosaic making, the colour, dimensions, and shape of *tesserae* are pivotal factors that influence the quality of the final artwork. Thus, the external colour served as a primary criterion for material selection and grouping.

Macroscopic images of the specimens were captured using a Canon EOS 5DS reflex camera. Colorimetric analysis was conducted on freshly cut surfaces of the *tesserae* to obtain measurements reflective of the original colour, thereby mitigating alterations resulting from weathering during burial or the presence of crusts or deposits on external surfaces. CIE colorimetric parameters L*a*b* were obtained using a portable spectrophotometer (CM-2600d Konica Minolta with a D65 illuminant), following guidelines outlined in EN 15886:2010 [79], with consideration given to the specular component included (SCI). A comparative analysis was also conducted between the colorimetric parameters recorded on freshly cut surfaces and the external coloration.

Each sample was prepared in the form of thin sections and subsequently examined using an Olympus DX-50 Polarised Light Microscope (PLM) equipped with a Nikon D7000 camera to capture digital microphotographs. Petrographic analysis facilitated the delineation of mineralogy and texture within the *tesserae*, thereby elucidating the petrographic characteristics of the materials and identifying the specific rock types utilized in their construction.

For micro chemical characterisation of specific mineral phases seventeen thin sections out of the total 153 samples, were subjected to Scanning Electron Microscope (SEM). The analysis was conducted using a FE-SEM Tescan Solaris coupled with an Oxford Instrument UltimMax 65 Silicon drift EDS detector. The analysis allow to complement the results obtained through PLM and to obtain additional petrographic details. SEM imaging and EDS spectroscopy were conducted at an acceleration voltage of 15 KeV and a beam current of 3 nA, with a working distance of 5 mm. High-resolution images were captured at 5 KeV, 300 pA, and a reduced working distance of 4 mm. Subsequently, the findings from the petrographic analysis were juxtaposed with the classification based on coloration.

---

[13] The results of research in this paragraph are presented on the article "Tracing the origin of Roman mosaic tiles in Aquileia: petrographic analysis of specimens from the suburbium" by Stucchi, Neva M. E.; Franceschin, Giulia; Coletti, Chiara; Vavasori, Andrea; Mazzoli, Claudio; Traviglia, Arianna. The article is currently under revision by the editor of the journal *Archaeometry*.

3.1.1 Macroscopic features of the analysed *tesserae*

The *tesserae* exhibit a range of shapes, including rectangular, cubic, rounded, and "tooth-like," with dimensions varying from 0.5 to 3 cm per side. Figure 20 presents photographic images of selected samples fragments of mosaic composed of black and white *tesserae* (respectively Figure 20 A and B) and single *tesserae* of different colours whitish-pinkish, black, white, grey (Figure 20 respectively from C to F). The red line present in the picture highlight the point where the samples has been cut in order to produce the thin sections.

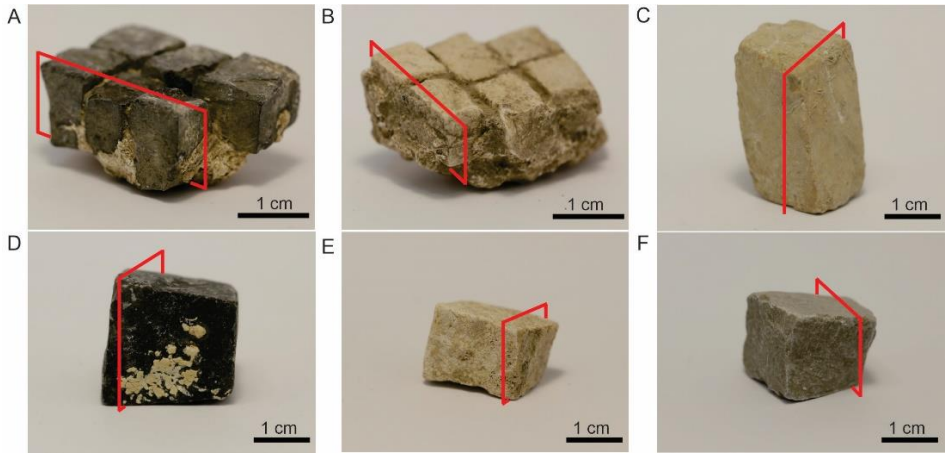

Figure 20 Photographic images of some of the analysed samples A) fragment made of 6 black *tesserae*, s. 9 ; B) fragment made of 6 white *tesserae*, s. 11; C) single whitish-pinkish tessera, s. 20C ; D) single black tessera, s. 10C ; E) single white tessera, s. 22D ; F) single grey tessera, s. 28A.

Because of the small dimensions of some of the selected specimens, in order to gain photographic images of the entire specimens, Optical Microscopy was applied. In particular, a small green tessera (sample 18C, Figure 21g) and a deep red tessera (sample 30C, Figure 21h). The green tessera is characterised by large, pale greenish plagioclase phenocrysts within a fine-grained deep green matrix, typical of mafic volcanic rock and resembling green. In contrast, the deep red tessera has a fine-grained compact matrix akin to red jasper [177].

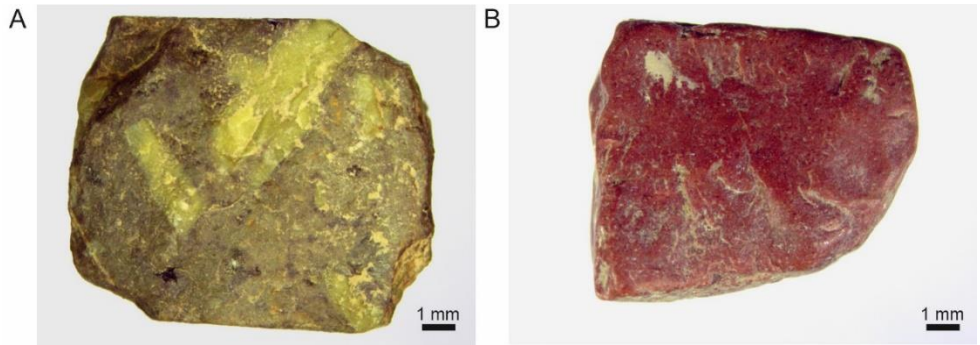

Figure 21 Microscopic images of 2 small *tesserae* A) green tessera, s. 18C ; B) red tessera, s. 30C.

The 153 analysed samples were characterised by a variety of colours with different tonalities and consequently categorised into seven colorimetric groups based on their visible colour: white (very pale-coloured *tesserae*, denoted as W), black (dark-coloured *tesserae*, denoted as B), grey (G), yellow (Y), pink (P), red (R), and green (Ge). In Figure 22 is reported the bar diagram with the distribution of specimens within each colorimetric group across the different subfields of the surveyed area. Specifically, there were 78 white, 31 grey, 24 black, 12 pink, 4 yellow, 3 red, and 1 green tessera.

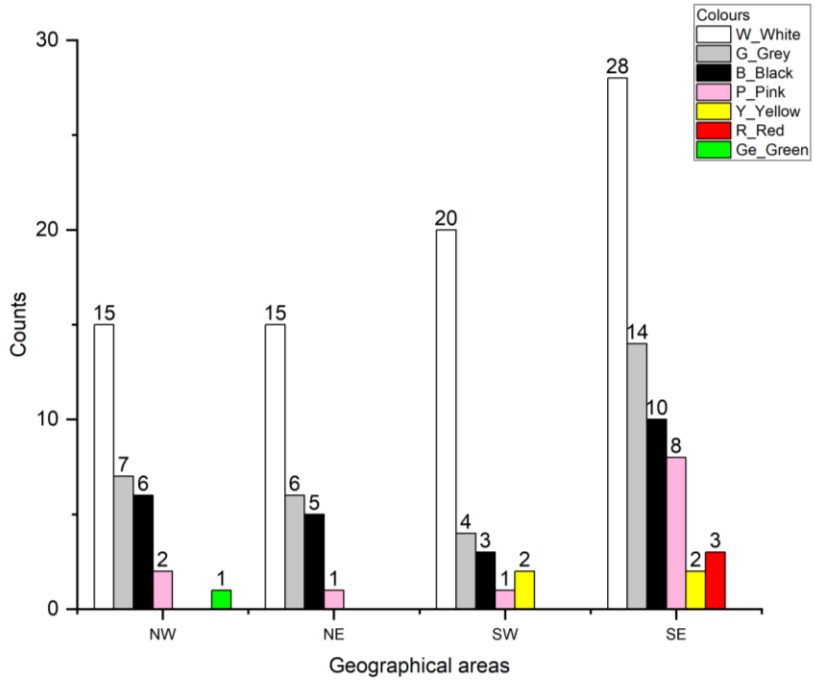

Figure 22 Bar diagram reporting the quantity of samples within each colour group across the various subfields of the surveyed area.

The 153 selected samples were grouped a priori based on their macroscopic appearance, in addition colorimetric analysis allow to effectively assess the colour without visive bias. The results achieved enabled plotting the relative colour in the L*a*b* space (Figure 23). The largest colour groups, including black, grey, white, and pink *tesserae*, exhibit a broad range of L*a*b* parameters. The colour space in Figure 23 shows no clear separation among adjacent groups, indicating significant colour variability even within individual groups. Analysing the overall distribution, the samples cluster within a specific broad range, with maximum variability observed in the L* parameter (ranging from 27 to 86). Data spread from the achromatic axis towards positive a* values for high L* values, resulting in very pale yellowish nuances. For low L* values, data shift towards slightly negative a* and b* values, indicating a predominant dark green component. The colorimetric distribution of the grey group highlights its wide range of values, continuously varying from light to dark shades (L* ranging from 42 to 81). A significant number of *tesserae*

belongs to the black group, which also shows extensive variability in the L* parameter (ranging from 27 to 64). Approximately half of the samples belong to the white group. These samples, while located in the lighter region of the colour space, display wide variability in L* (from 57 to 86). Most samples in the pink group and two yellow specimens (samples 12A, 20C, 23C, 33B, 39B, 41C, 42A, 52A and samples 32A, 32B, respectively) are positioned close to the wide field of the white *tesserae*, indicating a gradual shift in nuance for these materials, moving progressively away from the achromatic axes. Furthermore, sample 12A and sample 32B, macroscopically assigned to the pink and yellow groups, respectively, exhibit similar colorimetric parameters and almost overlap in the L*a*b* space. Only the red *tesserae* (samples 30C, 30D, 37D) display relatively homogeneous colorimetric parameters, occupying a confined area of the L*a*b* space with notably positive a* and b* parameters and intermediate L* values. The parameters recorded for the green *tesserae* (sample 18C) show a slightly negative a* value, suggesting a small yellow component in its colour. Its position in the L*a*b* space is close to the field of the black samples, which also exhibit a dark green component. To better visualise the colour distribution among the samples within the different groups, in Figure 23b are reported binary diagrams of the colour space respect to the a* and b* parameters, with information about the average value of the L* parameter. Samples in the white group (Figure 23b) are evenly distributed within a field characterised by a* values ranging from -0.2 to 3, and b* values between 2 and 16, encompassing shades of very pale grey, yellow, and pink. Figure 23c illustrates the distribution of the coloured samples. Specimens in the pink and yellow groups are projected very close to the area of the specimens in the white group, with slightly higher a* parameter values and lower average L* values, indicating deeper and slightly more vivid colours. Additionally, one of the pink *tesserae* (sample 31B) is positioned in the same area as the red samples, albeit with a significantly higher L* value (Figure 23). Two *tesserae* assigned to the yellow group (samples 30A and 30B) are located in a separate area of the diagram, displaying higher levels of saturation with b* values of approximately 20. Consistent with the observations in Figure 23c, the green specimen 18C is located near the specimens of the black group in the diagram in Figure 23e. The majority of the samples assigned to the grey group (Figure 23d) cluster in an area similar to that of the black specimens, although the latter exhibit significantly lower L* values (Figure 23e). Considering the differences in this parameter among the groups, there is a greater similarity between the grey and white samples than between the grey and black samples. Therefore, it is plausible that the tonality of specimens categorised as grey material bears a greater resemblance to those exhibiting white tonality. One of the grey specimens (sample 27A) is characterised by a* and b* parameter values that place it in the same area as some of the yellow specimens (samples 30A, 30B). Additionally, the L* parameter is similar among these samples, emphasising the challenges that can arise when defining colour solely through macroscopic observation. Finally, the black group shows a homogeneous distribution within a narrower range of a* (from -2 to 1) and b* (from -4 to 7) compared to other groups.

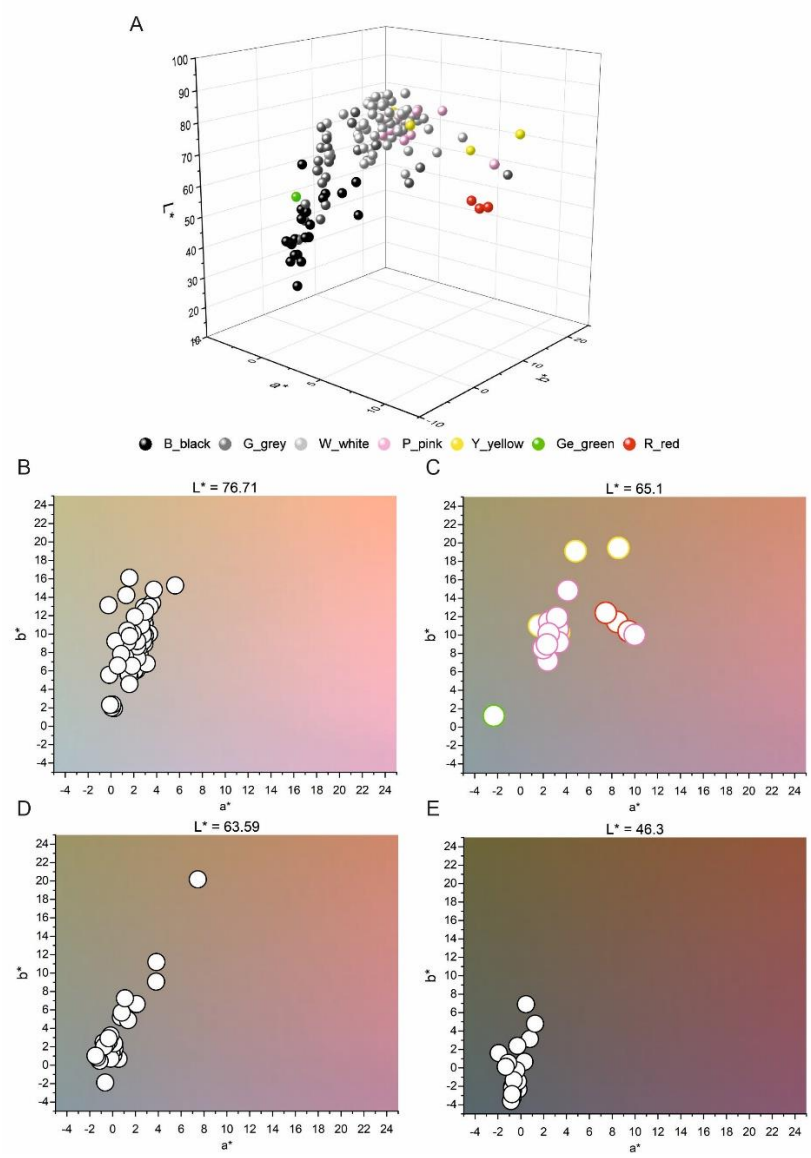

Figure 23 Graphical representation of colorimetric analysis results. (A) 3D plot in the Lab* colour space. To facilitate visualisation of the colorimetric distribution, specimens are plotted in the ab space: B) lightest coloured tesserae; C) coloured tesserae (pink, yellow, red, green); D) grey tesserae; E) darkest coloured tesserae.

3.1.2 Petrographic analysis of thin sections

A summary of the results achieved from the petrographic characterisation of the *tesserae* is reported in Table 1S of supplementary material section[14]. Mineralogy and textural composition of the lithotypes were defined thanks to microscopic investigation performed on thin sections of each specimens, allowing the identification of the specific mineral phases and rock types used in their realisation. This information allow the comparison with images of petrographic section of material allowing its identification and where possible the source of the raw material. Some of the *tesserae* exhibited distinctive microstructural features, establishing them as the exclusive representatives of particular petrographic classifications. It was observed that colour-defined groups of *tesserae* may encompass multiple lithologies, with individual rock types displaying chromatic variations that warrant their classification across diverse colorimetric categories. Photomicrograph acquired with microscopic analysis of thin sections of the materials identified are presented in Figure 24. Petrographic characterisation allow to assess that the majority of *tesserae* fall within a restricted range of petrographic categories, predominantly comprising limestones, while a small proportion consists of alternative lithologies or non-rock materials. Considering the external colours of the *tesserae*, it is possible to assess that despite their coloration, the material used to gain *tesserae* of specific colours is different and sometimes some materials are characterised by different shades, covering the necessities of production of a wide range of colours. Light-coloured *tesserae* primarily consist of various limestone types, such as wackestone, mudstone, grainstone, and packstone. These lithologies vary in their faunal composition and the abundance of fossils (also called grains), the occurrence of micritic versus sparitic cement, and the presence and quantity of a micritic matrix. Thanks to Dunham classification it is possible to define the exact typology of limestone considering the ratio of grains and type of cement [178]. From a mineralogical perspective, the distinction between light-coloured and dark-coloured *tesserae* predominantly arises from the presence and relative abundance of iron oxides, hydroxides, and other pigmented minerals. Additionally, SEM-EDX analysis conducted on thin sections of 17 lithic specimens (18A, 18B, 18C, 19B, 23A, 23B, 23C, 30C, 30D, 31A, 31B, 37A, 37C, 45B, 47A, 53C, 53D) revealed specific features and identified mineral phases that were not detected using PLM analysis. Although many of these specimens share the same petrographic characteristics, they differ in colour. To better understand these colour variations, the higher magnification capability of SEM, combined with chemical analysis via EDX, was employed.

[14] For more information please look at Annex_A, Table 1S Summary of the information acquired for each specimen.

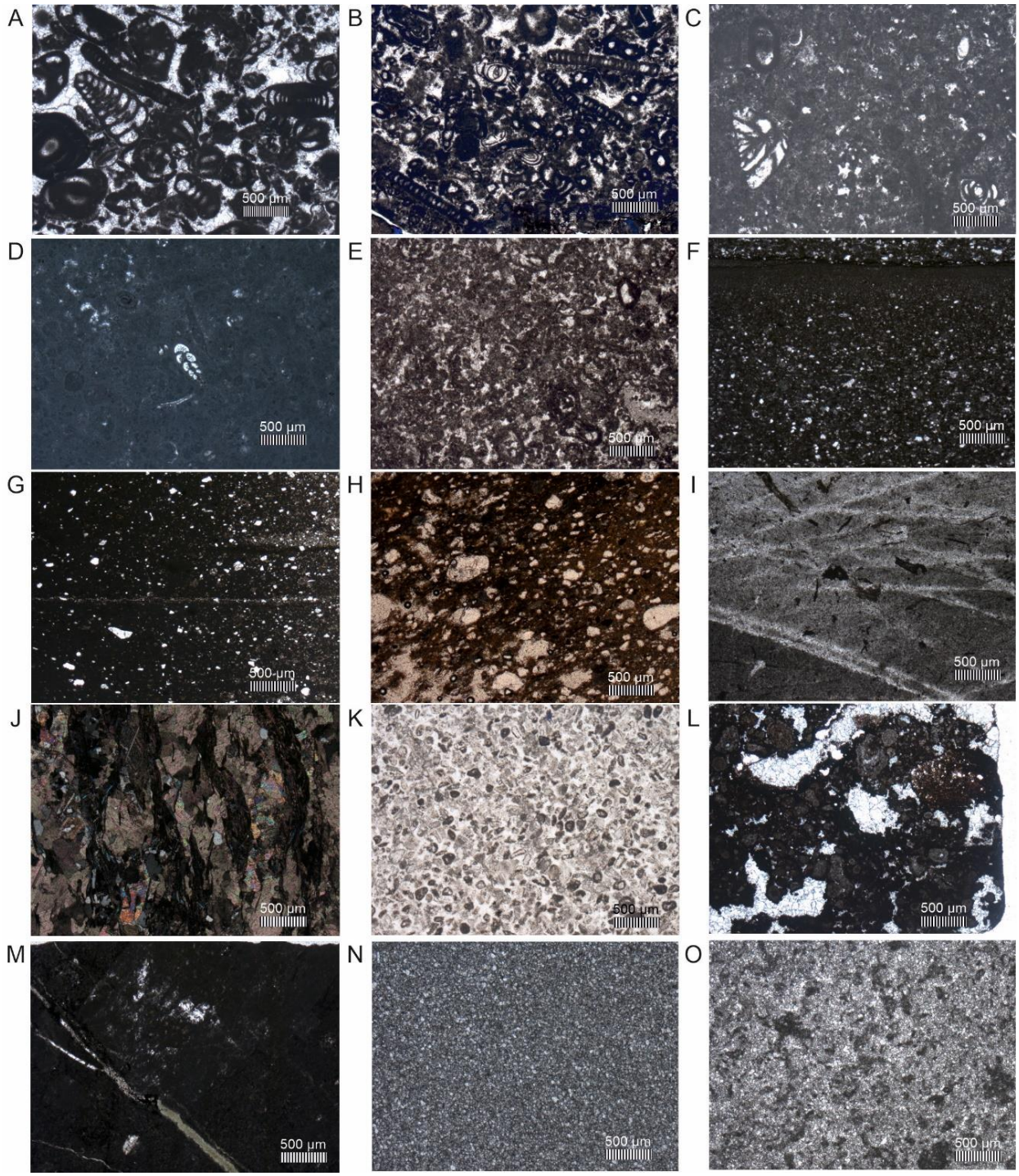

Figure 24 Microscopic images of thin sections are provided, featuring one example for each material: a) Grainstone, s. 13; b) Grainstone, s. 49A; c) Wackestone, s. 44B; d) Mudstone s. 3; e) Packstone, s. 48B; f) Laminated wackestone, s. 8; g) Ceramic material, s. 26D; h) 37D i) Chert, s. 18A; j) Impure calcite marble, s. 37C, in cross polarised mode; k) 45B; l) Hardground, s. 30D; m) Porphyry, s. 18C; n) Fine-grained crystalline limestone, s. 31B; o) 41B.

Grainstone

The predominant type of material recorded for the composition of the *tesserae* is grainstone, counting 38 specimens. This material is a peloidal limestone, comprising peloids, micritised ooids, and occasional benthic foraminifera shells, all cemented by a thin layer of sparitic cement. Figure 24A exemplifies a white *tessera* (sample 13) characterized by a texture supported by grains and a sparitic cement. The fossil content of these specimens typically includes abundant benthic foraminifera (Miliolida and Textulariidae), fragmented green algae (Thaumatoporella parvovesiculifera), and other foraminifera indicative of the inner-back edge carbonate platform, such as Broeckina balcanica, Chrysalidina sp., Vidalina sp., Nezzazata simplex, Moncharmontia apenninica, Scandonea samnitica, Cuneolina sp., as well as occasional echinoderms and sponges. This material can be of white colour, but its shades can veers to grey (e.g. sample 49A, Figure 24B), pink and yellow tonalities but also darker tonalities reaching a black colour, demonstrating the use of the same material for the production of *tesserae* of different colours.

Wackestone

The second type of material, for abundance, is wackestone (33 specimens), that differ from grainstone only for the prevalence of either sparitic cement or a micritic matrix. As well as grainstone, also wackestone can be characterised by different colours. Indeed, from the analysis was possible to assess the wackestone composition of *tesserae* of white, grey and pink colour. As possible to see in Figure 24C (e.g. sample 44B), this material is characterised by a micritic mud matrix where bioclasts are immersed. Some of the bioclastas that was possible to visualise are: benthic foraminifera (e.g. Nezzazata conica, Biconcava bentori, Miliolida), agglutinated foraminifera (e.g. Crysalidina gradata) and planktonic foraminifera (Whiteinella sp.), ostracods, and cyanobacteria (e.g. Decastronema sp.). PLM analysis indicated that several pinkish specimens, such as samples 23C and 31A, have similarities to greyish and whitish specimens like 37A and 18B, respectively. Microstructural analysis confirmed that these specimens are grainstone and wackestone from Aurisina. Furthermore, a comparison of the EDX patterns across a wide area indicated a higher iron (Fe) content in the pinkish samples. This suggests that variations in iron hydroxide content may account for the colour differences in the carbonate material, leading to shifts from white-grey to pink.

Biomicrite

24 samples of white, pink, grey and also yellow colour are made of mudstone (e.g. sample 3, Figure 24D). This material is distinguishable from the other presented for the biomicrite or microsparite matrix with dispersed ostracods that rarely presents foraminifera such as Chrysalidina sp. and Textulariidae, which have been recognised.

Packstone

Packstone with abundant skeletal fragments has been recognised as the one reported in Figure 24E (e.g. sample 48B). It was difficult to specifically determine the nature of bioclasts that in some cases were individuated as Pseudolituonella sp., Vidalina sp., Broeckina balcanica, and Textulariidae. Thanks to the faunal assemblages recognised, it is possible to suggest the geological period of formation as the late Cretaceous ages (from Cenomanian to Campanian). The dating of these materials aligns with the one of the formation of the Classical Karst region. This depositional environment encompass south-western Slovenia and north-eastern Italy, as the likely provenance for the raw materials used in *tesserae* production. In support of this, from bibliography [31,179] it is possible to know that this region was extensively exploited for building stone materials during the Roman period. However, the absence of rudist fragments in some of the analysed specimens, suggest in some cases that the source areas differ from the Roman Quarry present in Aurisina. This material was recorded for a totality of 17 specimens, only one of this is of grey colour, while the other are of white colour.

Laminated mudstone to wackestone

The great number of black *tesserae* and 23 grey *tesserae* present a matrix made of the rhythmical repetition of *strata* with more mud or bioclasts, this features are typical of laminated mudstone to wackestone stone (e.g. sample 8, Figure 24F). The laminae demonstrate a gradation in grain size, transitioning from coarse to fine particles. Interspersed between each lamina are thin layers enriched with iron hydroxide and clay minerals. The material is characterized by the accumulation of fossil fragment debris and small sparite grains within a micritic or microsparitic matrix. Occasionally, non-diagnostic bioclasts are identified, including Miliolida, recrystallized radiolarians, ostracods, and fragments of pelagic bivalves. These features indicates an intertidal sedimentary environment, it is possible to suggest an episodic high-energy depositional mechanism influenced by seasonal variations. Despite the deep-red colour, also sample 30C is made of laminated wackestone with bioclasts (e.g. silicified Globigerinoides, ostracod shells, radiolarians, and sponge spicules). This lithology is predominant among the detected materials, thus it is possible to assess the exploitation of quarries, during the Roman time, from the same geographical area. Possibly the source of this material are the quarry of Aurisina limestone where also wackestone and grainstone come from. Slovenian Roman mosaic are a good example for the identification of the typology of materials. Indeed, in the sites in Emona, Mošnje, on the Istrian coast, and in mosaics from Roman Celeia in Slovenia laminated wackestone has been found [70,72,179]. Moreover, Slovenian Karst area has been indicated as the possible provenience of this material considering the exploitation of black limestone during the Roman time [180]. Considering the location of the city of Aquileia, the nearest source of laminated wackestone is the Villaggio del Pescatore in Duino, near Trieste [181]. This site is particularly known for the great presence of fossils recorded which include reptiles, land plants, crustaceans, fishes, and dinosaurs [182,183].

Auirisina limestone comes from the upper part of the geological formation called Lipica formation [184] where also laminated limestone lies. This sequence is separated by a paleokarstic surface[185], forming the base of the Liburnian Formation, dated back from the Maastrichtian to the Paleocene period [186]. The analysis of the visible bio-microfacies allow the dating of the period of formation of the laminated limestone as the early Campanian [183]. Together with grainstone, wackestone, packstone, mudstone also laminated wackestone as the same carbonate composition and fall under Dunham classification considering the differences in texture and abundance of grains and bioclasts compared to mud [178]. Two samples one grey tessera (sample 19B) and one black (sample 53D) were analysed using SEM-EDX, in order to gain additional information that could improve the knowledge useful to drive supposition about the provenience. SEM observation confirm the composition revealed with PLM as laminated wackestone and EDX allow to assess the predominant carbonate composition with a detrital component of quartz and clay minerals. Additionally, Sample 53D contains a significant amount of pyrite, suggesting reducing conditions that explain the dark colour of the tessera. In contrast, samples 19B have varying amounts of iron oxide and hydroxide. Additionally, one *tesserae* of red colour (sample 30C) which materials was difficult to be identified was also analysed with SEM-EDX and surprisingly allow the assessment of laminated wackestone as material of its composition. Indeed, major carbonate composition, quartz and clay minerals, a high amount of iron oxide and hydroxide (which define the red colour) and also small quantities of fluorapatite were detected.

Ceramic material

6 out of 153 samples (samples 26D, 30A, 30B, 35C, 37D, 54C) are composed of ceramic material. These specimens are characterised of white, yellow, and red colour respectively 3, 2 and 1 specimen. In Figure 24G is reported the image of the analysis of the thin section of specimen 26D, a white terracotta tessera, which is characterised by an homogenous, fine-grained and isotropic matrix respecting the Whitbread definition for ceramic material [187–189]. Also all the other specimens made of ceramic materials are characterised by the same kind of ground mass. Typical colour of terracotta material, visible to the naked eye is the dark red one that characterise sample 37D. Indeed, this specimen analysed under PLM shows (Figure 24H) a dark brown to deep red optically active matrix, with a spotted b-fabric. Change in colour of other terracotta specimens analysed is due to the highly calcareous composition of the material, that present a crystallitic birefringent fabric (b-fabric), producing the yellow to white colour of the *tesserae*. The analysis show the presence of vughs and meso-voids in the matrix of the ceramic material and in small quantity also of micro voids. Through the analysis of the matrix, it was possible to record the presence of quartz and limestone fragments with rounded to sub-rounded shapes, along with rare argillaceous rocks and single foraminifers. These inclusions have a coarse:fine ratio of 10:90, with a single-spaced seriate grain size distribution, reaching the maximum size of around 300 μm. This result aligns with the recorded tendency of romans of use terracotta fragments for the production

of *tesserae* in absence of natural material of specific colour as demonstrated in the Aquileian Mosaic of the Wounded Beasts [59].

Chert

1 white sample (24C), 2 grey samples (50A, 53C) and 2 black samples (18A reported in Figure 24I) are composed of chert. This material is present in several carbonatic layers of Karst rock formations [186] being easily available. Indeed, chert and cherty limestones are frequently present in mosaics to produce *tesserae*, moreover they were also used by Romans to produce the aggregate material used in mortar formulations [63]. Three of these samples (18A, 23A, and 53C) were analysed through SEM-EDX analysis which revealed subtle differences among them. In addition to quartz, sample 18A contains calcite, dolomite, and abundant graphite, along with minor amounts of pyrite and apatite. Samples 23A and 53C consist of quartz, calcite, pyrite, and iron oxide/hydroxide.

Cipollino

Thin section of sample 37C reported in Figure 24J presents a medium to coarse-grained matrix with evident schistosity marked by spaced layers of chlorite and muscovite. Polycrystalline granoblastic aggregates of quartz, subhedral albite crystals generally larger than the average calcite grains, and accessory amounts of epidote and titanite are also present. This is the only *tesserae* presenting this features that are typical of impure calcite marble. According to literature material, some supposition about its precise composition and provenance has been made. The recorded composition is typical of *cipollino verde* (green cipollino). Green cipollino from the Apuan Alps is prevalently made of muscovite and contain also chlorite and often biotite [190,191], these minerals were not recorded during the analysis of our sample, excluding this provenance from the possible one. The matrix is also different from the impure marble or calc-shists of green and also of grey colour that comes from the north-western Italy more precisely from the Waldensian Valleys of Piedmont in the Cottian Alps. Indeed, the main characteristics of this material is the abundance of phengite, tremolite, also talc and diopside can be present, differently from chlorite which is generally absent of rare [192]. Considering this, the characteristics features recorded from our specimens is typical of an impure calcite marble that can be a green variety of *cipollino*, which is sourced from the Island of Euboea in Greece or a rarer grey variety of *cipollino*, called *cipollino bigio* also sourced in Greece from Karystos [177,193,194]. Considering, that the *tesserae* is characterised by a grey-black colour the latter kind of material can be the one that correspond to the one that compose our *tesserae*. Sample 37C is identified as an impure calcite marble with a texture and mineral assemblage similar to classical *cipollino verde or bigio*. This last hypothesis was confirmed also through the assessment of mineral composition conducted with SEM-EDX analysis, which revealed the presence of calcite, quartz, chlorite, muscovite, albite, titanite, apatite, and rutile (Figure 25).

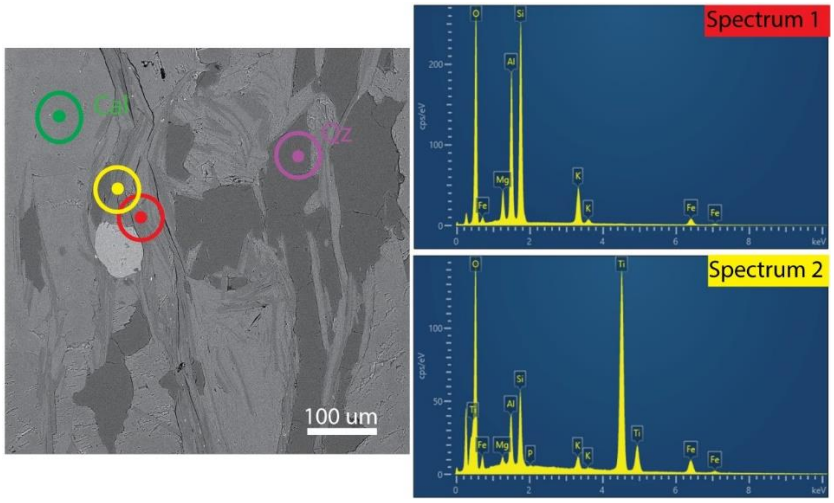

Figure 25 SEM-EDX analysis of sample 37C. Presence of calcite and Quartz are indicated in the figure following Warr 2021 abbreviations. Muscovite is identified in spectrum 1, while possibly a combination of rutile and muscovite is identified in spectrum 2.

Silicified grainstone

Only one grey *tesserae*, sample 45B, is characterised by a matrix typical of silicified grainstone (Figure 24K) with visible silica cements. Because of the few information acquired with simple PLM analysis, SEM/EDX was applied in order to gain more information about the mineralogy of the material, allowing the assessment of its composition. The analysis detected the presence of bioclasts composed of calcite within a fine-grained matrix of chalcedony, along with occasional grains of iron hydroxide and barite. The identified mineral phases are shown in Figure 26a, with abbreviations following Warr 2021 [195].

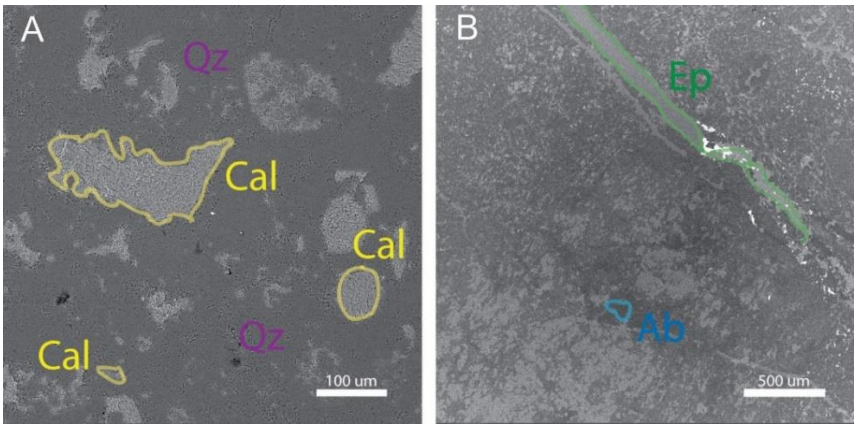

Figure 26 SEM-EDX analysis of samples: A) s. 45B, in yellow are highlighted the crystals of calcite, characterised by a light grey colour, that are visible in the silicate matrix (of dark grey colour); B) s. 18C, in blue is highlighted one phenocrystal present and in green the epidote vein.

Hardground material

Red *tesserae* 30D shows a textural characteristics typical of Hardground material (Figure 24L). The red colour is due to the ferruginous inclusions present in the clay. Irregularly shaped clusters of microorganism (ooids) are visible in the matrix which lack of distinct layering. Voids present within each clusters are filled with sparry calcite. The consideration that can be made through the evaluation of this thin section doesn't allow the evaluation of a precise provenance. However, in literature similar materials has been indicated as sourced primarily in the Slovenian Karst region and in lower quantity in the Italian Karst area [196] [197] . SEM-EDX analysis confirmed a high concentration of iron oxide/hydroxide, which accounts for its deep red colour. Quartz, clay minerals, and calcite were also identified (Figure 27).

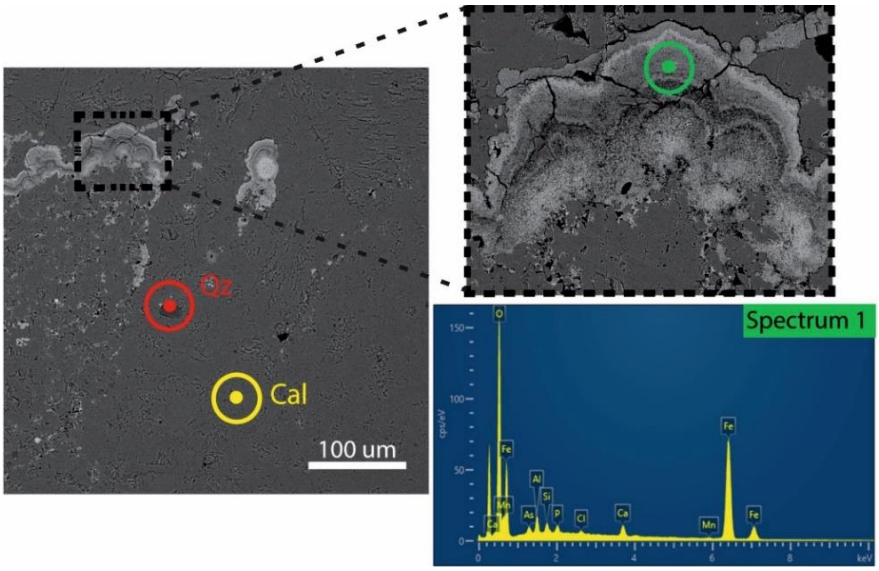

Figure 27 SEM-EDX analysis of sample 30D. A detail of the ferruginous ooids inclusions is reported in the upper left figure. Spectrum 1 shows the Iron oxide inclusions present, clearly visible in the microscopic picture on the left. The matrix is composed of Calcium carbonate (Cal) and Silica oxide inclusions (Qz).

Porfido verde antico

Only one *tesserae* (Figure 24M, sample 18C) presents a green colour. The matrix has the typical characteristics of a mafic volcanic rock with big rounded edges green plagioclase phenocrysts typical of porphyry material [177]. The plagioclase is extensively weathered into a fine-grained aggregate composed of saussurite and kaolinite. The phenocrysts are encased in a dark, microcrystalline matrix that contains scattered small, rounded grains of iron hydroxide. Many amygdales are filled with radiating aggregates of zeolite, chlorite, and epidote. Additionally, millimetric veins of chlorite, and less commonly epidote, are observed. These features suggest that this *tessera* could potentially be attributed to *porfido verde antico* (green ancient porphyry) [10]. Because of the singularity of this sample among the analysed, SEM-EDX was applied for the identification of the minerals. The results assess the presence of plagioclase as albite, with an

abundance of epidote [195] as a secondary phase in the matrix and veins, which primarily accounts for the green colour of this tessera (Figure 26B). The minerals identified confirm the nature of the material supposed by PLM analysis as *porfido verde antico*.

Giallo antico marble

Fine grained crystalline limestone is the material that compose a sole pink *tessera* (sample 31B, Figure 24N). The matrix of this material is easily recognisable, however it doesn't allow the definition of the provenance. In the Mosaic of the Wounded Beasts in Aquileia, a *tessera* made with a similar material was recorded [59]. The author have attributed it to *giallo antico marble* (yellow ancient marble, also known with the Latin name *Marmor Numidicum*), which despite the name can be also characterised by intense yellow to orange colour that can veers to pink tonalities as in this case. SEM-EDS analysis was used for the identification of the mineral phase, confirming the presence of quartz, clay minerals, iron hydroxide, and chlorite, with a predominant carbonate fraction (Figure 28). Additionally presence of Ce and La recorded by SEM-EDS spectrum can possibly be an additional assessment of the lithology of the material. Indeed, these two elements produce a mineral called monazite that is characterised by a yellow to green intense colour [198], additionally this kind of minerals has been recorded in the geological formation of the Namib desert, where *Marmor Numidicum* comes from [199].

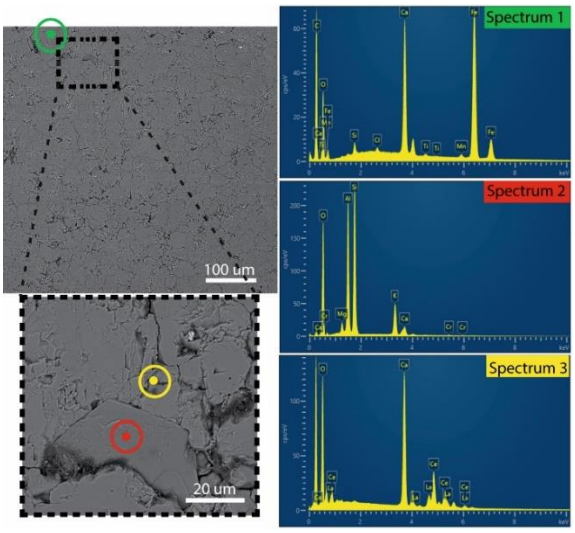

Figure 28 SEM-EDX analysis of sample 31B. A detail of the analysed area of acquisition of spectrum 2 and 3 is reported in the bottom left side figure. Spectrum 1 shows the Iron oxide inclusions. Spectrum 2 reveals the clay minerals inclusions. Spectrum 3 shows the predominant carbonate fraction.

Medium grained crystalline limestone

Finally, sample 41 B is a white single *tessera*, the PLM analysis of the thin section allow the individuation of a matrix similar to the one of sample 31B, indeed it is composed of a medium grained crystalline limestone (Figure 24O).

3.1.3 Same colour, different compositions: *tesserae* analysis results

The correlation between the results from petrographic analysis and colorimetric data shows that *tesserae* made from the same lithology can exhibit a wide range of colours, which are sometimes contrasting. In

Table 1 are reported all the type of material defined thanks to the analysis with the relative number of specimens of that specific colour and material, with information of the precise lithology and the possible provenance. Moreover, in Annex_A (Table 2S) are reported additional microscopic images of the thin sections analysed, divided according to the colorimetric group of belonging.

Table 1 For each colorimetric group are listed the different type of material, the amount of specimens made with the material, along with the specific lithology and the possible origin of the materials.

Colour	Material		Lithology	Provenance
White	Wackestone	20	*Aurisina marble*	Italian Karst region
	Grainstone	24		
	Mudstone	13		
	Packstone	16		
	Ceramic material	3	-	-
	Chert	1	Unknown	Classical Karst region
	Medium grained crystalline limestone	1	Unknown	Unknown
Black	Grainstone	*1*	*Aurisina marble*	Italian Karst region
	Laminated Wackestone	20	Unknown	Slovenian/Italian Karst area
	Chert	2	Unknown	Classical Karst region
	Impure calcite marble	*1*	*Cipollino bigio*	Karystos
Grey	Wackestone	*8*	*Aurisina marble*	Italian Karst region

	Grainstone	10		
	Packstone	1		
	Mudstone	6		
	Laminated Wackestone	3	Unknown	Slovenian/Italian Karst area
	Chert	2	Unknown	Classical Karst region
	Silicified grainstone	1	Unknown	Karst region
Pink	Wackestone	*5*	*Aurisina marble*	Italian Karst region
	Grainstone	2		
	Mudstone	4		
	Fine grained crystalline limestone	*1*	*Giallo Antico marble*	Unknown
Yellow	Grainstone	1	*Aurisina marble*	Italian Karst region
	Mudstone	1		
	Ceramic material	2	-	-
Red	Laminated Wackestone	1	Unknown	Karst region
	Ceramic material	1	-	-
	Hardground	1	Unknown	Unknown
Green	Porphyry	1	Unknown	Unknown

White *tesserae* were primarily composed of grainstone, wackestone, and packstone. The fossil assemblages found within these materials suggest a potential origin from the Italian Karst region [200]. Colorimetric analysis of most white *tesserae* showed consistent L*a*b* values, with $L^* > 70.0$, $1.5 < a^* < 3.0$, and $6.0 < b^* < 11.0$. Additionally, three white *tesserae* were made from

ceramic materials, such as bricks or pottery. Sample 24C, a white chert tessera, adds to the colour variability of this material, which was also used for grey and black *tesserae*.

Most dark *tesserae* consist of laminated mudstone to wackestone, featuring a micritic or microsparitic matrix and non-diagnostic bioclasts. Similar materials have been documented in mosaics from Aquileia [64] and various locations in Slovenia [70,72,179]. While some sources describe the origin of these materials as unknown [64], others attribute them generally to the Karst region [72,201]. Comparable rocks are found in various locations across the Dinaric Carbonate Platform in Slovenia, north-eastern Italy, and northern Croatia, including the Villaggio del Pescatore near Duino [182]. The grey tones range from light to dark, as confirmed by colorimetric analysis. Four samples were characterized by dark grey hues ($L^* \leq 50$), including three made of laminated wackestone (26A $L^* = 42.2$; 40C $L^* = 46.2$; 20A $L^* = 50.8$), which are petrographically similar to the majority of the black *tesserae* analysed. This observation aligns with findings by Miletić et al. (2016) [70], who noted that numerous dark-grey to black *tesserae* from a Roman villa rustica near Mošnje are made of the same laminated bituminous micritic limestone. It is possible that the grey laminated wackestone and the black ones originate from the same source, with the different tones reflecting natural variability in the pigmenting phases of the source rock. Several black and grey *tesserae*, specifically samples 18A, 23A, 50A, and 53C, are composed of chert. SEM-EDX analysis has provided further insight into their differing characteristics. For instance, sample 18A has a microcrystalline texture mainly composed of chalcedony, with relatively abundant graphite, calcite, and dolomite. In contrast, sample 23A contains chalcedony along with pyrite and iron hydroxides, while sample 53C consists of iron hydroxides and calcite. Another black tessera is made from impure marble, likely *cipollino bigio* (grey *cipollino*) [202].

The only dark-green tessera (sample 18C) is made of a volcanic rock with a porphyritic texture and petrographic features similar to *porfido verde antico* (green porphyry). Both stone types were widely used in Roman times, particularly for architectural elements and ornamental purposes, and have been identified in opus sectile, such as in the Domus of Coiedii in Suasa (Ancona, Italy) [203].

Most yellow and pink *tesserae*, with colours in the range of $L^* = 57.1–86.3$, $a^* = -0.2–5.6$, $b^* = 2–16.1$, are made of Aurisina marble. The colour differences are attributed to varying amounts of iron hydroxide. In contrast, two *tesserae* with more vivid hues (vivid pink for sample 31B: $L^* = 69.9$, $a^* = 10.0$, $b^* = 10.0$; red for sample 30D: $L^* = 53.8$, $a^* = 8.5$, $b^* = 11.4$) are petrographically different from Aurisina marble. The former is a crystalline limestone similar to *giallo antico marble*, known for its variable tones from yellow to pink, which was used in Aquileia for decorative purposes [55,184]. The latter is a hardground with ferruginous and clay-rich ooids. Although its provenance is difficult to determine, similar materials are common in the Slovenian/Italian Karst region. As mentioned earlier, some *tesserae* were crafted from ceramic

materials, displaying colours ranging from red to yellow and white, indicating the use of various brick materials to achieve specific visual effects.

3.2 Mortars composition

For the analysis of mortar layers, 29 out of the 153 specimens were selected due to the presence of mortar still attached to their surface (information regarding the samples are provided in Table 1S[15]).

Prior to any sampling procedures, a visual inspection combined with a photographic campaign of all samples was carried out. Dimensions and characteristics of all specimens were meticulously recorded during this phase. This approach facilitated the identification of the *tesserae* nesting direction within the mortar, potentially allowing for the differentiation, based solely on visual analysis, of the presence of each specific *stratum* of mortar the *tesserae setting bed* and *Nucleus*, and in addition a coarse mortar *stratum*, presents in 2 specimens, that can't be defined neither as *Nucleus* or *Rudus*. Owing to the significant size of the aggregate, the *Statumen stratum*, serving as the preparatory layer of the ground, thus it is not preserved in the small specimens examined in this study. For the sake of clarity in the presentation of results and scientific correction the following names will be employed in their abbreviated form as follows: i) *tesserae setting bed* (SB); ii) *Nucleus* (N); iii) coarse mortar *stratum* (CM).

In mosaic studies, distinguishing between the *Nucleus* and the *tesserae setting bed* layers can be challenging due to their similar preparation methods. Typically, the *tesserae setting bed* has a different composition than the *Nucleus*. In Aquileia, for example, the *tesserae setting bed* is composed of a thin layer of pure lime, sometimes mixed with sparry calcite or white marl dust, whereas the *Nucleus* is usually made of *cocciopesto* [58]. Generally, the *tesserae setting bed* layer is identified by the smaller aggregate sizes compared to those in the *Nucleus* layer [16]. Thus, following the initial analytical phase, Polarized Light Microscopy (PLM) was employed to examine all 29 specimens, previously prepared in the form of thin section, to assess the quality of mortar and its petrographic nature. An Olympus DX-50 Polarized Light Microscope equipped with a Nikon D7000 camera was utilised for this analysis.

Furthermore, 7 out of the 29 thin sections of selected samples underwent analysis using a Field Emission Scanning Electron Microscope (FE-SEM) Tescan Solaris, which was equipped with a Silicon drift detector EDS (Oxford Instrument Ultim Max 65). This instrumentation was utilised to ascertain the chemical and microstructural characteristics of the samples, as well as the hydraulic indices (HI) of the mortar. During this analysis, image acquisition and chemical characterisation were conducted at 15 KeV, with a current of 3 nA and a working distance of 5 mm. Additionally,

[15] For more information please look at Annex_A, Table 1S Summary of the information acquired for each specimen.

high-resolution images were captured at 5 KeV with a current of 300 pA and a reduced working distance of 4 mm.

X-ray diffraction analysis (XRD) was conducted on 18 out of the 29 samples to identify the mineralogical composition of the mortars. Due to the limited quantity of material available and the desire to minimize invasiveness, the analyses were performed on powder samples without fractionating the specimens. A PANalytical Empyrean X-ray diffractometer, equipped with a 1.8 kW Cu Kα ceramic X-ray tube and a PIXcel3D 2x2 area detector, was utilised for this purpose, operating at 45 kV and 40 mA. The diffraction patterns were obtained under ambient conditions using a parallel beam geometry in symmetric reflection mode. Analysis of the XRD data was performed using HighScore 4.1 software from PANalytical.

Specimens selected from specific points of the stratification underwent analysis using alsoThermal Gravimetric Analysis coupled with Infrared spectrometer (TGA-FTIR) to assess the composition of the binder phase. The experiments were conducted using a Perkin–Elmer Pyris 1 thermogravimetric analyser connected via a Perkin–Elmer TG–IR interface to a Perkin–Elmer Spectrum GX infrared spectrometer, equipped with a gas cell. Sample were subject to heating rate of 10 °C per minute, from 100°C to 1000 °C. Infrared spectra of the released gases were collected at intervals of 0.5 °C (approximately every 3 seconds).

3.2.1 Nature of the specimens

A summary table the number of samples analysed with the indication of their layers identified is reported in supplementary materials[16]. A preliminary visual inspection of the specimens enabled the partial identification of different *strata*. Examples of the analysed specimens are presented in Figure 29. The three specimens exhibits mortar still attached to the surface; *tesserae* face correspondent to the original floor can be individuate thanks to the smoother surface caused by foot traffic. As shown in Figure 29A, specimen 58A retains the SB and a thick N *stratum*, and seven white *tesserae* still nested in the bedding layer. In contrast, specimen 8 (Figure 29B) conserves only the two superficial mortar stratifications (SB and N). The mortar visible under the *tesserae* is smooth and 1 cm thick, with seven black *tesserae* still nested in this SB stratification, along with grouting mortar that fills the spaces between *tesserae*. Specimens 38B (Figure 29C) consist of single white *tesserae* with mortar attached to the surface.

[16] For the Table please look at Table 4S Summary of the results achieved by process of characterisation of mortars.

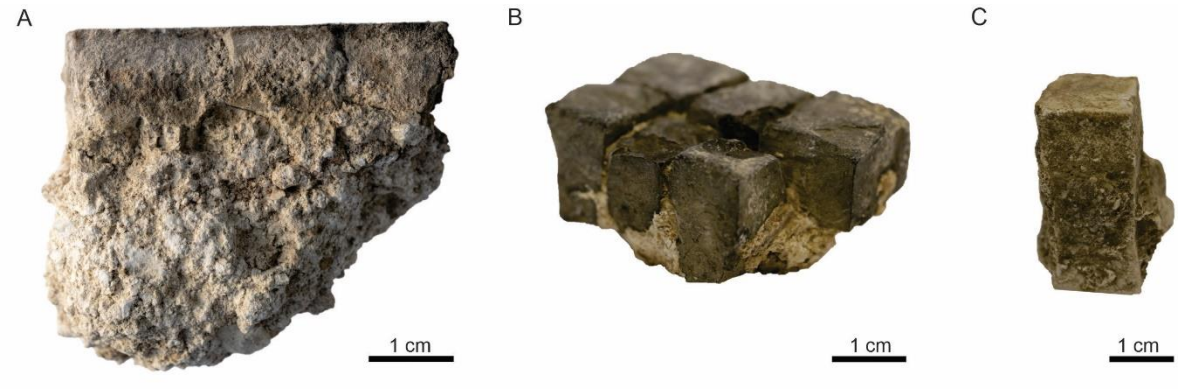

Figure 29 Samples of mosaic A) Mosaic fragment s. 58A; B) Mosaic fragment s. 8; C) Single *tesserae* s. 38B.

The analysis were focused on the stratification of two well-preserved specimens, 58A and 58B. These specimens retain a particular layering composed of a SB *stratum*, a well conserved cocciopesto layer (similar to *Nucleus*, thus we will refer to it as N) and a thick layer of coarse mortar, further investigation of this particular stratification are reported in the following paragraph.

3.2.2 Composition of mortars in the mosaic *strata*

PLM analysis of thin sections provided deeper insights into the morphology of the mortars, revealing the presence and composition of different stratifications based on Vitruvian guidelines and enabling the examination of the aggregates. To better understand the mosaic's setting direction and the sequence of layer deposition, images obtained from a previous photographic campaign of the entire specimens were compared with those acquired through PLM analysis of the thin sections. Despite PLM investigations, it was not possible to assess the nature of all the mortars and their chemical composition, thus elemental analysis were applied on selected samples. The SEM-EDS examination of seven selected specimens (2B, 8, 9, 14, 58A, 58B, and 58C) provided improved microscopic images and enabled elemental analysis. These specimens have well-preserved stratification, with both SB and N layers intact. The use of EDS for chemical analysis was essential for a semi-quantitative assessment of the oxides present, helping to define the hydraulic properties of each mortar type. Additionally to chemical information and microscopic images, SEM-EDS analysis of the *Nucleus stratum* was performed to evaluate the Hydraulicity Index (HI). This parameter is defined by considering the amounts of silicate oxides, calcium carbonate, aluminum oxides, magnesium, and sodium. A greater presence of oxides, such as Al, Na, and Si, indicates a

more hydraulic mortar. Following Boynton's formula [21], it is possible to calculate the HI, and according to Vicat [204], the value of HI indicates whether the mortar is aerial or hydraulic[17].

The elemental analysis allowed for the comparison of specimen compositions, which are presented layer by layer (from top to bottom) to enhance readability. This analysis also enabled the investigation of similarities and differences in the composition of the layers, assessing the presence and nature of each *stratum*. XRD analysis is considered the principal methods of characterisation of mortar[18], thus the technique was applied on the majority of the specimens. Finally, TGA-IR was performed on one samples for each *layer*, in order to assess presence of residues of organic compounds in mortar composition.

A summary of the results achieved by solo PLM analysis is reported in Figure 30. The graph shows the number of specimens characterised by the presence of specific stratification. However, the minimal amount of mortar present in seven specimens (specifically 1B, 6A, 21B, 44A, 45B, 51A, 57A) hindered precise stratification identification, necessitating further investigation (identified in the graph of Figure 30 with the "?"). By observing the lateral positioning on the *tesserae*, it was hypothesised that the mortar nature (summarised in the graph in Figure 30) is as follows: 9 samples are associated with SB mortar, 4 with N mortar, 7 with two distinct stratifications of SB and N mortars. Finally, 2 samples present an additional visible *stratum* made with coarser aggregates this *stratum* can be consider the *Nucleus* (in the paragraph we will referee to this layer as coarser *Nucleus*). While this initial analysis provides a means to identify different *strata*, more detailed microscopic and chemical investigations are required to accurately characterise the mortar's nature and stratification origin, allowing for complete discrimination of the *strata*.

Figure 30 Graph with the quantity of specimens for each type of stratification identified considering the different mortars visible with naked eye.

[17] If the HI is between 0 and 0.1, the mortar is aerial. It is feebly hydraulic if the HI is between 0.1 and 0.16, averagely hydraulic between 0.16 and 0.31, properly hydraulic with values in the range of 0.31 to 0.42, and eminently hydraulic when the HI is between 0.42 and 0.45.

[18] For more information please look at §2.2.2 Analysis of ancient mortar.

Tesserae setting bed

PLM analysis of SB mortar

Out of the 29 specimens analysed, 18 specimens exhibit mortar in the junctions between *tesserae* (Figure 31A) or on both sides of individual *tesserae* (Figure 31B) attributable to SB *stratum*, the solo presence of this *layer* was recorded in 9 of these specimen as only mortar conserved. Differently, 7 out of 18 specimens also contained N *stratum* and 2 specimens includes both N and an additional coarse mortar *strata*. These specimens featured a finishing layer, likely identified as *marmorino*. As shown in Figure 32A (sample 5A), this layer is composed of small angular fragments possibly of lithic material, ranging in size from 0.1 to 0.5 mm or of sparry calcite, bound together with calcic lime. A millimetre-sized stratification composed of sparse spathic calcite was found in mosaics of high quality. In this *stratum*, the *tesserae* are embedded, providing the mosaic with a more secure setting [50]. In some cases SB mortar was made by using lime, with the addition of few or none aggregate. This composition was recorded in some of the analysed samples as in sample 9 (Figure 31B). The binder-to-aggregate ratio (b/a) is greater than or equal to 1/3, indicating a fat mortar composition. This composition could have led, during the hardening process, to the formation of the visible big cracks (shrinkage phenomenon).

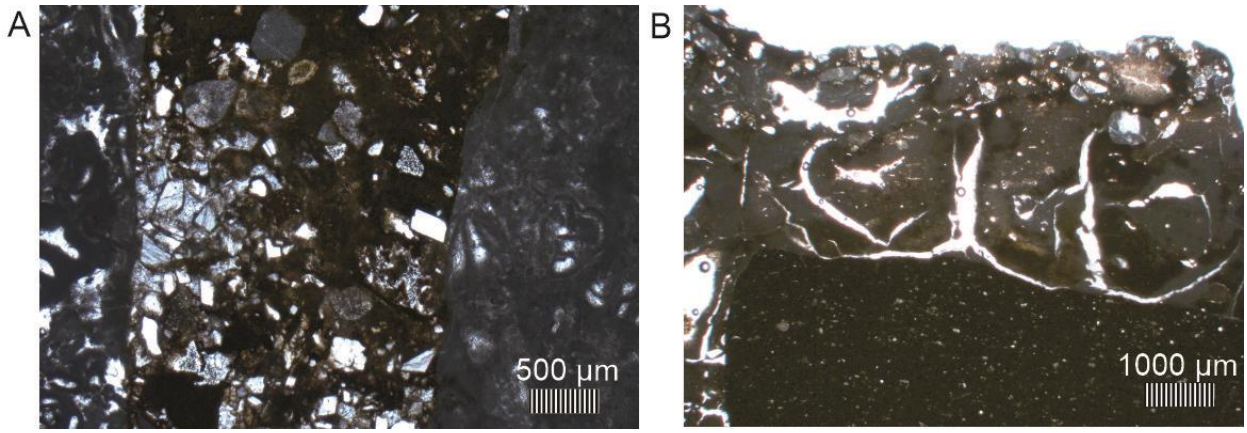

Figure 31 Microscopic analysis of thin sections of specimens with visible *tesserae* setting bed mortar: A) 5A; B) 9.

SEM-EDS analysis of SB mortar

An in-depth chemical analysis of SB using SEM-EDS was conducted to determine the nature of the aggregates and of the binder composing the mortar. Specimens 2B (Figure 32) and 58C are the most representative samples, showing the filling of the joints of *tesserae* with aggregates mixed with lime. The angular shape of these aggregates suggests a possible hand-crushing process. Chemical analysis of specimens 2B is composed of fine mortar made of calcium carbonate with Mg and Si in the composition, none aggregates are visible in the area under the *tesserae*. The presence of Mg minerals may indicate the dolomitic nature of the stone used to produce the slaked

lime. 2B and 58C identified the presence of mineral inclusions composed of aluminum, titanium, iron, and quartz. Evaluation of HI reveals the aerial nature of this mortar.

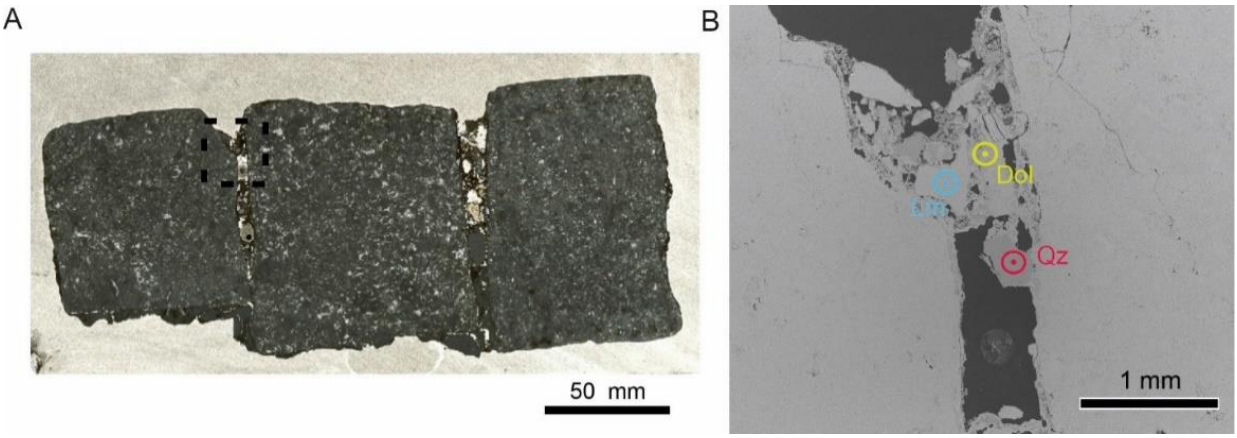

Figure 32 Analysis of sample 2B: A) Micrograph of the specimen with indication of the area of analysis; B) SEM-EDS of the analysed mortar, in figure are indicated the minerals forms present in the composition as reported by Warr indications.

The same matrix and composition of mortar 2B was recorded for the mortar still attached under the *tesserae* of specimen 8, and for specimen 58C. The specimen shows the presence of two different mortars under the *tesserae*, which are detached from one another, as visible in the figure. The SB mortar in specimen 8 is a fine mortar with no aggregates. The visible detachment of the two layers is a clear sign of degradation, which could lead to complete mosaic disintegration. This detachment might be induced by the different compositions of the mortars.

SEM-EDS analysis allow to individuate the nature also of SB mortar samples which composition was not possible to be assessed by solo PLM analysis. Nature of three specimens (21B, 51A and 58C) can be considered the finishing *stratum* made of lime mixed with sand, typical composition of SB *stratum* present in the majority of the specimens and despite the derisory amount of mortar the same composition can be assessed for specimen 44A.

XRD analysis of SB mortar

From all the analysis conducted with XRD analysis it is possible to confirm the presence of three different types of diffractogram. This analysis allow to discern the composition of the mortars, individuating three type of composition. In Table 2 are reported results of XRD analysis. SB stratification results in different samples has a different composition that can vary from type 1 to type 2 to type 3.

Table 2 Definition of type of mortar, example of diffractogram for each type of mortar and composition: type 1 sample 36B; type 2 sample 11; type 3 sample 5A.

Type	Diffractogram	Composition
1	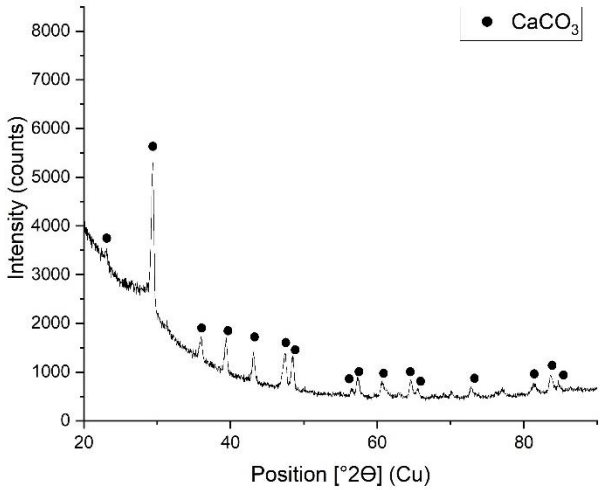	$CaCO_3$
2	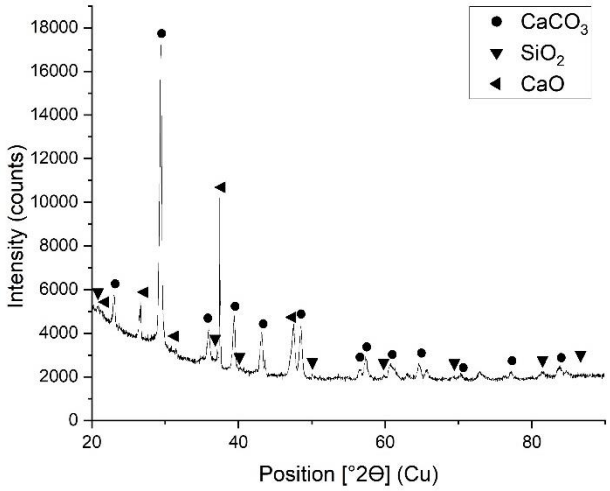	$CaCO_3$ + SiO_2

3	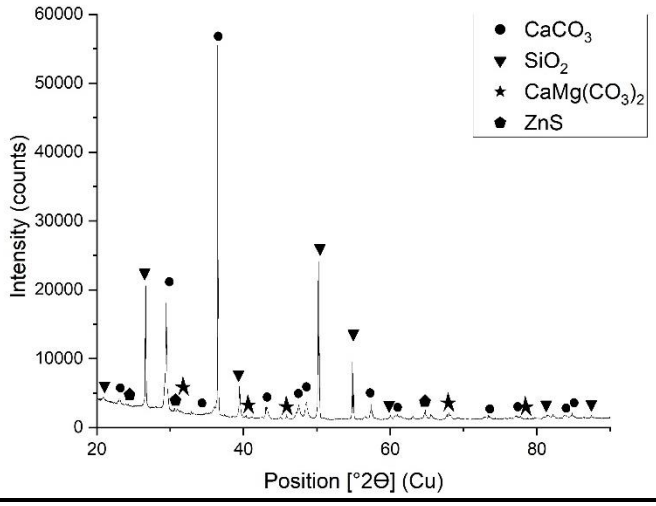	$CaCO_3$ + SiO_2 + $CaMg[CO_3]_2$

3 specimens (2A, 6A, 36B) of SB *stratum* are charaterised by a composition of Type 1 (Table 2, type 1, sample 36B), that is made of Calcium Carbonate, indicating the use of pure lime. Absence of other typology of minerals can indicate the lack of aggregates in the paste. This composition is typical of a finishing *stratum*. In specimens 2A, 6A some other minerals are present in trace amounts respectively Halite, Lime, Montmorillonite.

The majority of the specimens of SB (1B, 3, 11, 39A, 45B, 51A, 58C) are composed mainly of Type 2 mortar (Table 2, type 2, sample 11), which present typical peaks referable to calcite and quartz. The presence of quartz can be due to the possible use of sand as aggregate that function as inert. In some specimens (1B and 45B) was recorded the presence also of nitratine that comes from the products used as fertilizers. Specimens 3, 11, 39A, 51A, 58C present also traces of minerals referable to the use of stones, sands and ceramic materials for mortar composition, such as: Lime, Wurtzite, Halite (product of decay, due to the proximity to sea), Rutile. Comparing SEM-EDS of specimens 58C, 51A and being similar to specimen 2B, XRD result of the former specimen can be considered with a great certainty equal to the one of 2B.

Finally, 2 specimens (5A, 16) are composed of Type 3 mortar (Table 2, type 3, sample 5A) additionally to peaks of calcium carbonate and silica dioxide the diffractogram are characterised also by peaks of Magnesium Carbonate probably ascribable to the use of Dolomitic limestone (rich in Magnesium) for the production of lime. The co-presence of Mg and Si peaks can be related to the formation of the mineral phase Magnesium Silicate Hydrates (M-S-H). This phase in formed due to dolomitization of dolomite aggregates and the alteration of silica in alkaline conditions. This phase has been often detected in Aquileian mortars [2,58]. However, in order to assess its nature SEM-EDS analysis is required and will be performed in future.

In addition traces of Wurtztite mineral was assessed in the composition of some mortars, in Table 3S[19] is reported the diffractogram of sample 16.

TGA-IR analysis of SB mortar

Thermogravimetric analysis of sample 11, reported in Figure 33A, displays a typical weight loss curve of lime mortar [205]. A single weight loss of 40,9% is observed at 800°C corresponding to the decomposition of calcium carbonate, the primary component of the mortar, resulting in the release of CO_2. No additional weight losses were recorded confirming the absence of other materials in the mortar mixture. The IR associated with this weight loss (Figure 33B) clearly indicates the solo presence of CO_2 with a prominent peak around 2300 cm^{-1} and a minor signal around 500 cm^{-1}. None organic compound were recorded in the composition.

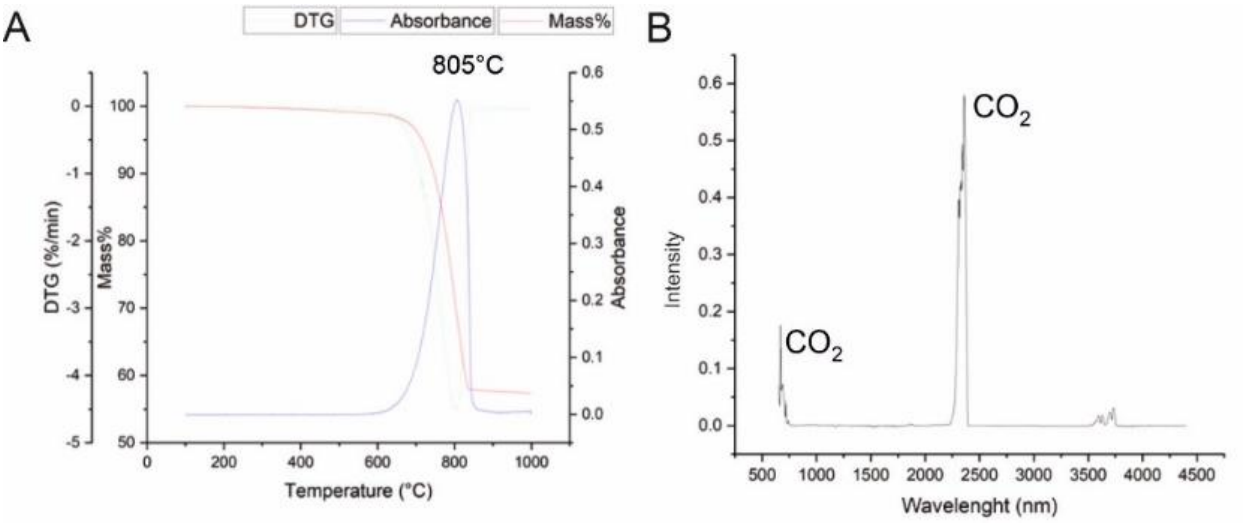

Figure 33 TGA-IR analysis of *tesserae* setting bed *stratum* of specimen 11: a) TGA result; b) IR acquired at the relative T of 805°C.

Nucleus

PLM analysis of N mortar

PLM analysis of the thin section of 13 specimens show the presence of *Nucleus* layer. 4 of them exhibit mortar residues attributable only to N stratification. Additionally, in 7 specimens N *stratum* is found in conjunction with SB and in 2 specimens also in presence of coarse mortar *stratum*. As shown in Figure 34A (sample 14), the aggregates primarily consist of angular ceramic fragments of varying sizes (ranging from 0.5 to 1.5 mm), which impart hydraulic properties to the mortar, along with an inert component, likely fluvial sand. The aggregate is mixed with a calcic lime binder in a 1:3 ratio of binder to aggregate (b/a). Microscopic analysis of the matrix revealed that the mortar in most specimens is of a fat nature. Large voids, or cracks within the mortar, visible in the

[19] For additional analyses please look at Annex_A, Table 3S Additional XRD diffractogram of the specimens.

N *stratum*, are due to shrinkage during the drying process, which is typical in fat mortars, resulting in a porosity of 5%. These shrinkage phenomena often occur near lime lumps within the matrix of most specimens. These lime lumps form due to the rapid slaking of lime clods with excess water during the preparation of the mortar binder or due to insufficient kneading of the mortar mixtures, which suggests a lack of precision in selecting and integrating raw materials [80]. In two specimens (37A and 38B), the mortar is thin, with a b/a ratio less than 1:3, indicating a higher proportion of aggregates compared to the other samples analysed as visible in Figure 34B. The aggregate is made of sub angular elements of possibly fluvial send.

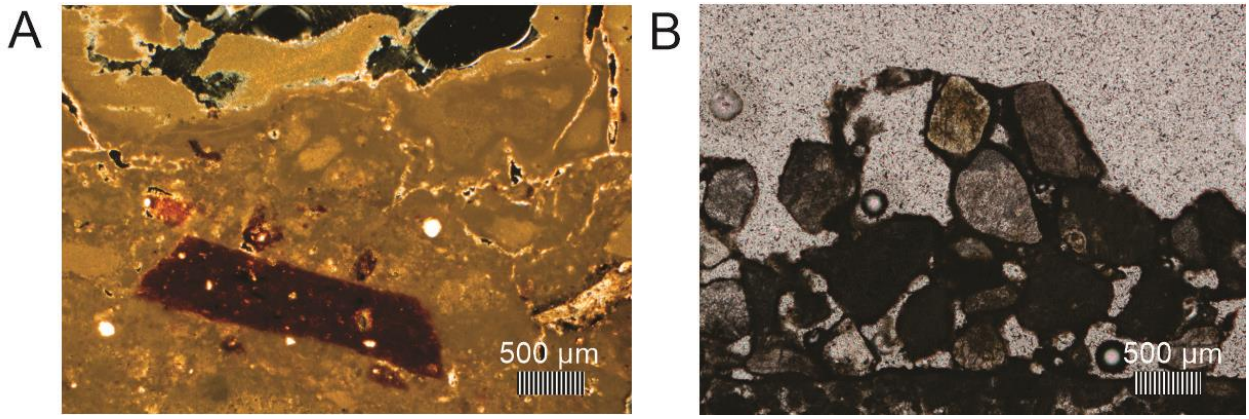

Figure 34 Microscopic analysis of thin sections of specimens with visible *Nucleus* mortar: A) Sample 14; B) Sample 37A.

SEM-EDS analysis of N mortar

As mentioned, sample 8 presents an area of detachment, possibly due to the use of two different mortars, as visible in Figure 35. Indeed, SEM-EDS analysis performed by moving from the top to the bottom of sample 8 (Figure 2S[20]), reveal the change of mortar composition, thus that 2 different mortars were used for SB and N *strata*. Mortar used for *Nucleus*, presents a greater amount of visible aggregates, which includes carbonate material and ceramic fragments , elemental analysis of this area reveals a matrix made of Ca and Mg. In Table 3 are reported results of the evaluation of HI in different points. The results demonstrate differences in hydraulic properties: the matrix of the material is aerial, reaching the proximity of ceramic fragments (with Aluminium, and few silica inclusions) HI increases, and inside the rim, near the aggregates of ceramic fragments, HI indicates hydraulic properties of the mortar.

[20] For additional analysis please look at Annex_A, Figure 2S SEM analysis of Sample 8.

Table 3 Evaluation of HI of specimen 8, area of analysis and results.

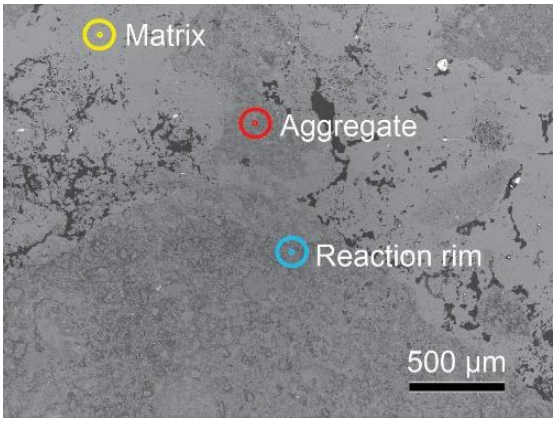

Element	Matrix	Aggregate	Reaction rim
Mg	0.78	1.86	6.14
Al	0.44	2.51	8.51
Si	1.66	8.61	31.5
Ca	49.9	42.5	16.6
Fe		0.75	3.13
HI	**0.04**	**0.27**	**1.9**

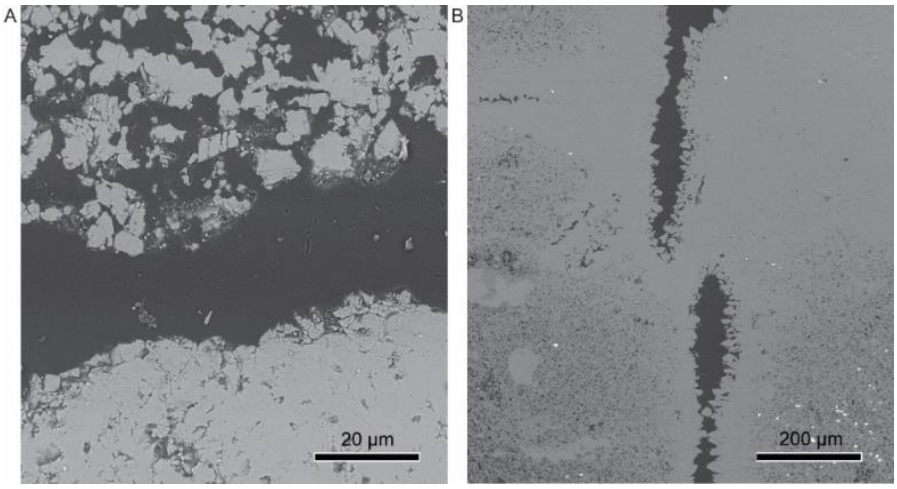

Figure 35 SEM analysis of samples: A) s. 8, area of detachment; B) s. 9, calcite of recrystallization present in the voids.

Investigation of *Nucleus stratum* of specimen 9 allows the individuation of calcite of recrystallization with the typical rhomboidal structures of sparitic calcite (Figure 35) Formation of these crystals is due to water that, inside the voids, dissolves the binder matrix, and the simultaneous decrement of pressure of CO_2, producing calcite precipitation in the pore [80]. Analysis of HI shows that this mortar is aerial in the matrix but with presence of visible aggregates. Thus, as for specimen 8, it is possible to assume that the increment of HI is induced by the presence of ceramic fragments in the composition. The same results were achieved for specimen 14 and specimens 58A and 58B. In Figure 3S[21] is reported the SEM-EDX image of the point of interface between *Nucleus* and coarse mortar *stratum* (highlighted with red line) of specimen 58B, the same

[21] For additional analysis please look at Annex_A, Figure 3S SEM analysis of sample 58B.

structure was also recorded for specimen 58A that presents the same microstructural and chemical composition. *Nucleus* is characterised by a fine matrix with few aggregates and big voids typically induced by shrinkage phenomena. From the SEM-EDS analysis it was possible to assess that *Nucleus* is composed of binder made of Calcium Carbonate with Magnesium minerals, indicating the use of lime obtained from stone rich in dolomite, with aggregates made of Quartz and Feldspar. The elemental map (Annex_A, Figure 3S B) shows the presence of minerals silicates and phyllosilicates, typical of ceramic fragments. Map analysis indicates Calcium Oxide in composition of the matrix, thus its aerial nature. Differently, evaluation of the HI in the area near ceramic aggregates indicates increment of hidraulicity, due to *cocciopesto* inclusions.

Elemental analysis of *Nucleus* of specimen 58C, reported in Figure 4S[22], shows the high presence of Calcium with Magnesium in the matrix, evaluation of HI indicates that *Nucleus* is composed of aerial mortar. Few aggregates are visible in the *Nucleus*, thus, no hydraulic properties are imparted to the mortar. This composition is similar to the *Nucleus* composition recorded for specimen 2B.

XRD analysis of N mortar

XRD analysis allow to assess the composition of 3 specimens (6, 14, 58B) as made of type 1 composition made of Calcium Carbonate, indicating the use of pure lime (as visible in the example reported in Table 2). Absence of aggregate can be due to the preparation phase of the sample. Indeed, few large aggregates nested in fine mortars were not included in phase of sampling of the material. Sample 14 is characterised not only by Calcium Carbonate, but also present other minerals in trace amounts respectively Halite, Lime, Montmorillonite (Table 3S[23], sample 14). Additionally XRD allow to assess the use of the same type of mortar for both *tesserae setting bed* and *Nucleus stratum* of sample 6.

As for SB *stratum* also *Nucleus stratum* of different samples results to be made principally of type 2 composition individuated by XRD, specifically 5 specimens (1B, 2B, 4, 7A, 8, 58C), XRD pattern of sample 4 is reported in Table 3S[23].

The XRD analysis of the cocciopesto layer, similar to *Nucleus*, of sample 58A shows a diffractogram equal to Type 3. It is characterised by peaks of calcium carbonate and silica dioxide and Magnesium Carbonate. Despite what expected mortar of *Nucleus* of sample 58A results different in the composition respect to mortar *Nucleus* of 58B, individuated as made of type 1 mortar made of pure lime only.

[22] For additional analysis please look at Annex_A, Figure 3S SEM analysis of sample 58C.
[23] For additional analysis please look at Annex_A, Table 3S Additional XRD diffractogram of the specimens.

TGA-IR analysis of N mortar

TGA results of specimen 58A is reported in Figure 36A, showing a calorimetric curve typical of lime mortar. Two weight losses were recorded: the first indicated by a hump at 479°C with a mass loss of 1.18% and a peak at 810°C with mass losses respectively of 1,2% of 41.7%. The initial weight loss is attributed to $Ca(OH)_2$ dehydration which occurs between 400°C and 520°C. The second weight lost, corresponds to endothermic peaks at carbonates at ca. 780°C [206]. The IR (Figure 36B) associated with the lower weight loss reveals two bands, one around 3000 cm^{-1}, corresponding to hydrocarbon saturated C-H stretching, and another around 1846 cm^{-1}, likely due to C=O stretching of anhydrides or other oxidised forms of hydrocarbons derived from carboxylic acids. Peak around 2300 cm-1 is related to CO_2. The IR analysis corresponding to the weight loss at 810°C (Figure 36B) shows a strong CO_2 peak and two peaks related to carboxylic acids.

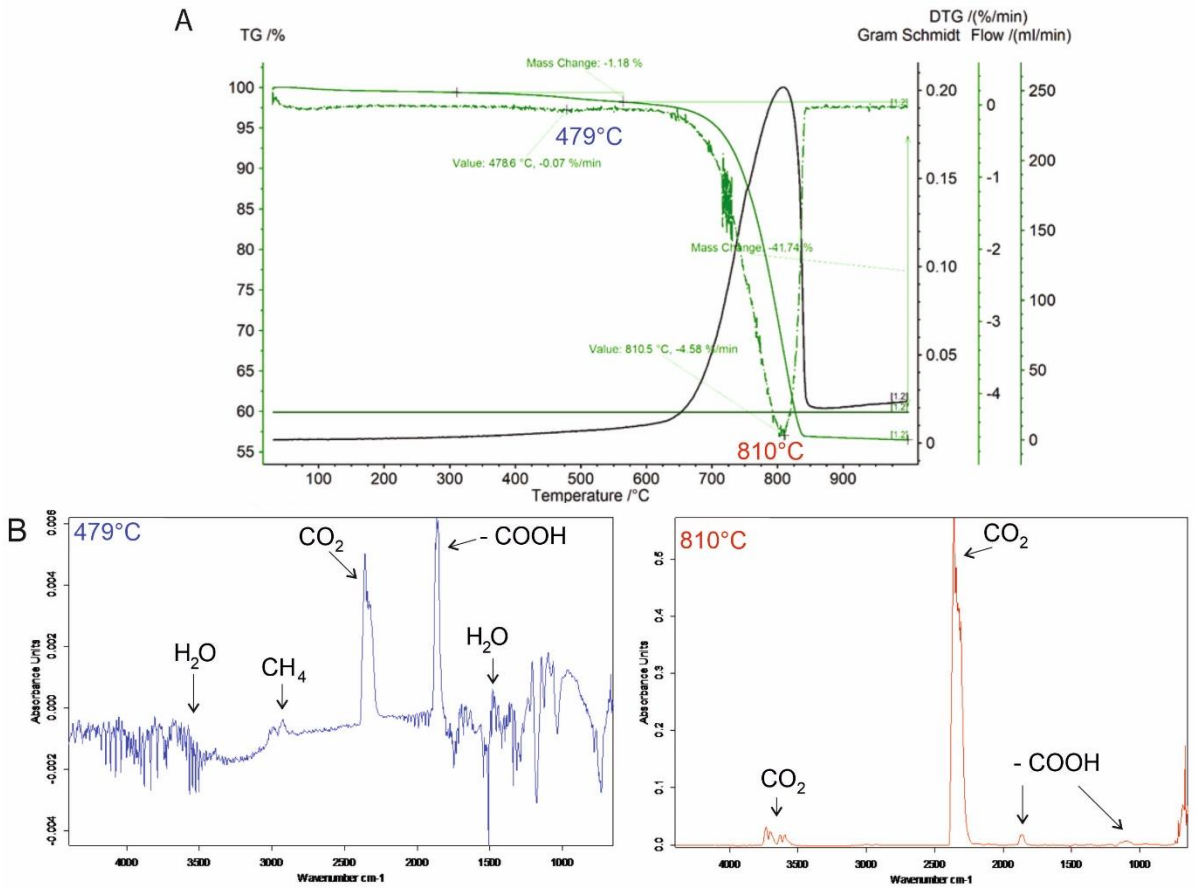

Figure 36 TGA-IR analysis of the *strata* of specimen 58A: a) TGA result; b) IR acquired at the relative weight loss.

Coarser mortar *stratum*

In Figure 37 are reported images of fragment 58A, which displays all stratifications as seen in sample 58B. The differentiation between these *stratum* is particularly evident when observed at various scales, from macro to micro dimensions. Both macroscopic and microscopic analyses reveal that the specimen is composed of white *tesserae* nested within the SB and N *strata*. When examining the entire specimen (as shown in Figure 29A), the mortar layers can be distinguished by their different colours and the presence of a fracture beneath the *Nucleus*. The distinction between the white and brown colours of the two mortar layers, representing the Setting bed (SB) and *Nucleus* (N), respectively, is more apparent in the micrograph of the cross-sectioned specimen (Figure 37A), allowing the assessment of the dimensions and characteristics of the *strata*. The first layer of filling of the tesserae is similar to SB layer, it is less than 1 mm thick (for practice we will referred to it as SB). The PLM analysis (Figure 37B) allows the individuation of lime mortar with visible few voids correspondent to pre-existing aggregates. Additionally, this mortar present a cracks along the side of the *tesserae* possibly formed due to the presence of voids that results interconnected. The *cocciopesto* mortar layer under the *tesserae* varies in thickness with a maximum height of 5 mm, it is similar to *Nucleus* mortar composition and we will referred to it as N. It is characterised by a dense, compact matrix with visible planar voids, possibly resulting from a shrinkage process. Figure 37B reports the PLM image of this mortar, which makes evident the different nature of this layer respects to the upper and lower ones. The mortar is composed of lime mixed with *cocciopesto* elements of variable sizes, lithic elements and quartz. The lowermost layer is made of coarse mortar, it has a thickness of 20 mm. It is composed of large aggregates ranging from 0.5 to 8 mm, with sub-angular shapes, no cocciopesto fragments were recorded, on the contrary the aggregate fraction is mainly composed of carbonatic material. The matrix of this mortar is clearly different form the others present in the specimens, thus it is possible to assess the presence of three different type of mortar that compose the specimen. Additional analysis of the coarse mortar *stratum* are presented in the following paragraph.

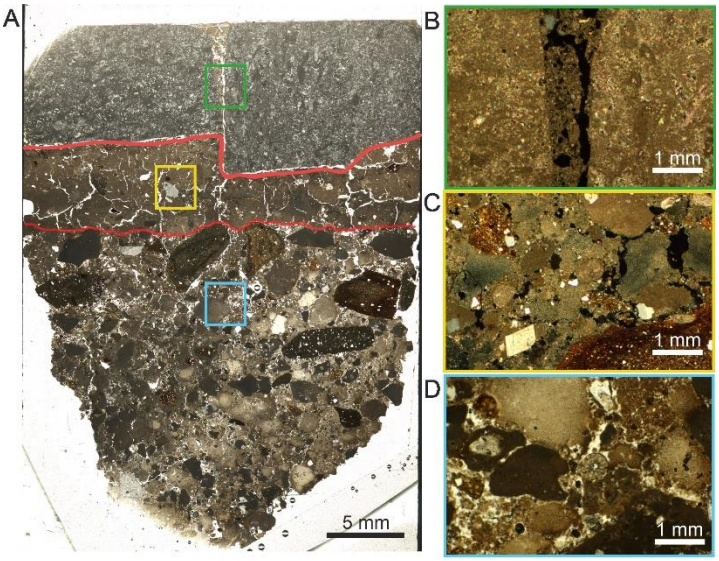

Figure 37 Sample 58A: A) micrograph of the thin section; B) PLM images of mortar filling the joint; C) PLM images of cocciopesto mortar; D) PLM images of coarse mortar.

PLM analysis of coarse mortar

Only two specimens (58A and 58B) present this type of mortar layer. These specimens are the most intact among those analysed and were therefore used as examples for identifying the stratification. They clearly demonstrate the compositional changes across the different mosaic layers (as visible in Figure 37). Microscopic images of the thin sections, in Figure 38A and B, illustrate the distinct composition of the *stratum*. It primarily consists of aggregates made of quartz and from carbonate material with sub-angular shapes and varying sizes, ranging from 0.5 mm upward, suggesting a possible hand-crushing process. The mortar in this layer has a binder-to-aggregate (B/A) ratio of less than 1/3, likely around 1/4, which is typical for mortars of this type. This mortar is characterised by porosity lower than 1%, making it less porous than the *Nucleus* and thereby providing better insulation for the mosaic.

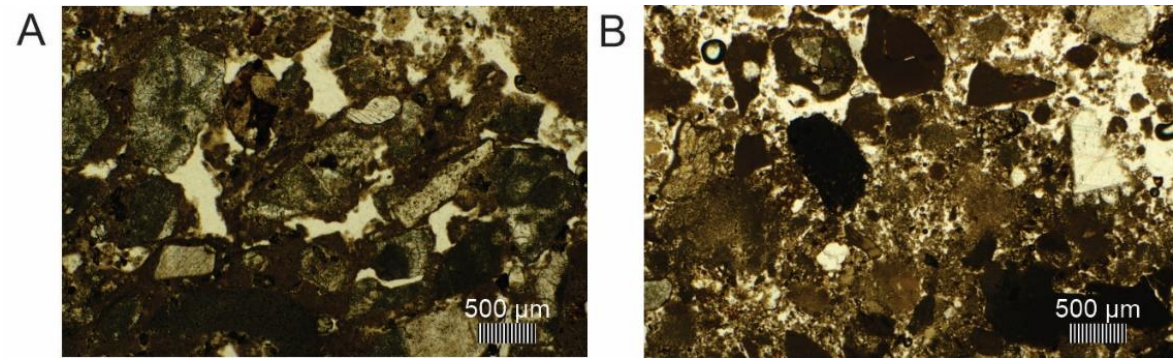

Figure 38 Microscopic analysis of thin sections of specimens with visible coarse mortar: A) Sample 58A; B) Sample 58B.

SEM-EDS analysis of coarse mortar

Application of SEM-EDS analysis allows to evaluate the nature of the aggregates and of the binder of the stratification (present in specimens 58A, 58B). Results reported in Figure 39 of the analysis of specimen 58A shows the presence of seashell in the composition, composed of Calcium carbonate, confirm by the calcium oxide recorded (Lm in figure). Aggregates are composed of minerals such as Feldspar, Quartz (Qz) and possibly Plagioclase (Anortite, An). Dolomite and K-feldspar minerals have been recorded in minor concentration, in the composition of the binder.
Co-presence of Si and Mg in the composition could be related to the formation of M-S-H mineral[24]. Punctual analysis made with SEM-EDS revealed the presence of Mg, Ca, Si, Al elements, possibly confirming the local presence of M-(A)-S-H, thus M-S-H enriched with alumina, and not of Anortite.

Presence of pieces of shells in the composition are assessed both by microscopic and chemical analysis also in specimen 58B.

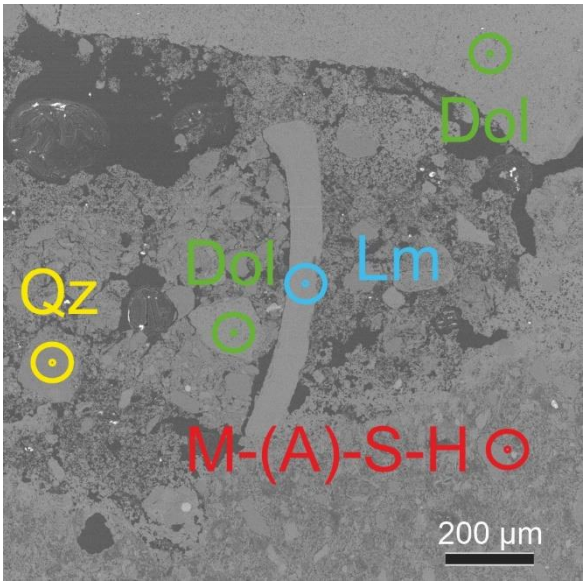

Figure 39 SEM-EDS of specimen 58A, mineral presents are indicated with different colours and the following abbreviations: Quartz, Qz; Dolomite, Dol; Lime, Lm; Magnesium alumina silica hydrate M-(A)-S-H.

XRD analysis of coarse mortar

In order to assess effectively the composition recorded with SEM-EDS, XRD analysis was performed on the *stratum* of both the 2 specimens. The diffractogram present typical peaks referable to calcite and quartz, but no presence of dolomite, thus a composition ascribable to Type 2 mortar. The presence of quartz can be due to the possible use of sand as inert. Additionally it presents also traces of minerals referable to the use of stones, sands and ceramic materials for

[24] For additional information about M-S-H please look at pg. 81.

mortar composition, such as: Lime, Wurtzite, Halite (product of decay, due to the proximity to sea).

TGA-IR analysis of coarse mortar

The coarse mortar of specimen 58B was analysed using TGA-IR, and the results, presented in Figure 40, differ from the analysis of *tesserae* setting bed and *Nucleus*, possibly confirming the effectiveness of the different composition of this layer and the others. Three distinctive weight losses were observed at 78° C, 478° C and 796°C. The IR analysis (Figure 40B) of the weight loss at 78° C indicates water release, suggesting that this mortar is highly hydrated. The IR correspondent to the hump recorded at 478°, shows the presence of two characteristic peaks of hydrocarbons, along with a prominent peak from the dehydration of $Ca(OH)_2$, as observed in the *Nucleus* sample. Weight loss at 796°C corresponds to the decomposition of carbonates [206]. The IR analyses (Figure 40B) shows a clear CO_2 peak at about 2300 cm^{-1} Along with signals at 1500 cm^{-1} and 3000 cm^{-1} which may be attributed to water contribution and the presence of peaks related to organic material partially covered by water signal. A possible hypothesis regarding the organic signals suggest the presence of shells in mortar composition. However, this remains speculative, and further analysis is required to confirm the nature of the organic compound detected with IR analysis.

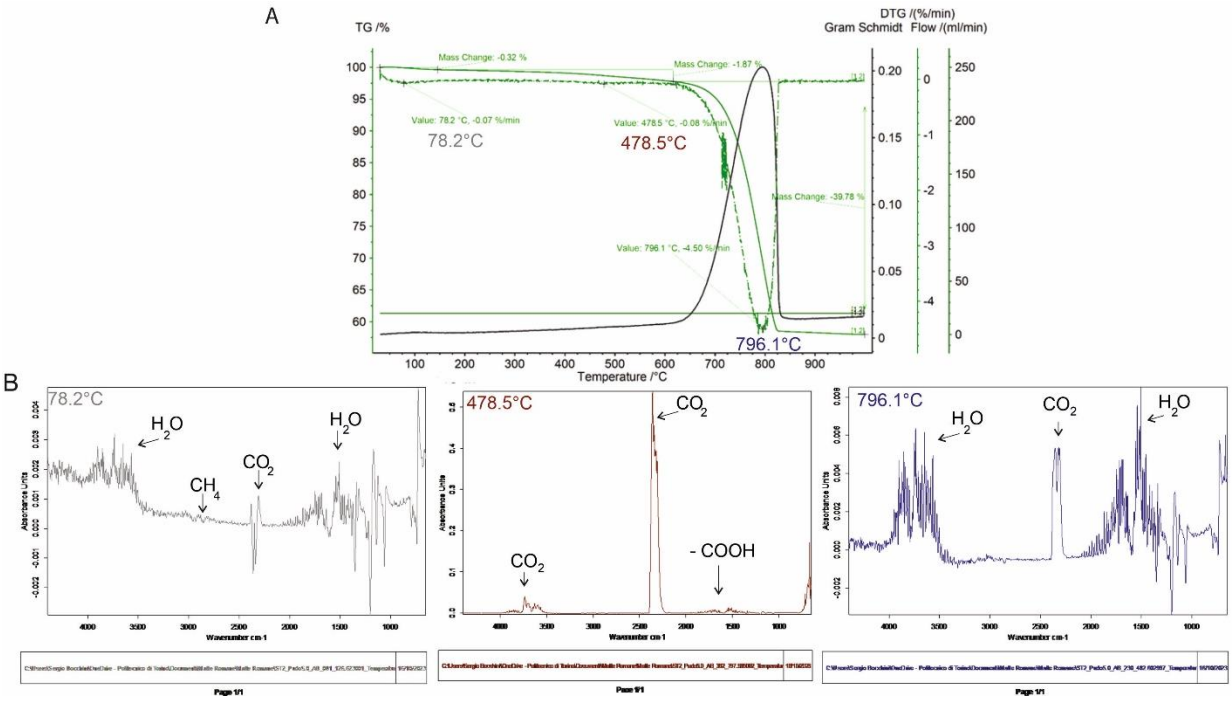

Figure 40 TGA-IR analysis of the coarse mortar of the lower *stratum* of the specimen 58B: a) TGA result; b) IR acquired at the relative weight loss.

3.2.3 Definition of mortar layering combinations

PLM analysis was insufficient for the individuation of the composition of the specimens and application of SEM and XRD analyses was fundamental, also supported by the comparison of results achieved by analysis of different specimens. In Figure 41 is reported the graph with the number of specimens characterised by a specific stratification. The analysis allowed to define the nature of the composition of the 7 not initially identified samples (namely 1B, 6A, 21B, 44A, 45B, 51A, 57A). Two of them specifically 1B, 6A result characterised both by SB and N *strata*, while other five specimens are characterised by the presence only of SB *strata* still conserved.

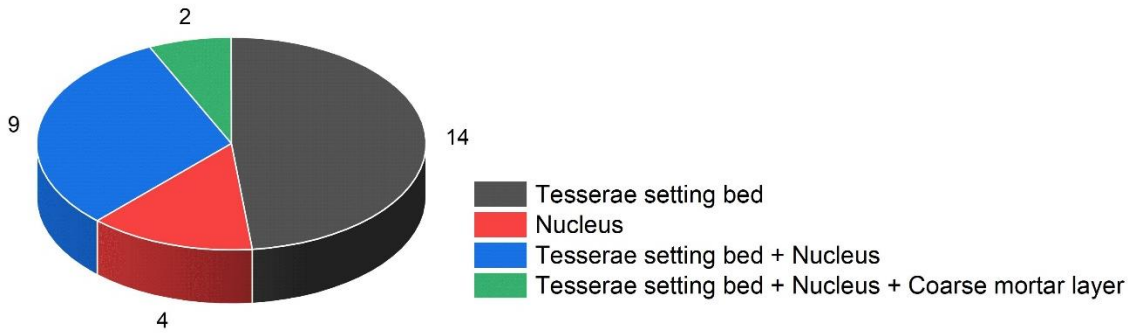

Figure 41 Graph with the quantity of specimens for each type of stratification identified.

The conducted investigation allows to assess the nature of the mortar of each *stratum* of the analysed specimens. In Table 4S[25] are reported details about the composition of the mortar of each stratification of the analysed specimens. Thanks to the multiple analysis performed it was possible to individuate different combination of *stratum* still present on the specimen, sometimes also characterised by different mortars. On the bases of the results achieved, it is possible to summarise the different types of compositions recorded in the analysed specimens as follow (for each type is reported the correspondent draw for a clearer comprehension, Figure 42):

1. Solo SB *stratum* with composition of pure lime or lime mixed with sand;
2. solo N *stratum* composed of lime with no or very few carbonate aggregates, in this case the finishing *stratum* is absent;
3. SB *stratum* made of lime mixed with sand with N *stratum* composed of lime with none or very few aggregates;

[25] For additional information please look at Annex_A, Table 4S Summary of the results achieved by process of characterisation of mortars.

4. SB *stratum* made of lime mixed with sand, N *stratum* made of hydraulic mortar with *cocciopesto;*
5. in some cases the use of one type of mortar made of lime with none or few aggregates for the production of both SB and N layer is recorded;
6. SB *stratum* made of lime mixed with sand, N *stratum* made of hydraulic mortar with *cocciopesto* and a lower *stratum* made of coarse mortar with no *cocciopesto.*

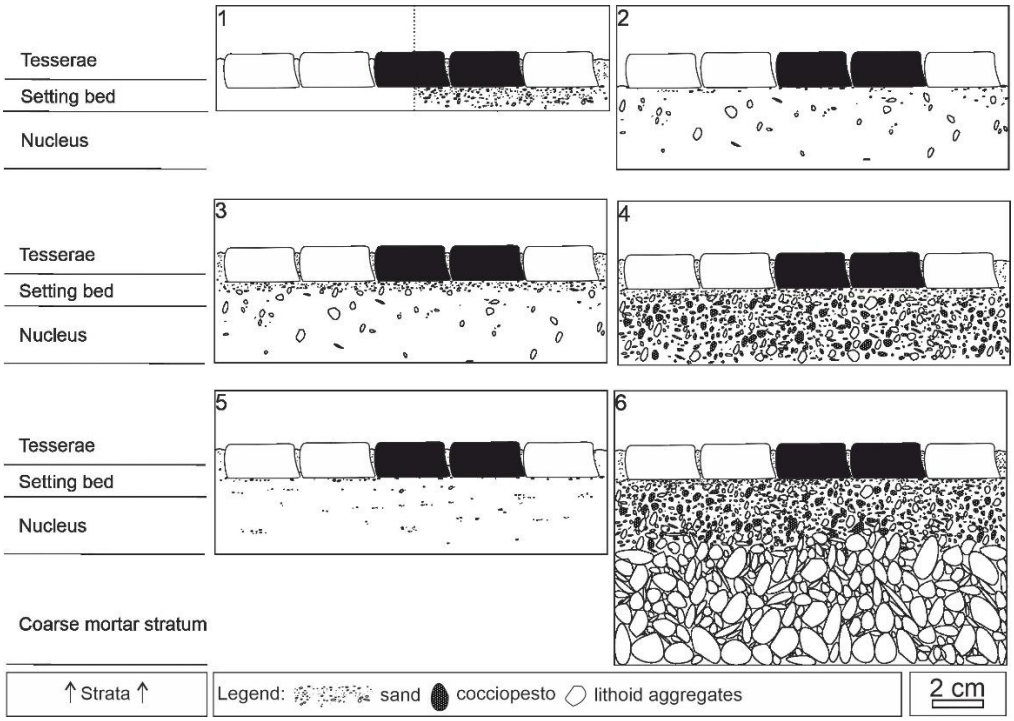

Figure 42 Schemes of the types of layering recorded. For the description please look at the text, each number correspond to the one present in the above list.

These results are crucial for understanding the technology behind mosaic production, particularly mortar production. Furthermore, they provide valuable insights into the level of attention and craftsmanship involved in the mosaics. As noted in the literature [50], the use of a single mortar layer and the absence of terracotta fragments as aggregates typically results in lower accuracy. This tendency might also suggest that the mosaic was produced during the Late Antique period, which coincides with a gradual decline in craft skills and economic power among patrons [56]. This hypothesis applies to specimens where *cocciopesto* was absent, and a single type of mortar was used for both the *Nucleus* and *tesserae* bedding layers.

Some mosaics documented in the literature feature an intermediate *stratum* similar to the first identified *stratum* below the *tesserae* [207]. This could be the case for the specimens mentioned

earlier, where only one type of mortar was recorded. However, further analysis is needed to confirm whether the two *strata* were made from the same or similar pastes.

The presence of a white mortar layer without aggregates and an inner *stratum* of *cocciopesto* mortar has been recorded in other mosaics from Aquileia [59,207]. In the specimens analysed here, the presence of a clearly visible stratification could indicate meticulous attention to the mosaic's production. Moreover, the use of a finishing layer made from lime mixed with sand is a clear sign of precision. This mortar type is typically used to fill the voids between *tesserae*, indicating its role as a finishing *stratum*. Therefore, the widespread presence of well-defined stratification or a finishing layer in most specimens suggests high-quality mosaics, potentially dating back to the Late Republican period [50].

3.3 Analysis of mosaic system

To fully uncover the historical and technological insights encapsulated within mosaics and to develop innovative preservation strategies, it is imperative to conduct a comprehensive examination of the material's density distribution and the intricate internal microstructure. Preservation of mosaics depends significantly on the stability of their supporting structure, a critical aspect influenced by the composition and quality of the *strata*. Thus, considerations of attachment, integrity, and interaction among layers are crucial in understanding potential causes of deterioration. Presently, investigations into mosaic fragments structure predominantly involve superficial analysis. Historically, tomography applications in literature have been cantered on assessing cracking and pore structure in cement and mortars [90]. This approach has facilitated considerations related to bond strength characteristics and the identification of cracks in mortar structures, allowing for the monitoring of mortar reactions to specific climatic conditions. Mosaic systems present a unique and intriguing case study for tomographic analysis due to their multiple mortar-based stratifications and *tesserae*. Each layer possesses a distinct composition, resulting in varied levels of porosity and microstructure.

To thoroughly examine the entire mosaic fragment avoiding a destructive sampling procedure, Synchrotron X-ray Computed Tomography (SXCT) was employed. The experiment was conducted at beamline ID10-BEATS of the Synchrotron-Light for Experimental Science and Applications in the Middle East (SESAME) research centre, in Jordan[26]. The analysis aims to extensively analyse the 3D distribution of various composing materials and internal cracks within archaeological mosaic artefacts. For acquiring microscale information, it proves to be a valuable tool, enhancing the resolution of reconstructed data and enabling phase contrast analysis. The objective of this study is to conduct an in-depth analysis of the three-dimensional distribution of various constituent materials and internal cracks within archaeological mosaic artefacts. Leveraging on the high image resolution and contrast provided by SXCT, the present non-invasive examination aims at establishing correlations between microscopic morphological variations and the underlying mechanisms of degradation and reaction of the compound that compose each specimen. Moreover, this analysis holds promise for elucidating traditional mosaic crafting techniques.

---

[26] The research presented in this chapter is presented in the paper "Non-destructive examination of ancient vitreous materials from Southwest Asia: synchrotron computed tomography at the BEATS beamline of SESAME" by Gianluca Iori*, Philipp Hans, Neva Maria Elisabetta Stucchi, Latif Ullah Khan, Abdellatif Saadaldin, Elena Possenti, Giulia Franceschin, Samah Al Khasoneh, Gian Luca Bonora, Gonca Dardeniz. The paper was accepted and it is currently in press on *Journal of Cultural Heritage*.

Due to the exploratory nature of our investigation of mosaics using SXCT, replica of ancient Roman mosaic were used. Samples were prepared ad-hoc, tailoring their size taking dimensional limits of the instrument (optical field-of-view) into consideration.

3.3.1 Preparation of the samples

Mock ups were prepared by the artisans of Scuola Mosaicisti del Friuli. The composition of samples adheres to the materials and production methods described by *Vitruvius*[27]. Indeed, analyses conducted on ancient samples confirmed the composition of original Roman mosaic[28] as reported by the ancient writer. The chemical information obtained enabled the reproduction of mock-ups of mosaics, facilitating the formulation of sacrificial materials that can undergo multiple analyses and treatments. The mortar layers, from bottom to top, were prepared as follow: a layer that resemble *Rudus stratum* composed of a coarse mix of *cocciopesto*, sand, and lime; *Nucleus*, a finer blend of *cocciopesto*, sand, and lime; and a thin finishing layer of pure lime (*Supra Nucleus*). *Tesserae*, which differ in size from 5 mm to 10 mm and material glass or stone depending on the sample, are nested inside the last layer. Smaller specimen for SXCT were obtained by isolating larger pieces of mosaic. In Figure 43 are reported images of the three produced specimens under analysis.

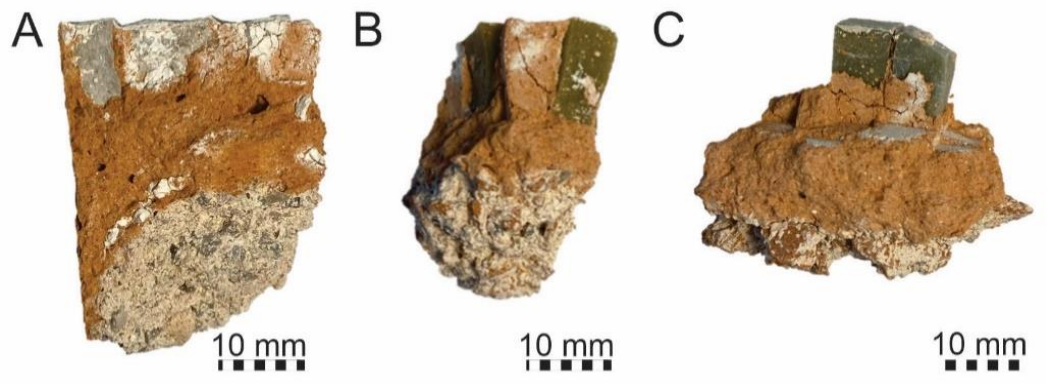

Figure 43 Mock-ups subjects of analysis: A) Petra; B) M01; C) Venezia.

The Petra specimen, shown in Figure 43A, is unique among the analysed samples, featuring 10 stone *tesserae* with regular shapes and dimensions of ~ 5 × 5 × 10 mm. During the isolating process, the *tesserae* remained firmly attached, with no issues of detachment.

[27] For more information please have a look at §2.1.2 Technology of Roman mosaic.
[28] For more information please look at §3.1 Characterisation of *tesserae* and §3.2 Mortar composition.

Figure 43B depicts specimen M_01, which consists of 5 green glass *tesserae*. This specimen is more irregular in shape due to the fragility of the glass mosaic system compared to stone. The glass *tesserae* are smaller than stone one, being characterised by a side measuring around 4 × 3 × 10 mm, and have irregular shapes. The specimen measures 15 mm × 25 mm in width and approximately 30 mm in height.

The Venezia specimen was designed to include only two *tesserae* (Figure 43). To preserve the integrity of this fragile specimen, the mortar layers were maintained. Breaking the mortar layer could cause significant detachment, potentially leading to the complete loss of the central *tesserae*. Therefore, downsizing was performed by carefully removing one *tesserae* at a time from around the central piece. The specimen measures 30 mm × 20 mm in width and approximately 25 mm in height, with each *tesserae* measuring 5 × 5 × 10 mm^3 approximately.

3.3.2 Synchrotron X-ray tomography experiments

All SXCT images were captured at the tomography end station of beamline ID10-BEATS of SESAME. The detectors, sample manipulation system and data collection procedure are described in detail in [208]. The broadband spectrum of the synchrotron X-ray source was filtered with glassy carbon (5 mm), aluminum (0.2 mm), and tungsten (0.5 mm) to reduce heat-load and the total dose of ionizing radiation on the specimen. This provided an X-ray beam with relatively narrow bandwidth and peak energy of 69 Kev, useful to minimize the effect of beam hardening (different absorption of the low and high energies of a polychromatic X-ray leading to image artefact). The distance between sample and detector was adjusted, and the beam left to propagate in air up to 900 mm after interacting with the specimen. This was done to exploit propagation-based X-ray phase-contrast enhancement as described in [209]. Samples were mounted using a custom 3D printed holder and wrapped in protective foam during SXCT scans. First, medium resolution scans (MR, voxel size: 13.65 µm) of the entire replica samples Petra and M_01 were performed. A Python script allowed the automated and sequential scanning of the sample at different heights (6 steps in total, capturing *tesserae, Supra Nucleus, Nucleus, Rudus as well as their interfaces*). This was done moving the sample along the rotation axis between scans. Each scan was performed collecting 8000 projections with exposure time of 0.07 s over 180° sample rotation, and had a Field of View (FOV) of 29.7 × 7.9 mm^2. Reference images (100 each) of the detector response without sample (flat fields) and without beam (dark fields) were collected before each scan for field inhomogeneity normalisation. An overlap of 100 slices (corresponding to 1.4 mm) was considered between successive scans in order to allow 3D image stitching during post-processing. Each 8 radiographic projections were averaged to improve statistics and compensate for the strong X-ray absorption of the mosaic. The total time of each MR scan was 1 h approximately.

After MR scans, additional data at high resolution (HR, voxel size: 3.1 µm) was acquired to improve the visualisation of the mortar layers, particularly of the area of contact between mortar and *tesserae*. For this, a custom 3D-printed 45-degree sample mount was fabricated. A HR scan was applied to the entire Petra sample and, using a procedure referred to as local tomography, to the core of the Venezia sample. In Figure 44 is reported the image of Venezia specimen, in red is highlighted the area of interest for the HR scan of the sample, indicating that the analysis was focused on the central portion of the specimen. HR beamline setup was made setting a 360° rotation of the sample and extending the FOV horizontally (the vertical FOV remained 6.7 mm). The distance between sample and detector was set to 500 mm. The scan was performed in 5 steps, each consisting of 2016 projections with exposure time of 0.448 s.

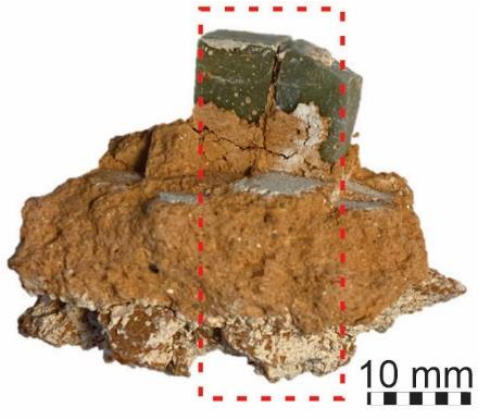

Figure 44 Venezia sample, the area of analysis is highlighted in red.

3.3.3 3D image reconstruction and analysis

SXCT volume images were reconstructed using the Python software TomoPy [210] and the web application alrecon [211]. Sinograms (series of projections under different projection angles) were normalized for the beam inhomogeneity (flat-field correction). A sinogram stripe removal algorithm [212] was applied to avoid ring-shaped artefacts in the reconstructed images. Propagation-based phase-contrast images were generated by applying a phase-retrieval step [213]. CT reconstructions were computed on the beamline high-performance-computing facility with a GPU-accelerated implementation of the Filtered-Back-Projection algorithm. All 3D images were stored as stack of 16-bit TIFF files. The sequential scans of a single specimen could lead to up to 126 GB of reconstructed volume images. After reconstruction, all images were inspected and cropped using ImageJ [214] where necessary. Stitching of the vertical scans of each specimen, 3D rendering, and further image processing for the visualisation of the microstructure were performed using Dragonfly (Comet Technologies Canada Inc., Montreal, Canada). Theoretically, the

evaluation of porosity consists of assessing the ratio between the volume of empty space present in the sample and the total volume of the sample. The visualization and evaluation of the porosity in the mosaic structure were performed by applying the following steps to the image reconstruction of the SXCT scan of a portion of mosaic fragments. The images were filtered using a median filter to reduce noise and simplify the segmentation process, which is a fundamental step for identifying the pores. A K-means segmentation algorithm was applied, which divides the data based on their features, grouping the most similar elements. The initial segmentation was performed to include the entire sample in the process. To avoid the possible inclusion of artefacts and noise in the evaluation, a 3D morphological opening was applied with a kernel size set to 3 voxels, effectively cleaning the mask. This process was repeated throughout the creation of the mask to accurately include or exclude areas of interest. A second mask was applied to the reconstruction of the specimen, focusing on the voids and the background. In this case, a refinement process was also performed to ensure that only the areas of interest were included. After preparing the two Regions of Interest (ROIs), a multi-ROI was created. A background removal process was applied to allow the software to focus solely on the whole sample and the internal voids. By comparing the prepared multi-ROI with the single ROI of the entire sample, it is possible to determine the volume of the internal pores. Additionally, the refinement process allowed for the evaluation of the larger pores present in the analysed area.

3.3.4 Insights in the microstructure of mosaic

Thanks to the analysis it was possible to evaluate the microstructure of each specimen, presence of cracks and porosity were assessed. In Figure 45A is reported the 3D reconstruction of Petra specimen. The analysis allows to differentiate using different colours to highlights cracks (in blue) from open (in purple) and close porosity (in green). As visible, the *Supra Nucleus* and *Rudus* are characterised by cracks, possibly due to shrinkage phenomena. Differently, the *Nucleus* is characterised by open and close pores, produced in phase of casting by the air trapped inside the mortar. In Figure 45B is reported the 2D section of Petra specimen, in each coloured square are indicated the analysed area, which results are reported in the planar images reported nearby. Additionally, results of the material porosity, expressed in %, and evaluated for each stratification and specimen, are reported in Table 4, together with the corresponding, size of the analysed volume. A lateral image of Petra specimen (Figure 45B) shows no porosity within the *tesserae*, while allows the clear visualisation of the cracks below the *tesserae* of *Supra Nucleus*, also visible in the planar view (Figure 45B). These big cracks are produced by the shrinkage phenomena of the mortar in contact with the *tesserae* and lead to a SB porosity of 8%. *Nucleus stratum* is characterised by a porosity of 5.2%, one big pore is visible in the centre of the stratification and one vescicle is visible below. It is possible to see that pores are source of micro cracks that

propagate in the *strata*. This suggests that the process of compaction should be performed carefully in order to reduce the formation of pores and thus the production of cracks. The image allows also to differentiate visibly the different mortars, underlying that *Rudus* does not cover the entire size, but is partially submerged by *Nucleus*. Big aggregates with angular shapes are visible in R and cracks are distributed along the perimeter of each aggregate, the porosity of this *stratum* is of 4.7%. The analysis allows also to evaluate the largest interconnected pore, which can link different pores and span a large portion of the *strata* volume. This information can be indicative in order to assess the level of damage of the *strata*. Indeed, to parity of cracks we have greater possibility to have a detachment or a disaggregation. This effect is enhanced depending to the dimensions and give information about the fragility of the system. Images of the evaluation of largest interconnected pores are reported in Figure 5S[29]. The 76.3 % of the cracks of *Supra Nucleus* are all interconnected, while for *Rudus* correspond to the 46% of the porosity, cracks are naturally shaped to be interconnected, and to propagate inside the structure also producing a chain reaction effect of propagation. This data is not available for *Nucleus*, possibly because of the small dimension of the largest of pores, thus the possible absence of interconnection. Indeed, the image of Figure 5SB[29] shows clearly a pore with a circular vescicle which is the largest pore interconnected of *Nucleus stratum* and the interconnection of cracks inside SB and R. The different densities of the aggregates constituents correspond to different grey-levels in the phase-contrast SXCT image, allowing to distinguish the composition of each layer. Figure 6SA[30] shows a 3D rendering of the Petra specimen with opacity set to highlight only aggregates more radio-opaque (i.e. elements with greater density). This allows to visualise the *tesserae* and the prevalent distribution of big stone aggregates in *Rudus*, while the *Supra Nucleus* and *Nucleus* are revealed to be with less aggregates of smaller dimension thus less dense. Moreover, as reported in Figure 6SB[31], it is possible also to visualise the pores depending on their volume thickness, thus allowing the direct analysis of the pores.

[29] For more analysis please look at Annex_A Figure 5S Large interconnected pore of Petra specimen.
[30] For more analysis please look at Annex_A Figure 6S 3D image of Petra specimen.
[31] For more information please look at Annex_A to § Additional materials of §3.3 Entire specimen.

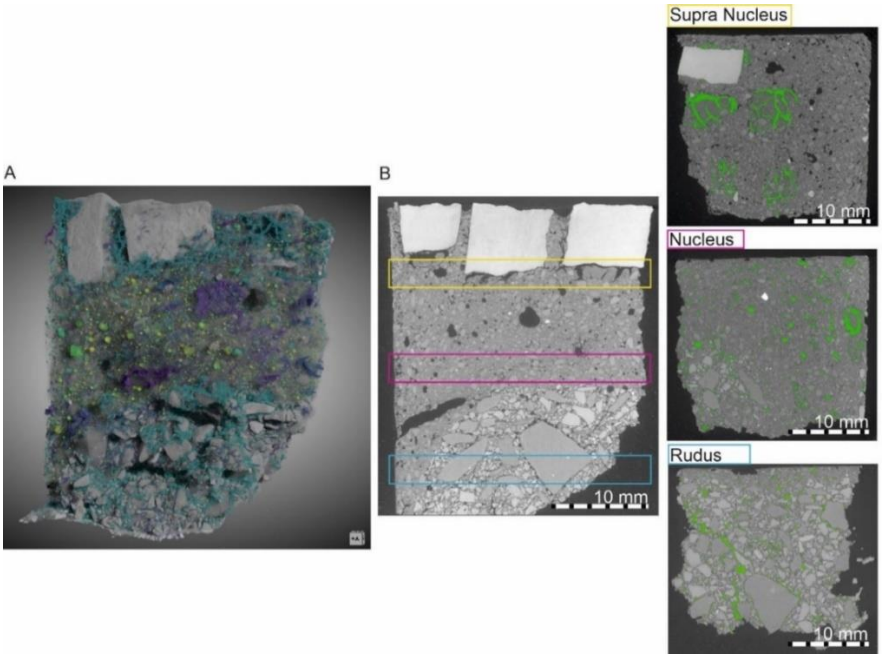

Figure 45 Analysis of Petra specimen: A) 3D reconstruction; B) 2D reconstruction with the relative planar analysis of each layer, pores are highlighted in green colour.

Table 4 Results of porosity evaluation for each specimen for each *stratum*.

	Petra		**Venezia**		**M_01**	
Stratum	**Porosity (%)**	**Analysed volume (mm^3)**	**Porosity (%)**	**Analysed volume (mm^3)**	**Porosity (%)**	**Analysed volume (mm^3)**
T	-	-	25.6%	3817.6	-	-
SB	8%	56.7	-	-	-	-
N	5.2%	36.7	5.9%	72.5	3.2%	0.91
R	4.7%	125.4	17.3%	167	12.9%	195.6

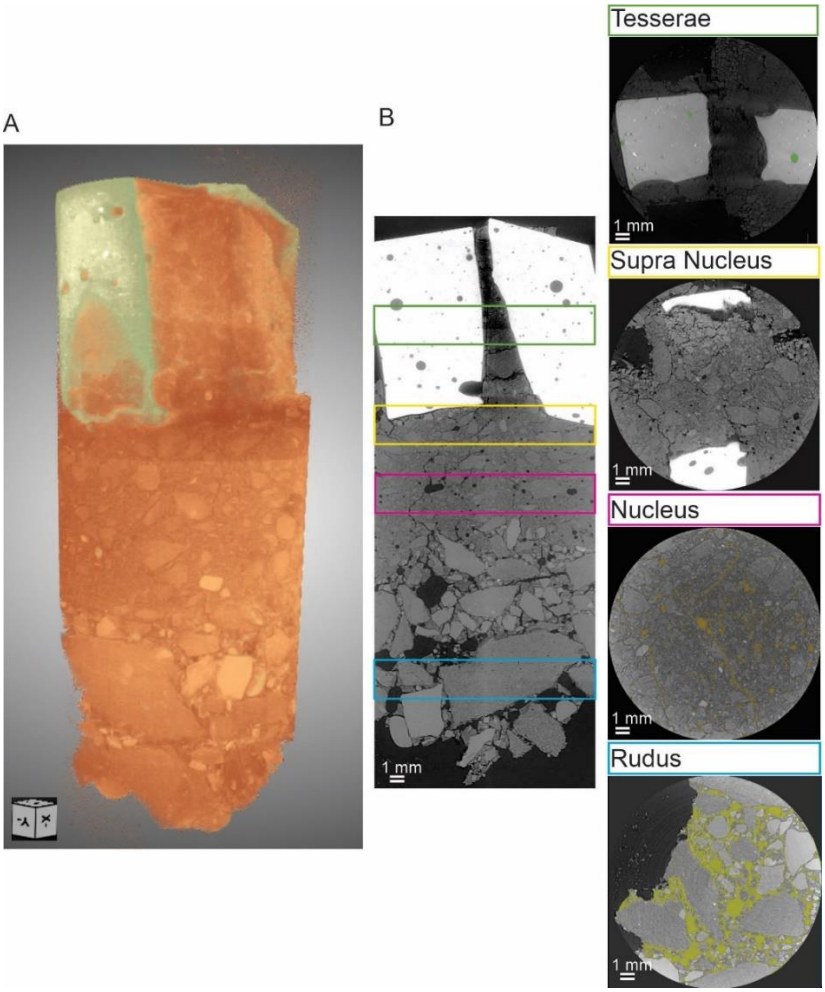

Figure 46 Analysis of Venezia specimen: A) 3D reconstruction; B) 2D reconstruction with the relative planar analysis of each *layer*, pores are coloured.

In Figure 46 are reported 3D and 2D images of Venezia specimen. The specimen was analysed in high resolution mode and for this reason the analysis was focused only to the central part of the specimen. A 3D rendering of the specimen with realistic colour is shown in Figure 46A. Differently from stone *tesserae*, glass ones are porous as clearly visible in the longitudinal virtual section of Figure 46B. The porosity of the *tesserae* was calculated to be 25.6%. Despite the visible presence of *Supra Nucleus stratum*, it was not possible to evaluate its porosity due to discontinuities of the *strata* that is only partially visible in small portion of the surface, making its evaluation difficult. Differences between SB of mosaic produced with glass and stone *tesserae* are visible in Figure 7S[32]. Particularly, larger cracks are visible in the Petra specimen, while in the Venezia specimen only few very small cracks are present. This element can indicate a better adhesion of the mortar to the surface, thus a possible lesser degree of deterioration. Cracks seem

[32] For more analysis please look at Annex_A Figure 5S *Supra Nucleus* analysis of the internal cracks.

to be produced in proximity of irregularities of the surface of the *tesserae*, thus stone *tesserae* being more irregular are source of more cracks indicating the importance of having a regular *tesserae* surface. *Nucleus stratum* whit a porosity of 5.2% is characterised by similar porosity of N *stratum* of Petra. This was expected, since the production of mock-ups, despite the use of different type of *tesserae* was performed following equal recipes and procedure between *strata*. Big aggregates present in the *Rudus stratum* have brought to the production of large voids which act, in turn, as source of cracks, and bring the porosity of this layer to 4.7%.

M_01 specimen is made of glass *tesserae* and results achieved from analysis were used as support for the results achieved from Venezia specimen. The 3D rendering of Figure 47A shows the complete reconstructed specimen, with realistic virtual colouring. *Nucleus* and *Rudus strata* are characterised by a porosity equal to 3.2% and 12.9%, respectively. These results are in line with porosity measurements achieved on the Venezia specimen. The analysis allows to evaluate the largest interconnected pores of *Nucleus* which represent the 9.8% of the total *Nucleus* porosity (Figure 8SA[33]). In contrast the largest interconnected pore within the *Rudus* accounts for as much as 97.4% of the total *Rudus* porosity, underlying how virtually all the pores are connected within this *stratum*. This result can give an idea about the internal microstructure and the possible point of failure of the specimens. Figure 8S (A-C) illustrate the evaluation of pores, largest connected voids, and volume thickness of voids (i.e. void size) in the *Nucleus* of the M_01 specimen.

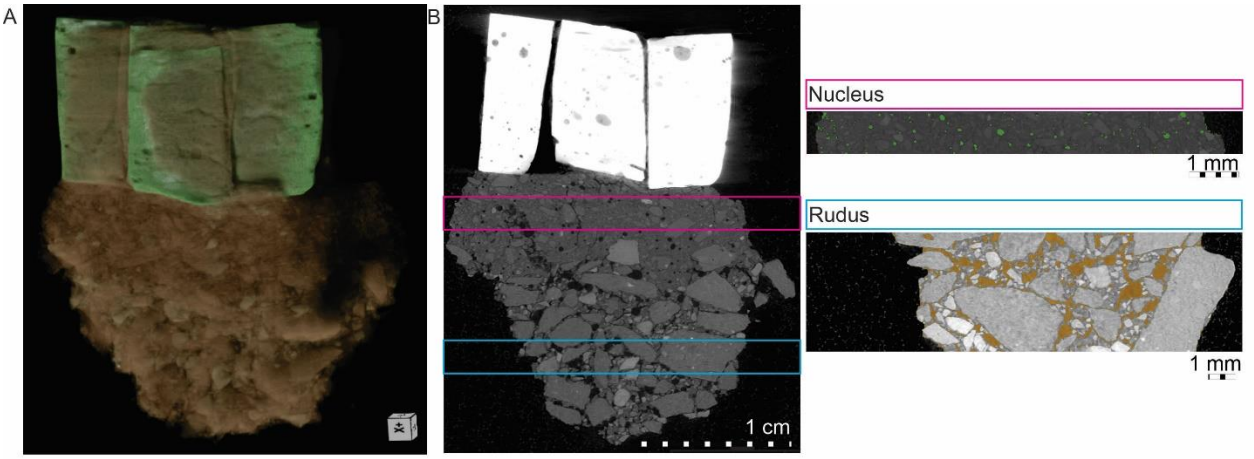

Figure 47 Analysis of M_01 specimen: A) 3D reconstruction; B) 2D reconstruction with the relative planar analysis of each layer, pores are coloured.

The acquisition of spatial distribution across the entire specimen, as well as the detailed analysis of aggregate distribution within the mortar, allows for a comprehensive understanding of the material's internal structure. Complete visualisation of cracks and pores enables the identification

[33] For more analysis please look at Annex_A *Nucleus* analysis of M_01 specimen.

of potential networks formed by these pores and their connections to the external surface. In specimens with multiple layers, this visualisation can further facilitate the assessment of specific characteristics of different types of mortars. Evaluation of the porosity of the *tesserae* was possible for one specimen, demonstrating the presence of voids in glass *tesserae*. Despite the fine mortars used for the *Supra Nucleus stratum* showing a porosity value comparable to that of the *Rudus* layer, this is due to shrinkage phenomena that affect the mortar during the drying phase, producing cracks. The *Nucleus stratum* of all the specimens are characterised by similar values of porosity, demonstrating that the mortar is finer, with smaller aggregates. In conclusion, it is possible to assess that the *Rudus stratum* is the layer with the greatest differences in porosity when comparing the different specimens. This result is due to the use of large aggregates in preparing the mortar, whose high dimensional and shape variability induces greater variability in porosity.

The results achieved demonstrate the feasibility of using SXCT analysis for the study of fragments of archaeological materials.

4 Development of a mortar for restoration

The analysis of ancient materials presented in Chapter 3 enabled the understanding of the composition of ancient Roman mosaics in the city of Aquileia. The composition of the stratification observed in the 153 specimens analysed matches that reported by Vitruvius [42]. Additionally, petrographic analysis of thin sections and results from Synchrotron radiation tomography have highlighted that the *Nucleus* stratification is responsible for the stability of the *tesserae* due to its role in attaching both the *tesserae* and the *Rudus stratum*. In this framework, the research focused on the development of innovative mortars by designing six different formulations. The mortars were prepared considering *Nucleus* composition, assessed during characterisation process, and on the data reported in the literature.

The new products were developed in the framework of two standpoints: compatibility and sustainability. Compatibility is a key parameter to consider during restoration intervention, thus using the designed materials, it is ascertained thanks to the similarity of the composition of these mortars to the composition of original roman mixture. Sustainability was ensured by producing two mortar pastes in which a natural gel (called Nopal gel or *Opuntia ficus indica* gel) was added, produced by the waste of pruning of the plant of *Opuntia ficus indica*. The methodology of production of this gel is easy, fast, and necessities only of water, leading to a material that has a low environmental impact. In the framework of sustainability two more mortar pastes were produced by the addition of self-healing material (labelled as “CSMMA”) made of calcium and silica oxide encapsulated with poly(methyl 2-methylpropenoate), named also poly(methyl methacrylate) in Figure 48. It is a common knowledge that the addition of self-healing materials can be considered sustainable because, thanks to their properties, they improve the durability of the mortars, in which they were added, reducing the number of restoration interventions to apply.

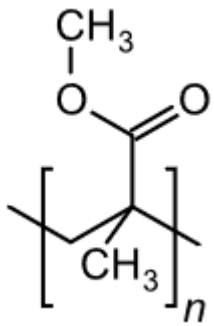

Figure 48 Skeletal formula of Poly(methyl 2-methylpropenoate).

In Table 5 are reported the composition of the 6 mortars used in this study: Mortars made with slaked lime (X) as binder were labelled as X, XN, XCS, differently mortars with NHL 3.5 (Y) as binder were labelled as Y, YN and YCS. In formulations XN and YN Nopal gel (N) was used instead of water, while self-healing material (CS) were added to the mortars X and Y developing mortars XCS and YCS.

Table 5 Composition of the designed mortars.

Mortar	**Aggregate**	**Binder**	**H_2O% (on weight B+A)**	**Additive**
X	Mix of Sand : *Cocciopesto* 1:4	Slaked lime	H_2O 4%	-
XN			-	Nopal 4%
XCS			H_2O 4%	CSMMA 1%
Y		NHL 3.5	H_2O 20%	-
YN			-	Nopal 20%
YCS			H_2O 20%	CSMMA 1%

The Figure 49 shows the analysis conducted on the mortars.

First of all, the workability of the new mortars was tested. On hardened mortar, morphological characteristics were evaluated applying microscopic investigation, colorimetric analysis, water absorption test and porosimetric analysis on specimens or fragments of hardened mortars. Moreover, along the curing time, physical mechanical properties were tested as flexural strength test and compressive strength test. The composition of mortars were analysed by SEM-EDS, XRD and DSC-TGA analysis. The results reported allow the definition of the formulated mortar more suitable for the restoration of the mosaic system.

Finally, consideration about the compatibility of the prepared mortars with the ancient one were made by the application of micro mechanical analysis on small fragments of mortars, both new and ancient and a comparison of the chemical analysis performed.

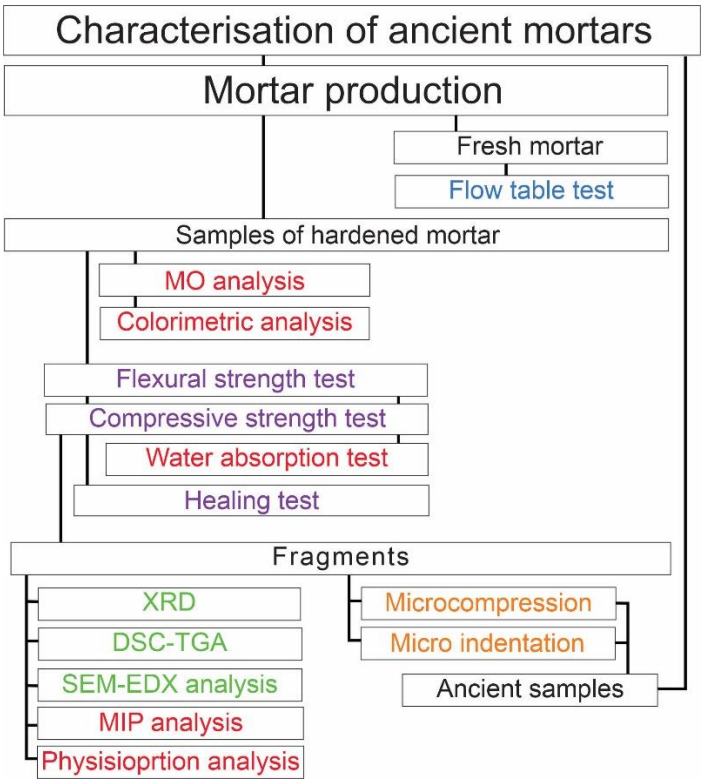

Figure 49 Diagram of analysis and tests conducted on the developed mortars. In red are indicated morphological tests, physical mechanical test are indicated in purple, in blue the one tested at the fresh state of the mortar, in orange are indicated the test made also on ancient mortars, in green are indicated chemical analysis.

4.1 Application of reverse engineering for the design of mortar

From the analysis conducted on samples from the archaeological site of Aquileia, it was possible to assess the hydraulic nature of *Nucleus* stratification, because of the presence in its composition of *cocciopesto* fragments (bricks powder). As is known, Romans used to add *cocciopesto* [56], because of its demonstrate good pozzolanic properties [215]. Particularly it was used when *pozzolana* (volcanic material) was not easily available, as in the case of the Aquileia region. In addition to *cocciopesto*, sand was recorded in the composition of the aggregate phase of the mortar analysed, according to the tendency typical of Romans to use sea sand [45,52] or fluvial sand to produce mortars [56].

On these bases, two mortars, X and Y, were designed reproducing the ancient composition. The two mortars, as detailed in Table 5, are prepared using the same materials, in the same ratios, differing only for the type of binder used. Slaked lime was the common type of binder used during roman period, the relevance of its use [56,216] and its production are known nowadays [217]. NHL 3.5 was used as a binder in place of slaked lime, as this type of binder is commonly used for making mortars for restoration [218]. For mortar X, slaked lime was used as binder (calcium hydroxide, $Ca(OH)_2$, with excess H_2O) purchased from "C.T.S. Conservation", while for mortar Y, NHL 3.5, purchased by "Lafarge", was used.

The aggregate phase consists of a mix of *cocciopesto* powder (grain size < 0.4 mm) and quartz sand (medium grain size 0.1 - 0.3 mm), both purchased from "C.T.S. Conservation", in a 1:4 ratio defined on the bases of preliminary tests reported in Annex_B[34]. The binder-to-aggregate ratio used adheres to the Vitruvian recipe of 1:3 [42]. Water was added in different percentages depending on the binder used. Slaked lime contains excess water, which increases the total water content and reduces the need for additional water. Conversely, the powder nature of NHL 3.5 requires more water.

[34] In Annex_B are reported results of preliminary test conducted for the definition of the composition of the aggregates ratio.

4.2 Innovative mortars with Nopal gel

The good effect of the addition of natural elements in the mortar was known since Roman time [6] [35] and the practice continuous along centuries [219], until nowadays, when this tendency is particularly boosted considering the general interest in the production of new greener materials [158,220,221].

As explained in Chapter 2, paragraph 2.4.2, among the natural compound tested as additive for mortars and cements, gel produced from *Opuntia ficus d'indica* plant (also known as Nopal gel) gave the greatest results. Indeed, its addition to lime based mortars or concrete has been demonstrated to improve the mechanical resistance, reducing the formation of cracks, improving the workability, having a low bio receptivity despite its organic nature [158,156,132]. Moreover, the use of this gel represent a sustainable choice, indeed the gel can be extracted from the waste of seasonal pruning which are subjected the plant, avoiding the employment of other resources.

In this framework, two different kind of mortars labelled as XN and YN were prepared using *Opuntia ficus d'indica* gel. To allow the comparison of all the prepared mortars, the same procedure of production and the same ratio of binder and aggregates was used for all the mixes. Thus, the results achieved from their analysis and testing are completely comparable, being X a reference material for mortars XN and XCS as Y for YN and YCS. Considering the different binder used, a different quantity of gel (in substitution to water) was added to XN and to YN, but always respecting the amount of liquid phase used in the reference mortar.

4.2.1 Nopal gel production

Nopal gel was produced using the traditional and simplest method described in multiple studies [132,146]. Images of the cladodes and steps of production are reported in Figure 50. Fresh cladodes of *Opuntia ficus-indica* were peeled (Figure 50B) and cut into pieces (Figure 50C), which were then soaked in water at a ratio of 1:2 (in weight of cladodes to water) for 24 hours (Figure 50D). After this period, the water transformed into gel, which could be separated from the leaves through a filtration step (Figure 50E). The choice of 24h as time of immersion is in accordance to literature [132,146]. However, preliminary analysis was conducted to test if a different time of immersion can change the composition of the gel. The gels obtained were weighted and characterised through

[35] For more information please look to § 2.4.2 The use of natural additives in mortar pastes.

DSC analysis and FTIR spectroscopy. The results confirmed that despite the change of time of immersion the gel obtained is the same.

Tests for the evaluation of the growth of biological material were conducted by adding different concentrations of bioactivity inhibitor, method and results are reported in Annex_C[36], and sodium benzoate was selected to be incorporated into the gel extraction in concentration of 1 mg/ml. Indeed, sodium benzoate is one of the most commonly used agents for food preservation [222] and is easily adaptable for other purposes.

The solid content into the gel has been also evaluated: 50 ml of gel were dried at 60°C for 48 hours. The samples were weighed before and after the drying process, and the difference provided the amount of dry residue. It results that the gel is composed for the 98% of water.

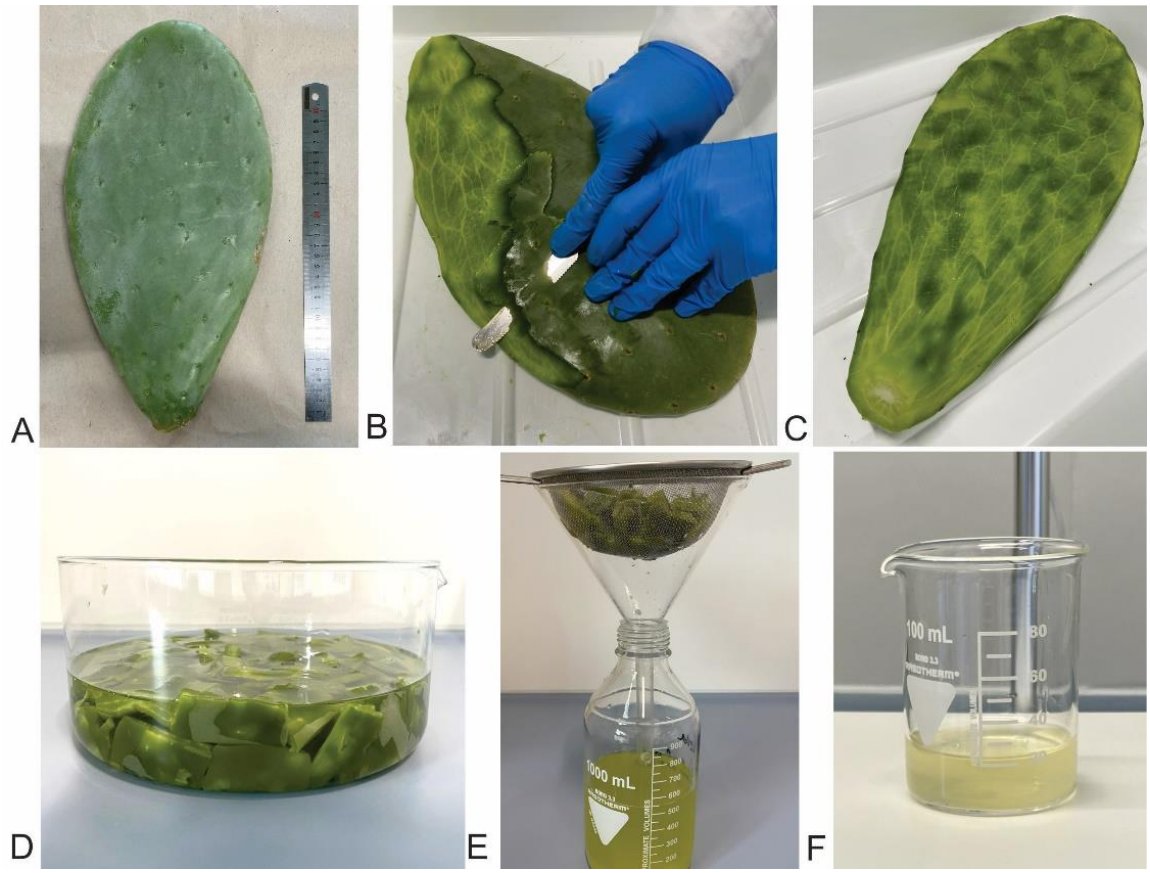

Figure 50 Phase of preparation of Nopal gel: A) Cladodes of Opuntia ficus indica; B) Process of peeling of the cladodes; C) Peeled cladodes; D) Fresh cut and peeled cladodes immersed in water; E) Filtration phase of the pieces of cladodes; F) Gel of Nopal

[36] In Annex C are reported test for the evaluation of prevention of biological growth in addition of different quantity of Sodium Benzoate.

4.2.2 *Opuntia ficus indica* gel composition

Due to the complex composition of the produced *Opuntia ficus indica* gel, different analysis were applied for the evaluation of the nature of the gel used for the production of the mortar:

- Fourier Transform Infrared Spectroscopy (FTIR)
- Thermogravimetric analysis coupled with Differential Scanning Calorimetry (TGA-DSC)
- Inductively Coupled Plasma Mass Spectrometry (ICP-MS)
- Scanning Electron Microscopy (SEM)

Fourier Transform Infrared Spectroscopy (FTIR)

FT-IR analysis was conducted in KBr using a Perkin Elmer Spectrum One Instrument. The analysis were conducted on different sample of gels produced using an increasing time of extraction, the results are reported in Annex_C[37] and no substantial differences are visible.

In Figure 51 is reported the spectrum achieved from the FT-IR analysis of the gel used for the production of the mortar, extracted during a process of immersion of 24 hours. According to literature, the signals in the range 3000-3600 cm^{-1} are related to the stretching frequencies of hydroxyl groups (-OH, present in R–OH and –C(O)–OH moieties) of the polysaccharides that compose the gel. These groups are responsible of the intermolecular hydrogen bonds of mucilage molecules, water and heavy element ions [21,147,153,223]. Signals around 2940-2853 cm^{-1} are related to the vibrational bond C-H, that can be due to the presence of methylene, pyranose and glycoside in the composition [153,223,147,21]. Peaks at 1598 cm^{-1} and 1432 cm^{-1} can be assigned to the carbonyl (C=O) and COO^- stretching modes, respectively, of the D-galactopyranosyl uronic acid residues and of the carboxylic acid (RCOOH) [147,223]. Signals cm^{-1} at 1318 and 1267 cm^{-1} are related to C-N stretch of the amine [147]. Signals at 1177 cm^{-1} and 1122 cm^{-1} carbohydrates fingerprint and it allows the identification of some functional groups of polysaccharides such as stretching C-O-C, bending O-H, and deforming (CH_3) vibrations [21]. Vargas Solano [147] interprets the peak at 1047 cm^{-1} vibrations of the stretching (extension) the C-O bonds of primary and secondary alcohol of the pyranose ring and the signals present between 935-777 cm^{-1} as the vibration of C-H out of plane bend and to monosubstitution (phenyl) on phenolics compounds.

[37] In Annex_C are reported FTIR analysis for the evaluation of *Opuntia Ficus indica* gel at different stages of extraction of the gel.

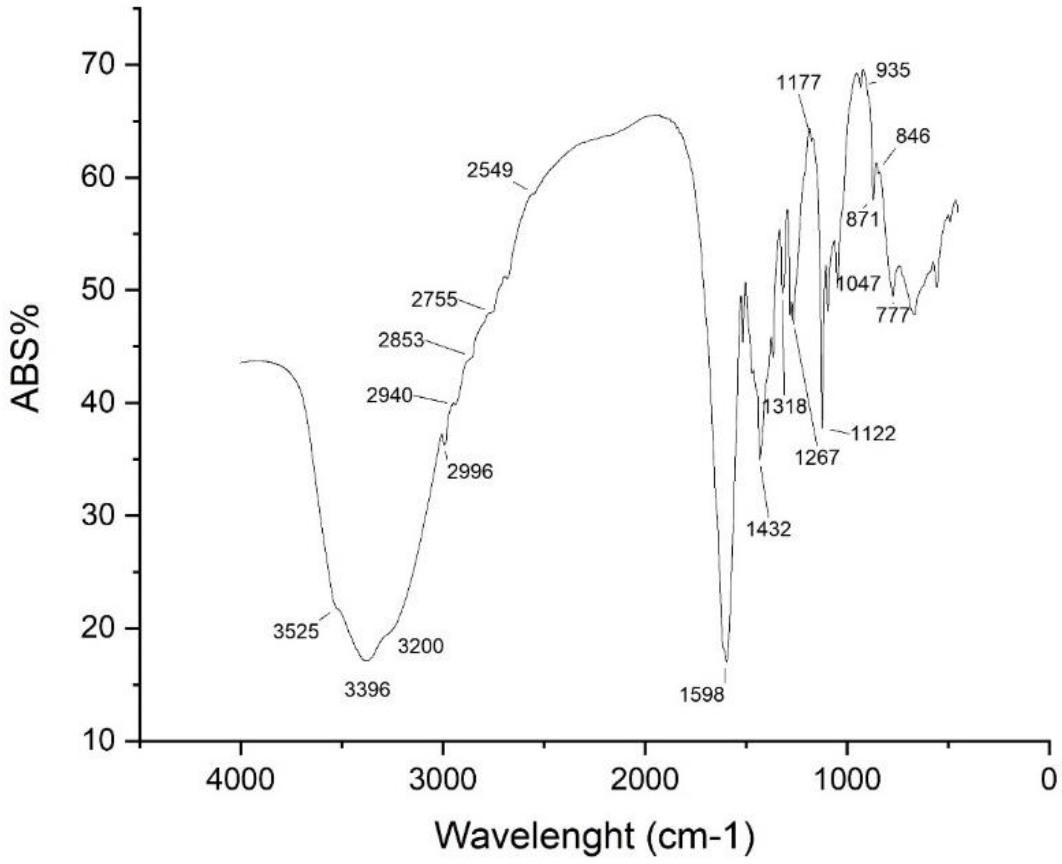

Figure 51 FT-IR spectra of Nopal gel.

Differential Scanning Calorimetry coupled with Thermogravimetric analysis (DSC-TGA)

DSC-TGA analysis technique was employed to characterize the gel as well as binders and mortar fragments. The analysis was performed utilizing the Linseis STA PT-1000 thermobalance instrument. The analyses were conducted on alumina crucibles in a nitrogen inert atmosphere, following a specific temperature schedule:

- Ramp rate of 10°C/min up to T = 30°C, with a dwell time of 3 minutes

- Ramp rate of 20°C/min up to T = 900°C, with no dwell time

The thermal behaviour of Nopal gel was assessed by the analysis of powder of lyophilised gel. The analysis was conducted on samples of gels produced with different time of immersion, in order to assess change in composition of the hydrogel to parity of increment of time of immersion.

Results of this research are reported in Annex_C[38], and show that there are no substantial differences in the composition.

The thermogram achieved from the analysis of *Opuntia ficus indica* gel used for the production of the mortar is reported in Figure 52. The blue line is correspondent to the heat lost, while the red line is correspondent with the loss of weight.

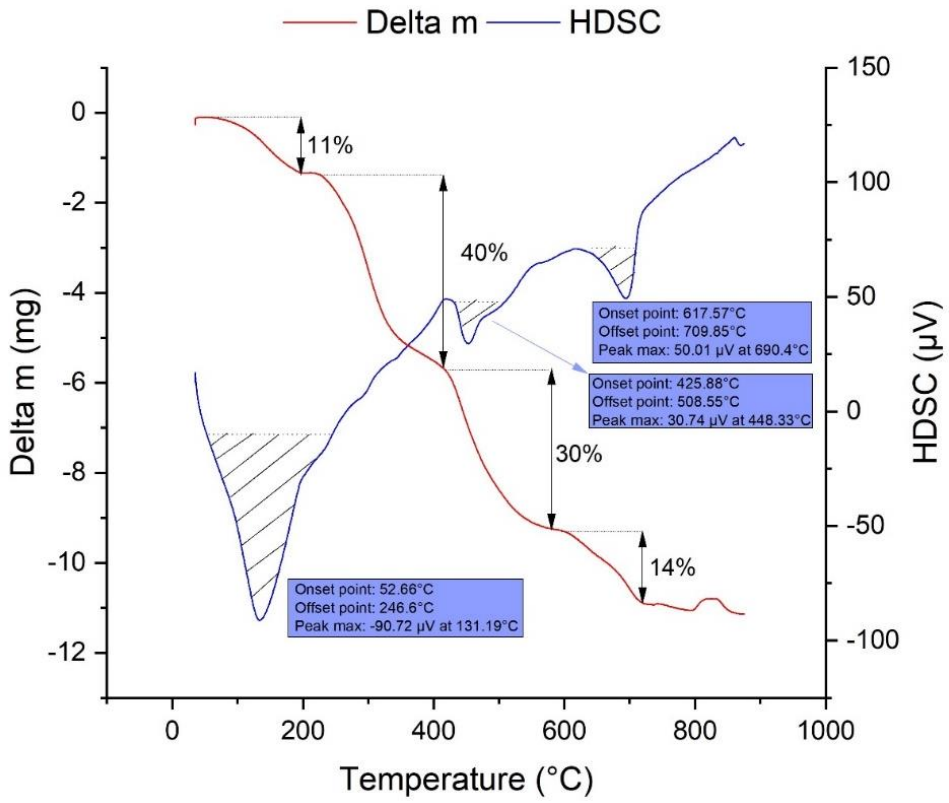

Figure 52 DSC-TGA of Nopal mucilage with the indication of the reduction of weight.

Heat flow curve (blue line) is typical of material that retain water. Indeed there is a huge initial variation [21] followed by other two processes of change of the heat flow. This trend is in accordance to the weight flow curve (red line). The first event of mass lost happen between 25°C and 200°C, it is related firstly to free water lost (till 100°C) and secondly also to bonded water lost [223]. In literature, this event is explained considering the moisture present inside the sample of gel that is hygroscopic [21]. The second important mass loss is around 250°C due to organic compound combustion and more precisely to the degradation of polysaccharide [153,224]. While

[38] In Annex_C are reported DSC-TGA analysis for the evaluation of *Opuntia Ficus indica* gel at different stages of extraction of the gel.

the last huge mass loss happens at about 400°C, as reported in literature [21] this can be indicator, that at this temperature, there is still a residual part of material capable to retain water.

Inductively Coupled Plasma Mass Spectrometry (ICP-MS)

The minerals and metals content of the gel was analysed through Inductively Coupled Plasma Mass Spectrometry (ICP-MS). The instrument used is a Thermo Fisher iCAP7600, set up with the following settings: Plasma Power 1150 W, Auxiliary Gas 0.5 L/min, Coolant Gas Flow 12 L/min, Nebulizer Gas Flow 0.50 L/min.

1 ml of gel was previously lyophilised and then the sample was digested in 1 mL of solution of HNO_3/H_2O_2 (1:1) for 2 hours at 65°C in an ultrasonic bath and then brought to a final volume of 10 mL. The solution was filtered through a 0.45 µm RC filter and then analysed. For elements Ca, Mg and K the measurements was repeated applying a dilution of the sample. In Table 6 are reported the content in ppm of the elements present in the gel with Relative Standard Deviation %. Ca, Mg and K were recorded through the analysis of diluted sample.

Table 6 Result of ICP-MS analysis.

Category	**Ca**	**Cu**	**Fe**	**K**	**Mg**	**Mn**	**Na**	**Zn**
AVG (ppm)	62.850	0.020	0.039	96.954	28.630	0.101	6.520	0.157
RSD %	0.735	0.190	2.896	0.252	0.342	2.497	1.068	4.533

Main metals present in the composition of the gel are K, Ca and Mg, moreover good concentration of Na was recorded while the lowest concentration were recorded for Cu, Mn, Zn. These results are partially in accordance with what reported in literature, indeed the bibliographic material report the analysis of cladodes, fruits or peel of *Opuntia ficus indic*a and differently we have analysed the composition of the hydrogel [225,226]. This comparison can be interesting in order to define if the process of production of the gel brings to the complete extraction of all the elements present inside the process cladodes. Despite what reported in literature, our sample lack in concentration of Fe. Following bibliographic indications, the analysis was conducted in order to assess the presence also of Co, Cr, Li, Mo, Ni, but the concentration of these elements were derisory and the results of analysis of this elements can be considered not significant. Thus, it is possible that the process of extraction of the gel brings only to the conservation of minerals present in greatest quantity in the plant used for gel production. Moreover, it must to take in consideration that these differences could be related to a different species of plant, geographical origin, maturity stage, process of harvesting, season of pruning and age of the plant [147,225,148].

Scanning Electron Microscopy (SEM)

Morphology of the gel was analysed employing Scanning Electron Microscopy (SEM). The analysis was conducted on lyophilised sample of the gel. The samples were dehydrated using ethanol gradients (30%, 50%, 70%, 90%, 96%, and 100%, twice for each step) and finally left in pure ethanol for 2 days. The SEM analysis was performed using a Zeiss GeminiSEM 560 (Zeiss, Oberkochen, Germany) field-emission gun operating at 5 kV acceleration voltage. The sample was previously coated with gold for increasing the conductivity and avoiding charging effects. Secondary electrons detector (InLens) were used to enhance the morphologic differences between the samples.

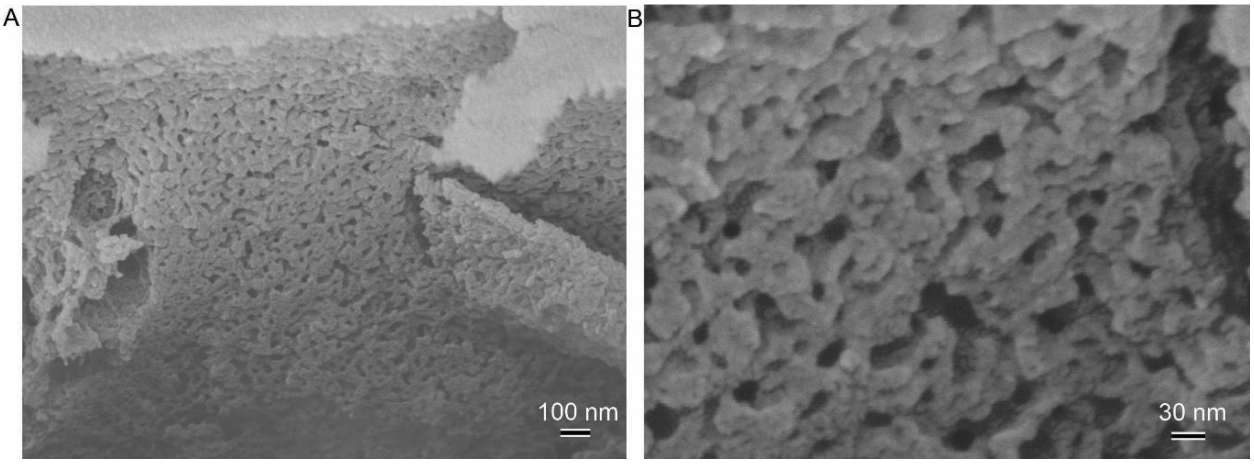

Figure 53 SEM analysis of lyophilised Nopal.

SEM images reported in Figure 53 clearly shows a spongy-like structure with interconnected fibrils. The interstitial structures are evenly distributed and have uniform dimensions, with an average size of 76 nm ± 25. This spongy structure may be responsible for the gel's high water retention capacity, as it is possible for the network to be filled with water while maintaining its integrity. This behaviour could influence the workability properties of the mortar and explain the delayed setting time of mortar containing Nopal gel, as reported in the literature. To evaluate the effect of Nopal gel on mortar retention, slump tests were conducted immediately after the mortar was produced and again after 50 minutes. These tests demonstrated a change in retention time. The results are provided in the Annex. Further SEM analysis of the gel itself (without the lyophilisation process) is necessary to confirm this hypothesis, considering that the gel remains in liquid form when added to the mortar.

4.2.3 Rheological properties of *Opuntia ficus indica* gel

In addition to the analysis conducted to define the composition of Nopal gel, two different types of tests were conducted to evaluate the workability properties of the gel when added to the binder: rheological tests and flow table test.

Rheological test

Rheological test were performed on pastes composed of slaked lime with different concentration of Nopal gel expresses in water/cement ratio, in this case Nopal/lime ratio.

The shear viscosity and yield stress of each mixture were determined using a controlled-stress rheometer (Anton-Paar MCR 102) comprised of a stationary lower plate with a thermostat set at 25°C and a measuring geometry with a flat bottom plate connected to a motor that initiates its rotation. The instrument conducted the analysis applying continuous rotation at a controlled rate, gradually increasing speeds over time. Through the application of a shear rate (γ) [1/s] the analysis evaluate the shear stress applied (τ) [Pa]. As a result, the yield viscosity was calculated as the ratio of shear stress to shear rate expressed in Pa*s (Equation 1).

$$\eta = {}^{\tau}/_{\dot{\gamma}} \qquad (1)$$

This enabled the measurement of how viscosity changes with varying shear rates, aiding in understanding the fluid type under analysis.

From the results (Figure 54) it is possible to see the decrement of viscosity obtained by increasing the amount of Nopal gel.

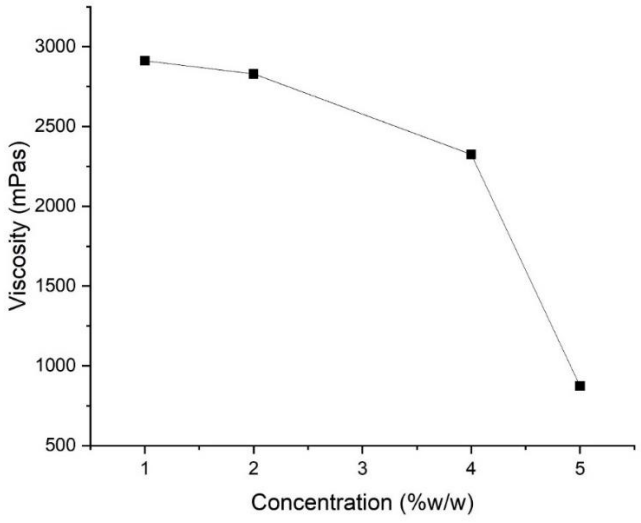

Figure 54 Influence of Nopal concentration on viscosity of mortar paste

Slump test for the evaluation of influence of Nopal on workability of the slaked lime

The mixtures analysed with rheometer, were also tested with slump tests to verify the correspondence between the results obtained with the two techniques. Slump test, also known as Abrams cone, is a fast and simple test used on-site for the assessment of viscosity and workability of cements, mortars and pastes. However, the large size of the Abrams cone requires substantial quantities of material, which is impractical for laboratory research. To address this issue, we used the mini-slump test, a scaled-down version of the slump test utilising a smaller Abrams cone [227]. In practice, the analysis is conducted for each formulation immediately after the mixing, ensuring the homogeneity of the mixture. The cone is placed on a flat surface and filled from the top with fresh mortar, ensuring it is completely filled. After waiting approximately one minute, the cone is lifted very slowly to avoid deforming the mixture, allowing the material to expand naturally. The diameter of the expanded mortar on the calibrated platform is then measured, providing comparative data on the fluidity of different mixtures. It is important to note that measuring viscosity using the slump test has inherent issues with low repeatability and precision. Nevertheless, it remains a straightforward and widely used method for the instantaneous evaluation of the viscosity of fresh mortar mixtures.

Results (average of 3 measurements) of Slump test are reported in Figure 55. As possible to see at increasing quantity of Nopal gel there is an increment of the diameter of expansion of the pastes. These results are completely in accordance with the results achieved with rheometric analysis.

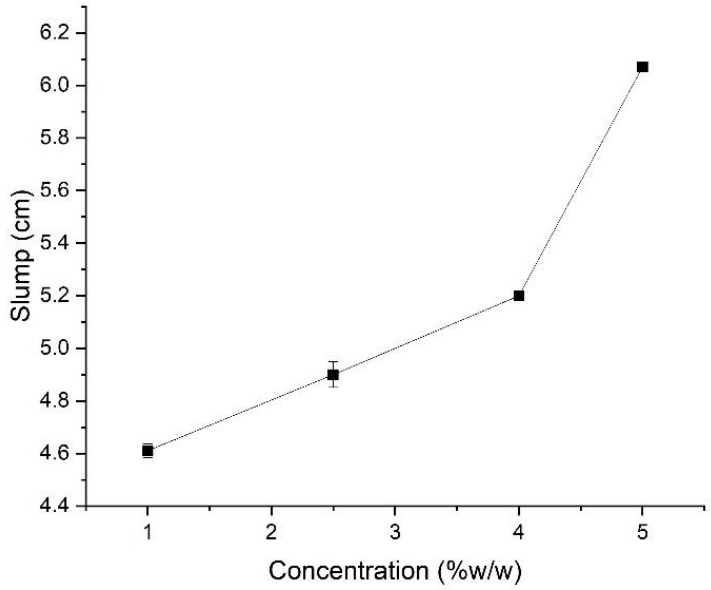

Figure 55 Results of slump test for the evaluation of the change in viscosity at increasing quantity of Nopal.

4.3 Mortars with Self-healing materials

As explained in detail in Chapter 2.4.3, self-healing materials are capable of repairing the system were they are introduced themselves. Indeed, these materials contain elements that react under conditions of damage, restoring the system. Given the importance of durability in restoration interventions, self-healing materials are a suitable choice for producing restoration mortar. Additionally, the growing interest in mortars and concrete with self-healing properties aligns with the trend towards sustainable materials that can repair themselves without the need for further intervention. Consequently, two mortars with self-healing agents were designed and investigated.

The mortars labelled as XCS and YCS were prepared based on the compositions of mortar X and Y, using the same quantities, ratios, and materials. The self-healing material called CSMMA (see Chapter 2.4.3) was added at concentration of 1% of the total weight. This decision was based on the studies carried out under my supervision and described in a thesis [228].

4.3.1 Self-healing material production

The self-repairing additive, labelled as CSMMA, consists of an active binding core, formed with hydrated lime and silica calcined together at 900°C for 24h (labelled as CS), encapsulates with a layer of Polymethyl Metacrylate (PMMA). To form the self-healing additive, a polymer solution (30 g/L) was prepared by dissolving the flake polymer (1.5 g) in chloroform (50 mL) under stirring for 1h and then a dilution (10 mL chloroform) was applied, resulting in a 30 g/L concentration of polymer. Chloroform ($CHCl_3$) was chosen for solubilising PMMA, as it was identified as the most effective solvent [229]. 300 g of CS was dispersed in 70 mL of chloroform, under mechanical agitation for 1 h to form a homogeneous suspension. This mixture was then combined with 50 mL of polymer solution, previously prepared and stirred for approximately 24 h allowing solvent evaporation, resulting in the powdered additive called CSMMA.

4.3.2 Evaluation of the composition of self-healing material CSMMA

In order to characterise the self-healing agent used for the purpose of research, two different analysis were conducted:

- Fourier Transform Infrared Spectroscopy (FTIR)
- Thermogravimetric analysis coupled with Differential Scanning Calorimetry (TGA-DSC)

Moreover, also in this case rheometric behaviour of the binders added with the self-healing material was assessed. The rheological investigation was conducted applying:

- Rheometric analysis
- Slump test

Fourier Transform Infrared Spectroscopy (FTIR) of CSMMA

FT-IR spectroscopy was used[39] in order to assess if the synthesis of the self-healing additive has a positive result. The analysis was performed on samples of CS and CS encapsulated in PMMA (CSMMA), the comparative analysis is reported in Figure 56, substantial difference in composition of CS and CSMMA is not visible. The FTIR were compared also with the reference FTIR of PMMA[40].

Peak at 3645 cm^{-1} is typical of portlandite formation [230], thus it could be related to $Ca(OH)_2$-SiO_2 or the indication of the presence of Calcium hydroxide [231] not completely calcinated (CaO). The enhancement of intensity of this peak in CSMMA IR it is due to the presence of PMMA. Bands at 3417 cm^{-1} and at 1628 cm^{-1} are related to deformation vibrations and stretching vibrations of –OH. This wide band is precisely of H-O-H stretching mode of $Ca(OH)_2$ [166]. Comparison with PMMA spectra allows to assess that the picks between 1500 and 1400 cm^{-1} can be assigned to asymmetric bending vibrations of ($C-CH_3$) and ($C-CH_2$) bonds [232]. Peaks at 1407 cm^{-1} and 887 cm^{-1} can be related to the CaO [231], formed during the calcination of the $Ca(OH)_2$. Peaks at 992 cm^{-1} and 771 cm^{-1} can be related to stretching of Si-O-Si [166,230], respectively symmetric and asymmetric. These frequencies are an indication of the degree of polymerization of Si network [230].

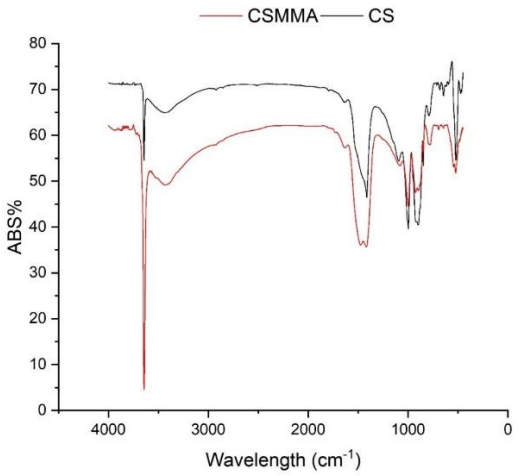

Figure 56 FT-IR analysis of the self-healing material CSMMA (blue line) and of the sole core of the self-healing material CS (black line).

[39] For additional information about FT-IR instrument and mode please look to § 4.2.2 Opuntia ficus indica gel composition.
[40] Image of FTIR of PMMA is reported in supplementary material Annex_D Figure 14S.

Differential Scanning Calorimetry coupled with Thermogravimetric analysis (DSC-TGA) of CSMMA

The analysis was conducted using the same instrument and mode for the DSC-TGA analysis conducted on Nopal gel[41]. This analytical investigation aimed to assess the presence of the polymer capsule in the additive. The analysis report a graph with variation of the differential calorimetry (HDSC) (expressed in µV) and mass change (delta m, expressed in mg) related to increasing temperature.

Comparing the result of analysis achieved (Figure 57) with DSC-TGA conducted on the PMMA and the binder mixture CS, is it possible to assess the effective presence of both elements in the prepared self-healing material CSMMA. Indeed, in HDSC results, the peak around 350-450°C is present in all the three analysis, corresponding also to the major weight loss of analysis recorded with TGA. Particularly, for PMMA this heat loss is visible from the huge peak shifted to lower temperature at about 350°C. Differently, this peak is really small for CS and it correspond to the decomposition of $Ca(OH)_2$ [230]. While, it is marked as the one recorded for PMMA at 450°C for CSMMA. TGA analysis give back three similar results for the three samples. As already mentioned the main weight loss correspond to the main heat loss, CSMMA curve is more similar to CS one but at high temperature there is a change in weight not recorded for CSMMA.

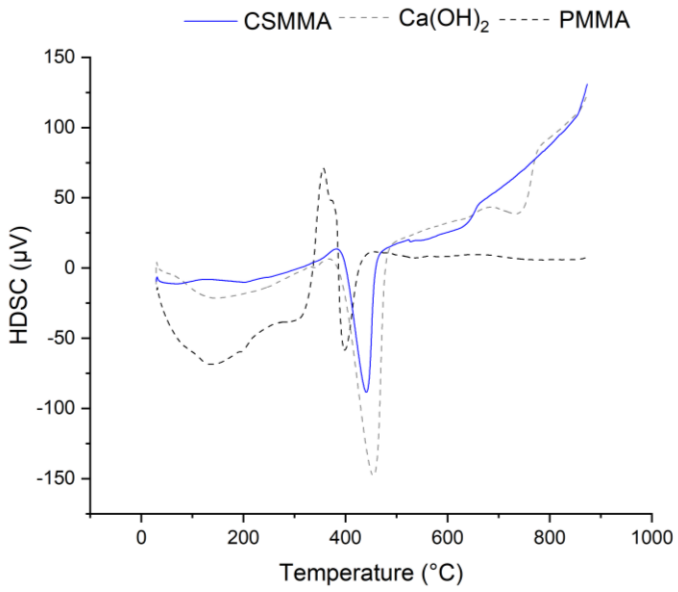

Figure 57 DSC analysis result of CSMMA self-healing material, Calcium hydroxide and Polymethilmetracrylate

[41] For additional information about DSC-TGA instrument and mode please look to § 4.2.2 *Opuntia ficus indica* gel composition.

Change of rheology of slaked lime with the addition of CSMMA

As performed for Nopal gel, in order to assess the influence of CSMMA on viscosity properties, rheological measurements were conducted by using the same instrument and parameters[41]. Three different mixture composed of slaked lime with additive in three different concentrations 1%, 3% and 10 % (in %w/w) were analysed, together with the pure slaked lime in order to allow the comparison of the results (see Table 7). More investigation of the effect of this additive to workability are reported in Annex_D[42], this preliminary research has been used in order to define the best concentration of CSMMA to use for mortar formulation.

Table 7 Results achieved with rheometer and slump test on pure slaked lime and slaked lime with self-healing material in different concentrations.

Composition	**Rheometer**	**Slump test**
	Viscosity (Pa*s)	**Diameter (cm)**
Slaked Lime (SL) with water/cement ratio 0,5 (w/c)	4.48	8.70
SL 0,5 (w/c) + CSMMA 1%	5.57	7.75
SL 0,5 (w/c) + CSMMA 3%	5.88	7.55
SL 0,5 (w/c) + CSMMA 10%	5.73	7.15

From the results of rheometric analysis, it is possible to assess that the addition of CSMMA increases the viscosity with an increment of concentration from 0% to 1% to 3%. Slight decrement recorded from 3% to 10% can be related to a different quantity of intrinsic water (not controllable) present in slaked lime used for the test (in this case dryer). Thus, we can consider it stationary or related to an error.

Slump test was conducted on the same samples analysed with Rheometer in order to complete and to assess the rheometric measurement conducted. The results (in Table 7) indicates a decrement of the diameter of the paste, with a continuous increment of self-healing material added, thus, an increment of the viscosity of the paste. These results accord with the rheometric measurements and generally, it is possible to assess that by increasing the quantity of CSMMA additive an increment of the viscosity and cohesion of the binder has obtained together with a decrement of

[42] In Annex_D are reported results of the rheometric analysis performed on mixtures of binder with different concentrations of CSMMA.

fluidity. These results highlights that the mortar produced with this additive could lack in workability, a fundamental parameter to consider for the development of an injection mortar.

4.4 Mortars production

In the Table 8 are reported the information about materials and methods used for the preparation of the mortars.

Table 8 Information about materials and methods used for the preparation of the mortars

Mortar	Binder	Aggregate	H_2O%	Additive	n. of samples	Mixing time	Vibrating table
	1	3					
X	Slaked lime	Sand:*cocciopesto* 1:4	H_2O 4%	-	18 (4*4*16 cm) 15 (5*5*5 cm)	10 min	50-45 Hz
XN			-	Nopal 4%	18 (4*4*16 cm) 15 (5*5*5 cm)	10 min	50-45 Hz
XCS			H_2O 4%	CSMMA 1%	18 (4*4*16 cm) 15 (5*5*5 cm)	10 min	50-45 Hz
Y	NHL 3.5	Sand:*cocciopesto* 1:4	H_2O 20%	-	18 (4*4*16 cm) 15 (5*5*5 cm)	10 min	50-45 Hz
YN			-	Nopal 20%	18 (4*4*16 cm) 15 (5*5*5 cm)	10 min	50-45 Hz
YCS			H_2O 30%	CSMMA 1%	18 (4*4*16 cm) 15 (5*5*5 cm)	10 min	50-45 Hz

Aggregate part was composed of two materials fine quartz sand and *cocciopesto* in ratio 1:4 which were pre-mixed homogeneously. The mixtures were prepared by the use of an automatic mixer, keeping the mixture under constant agitation. The binder (Slaked Lime or Natural Hydraulic Lime 3.5) was then mixed with aggregate in appropriate quantities to maintain the 1:3 b:a Vitruvian ratio. Water or when necessary *Opuntia ficus indica* gel were added as last element, adjusting the consistency. Finally, when necessary, the self-healing additive[43] was incorporated mixing the mixture for other 10 minutes. Approximately 15 kg of mortar was produced for each type of paste based on the requirement of research. The mixtures were analysed both at the fresh and hardened state.

The designed six mortars were cast into prismatic moulds (40x40x160 mm) to obtain 18 specimens and cubic moulds (50x50x50 mm) to produce 15 specimens (Figure 58A). In order to assess the change of the properties of the mortars along curing time, and to conduct all the necessaries test,

[43] In Annex_D are reported results of preliminary test conducted for the evaluation of the concentration of CSMMA to use in order to achieve the greatest results.

at least 33 specimens of each type of mortar were produced (Figure 58B), resulting in a total of 216 samples. Prismatic specimens were used to evaluate primarily flexural strength; the resulting cubes achieved from the rupture with flexural strength were then used for the evaluation of compressive strength and water absorption. Cubic specimens were used for the evaluation of the self-healing properties of the materials. The specimens were cured under the same environmental conditions for a total of 7 days [233], to prevent formation of cracks they were covered for 5 days by wet hessian tissue, creating an environment characterised of high humidity level (RH% of 90%), then let hardening in air for other 2 days. After 7 days, since the casting, the specimens were demould, labelled and let to harden in laboratory condition (T of 25°C, RH% of 60%) until the moment of analysis of each of them (14, 28, 56, 89, 365 days).

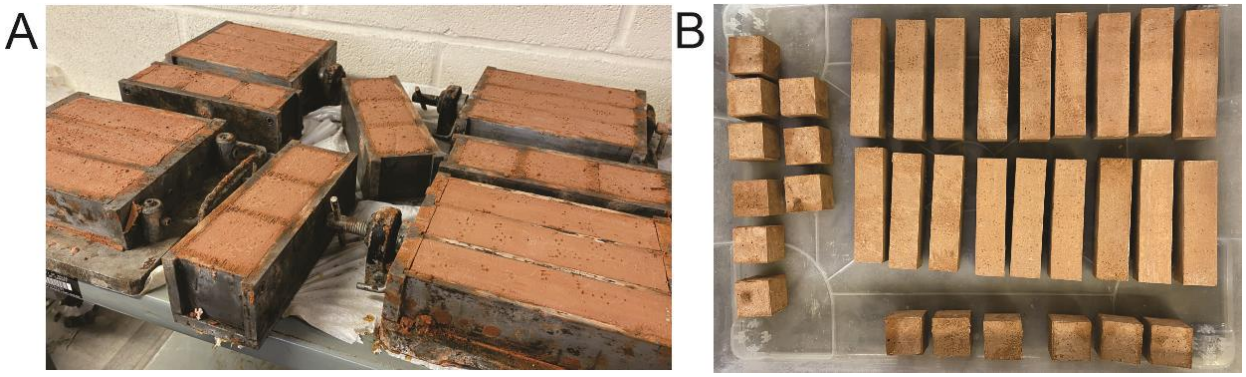

Figure 58 Phase of preparation of the samples of mortars: A) moulds used for the process of casting; B) demould set of 33 specimens of one type of mortar.

4.5 Mortars analysis

In Table 9 are reported information about the tests performed on the mortars.

Table 9 Analysis conducted on specimens of mortars.

Parameter	Test	Analysed specimens	Dimensions (mm)	Time of curing (days)	Normative
Workability	Flow table test	X, XN, XCS, Y, YN, YCS, fresh mortar	-	0 (fresh mortar)	ASTM C230
Mechanical	Flexural strength	X, XN, XCS, Y, YN, YCS, hardened mortar	40*40*160	14, 28, 56,90	EN 1015-11:2019
	Compressive strength		40*40*40		BS EN 12390-3:2009
	Pull-out test	X, XN, Y, YN	40*40*40	28	-
Physical	Immersion test	X, XN, XCS, Y, YN, YCS	40*40*40	14, 28	UNI NORMAL 7/81
Microstructural	Microscopic images	X, XN, XCS, Y, YN, YCS	Pieces of mortar	56	NORMAL 43/93
	Colorimetric analysis				
	Porosimetry		Fragments	360	NORMAL 4/80
	BET				
Chemical	XRD	X, XN, XCS, Y, YN, YCS	Fragments	360	
	SEM-EDS				
	DSC-TGA				

4.5.1 Analysis of fresh paste

Considering that we want to produce an injection mortar, proper workability is required. To assess this property, the mixtures have been characterised through flow table test, following the

procedure reported in ASTM C230 [234]. This test involves placing the mortar into a mobile cone. The cone is then moved, allowing the mortar to expand. After a set number of regulated movements (25 times in 15s), the cone is lifted. The diameter achieved by the mortar paste is measured, thus allowing to record the fluidity of the mortar.

4.5.2 Morphological analysis of hardened mortar

Microscopic and colorimetric analysis

Evaluation of the morphological features of the mortars were determined at 56 days of curing through microscopic analysis of both outer and internal surfaces. High resolution images of the surfaces with different magnification were acquired using a Keyence Digital Microscope VHX-7000. Thanks to the comparison of the images acquired for each specimens it was possible to determine effectiveness of similarity or differences of the different mortars.

Colorimetric analysis were also performed on the outer surface of the specimens in order to assess the possible colour variation induced by the addition of additives. The analysis was performed using a spectra colorimeter Konica Minolta CM-2600d spectrophotometer and the CIE L*a*b* system, in accordance with NORMAL 43/93 standards [235]. This technique utilizes the acquisition of reflectance spectra from coloured surfaces, recorded by numerically capturing colorimetric parameters corresponding to the CIE L*a*b* colour space [236]. The mathematical transformation of the CIE space allows for an immediate interpretation of the surface colour through the acquisition of a colorimetric spectrum and of three spatial coordinates: two on the x, y plane (respectively a* - redness-greenness, b* - yellowness-blueness) and one associated with the brightness measure along the z-axis (L*) [235]. With the aid of a reference mask, five measurements were taken from each surface, each from a different area of the sample, and each obtained as the average of three successive scans. For the purpose of the research, for each sample, the average colorimetric spectrum was evaluated in order to see possible colorimetric differences.

Analysis of micro and macro pores of the mortars: MIP and BET

As presented in §2.2.2 mechanical, chemical properties of mortars as well as their conservation are related to their intrinsic porosity. Thus, application of methods of investigation that can give all the information about porosity and cracks present in the material, became fundamental in order to foresee the durability of the mortar and to define restoration materials and approach to use.

Mercury Intrusion Porosimetry (MIP) is based on the applied pressure used to push the mercury inside the porosity against the mercury surface pressure [237]. The analysis is based on the

Washburn equation [238] (Equation 2) which correlates pore radius r and pressure P (Kg/m^2), with the surface tension (γ) (for mercury is 480 mNm^{-1}).

$$Pr = -2\gamma cos\theta \quad (2)$$

From the analysis it is possible to achieve different information related to porosity. It is possible to assess the surface area of the pores that is a correlation of the penetration curve with pressure and radius. The mean pore diameter evaluated as the ratio of the Volume of mercury and the surface area, and the volume pore size distribution as the pore volume per unit interval of pore diameter [237]. MIP analysis allows the quantification of pores from 200 micron to 3 nm. Variable porosity within the same material causes it to react differently to both degradation phenomena and treatments. The processing and implementation of the material itself lead to an increase in porosity over time, the impact of which is important to consider [87]. For this reason, Physisorption analysis (also known as BET analysis) was applied allowing the evaluation of micro and meso-pores within the range of 300 nm to 0.2 nm. Thus, the two analysis results complementary covering the investigation of macro to meso to micro pores [237]. Physisorption measures gas adsorption on a solid to determine surface area, pore volume, and pore size. It uses Brunauer-Emmett-Teller (BET) theory to analyse adsorption, providing surface area through a linear plot of gas adsorption data at low relative pressures [239]. For analysing pore size distribution, the Barrett-Joyner-Halenda (BJH) theory is applied at higher relative pressures [240], specifically targeting mesoporous materials [237].

Small fragments of mortars were subjected to Mercury Intrusion Porosimetry (MIP) to assess and quantify the volume of open and close pores present in the specimens. The evaluations were made following NORMAL – 4/80 [241]. For MIP analysis was used an Automatic apparatus with a capacitive system for mercury intrusion detection and composed of two units. The first is a Pascal 140 for the analysis of elements with pore diameter ranges 116 - 3.8 μm and particle diameter of 330-15 μm. The second is a Pascal 240 for macropores, micropores, and powders with pore diameters of 15 - 0.0074 μm and particle diameter of 40-0.015 μm. Analysis has been conducted with the following parameters:

- Hg contact angle: 140°
- Max pressure: 200 MPa
- Pressure: 0.01 KPa - 400 KPa
- Increasing speed rate: 1-5 MPa/min
- Decreasing speed rate: 6-14 MPa/min
- Temperature: around 22°C

Powder of mortars were subjected to the BET analysis employing a Micromeritics TriStar II Plus employing Nitrogen as adsorptive gas. Samples were pre-treated using a Micromeritics VacPrep 061applying a thermal treatment for 3h at 150°C under vacuum. The analysis produced the isothermal curve of absorption and desorption of the gas having relative pressure [p/p_0] and the quantity of adsorbed gas [g/cm^3] respectively on X and Y axes.

Imbibition capacity: water absorption by total immersion

Water imbibition capacity is a crucial aspect in the study of construction and restoration materials. This analysis is commonly used as an efficient indirect method for porosity evaluation, due to its ease, repeatability, and cost-effectiveness [91]. Water absorption is strictly related to porosity, a key factor influencing the physical and technological properties of materials. Indeed as already mentioned, porosity variations, dictated by pore size, structure, and arrangement within composite material matrices, directly impact strength and durability [91,242]. In this study, mortar specimens were analysed for their water absorption ability allowing to complete the evaluation of the internal properties, specifically porosity.

Three cubic samples of 40x 40 x 40 mm of each mortar, were subjected to total immersion. These samples were placed in containers, elevated on plastic rods to minimize contact surface, and fully submerged in deionized water at room temperature. The water level was maintained 2 cm above the samples. The measurement process involves weighing the dry samples before immersion to record their initial mass, then regularly weighing them at intervals (1, 6, 24, 48, 72 hours) from the start of immersion, water absorption capacity was measured at each time following Equation 3.

$$\frac{\Delta M}{\mathrm{M\%}} = \frac{M1-M0}{M0}\ 100 \qquad (3)$$

This ratio expresses the absorbed water amount at each weighing, expressed as a percentage of the sample's dry mass. To obtain a trend of imbibition capacity for comparison across various curing days, the average value of absorbed water is calculated using the previously mentioned formula, resulting in: ΔMavg %. This average percent imbibition capacity is determined for each sample at every day of mortar curing.

4.5.3 Chemical analysis of mortars

Scanning Electron Microscopy with EDX probe (SEM-EDX)

In order to analyse microstructural features of the mortar and their elemental composition, Scanning Electron Microscopy coupled with Energy Dispersive X-Ray Analysis (SEM-EDX) of small fragments was performed. The SEM analysis was performed using a Zeiss GeminiSEM 560 (Zeiss, Oberkochen, Germany) field-emission gun, operating at 20 kV acceleration voltage. The

detector used was the VPBSE, back-scattered detector, used for enhance the differences of the elements present in the samples. Energy-dispersive spectroscopy (EDX, Oxford instrument, X-Max, 80 mm2) operating at 20 kV was utilized to evaluate the elemental ratios of mortars.

X-Ray Diffraction analysis (XRD)

X-ray Diffraction analysis was conducted in order to achieve a proper evaluation of the mineral phase present in each mortar. XRD analysis was carried out on PANanalytical Empyrean X-ray diffractometer equipped with a 1.8 kW Cu Kα ceramic X-ray tube and a PIXcel3D 2x2 area detector, operating at 45 kV and 40 mA. The diffraction patterns were performed under ambient conditions using a parallel beam geometry in symmetric reflection mode. HighScore 4.1 software from PANalytical was employed to analyse XRD data.

Differential Scanning Calorimetry coupled with Thermogravimetric analysis (DSC-TGA)

Differential Scanning Calorimetry coupled with Thermogravimetric Analysis (DSC-TGA) was performed on all mortars, analysing one specimen of material at 360 days of curing. The analysis was conducted using the same instrument and method used for the analysis of additives[44]. Application of this analysis on mortar fragments allow evaluating the peak of absorption of calcium carbonate. Thus, to evaluate the effective carbonation occurrence of the mortar as well as its difference for each different type of mortar. Moreover, from the analysis is possible to assess also different heat variation and mass lost related to the presence of additive in the mortar.

4.5.4 Mechanical test

Flexural strength test

The test was conducted repeatedly at various hardening intervals (14, 28, 56, and 89 days) to examine the relationship between the variation in characteristics and hardening time. Each test was repeated in triplicate for each mortar at each interval, and the average value of each measurement was considered, along with the respective standard deviation. Flexural analyses were performed on prisms using a Controls Automax 50-C52D02 machine, employing displacement control at a rate of 0.03 mm/min until complete specimen failure, in accordance with the UNI EN 1015-11:2019 standard [243]. Flexural strength values (*ef*) were evaluated using Equation 4, which takes into account the load applied at the fracture point (F), the length of the support span (l), and the dimensional parameters of the specimen (width b and area A).

[44] For more information please look at §4.2.2 *Opuntia ficus indica* gel composition.

$$ef\left(\frac{N}{mm^2}\right) = 1.5\frac{F\ x\ l}{b\ x\ A} \quad (4)$$

Compressive strength test

Fractured specimens resulting from the flexural analysis were then used to derive two specimens measuring 40x40x40 mm^3 each, which were utilized to assess compression strength and water absorption capability. Compression strength was determined using a Controls Automax 50-C52D02 machine with displacement control set at 0.2 mm/s, following the procedure outlined in UNI EN 12390-3:2009 [23]. Similar to the flexural strength evaluation, the values for compression strength (σ) are based on the load applied (F) divided by the surface area (A), as described in Equation 5.

$$\sigma\left(\frac{N}{mm^2}\right) = \frac{F}{A} \quad (5)$$

Healing test

To evaluate the healing abilities of the mortars 3 samples of each type of mortar were subjected to a partial fracture, meaning that a breaking stress of 70% of the full compressive strength obtained on the same day of curing was applied. Partial fracture is a process that induces partial cracks in the sample with the purpose of breaking the polymer capsule containing the binding core, which can initiate the self-repair process of the crack. Therefore, the partially fractured samples were then placed in a repair environment at an average temperature of 22°C and 96.5% of relative humidity. After seven days, the samples were subjected to full fracture at 100%, thus obtaining the compressive strength value of the self-repaired sample.

4.5.5 Assessment of the compatibility of ancient mortars and new pastes

Compatibility is a key parameter to take in consideration during restoration phase. Indeed, the compound used for the restoration process and the substrates must to react similarly from the mechanical point of view, considering the interaction that will undergoes between the restored substrate and the material applied. Despite the fact that in their composition the mortar produced are similar with the ancient material, comparison of elemental analysis conducted was performed. Furthermore, in order to effectively test the mechanical compatibility, test for the evaluation of mechanical properties were performed both on ancient fragments and new mortars. Because of the small amount of material from original Roman mosaic, analysis that necessitates of small quantity of specimens were used such as the micro-indentation and the micro-compression. Thus, a downsizing of specimen of the innovative mortars produced were performed in order to have specimens of comparable dimensions to the one of ancient mortar.

Micro indentation analysis

Local mechanical properties were characterized using a micro hardness test on an Anton Paar MicroCombi scratch/indenter system equipped with a Vickers tip. The measurement give back curves corresponding both to the loading and unloading measurement, displaying the indentation force apply versus the depth reached by the tips in the surface. The maximum load applied was 10 N, at a rate of 10 N/min, and removed at 20 N/min, with a dwell time at maximum load of 15 seconds. Due to the high roughness of the samples, traditional visual analysis of the Vickers imprint was impractical. Instead, hardness (H) was calculated from the unloading curves using the classical Oliver & Pharr method [244]. The method considers the maximum load applied (Pmax) to a real area of contact of the tip with the analysed surface (A) as reported in Equation 6.

$$H = \frac{P\,max}{A} \qquad (6)$$

Two specimens of each material were analysed performing at least 10 measurements for each surface.

Micro compression analysis

Micro compression test was performed using an Instron 3365 dual-column dynamometer, equipped with a 2 KN load cell. The analysis were performed on small prismatic samples (about 8*8*5 mm^3) at least three specimens for each material were tested.

Load was applied at 1 mm/min rate, and tests were interrupted when a drop in load indicated fracture of the sample, or, in the case of non-catastrophic failure, when a deformation of 30% was reached.

From the stress-strain curves achieved, compressive strength value is acquired from the maximum of the curves, while Young's modulus was extracted from the initial, linear, region of the curve.

4.6 Results of mortars analysis

4.6.1 Evaluation of the workability of mortar pastes

All the test of workability were made in triplicate, average of the achieved results are reported in Figure 59. The standard deviations of all the results are around 30%.

Considering the nature of the binder used it is necessary to make a premises. NHL allows, differently respect to slaked lime, to have a greater control of the fluidity. Slaked lime has a natural water of hydration and a greater capacity to retain it, avoiding controlled modification of workability. Accordingly, mortar Y has greater workability respect to mortar X. As clearly visible in the histogram, substitution of Nopal gel to water in both the mixtures (added in the same quantity) improves the workability, YN has the greatest value respect to all the mixtures.

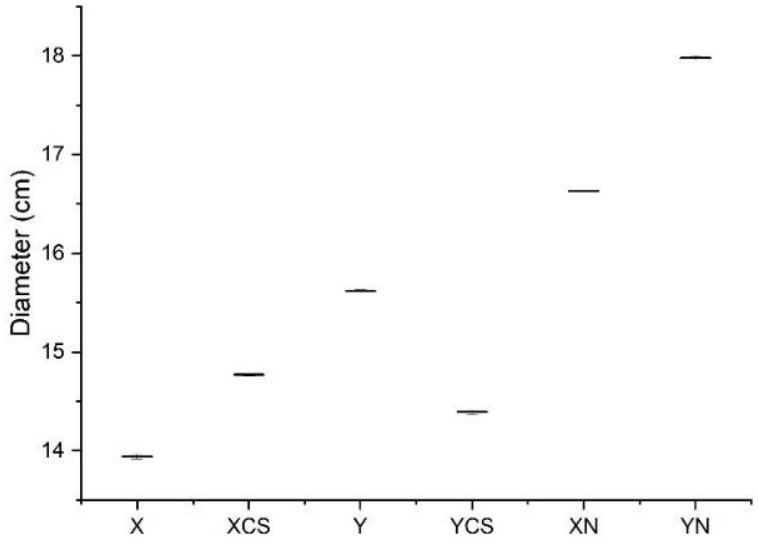

Figure 59 Results of workability expressed in diameter achieved by each mortar.

In order to have a clearer vision of the effect of the additives on X and Y in

Table 10 are reported the results of change expressed in percentage. Moreover, considering the passage of time from the begging of the casting, when the mortar is fresher, and the ending of this process, mortar is subjected to drying process that reduce its workability. Thus, evaluation in the change of the workability of the pastes from the beginning and the end of the process is also reported expressed in %. Nopal increases the workability of 19% and 15% respect mortars X and Y. CSMMA increases the workability of mortar X in lower quantity of 6%, but it decreases the workability of Y of 8%, indeed this paste was stiffer in phase of production. Indeed, during the

test water came off from the mortar if pressed. Passage of 50 min of time induce a decrement of the workability of all of approximately 8% to 10%. Hardening of mortar is fast inducing a strong decrement of the fluidity and possibly the necessity to add more water in order to have an enough workable paste. Self-healing material does not change the workability.

Table 10 Evaluation of flow table test results.

Mortar	Before casting diameter (cm)	Std. dev	After casting diameter (cm)	Std. dev	Change in diameter (cm)
X	13.9	2%	12.8	2%	1.1
Y	15.6	1%	14.2	1%	1.4
XN	16.6	2%	15.2	3%	1.4
YN	18	2%	16.7	2%	1.3
XCS	14.8	2%	13.6	3%	1.2
YCS	14.4	2%	13	3%	1.4

Effect of the addition of Nopal gel to mortar pastes

Investigation of the effect of the increment of quantity of Nopal in mortar for the modification of the fluidity was investigated (Figure 60). Each result is the average of the results achieved by the repetition of the test for three time. A quantity of 1 kg of mortar X and Y were prepared and their fluidity property was tested. Rate of 25 ml of Nopal gel was added subsequently to the initial mixtures, and the test was repeated after each addition.

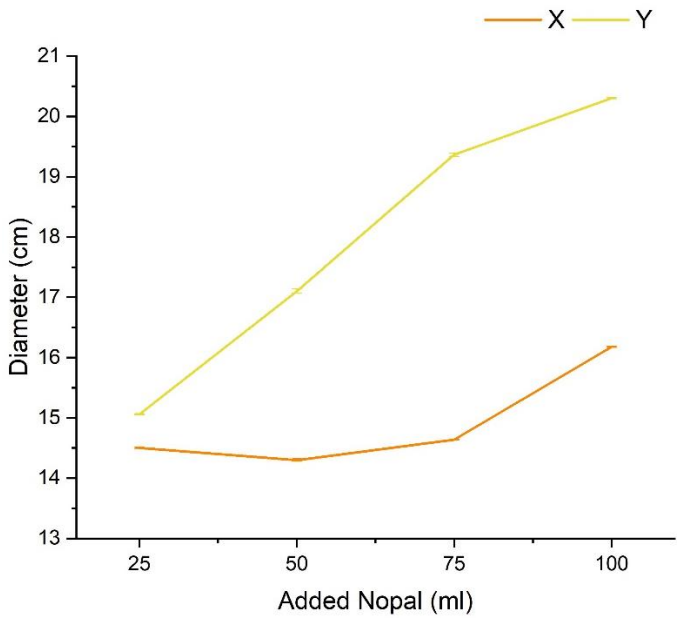

Figure 60 Plot of data of evaluation of increment of fluidity of mortar to parity of addition of Nopal gel to the paste.

Increment of the fluidity with the subsequent additions of gel is quite constant for both mixtures. Addition of increasing quantities of Nopal to mortar X shows a linear increment of workability at increasing addition of gel.

4.6.2 Morphological

Microscopic analysis

Evaluation of the morphology of the specimens was made using optical microscope. In Figure 61 are reported images of the external surface of mortar cubes. Microscopic observations of the surface of the specimens show similarity of the texture. As is possible to see mortars produced with slaked lime X, XN and XCS show generally a greater presence of cracking. Generally, no huge colour differences are visible comparing the surfaces of the specimens made with the same binder.

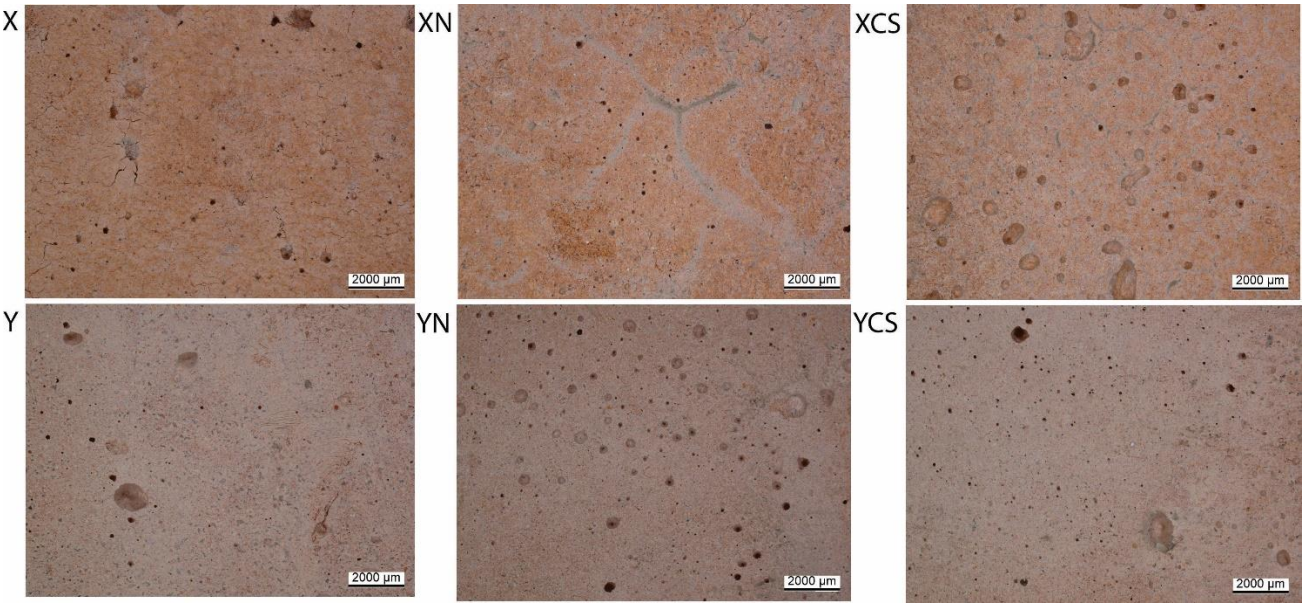

Figure 61 Microscopic images of the surfaces of mortar specimens.

Investigation performed with greater magnification, shows presence of particular elements for mortar containing Nopal. Presence of white saline like structures (Figure 62A), Presence of vegetable fibre (Figure 62B), presence of thick white patina, particularly accumulated and visible on edges of the specimens (Figure 62C).

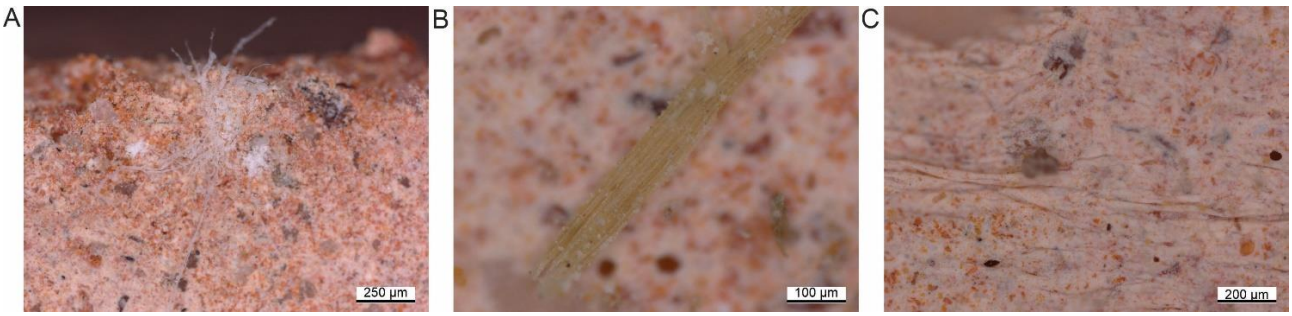

Figure 62 Images of the external surface of mortar with Nopal: A) YN efflorescence, B) YN fibre of Nopal, C) YN Nopal patina.

Internal surface of specimens was exposed after compressive strength analysis and was analysed in order to see the internal side of mortars cube. As visible in Figure 63, no differences are present in the morphology of specimens.

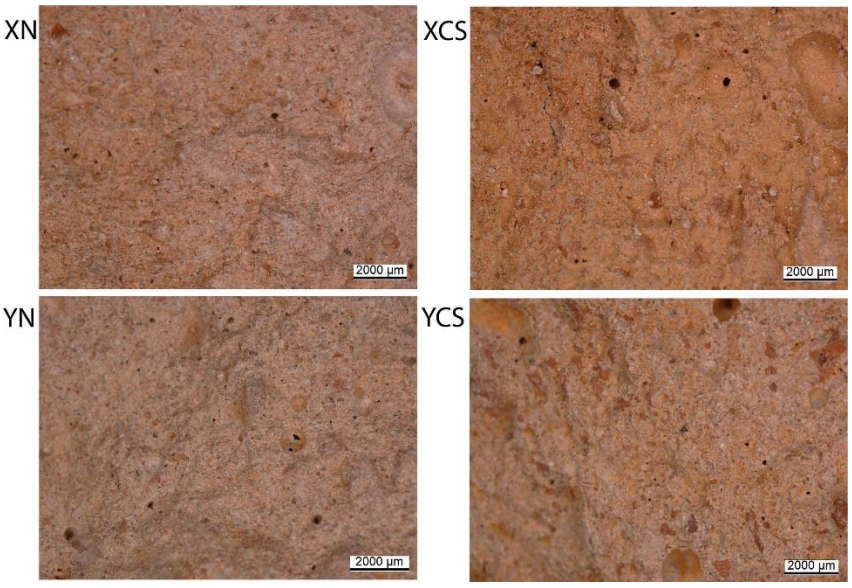

Figure 63 Microscopic images of the internal side of mortar specimens.

From microscopic evaluation of the internal side, all the specimens show the same morphological characteristics, with the presence of white and orange efflorescence uniformly distributed. The only visible difference is noticeable thanks to the increment of magnification. A thick white patina, slightly present inside voids in mortar Y and YCS is particularly present in mortar YN (Figure 64).

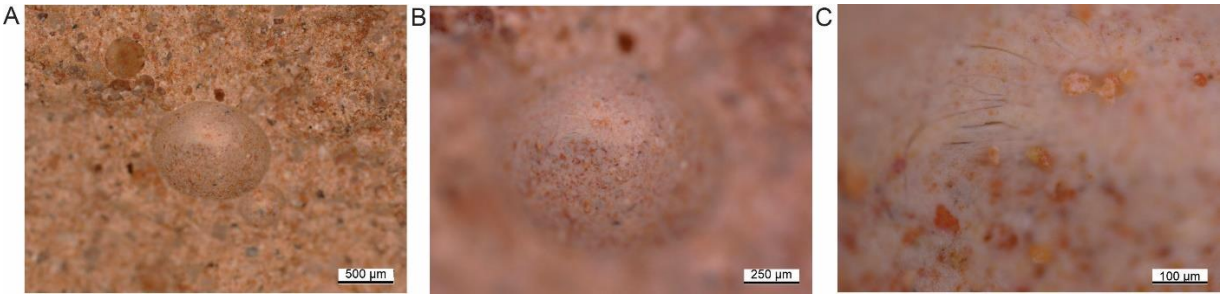

Figure 64 Microscopic images of the white patina present inside mortar YN

Colorimetric analysis of the mortar

Colorimetric analysis was performed on external surfaces of each specimen. In order to avoid bias the analysis were performed in area without holes. As possible to see in the graph (Figure 65) all the mortars show a similar spectra. Mortar X is the only one which show a slightly darker tonality, possibly due to the presence of pores on the surface that cannot be avoided in phase of analysis. This equality of the parameter recorder indicates that the colour of these mortars is not affected by the change of binders, neither by the addition of additives or by the substitution of water with the natural gel.

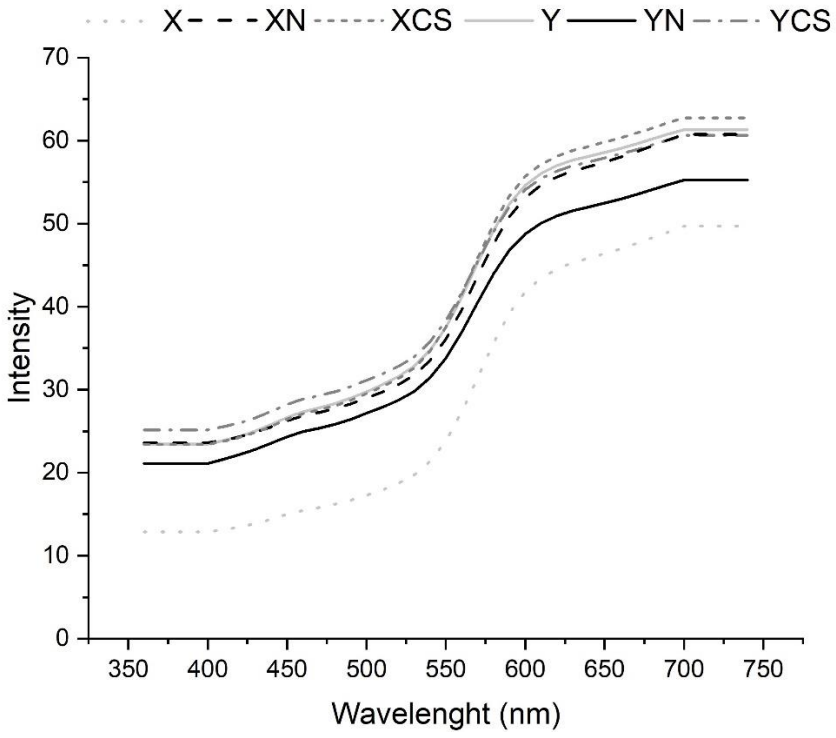

Figure 65 Colorimetric spectra of each specimen of mortar.

Micro and macro porosity of the mortars

From the application of MIP analysis it was possible to assess the porosity of the designed mortars. In Figure 66 are reported the plot of the results achieved from MIP analysis of the evaluated surface area and the average pore radius.

Greater pore surface area was recorded for mortar XCS and X, that are charaterised by similar results (19.9 m^2/g and 18.8 m^2/g, respectively). Thus in this case the addition of self-healing compound didn't change the property of the mortar, according to the compression and flexural strength analysis.

Differently, mortar YCS and Y show complete different results of surface area (15.8 m^2/g and 11.3 m^2/g, respectively) possibly indicating the effective change of porosity induce by additive addition. Also the use of *Opuntia ficus indica* gel shows contrasting results bringing to the improvement of surface pore area for mortar with NHL, thus in mortar YN (14.8 m^2/g), and a reduction of surface area in mortar produced with slaked lime, thus XN (11.8 m^2/g), if respectively compared to mortars Y and X. This results must to be correlated with the dimension of the pores, indeed as stated by Morgan and Gordon (1970) [245] larger pores have a smaller surface area, while smaller pores have a greater one.

Average values of pore radius has been analysed for each mortar, mortar X is characterised by the lowest pore radius equal to 0.019 µm. Use of *Opuntia ficus indica* gel brings to the improvement of surface area, indeed mortar XN shows the greatest value 0.0369 µm. Differently, mortar YN shows lower value equal to 0.025 µm. Thus, also in this case the use of gel gives completely different results if added to mortar with NHL or to mortar with slaked lime. Similarly, also the addition of self-healing material gives different results. It improves slightly pore radius value for mortar with slaked lime (XCS 0.021 µm), and it reduces it for mortar with NHL, passing from 0.033 µm for Y to 0.022 µm for YCS. Considering this, the results of total surface area and average pore radius can be considered in accordance, assessing the effectiveness of the results achieved.

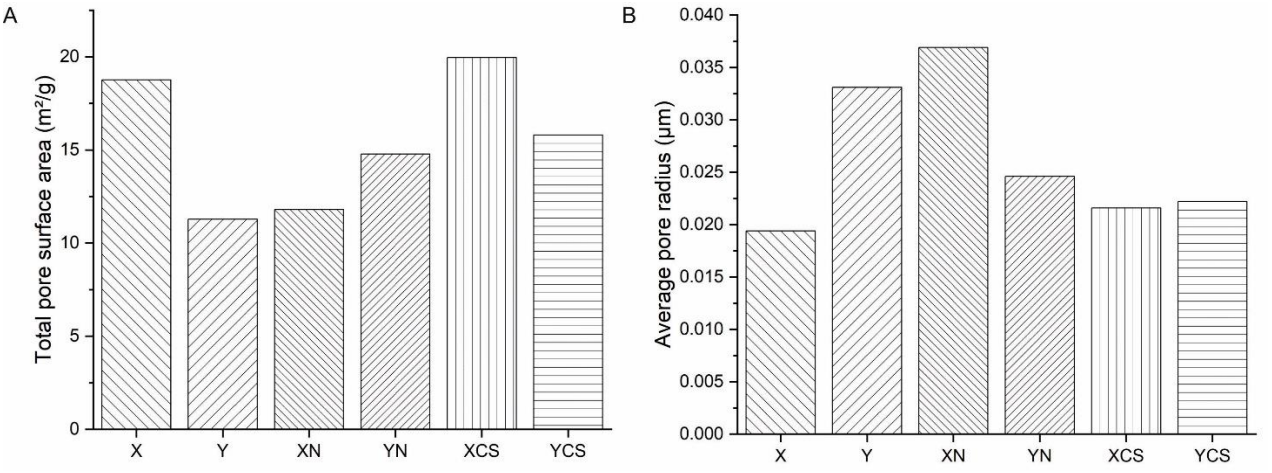

Figure 66 Results of MIP analysis: A) pore surface area; B) average pore radius.

Additionally, the analysis allow the evaluation of the total pore volume (Figure 67). The results indicate that mortars XN and XCS are the most porous (218 mm^3/g and 215 mm^3/g, respectively). The relative starting mortar X, are characterised by porosity value equal to182 mm^3/g. Despite the use of different binder mortar Y is characterised by similar result equal to 186 mm^3/g. In this case both the use of gel or addition of self-healing bring to a slight decrement of porosity (181 mm^3/g and 175 mm^3/g, respectively).

In conclusion it is possible to state that mortar X is characterised by an average values of porosity but the pores with the smaller dimensions. Differently, mortar Y shows a porosity similar to the one recorded for YN, indeed it has the lowest porosity but the biggest pore. Mortar XN is the most porous, indeed it is charaterised by the highest pore radius value.

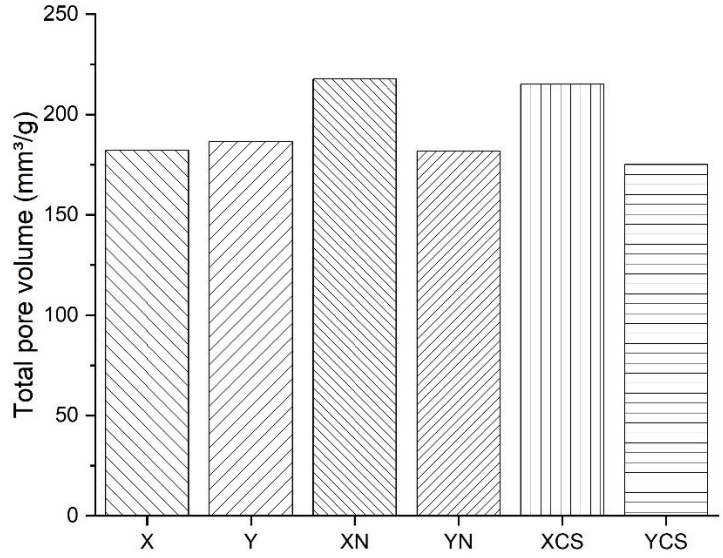

Figure 67 Results of MIP analysis evaluation of the total pore volume.

Thanks to physisorption analysis it was possible to evaluate the presence of the micro and meso pores of the mortars, the curve achieved from the analysis are reported in Figure 68. The curves present hysteresis after 0.4 p/p° typical for plate-like particles or pore network consists of macropores.

Generally, it is possible to assess the absence of microspores to parity to the presence of mesopores indeed for mortars produced with NHL the pore size dimensions fall between 510-586 Å, while the dimensions increase for mortars with slaked lime with dimensions between 780- 860 Å.

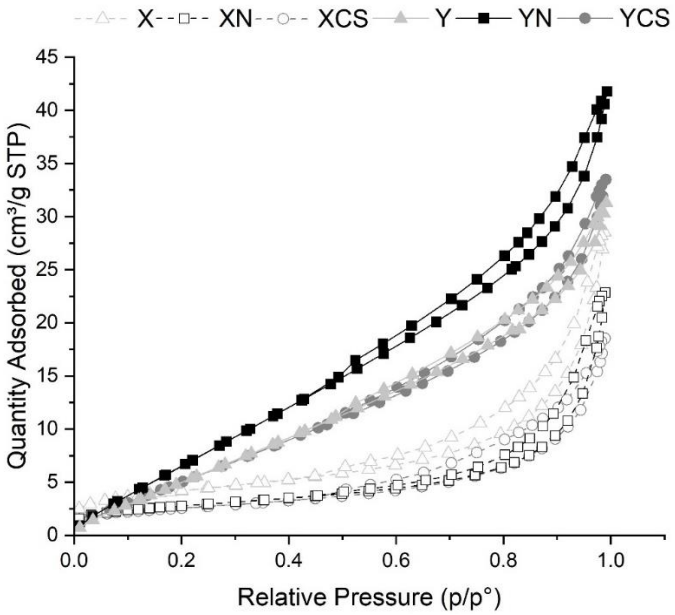

Figure 68 Curve of physisorption of each analysed mortar

In Figure 69 is reported the plot of the surface area results achieved with physisorption analysis.

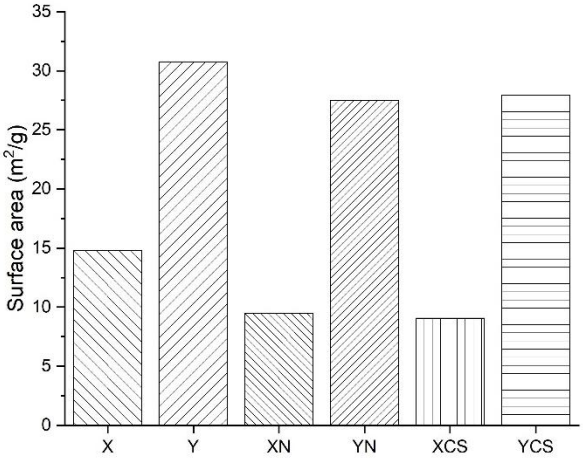

Figure 69 Results of surface area analysed with physisorption of each analysed mortar.

To evaluate the superficial area it was used the BET (Brunauer–Emmett–Teller) theory. It is possible to assess that use of slaked lime induces a reduction in surface area of the mortar (X, XN and XCS) respect to mortar prepared with Natural Hydraulic Lime (Y, YN and YCS). Addition of self-healing material brings to a general reduction of the surface area both on mortar with slaked lime from 15 m^2/g of X to 9 m^2/g of XCS, while for mortar with NHL from 31 m^2/g of Y to YCS 28 m^2/g. Substitution of water with natural gel to mortar brings to the reduction of SA to mortar XN 10 m^2/g and to the improvement to mortar YN 40 m^2/g.

Rate of absorption of water

Results of immersion test applied to cubic specimens of mortars at 28 days of curing are reported in Figure 70. Despite the use of different binders, mortars X and Y have the same water absorption trend, so it is possibly to suppose that the use of NHL for mortar formulation respect the characteristic of porosity of slaked lime based mortars.

Use of *Opuntia ficus indica* gel induces a change of absorption respect to mortar X and Y gaining maximum and minimum values of absorption respectively for mortar XN and YN. Lowest absorption of water, possibly indicates the lowest porosity of the mortars and more compact matrix, thus the use of *Opuntia ficus indica* gel can act as a reducer of water absorption.

Addition of self-healing material induces an increment of absorption to both the mortars, possibly due to the intra-granular spaces formed by the addition of the self-healing which keep the granules separated. Moreover, the self-healing material being composed of Silica can itself absorb water.

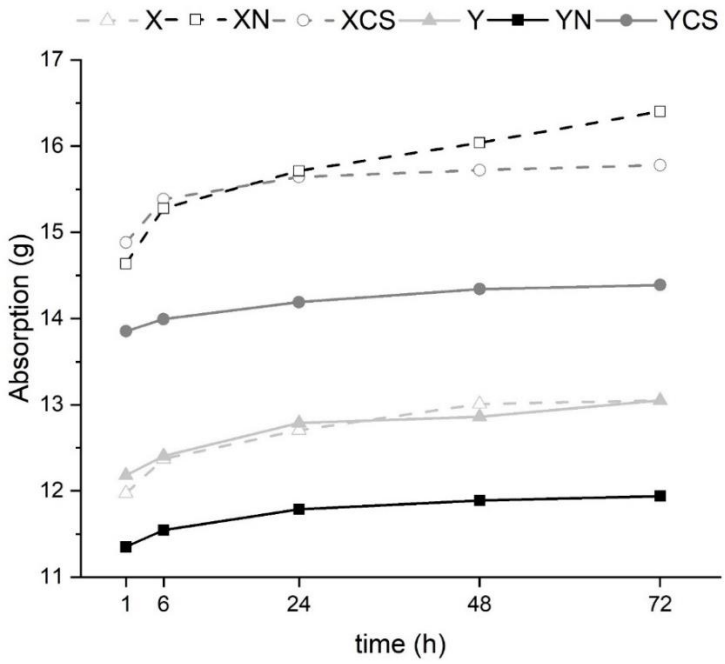

Figure 70 Results of immersion test analysis of mortars at 28 days of curing.

In order to assess the effectiveness of the results achieved both by absorption test and porosimetric analysis they were compared. In theory, we expected that to parity of greater porosity correspond greater absorption. From the results achieved we can define that the results of porosity with the one of absorption are in accordance. Only YCS results less porous respect to the amount of water absorbed. However, these results can be considered good considering the high standard deviation of absorption test.

4.6.3 Chemical

SEM-EDX analysis

Investigation at microscopic level with SEM of the matrices of the mortars, show that are all characterised by the same structure, as visible in Figure 71. SEM-EDX analysis was performed in order to analyse the elemental composition of the mortars, in Table 11 are reported the concentration of the elements with great abundance (expressed in atomic %). Comparing mortars X and Y it is possible to assess the presence of greater abundance of Ca in mortar Y, despite to a greater abundance in Mg in mortar X. This discrepancies can be due to the use of different binders. Indeed, mortar X is composed of slaked lime usually produced with limestone containing dolomitic minerals, while mortar Y is produced with NHL that can be richer in Ca. Comparing mortar XN and YN to mortar X and Y, respectively, the quantity of Ca improve, possibly due to the mineral composition of *Opuntia ficus indica* gel. No particular change in composition can be assessed for mortars XCS and YCS. The drawn conclusions has been drawn considering that the analysis has been conducted on specimens where aggregates and binders are mixed. Thus, further investigations are necessary.

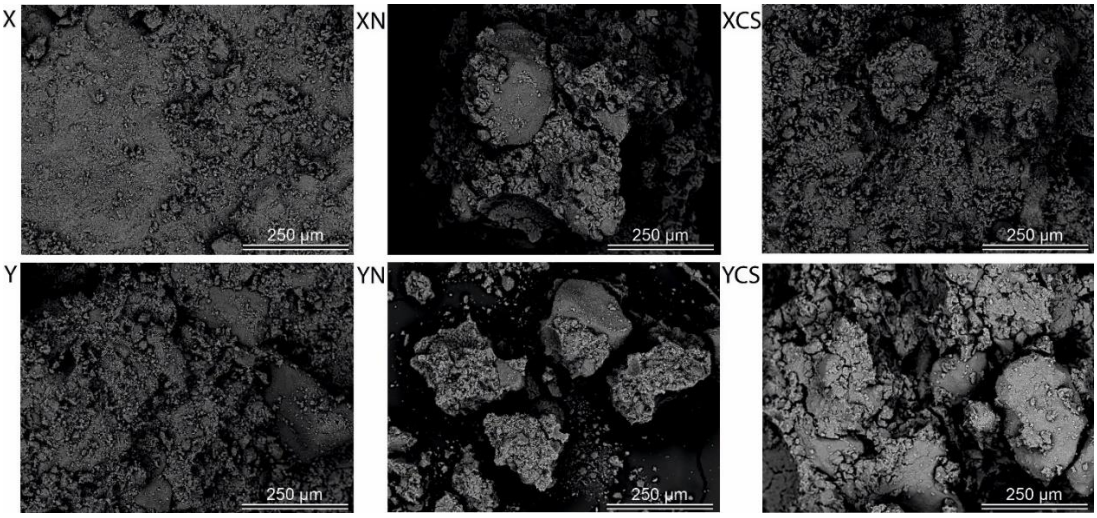

Figure 71 SEM analysis of mortars.

Table 11 SEM-EDX analysis, elemental composition of mortars.

	X	XN	XCS	Y	YN	YCS
Ca (atm %)	24.75	42.58	34.19	57.79	60.29	56.49
Si (atm %)	29.5	29.81	31.93	28.76	27.17	28.13
Mg (atm %)	30.32	13.31	15.99	1.08	1.55	1.69
Al (atm %)	11.32	8.93	10.71	6.49	6.47	8.58
Fe (atm %)	2.55	3.16	3.54	2.47	2.11	2.49
K (atm %)	1.07	1.23	1.99	1.87	0.68	0.82

Application of greater magnification in phase of SEM analysis allows to assess the presence of wire and needle like structures. Wires are particularly abundant, creating intricate structures in mortar YN (Figure 72) and with greater magnification and in smaller quantity are also present in mortar X, Y and XN. Map analysis conducted on mortar YN shows the calcium composition of these structures, as visible in Figure 73. Moreover, the sum spectrum of the area analysed with elemental map demonstrate the presence of silicate and aluminium in the composition. This elements are responsible of the formation of aluminates crystals that are characterised by a typical shape as the needle like one visible in the picture. This abundance can be responsible of the formation of the typical also of the increment of mechanical strength, indeed calcium silica and alumina participate directly to the formation of CASH and CSH structures that are responsible of the improvement of mortar strength.

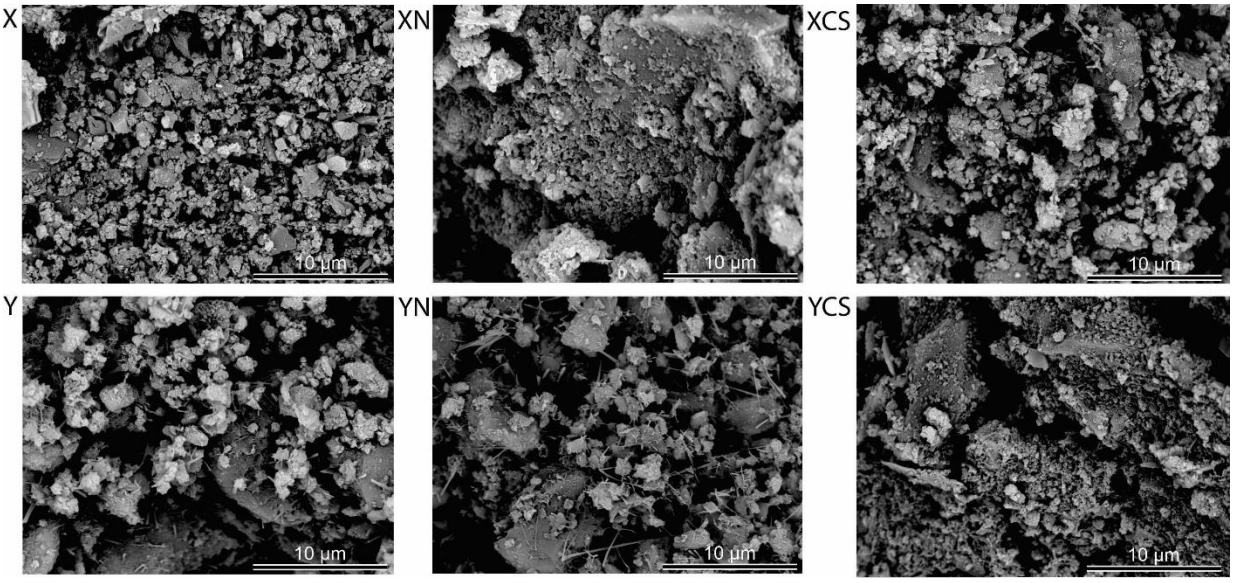

Figure 72 SEM analysis of mortars, with greater magnification.

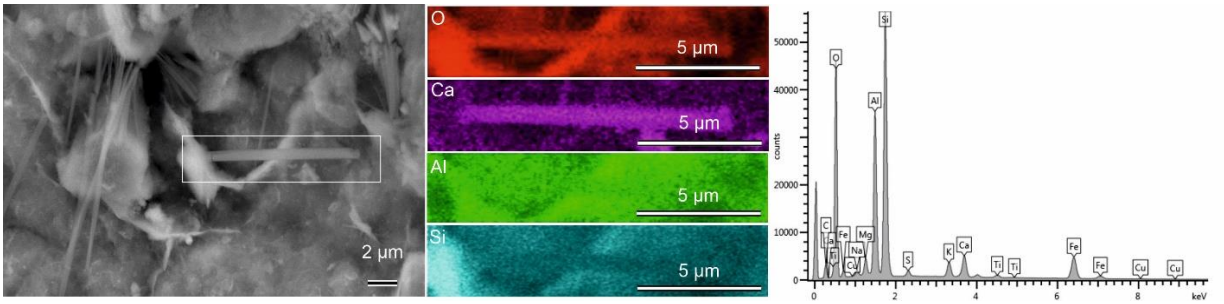

Figure 73 Map analysis of needle like structure of mortar YN.

Characterisation of the produced mortars has been conducted also by the application of XRD, the results are reported in supplementary materials[45] and confirmed what expected.

DSC-TGA analysis

Results of analysis of DSC-TGA of mortars Y and YN are reported in Figure 74. The grey lines represent the calorimetric curves, the black curves are correspondent to the mass variation, and it is possible to see how the decrement in mass correspond to the thermal exchange, indicating the reaction of decomposition. The three curves show equal pattern, with 2 main points of degradation at about 480°C and 800°C, which respectively correspond to the decomposition of $Ca(OH)_2$ and $CaCO_3$. This result highlights that addition of Nopal doesn't cause change in composition, possibly demonstrating that addition of *Opuntia ficus indica* gel to the mortar doesn't change its composition.

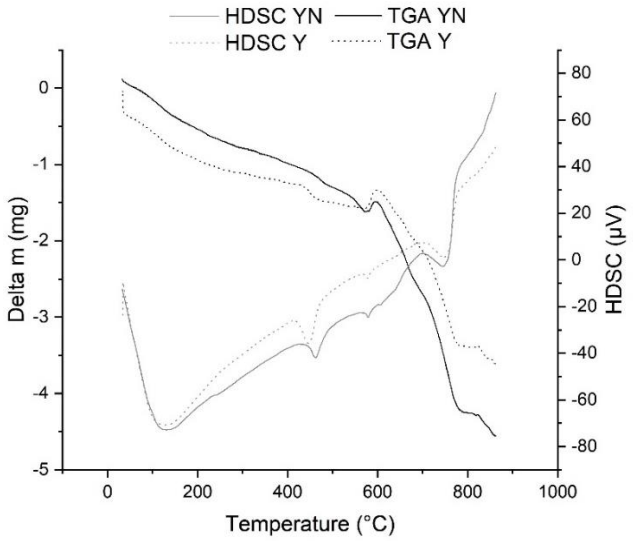

Figure 74 Results of DSC-TGA analysis performed on mortar Y and YN.

[45] For results of XRD analysis please look at Annex_E Further characterisation of prepared mortars.

In Figure 75 results of DSC analysis of mortar Y is correlated with the one of mortar YCS and with the analysis performed on self-healing compound CSMMA. No differences can be evaluated between Y and YCS, and also CSMMA is characterised by a similar pattern, which indicate the decompositions of $Ca(OH)_2$ and $CaCO_3$ respectively at 480°C and 800°C.

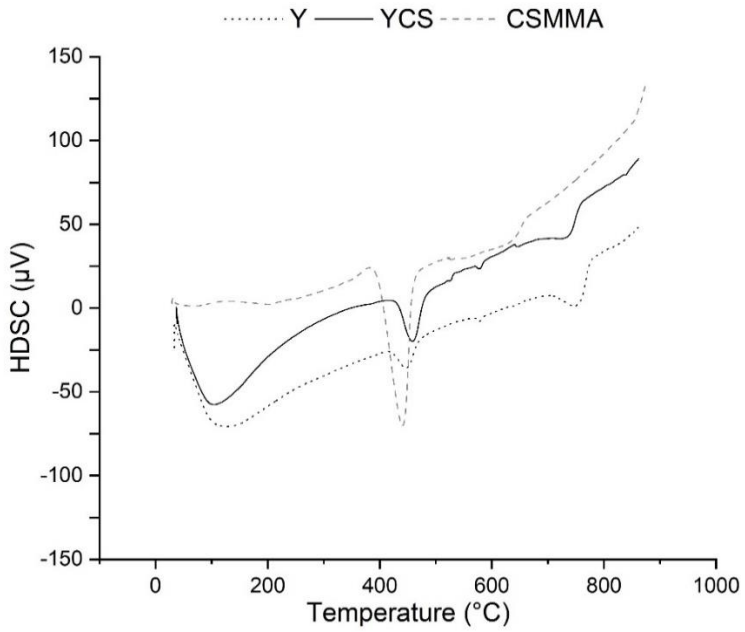

Figure 75 Results of DSC-TGA analysis performed on mortar Y and YCS.

4.6.4 Mechanical test

Evaluation of the flexural strength

Flexural analysis was conducted on prismatic specimens at different curing time in change of flexural modulus along hardening phase, the results are reported in Figure 76. The results allow to evaluate if change in binder and presence of additives in composition can produced changes of flexural strength.

Generally, it is possible to state that all the mortars prepared with NHL as binder (Y, YN, YCS) are characterised by greater *ef* respect to mortar prepared with slaked lime. At 89 of curing mortar YCS shows the greatest flexural strength, thus it is possible to assess that the flexural strength of Y (0.41 N/mm^2) increases by adding CSMMA (0.57 N/mm^2). However, this results is not in line with what expected, as it could be due to a possible premature reaction of the self-healing material. Differently, mortar XCS has similar results achieved with mortar X, with a slight increment along

hardening time and reaching similar plateau values (0.19 N/mm^2 and 0.17 N/mm^2 respectively at 89 days of curing). This can indicate that, differently from mortar with NHL, the self-healing additive stay unreacted, being not released.

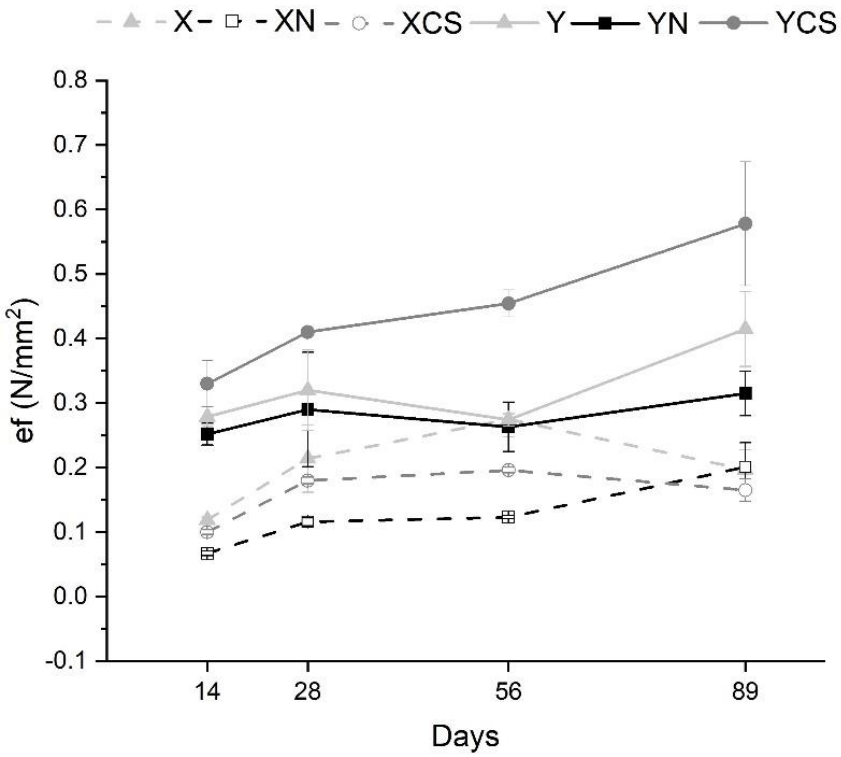

Figure 76 Variation of values of module of flexural strength during curing time.

Mortar YN demonstrates greater results respect to mortar XN (0.31 N/mm^2 and 0.20 N/mm^2 respectively, at 89 days), this difference in results can be solely related to the use of different binders. NHL mortars undergo hydraulic reactions that contribute to early strength gain and higher final strength. This hydraulic setting results in a denser and more cohesive matrix, which resists flexural stresses more effectively than non-hydraulic, slaked lime mortars.

Flexural strength of mortar XN is lower, both at 14 and at 28 days, respect to mortar X, but reach a higher value at 89 days of curing, possibly indicating that use of Nopal produced an increment of time of hardening. Differently for mortar YN, the gel induces only a slight reduction of *ef* value that, considering the standard error, can be define as absent.

Compressive strength test and evaluation of the Young Modulus

In Figure 77 are reported the results of compression achieved by the analysis of the mortars during curing time.

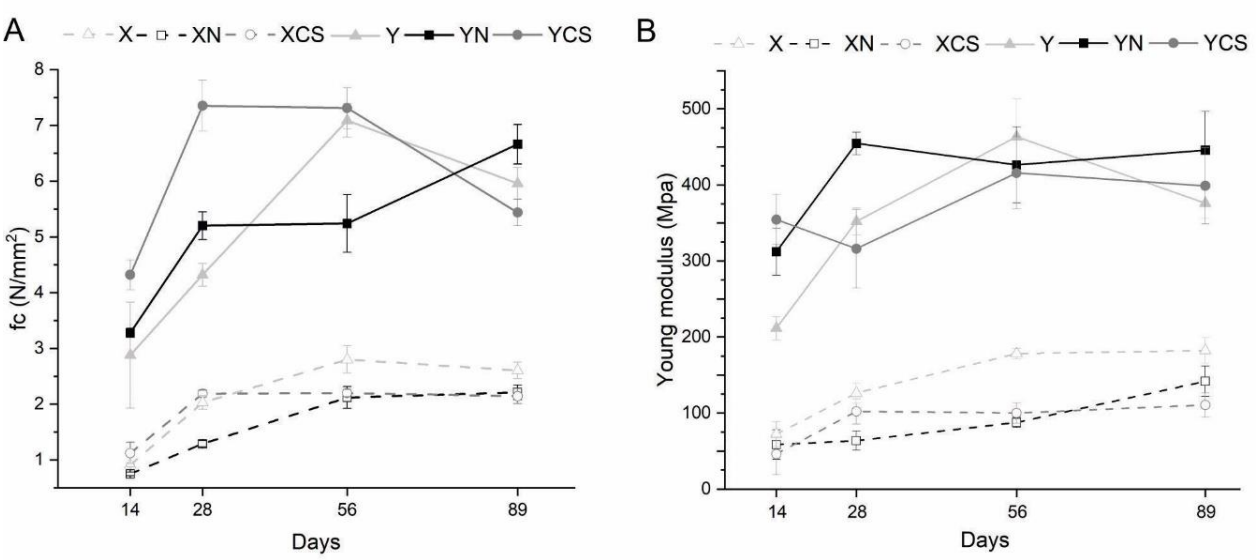

Figure 77 Compressive strength results at different days of curing: A) Compression; B) Young modulus.

Results of compression test of mortars X e Y are in accordance to results of flexural strength. Indeed, at 89 days Y reaches greater value of compression strength respect to X (respectively of 5.96 N/mm^2 and 2.61 N/mm^2), and generally all the mortar produced with NHL 3.5 as binder show greater compression strength values respect to slaked lime mortar based one. Elastic modulus was evaluated from the results achieved with compression strength, and as it is possible to see in the graph (Figure 77B) the results follow similar trend to compression one. X has a low increment of the value from 28 to 89 days of curing (126 MPa and 182 MPa respectively), the same trend is recorded for mortar Y, but it reaches greatest values at the same curing time (351 MPa and 376 MPa respectively).

As for flexural strength also in this case mortars X and XCS show similar trend having a low increment of value along the hardening time. Mortar with self-healing shows a slow initial increment of *fc* value at 14 and 28 days that considering the standard deviation can be considered equal to the value reach by X. The compression strength of XCS reduced slightly respect to mortar X between 28 and 89 days of curing. Nevertheless, at 89 days of curing the mortars show similar compression strength values equal to 2.61 N/mm^2 for X and 2.14 N/mm^2 for XCS. The slightly lower compressive strength of XCS might suggest that the self-healing additives remain inert and act as inclusions within the matrix. Also in this case, elastic modulus obtained are in line with the one recorded for compressive strength test. XCS reach a plateau after 28 days and has the lowest value of Young modulus (110 MPa).

Mortar YCS shows a sudden strong improvement of compression values at 14 days, but along the curing time it reaches a plateau value of 398 MPa.

By the comparison (Figure 77A) of results achieved with mortar X and Y to respectively XN and YN it has been pointed out that mortar YN, reach the greatest value of compressive strength at 89 days of curing respect to all the mortars. Indeed, the addition gel induces an increment of the 14% to the compressive strength at 14 days, and of 16% at 28 days for mortar prepared with NHL binder. Differently, in mortar with slaked lime, after an initial reduction of the value of compression, mortar XN reach similar value to mortar X (2.21 N/mm^2 and 2.60 N/mm^2 respectively at 89 days).

Evaluation of the elastic modulus (Figure 77B) shows that the value increase constantly for mortar XN, however being less elastic respect to mortar X. Mortar YN is the one that reach the greatest value among all the mortars, along the hardening time and reaching at 89 days 445 MPa.

Healing test

Evaluation of the healing properties was conducted on all the mortars. However the test was mainly focused to evaluate if self-healing additive CSMMA produced can impart healing properties to the mortar. The results of this test were negative demonstrating the absence of healing behaviour of the mortar. The negative result of healing tests together with the compressive tests let to suppose that the self-healing compound was already reacted inside the mortar during the curing.

The different influence on the compressive test of the self-healing material depending also to the binder used for mortar production related to the nature of the core of the additive.

It can be assumed that, rather than remaining dormant until the time of damage, the self-healing additives participated in the hardening reaction in the case of the NHL mortar. This is likely due to an incomplete coating process.

With slaked lime, the presence of water and the availability of CO_2 possibly favour the sudden reaction, and the subsequent formation of carbonate, within the 28 days of curing, of the additive in the mortar, without imparting any kind of change to the mortar. Moreover, effect of the improvement of strength imparted by CSMMA is less visible with slaked lime.

Further investigation need to be conducted in order to optimise the process of encapsulation of the self-healing agents.

4.6.5 Mechanical compatibility of ancient mortars and designed pastes

In order to assess if the designed mortars are characterised by similar mechanical characteristic respect to the ancient one (labelled as M), micro indentation test and micro compression test has been conducted on small mortar fragments of both new and ancient material.

Micro indentation analysis

Figure 78 reports the force-displacement curves achieved from the micro-indentation test which can give information about material behaviour at micro level. Irregularities in the curves can be due to large voids or cracks that can be present on the mortar surface, while discontinuities of the curves can be due to the cracking of the surface while the force-driven indentation tests is applied. The curve of M is similar to the curves obtained with mortar XN, YN, and Y, demonstrating similar behaviour under indentation test. Differently, mortars YCS, X and XCS show different behaviours where the curve of mortar YCS is typical of hard material. From the analysis it was possible to quantify values of hardness of the analysed surfaces applying Oliver and Pharr method.

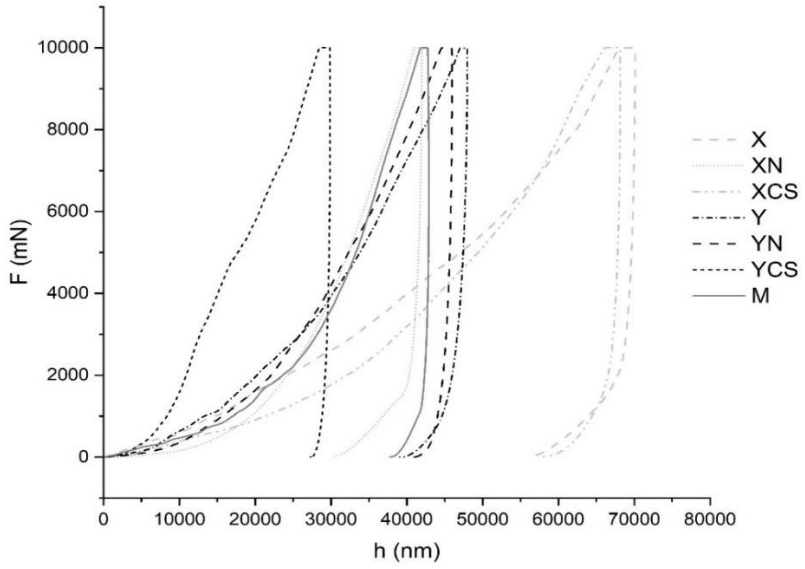

Figure 78 Curves of micro indentation test results for new designed mortars and ancient mortar.

Ancient mortar "M" is characterised by value of hardness equal to 203 MPa ± 14 similar to mortar YN (186 MPa ± 20), considering the standard error the two mortars can be considered characterised by equal hardness value. Also mortar Y show similar result to mortar M with value equal to 183 MPa ± 9. Despite the use of a different binder also mortar XN 238 MPa ± 13 show results in line with the one achieved for the ancient material. A completely different results was achieved by the analysis of mortar X and XCS which are characterised by lowest parameters (both with value ~84 MPa ± 3) of hardness, making them not compatible with the ancient mortar. Finally,

also mortar YCS result to be not compatible from hardness point of view with mortar M, having very high value of hardness equal to 457 MPa ± 35.

Micro compression analysis

Results of micro compression analysis allow to evaluate the parameter of strength of ancient mortar, and to compare them with the results achieved for new developed mortars. In Figure 79 shows that the highest value of micro compression was achieved by mortar Y (10 MPa ± 1.7), which results to be similar to mortar M that is characterised by compression strength value equal to 9.22 MPa ± 1.6. Furthermore, the two mortars M and Y have similar elastic modulus values equal to 212 MPa ± 9 and 204 ± 39, respectively. However, the highest values of Young modulus was recorded for mortar YN that reaches 263 MPa ± 3, similar also to the ancient in term of value of compression (7.6 MPa ± 0.8). Mortar XCS shows value of compression (7.1 MPa ± 0.6) and of elastic modulus similar to ancient mortar. Differently mortars XN, X are characterised by lowest values of hardness (4.1 MPa ± 0.1 and 2.7 MPa ± 0.8, respectively) and of Young modulus (166 MPa ± 9 and 167 MPa ± 23, respectively), being not associable to ancient mortar. Finally, YCS show the lowest value of strength among all the tested mortars. This last result can be considered one outlier, indeed during the process of analysis this mortar bring to the complete failure of the test. This effect can be due to the high value of strength of the mortar that exceed the limit of the instrument. These results reached by the analysis of new mortars align with the results of macro compression, making this test reliable and the correlation between ancient and new mortar extremely valuable. This result is a primary significant result of mechanical compatibility of the innovative mortar with the ancient material.

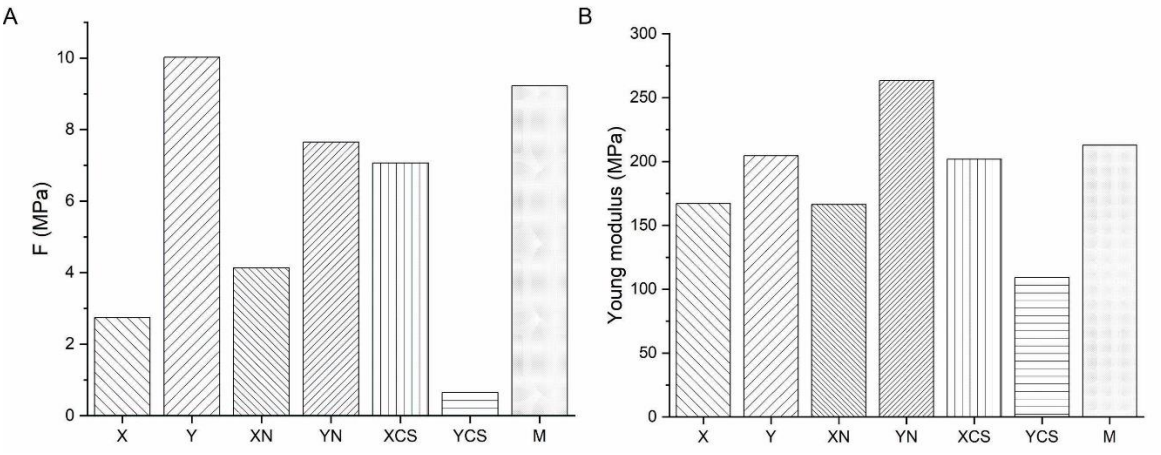

Figure 79 Results of micro compression analysis: A) Compression; B) Yung modulus.

5 Properties of mortar for restoration intervention

5.1 Design of Pull Out Test

The promising properties demonstrated by the mortars, particularly the one of mortar YN, as highlighted in Chapter 4[46], have led to the next phase of the research. As a result, the focus shifted to the final step: testing and evaluating its effectiveness as a restoration mortar.
Adhesiveness is one of the desirable characteristic for mortar used in restoration. The common test present in literature are not feasible to test mortar for restoration of mosaic system. Thus, to evaluate the adhesiveness property a new method was necessary which includes the production of mortar attached to a replica of a *tesserae* and the application of a Tensile Strength Test. For the test was used a Lonos Tenso-Test 5000 instrument with a Maximum Load of 50KN.

The tests were made designing a system similar to a mosaic system compatible with the instrument. The system accounts the nesting of a *tesserae* of mosaic inside the mortar, thus the presence of mortar on the 4 lateral sides and on the bottom side of the *tesserae* considering the characteristic of a real mosaic *tesserae*. Different trial test were conducted in order to reach the best system for the production of this testing method. In

Figure 80 is reported a schematic representation of the type of specimens designed for the purpose of the test.

The following paragraph provides detailed information about the method of treatment and production of *tesserae*, mortars and system produced in order to replicate the characteristics of the materials as closely as possible to the original system.

[46] For more information about the properties of the mortars please look at §4.6 Results of mortar analysis.

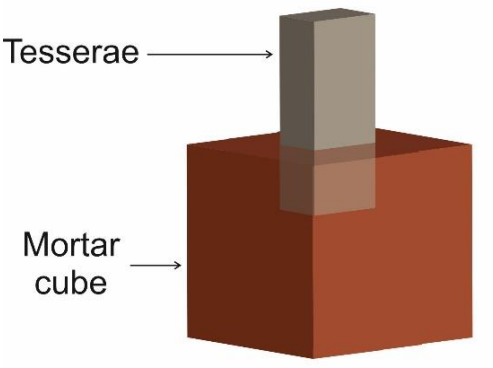

Figure 80 Schematic representation of the produced specimen.

5.1.1 Production of the system

Tessera

The material used for the production of the *tesserae* is quite similar to that identified as the most commonly used in the production of Aquileian mosaics[47], which are the focus of this research. Specifically, a light-coloured carbonatic limestone known as Biancone, sourced from the nearby Aurisina caves, was used. The material was cut with dimension of 15x15x40 mm in order to allow the nesting of the *tesserae* for at least 10 mm and the sufficient dimension to allow the attachment of the tensile instrument.

Ancient stone *tesserae* were split-cut by the Romans, a technique that imparted a rough surface to the *tesserae*. In this context, the roughness of two ancient *tesserae* was analysed using a Digital Microscope (VHX-7000, Keyence) in profilometer mode. Each side of the original tiles was analysed by performing 2 measurements, one with perpendicular direction with the other. In Figure 81 is reported the image of the interface of the instrument in phase of measurement of the material. The analysis of the roughness is conducted along the traced red line along the surface. As a result the software give back the measurement profile, reported in the table (visible in Figure 81), with different values of roughness as the average, the maximum profile valley and the total height profile and other parameters. The results are associated with a 3D image of the analysed portion of the surface and a 2D image with indication of the scan line (in red) along which the analysis is ongoing. On the bottom side are reported the total profile and the roughness profile evaluated along the scan line.

[47] For more information please look at §3.1 Petrographic nature of *tesserae.*

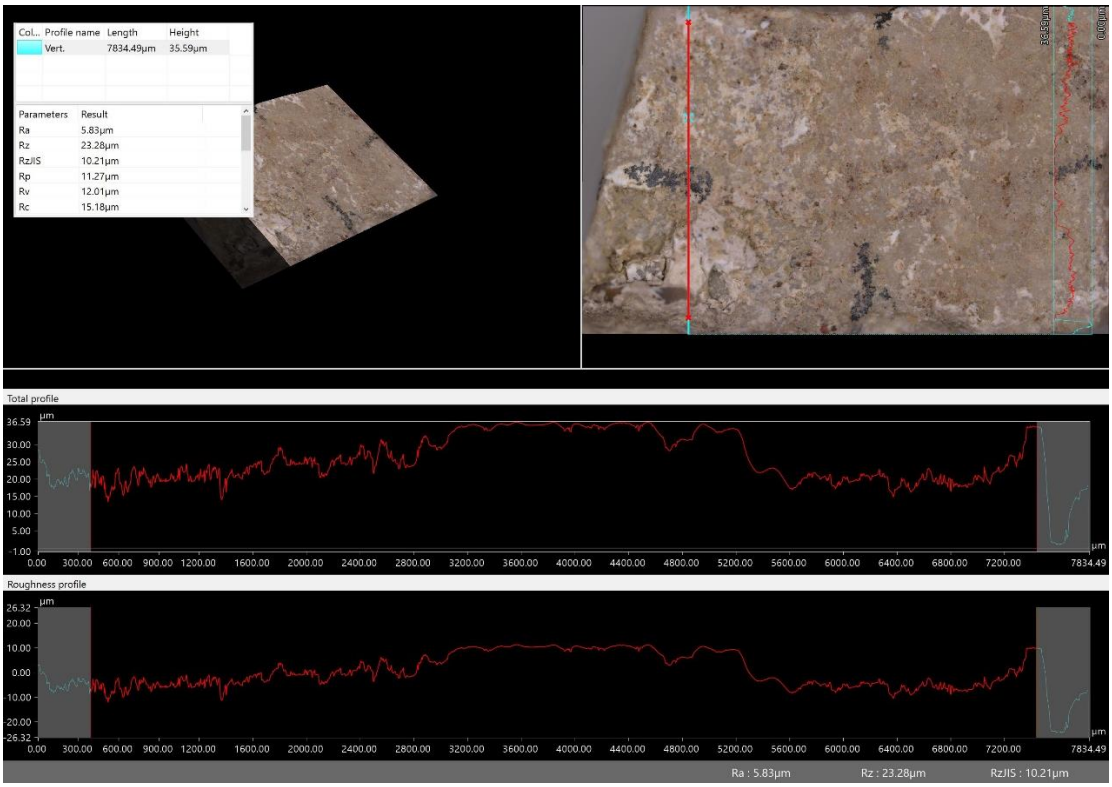

Figure 81 Interface of the results given by the software in phase of analysis of roughness

The average of the results of analysis of the roughness of two ancient *tesserae* are reported in Table 12. The analysis was conducted on three side of each sample, the results are an average of three measurements taken along both the longitudinal and lateral lengths of the *tesserae*. The parameter taken in consideration from the analysis with the profilometer is an average of 10 measurements conducted on the scan line analysed. These results allow us to determine the average level of roughness of substrates of ancient *tesserae*.

Table 12 Results of analysis of roughness of 2 original *tesserae*.

Side	Original 1 (µm)	Original 2 (µm)
1	19.37	3.8
2	15.17	15.17
3	4.92	16.82
Average	13.15	11.93

Subsequently, different type of treatment were performed on trial *tesserae* to achieve a roughness similar to the one of ancient material. The *tesserae* were treated with a sand blaster by changing the type of sand used in the sand and the time of application of the treatment. Then, materials treated following different processes were analysed with the profilometer and compared with the

results achieved by the analysis of ancient *tesserae*. The processing that allow to achieve a compatible roughness with the ancient material was conducted applying the following parameters to treat each side of the *tesserae*:

- sand of dimensions of 0.2/1.5 mm
- for a time of 10 s for each side
- maintaining 100 mm of distance between the needle of the sand blaster and the sandblaster
- moving the needle along the length of each *tesserae*

Casting of mortar and process of nesting of *tesserae*

Ad hoc mould were prepared for the test, in Figure 82 is reported a schematic representation of the mould. The mould has lateral voids that allow the insertion of the *tesserae*. Thus, the produced specimens are cube of 40 mm each side with *tesserae* nested inside.

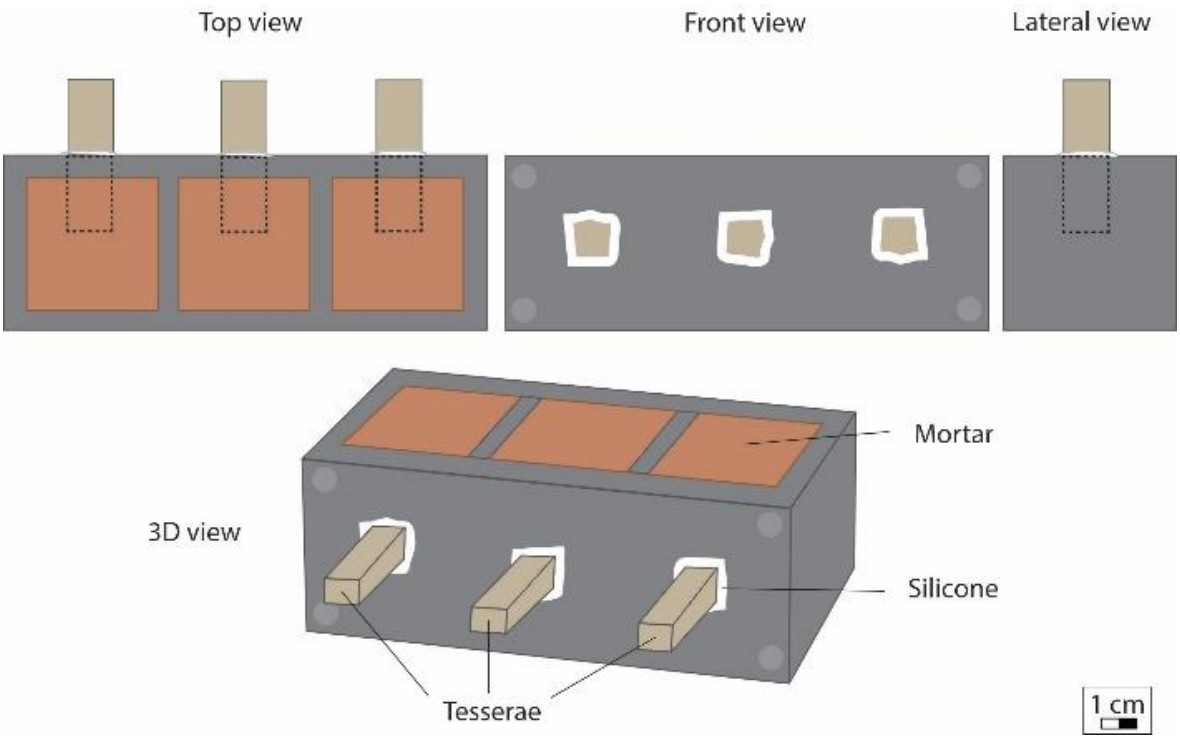

Figure 82 Schematic representation of the designed mould.

After several trial, the best method of embedment was achieved using the following process. As first step, the mould was pre-prepared by positioning the tiles inside the voids to the desired depth and securing them to the sides using silicone (Figure 83A). The use of silicone also helps to prevent mortar spillage from the gaps between the mould and the *tesserae* and keep the *tesserae* fixed to the mould in phase of casting. The *tesserae* were attached to the system in order to allow a depth

of the tiles in the mortar of 10 mm and having an outer length correspondent to 30 mm (Figure 83B). The mortars were prepared following recipes and condition used for the production of specimens of mortars used for compressive and flexural test[48]. Mortars were cast pouring little by little quantity (Figure 83C) and vibrating the mould in order to avoid the formation of bubbles and giving homogeneity to the mortar. The casted mortars were let hardening[48] achieving specimen as the one reported in Figure 83D. The test was designed and conducted for testing 4 out of 6 developed mortars: the two references mortars (X, Y) and the two with *Opuntia ficus indica* gel (XN, YN).

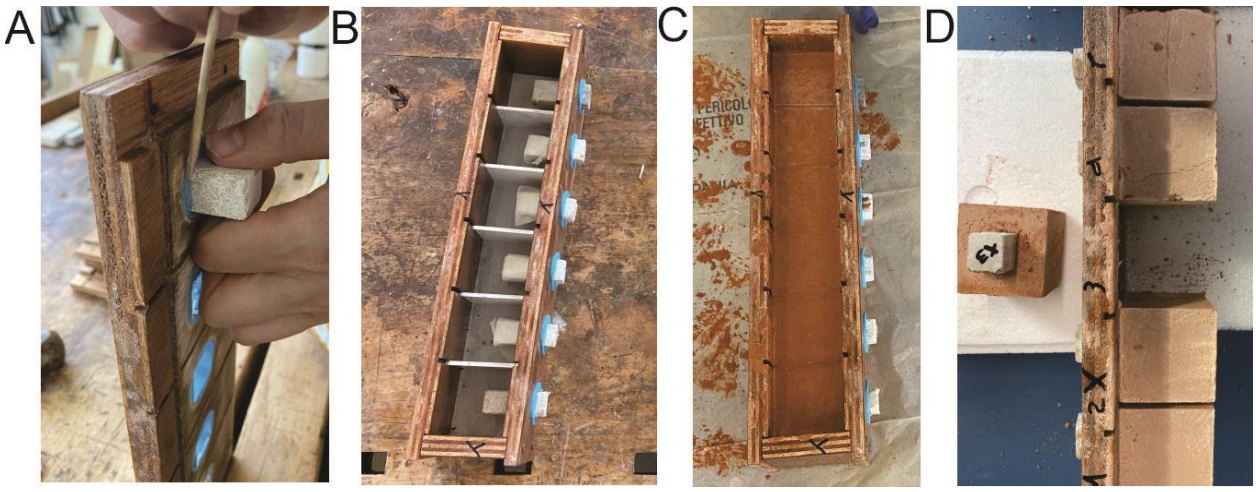

Figure 83 Production of Pull out test specimens: A) *Tesserae* attachment, B) the prepared mould, C) the mould filled with mortar, D) the hardened specimens.

Design of the attachment system for Tensile Machine

Considering the dimensional limit and the type of tensile machine used, an ad hoc system for the attachment of the cube of mortar to the tensile machine was prepared. A scheme of the system designed for the attachment of the mortar cube to the tensile machine for pull out test is reported in Figure 84. The system is composed of an upper plate (Plate 1) that is the point of attachment of the tensile machine, this plate is linked to the *tesserae* slot. Inside this slot the tiles are located and screwed to the system with screw 1. *Tesserae* slot is linked to the below system called cage that is composed of an upper edge of containment of the cube and a lower plate (Plate 2) which are linked with screws (Screw 2). Plate 2 serve to attach the system, thus the specimen, to the plate of allocation of the tensile machine, where the cube will be positioned.

[48] For additional information please look at § 4.4 Mortars production.

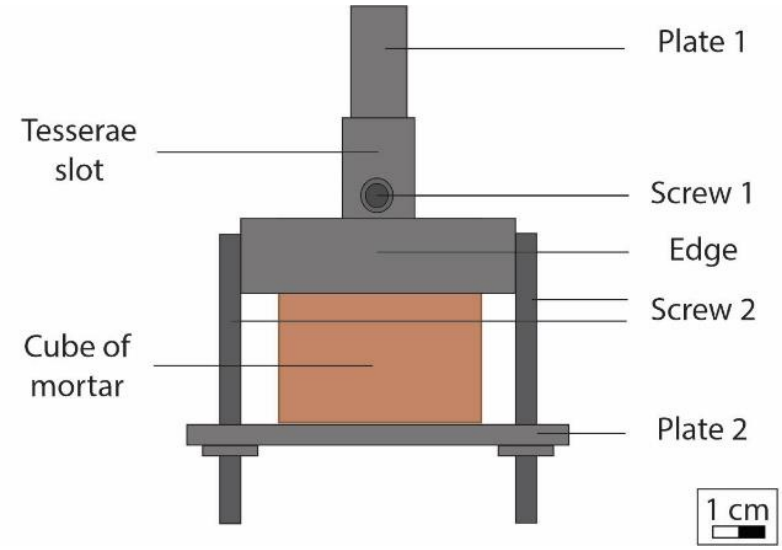

Figure 84 Schematic representation of the cage designed for the Pull out test.

The system was prepared considering that the specimen must to be tied to the lower plate present in the machine and gripped to the clamp present above, thus a sort of cage was prepared. Two metal bars were used in order attach the system to the lower plate. The metal bars are screwed to angular threaded screws that are attached to the upper system. The top part of the system is prepared as a metal cage present a void were the tile come out. The tile is constrained inside a squared tube of metal that envelop it completely and it is attached using 2 screws. The system of constrain of the *tesserae* presents a top metal plate that allows the attachment of the *tesserae* to the clamp of the tensile machine. Images of the system produced and of the system placed on the tensile machine are reported in Figure 85.

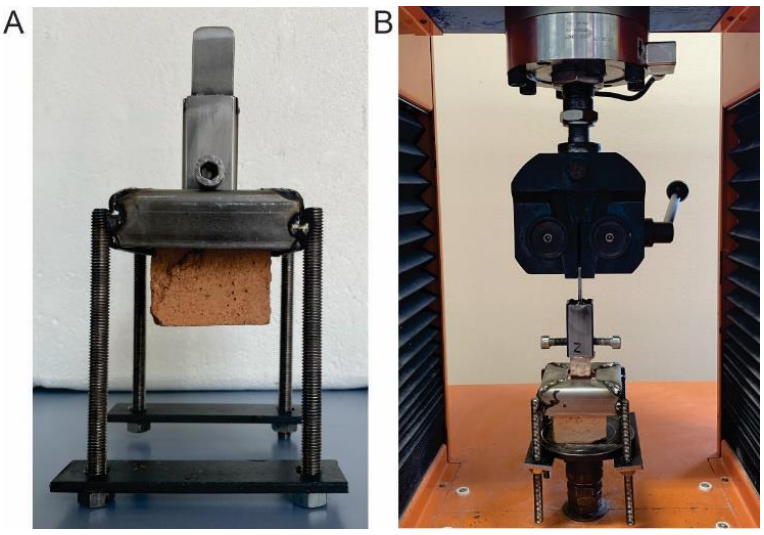

Figure 85 System produced for the pull out test of the *tesserae*: A) the specimen attached to the system, B) the system located in the machine.

5.1.2 Evaluation of the adhesiveness of the mortar

The Tensile Strength Test was conducted after one month of hardening of the specimen. It allows to achieve value of the Maximum Force endured by each sample before the detachment of the nested *tesserae* form the host mortar. The scheme reported in Figure 86 show 3 possible outcomes of the test. In the first case the *tesserae* is still nested inside the mortar without being removed. In the second case the applied force conducted the detachment of the *tesserae* lifting it from its seat. The last scenario consider the breaking of the *tesserae* without its removal from the seat, the *tesserae* still nested partially inside the mortar. The most desirable case is the number 3 because it consider that the mortar has a great adhesive power that did not allow *tesserae* detachment. However, considering our system this scenario can be also due to the presence of the two screws of attachment of the *tesserae* to the external cage. Thus, the rupture can be due to the force applied in the point of contact of the screws.

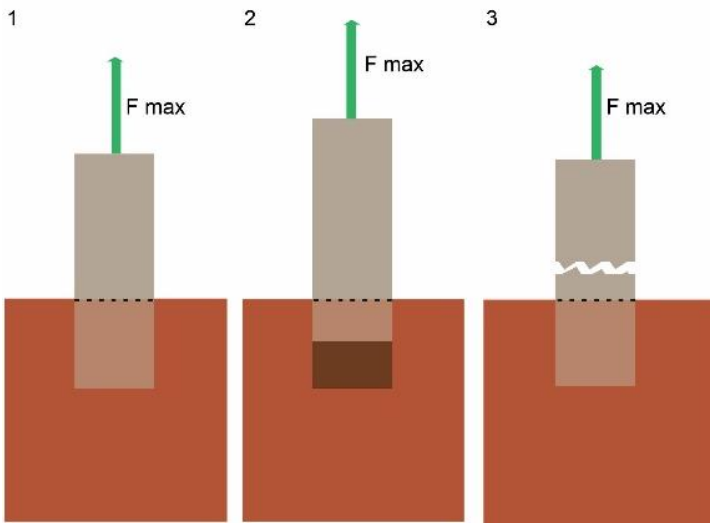

Figure 86 Possible outcomes of the test.

The test was conducted on several specimen for each type of mortars. The results of the measurements conducted on three sample and the relative Coefficient of Variation for each type of mortar are reported in Table 13. From the results it is possible to assess that both mortar with Nopal gel (XN and YN) resist to greater force respect to their counterpart (X and Y). Above all, mortar YN is the one that endured the maximum force before the detachment of the *tesserae*.

Table 13 Results of Pull out test.

Mortar	Sample	F max (N/mm^2)	CoV
X	1	7.89	0.061
	2	2.89	
	3	7.53	
XN	1	8.31	0.005
	2	7.53	
	3	7.59	
Y	1	8.55	0.035
	2	5.72	
	3	12.47	
YN	1	10.90	0.015
	2	8.19	
	3	12.23	

5.2 Simulation of restoration intervention

The results of the pull-out test[49], along with several other tests and analyses conducted[50], have confirmed that mortar YN (made with *Opuntia ficus indica* gel and NHL as binder) is the best among the designed mortars. To evaluate the restoration properties of this mortar, a simulation of the restoration intervention has been performed. Thus, mock-ups of mosaic were produced and, in order to simulate the real state of the art, were degraded using degradation process. The so produced mock ups were then subjected to restoration process, simulating the commonest passages performed for the restoration of mosaic. In order to evaluate if the degradation has effectively impacted the mock-ups evaluation of the Ultrasound Pulse Velocity (UPV) has been applied in order to assess the possible increment of voids and porosity in the mock-ups. The analysis was conducted also after the restoration intervention in order to evaluate if the restoration intervention has been restored the quality of the material in terms of porosity to the original stage.

5.2.1 Production of mock-ups

For restoration test mock-ups of mosaic were produced by masters of *Scuola Mosaicisti del Friuli*. The mock-ups present the same stratification and composition of the specimens produced for the analysis performed with Synchrotron Radiation Tomography[51] but are characterised by greatest dimensions. *Tesserae* are made of black (Figure 87A) and white stone (Figure 87B) and coloured glass (Figure 87C) with variable dimensions from 10 to 3 mm of side.

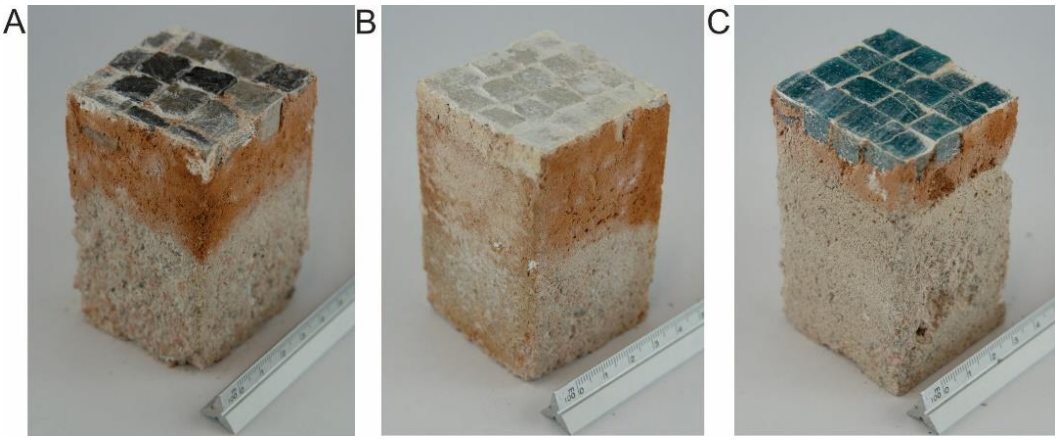

Figure 87 Mock ups of mosaic: A) black *tesserae*; B) white *tesserae*; C) glass *tesserae*.

[49] For more information about pull out test outcomes please look at § 5.1.2 Evaluation of the adhesiveness of the mortars.
[50] For more information please look at §4.6 Results of mortars analysis.
[51] For more information about the composition please look at §3.3 Analysis of mosaic system.

5.2.2 Degradation of mock ups

Degradation of mortars is strictly related to intrinsic aspect of porosity of the mortars and its strength. Thus, evaluation of the degradation effect can contribute to increase the knowledge about the properties of the mosaic system interaction with the environment. The environmental place of city of Aquileia (where the reference mosaic comes from) is a humid area subjected to cycle of frost an thaw that happen along the winter period. These cycles are responsible for the deterioration of mortars and stone [100] and affecting particularly mosaic conserved in situ[52]. Thus, in order to simulate degraded mosaics, process of frost and thaw, cycles of degradation produced in laboratory was applied following UNI EN 12371 [246] on the produced mock ups. A totality of 13 specimens were subjected to the process, 5 made of white stone *tesserae*, 5 with black stone *tesserae* and 3 whit glass *tesserae*. The specimens were selected considering to have specimens with *tesserae* of different dimensions, In order to assess if the change in dimensions of the *tesserae* affect the process of degradation, stone specimens were selected in order to have small (5 mm ± 1 each side), medium (7 mm ± 1 each side) and large size (10 mm ± 2 each side) of the *tesserae*. The specimens were immersed in water for 48 h, in order to achieve complete imbibition. Then, 13 cycles were performed each including frost in air and thaw in water. For time constrain, differently from what reported in norm, changes of time of each cycle were applied: frost in air was conducted for 8 h and thaw in water for 14 h.

In Table 14 are reported information about the name of the mock ups, the type of *tesserae* that compose it (material, colour, dimensions), and the number of cycles of degradation endured by the mock-ups.

Table 14 Information of the degraded mock ups.

Name	*Tesserae*	n. cycles	Effect
M1	Stone, black, medium size	13	Loss of majority of the *tesserae*, N mortar fragmentation
M4	Stone, black, medium size	13	Loss of few *tesserae*, big fractures in N *stratum*
M5	Stone, black, small size	13	Loss of few *tesserae*
M8	Stone, black, medium size	13	Loss of few *tesserae*, disruption of R that avoid specimen to stand up
M12	Stone, black, big size	7	Loss of some *tesserae*
M16	Stone, white, small size	13	Loss of few *tesserae*, big fractures on N *stratum*, disruption of R
M17	Stone, white, medium size	13	Loss of few *tesserae*, disruption of R
M20	Stone, white, big size	6	Loss of all the *tesserae*, N *stratum* partially lost

[52] For more information about degradation phenomena of mosaic please look at §2.3.1 Conservation procedures of mosaic.

M22	Stone, white, medium size	6	Loss of all the *tesserae*, N *stratum* fragmented and partially lost
M26	Stone, white, medium size	8	Loss of few *tesserae*
MV1	Glass, green	4	Complete detachment of N from R *stratum*
MV2	Glass, purple	3	Detachment of all the *tesserae* from N, loss of some *tesserae*, big fracture in N *stratum*
MV4	Glass, mix of colour: green, purple, blue	3	Loss of the majority of the *tesserae*, partial loss of N *stratum*

From the results, no correlation can be assessed between the number of cycles endured by the mock-ups and the dimensions of the *tesserae*. Nevertheless, glass mosaic degraded before stone one, thus a correlation with the material can be assessed. Indeed, after few cycles the glass *tesserae* were detached and in some cases also the complete detachment of *Nucleus stratum* (

Figure 88). This different behaviour of stone and glass *tesserae* to the process and their detachment was not expected considering the tomography results of analysis that show the greater presence of fractures below stone *tesserae*[53]. This results of degradation highlights that system of attachment of stone-mortar is stronger respect the glass, possibly due to the roughness of the *tesserae* surface.

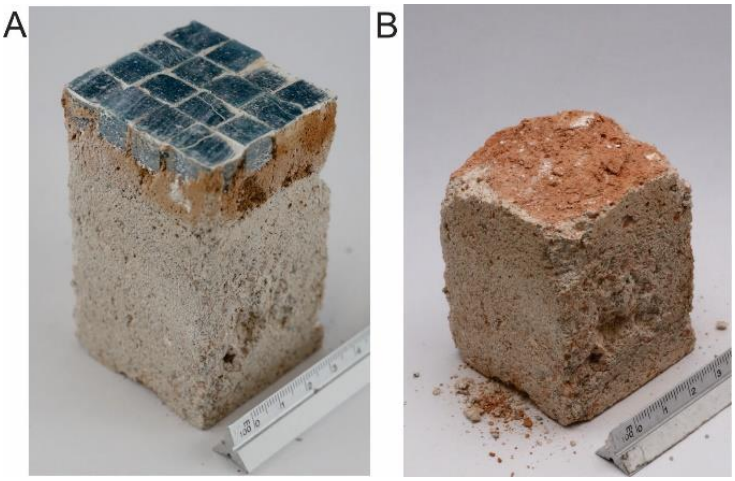

Figure 88 Specimen MV1 before and after degradation process.

The images allowed to assess how degradation affects different mortar *stratum* in varying ways. For instance, in Figure 89, the decay process has caused the disintegration of the *Nucleus*, leading to its partial loss and the complete detachment of *tesserae*, while the *Rudus stratum* remains largely intact. This variation in response to decay can be attributed to the porosity of the mortars. The *Rudus* layer, being more porous with larger voids, as previously demonstrated[53], allows water to

[53] For more information please look at §3.3 Analysis of mosaic system.

enter, pass through, or freeze without causing damage because there is sufficient space for expansion. In contrast, the *Nucleus*, with its more compact structure and smaller voids, traps water within its pore network. As the water freezes, it exerts pressure on the pores, leading to fractures and disintegration as visible in Figure 90A. The *Supra Nucleus stratum*, which is the densest and most decorative layer, is almost completely disintegrated in most cases. Finally, all specimens exhibit the detachment of some or all *tesserae* during the degradation process (Figure 91 and Figure 92), underscoring the fragility of this part of the mosaic. This highlights the critical importance of using a mortar with strong adhesive properties for the restoration of such a delicate system.

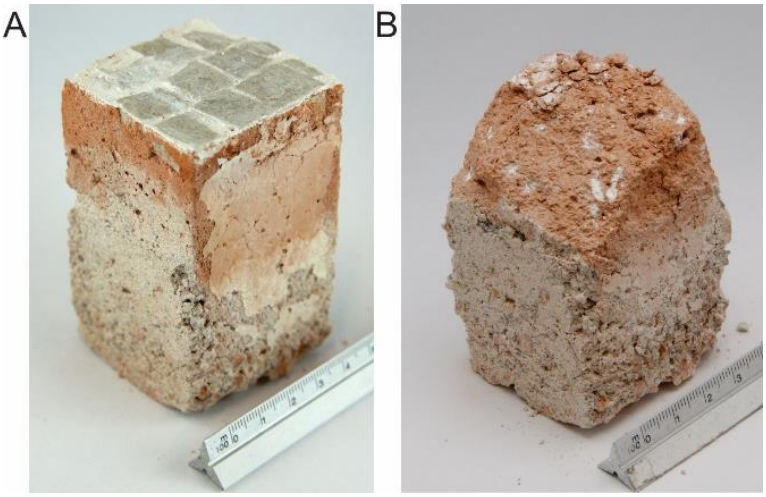

Figure 89 Specimen M20 before and after degradation process.

5.2.3 Process of restoration

As reported in §2.3[54] process of restoration primarily includes the use of mortar to perform a consolidation of the edges and of the bottom side of the mosaic, to fill the cracks of the material, to reattach the *tesserae*. Thus, the process was conducted by applying the YN mortars on the degraded mosaics. Mortar was used in order to consolidate the *Nucleus* part of Specimen and to fill the cracks formed in phase of degradation (Figure 90B). In Figure 91 are reported images of specimen M26 before and after degradation process that as is possible to see induced the loss of some *tesserae*. The lost *tesserae* were reattached thanks to the restoration intervention and the sides of the specimens, particularly the one of *Nucleus*, were consolidate in order to reinforce the *stratum* correspondent to the point of attachment of the *tesserae*. A similar intervention was

[54] For more information please look at § 2.3 Introduction to the Conservation of mosaics.

conducted on specimen M17 (Figure 92), however in this case the *tesserae* were completely detached, thus their reattachment was conducted by the help of a mould.

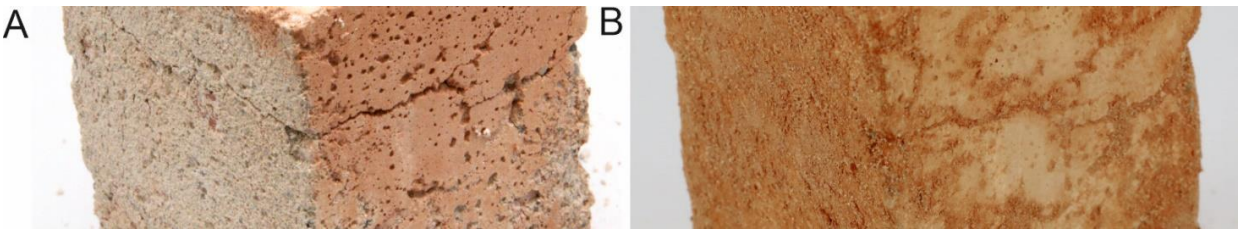

Figure 90 Specimen MV2 before and after restoration process.

After the application of the restoration, the mortars were let to harden following hardening condition applied during mortar design[55], and then let to harden the material in laboratory condition. As is possible to see the mortar effectively allow the reattachment of the material and the filling of the external cracks. However, to assess the effective filling also of the internal cracks Ultrasound Pulse velocity measurement was applied.

Figure 91 Specimen M26: A) Before degradation process; B) after degradation; C) after restoration process.

Figure 92 Specimen M17: A) Before degradation process; B) after degradation; C) after restoration process.

5.2.4 Application of UPV analysis and evaluation of the restoration intervention

Ultrasound Pulse Velocity (UPV) is an easy test to evaluate the quantity of voids present inside the material. The test is based on the application of two probes in contact with the surface of two

[55] For more information please look at § 4.4 Mortars production.

opposite sides. The UPV send the ultrasound and record the time of flight of the passage of the ultrasound from one probe to the other. Knowing the length of this space it is possible to achieve the Velocity of the Ultrasound and to parity of its velocity knowing the increment or decrement of the voids. The evaluation of this velocity before, after degradation allow to see the effective increment of voids induced by the decay. The application of this test after the restoration allow to assess the reestablishment, thanks to the restoration, of the original pores or at least the reduction of porosity formed in phase of degradation. Velocity of ultrasound is inversely proportional to the quantity of voids, thus greater is the velocity lower will be the quantity of voids. Thus, application of the test on different type of specimens allow, through comparison, to assess the effective change of this parameter.

UPV test was conducted following normal UNI EN 14579 [247] by the use of a Matest portable instrument with measuring range of 0 - 3000 micros and a resolution +/- 0.1 micro sec. By the application on the specimens of two probes of 55 kz, with adjustable ultrasonic pulse width selection from 250 to 1000 v. UPV test assess the effective achievement of the increment of voids induced by the degradation indeed the average velocity of ultrasound for different specimens before the degradation was variable around 0.12 Km/s to 0.17 Km/s. After the degradation the velocity decreased for all the specimens indicating the increment in porosity. In Figure 93are reported the results of Ultrasound pulse velocity recorded before and after the restoration.

From the results it is possible to assess that the restoration intervention maintain the values of velocity for the majority of the analysed specimens, thus that the intervention didn’t bring to the filling of the internal porosity. Nevertheless, some selected specimens show the effective increment of the results of velocity indicating the reduction of the cracks and porosity of the specimens (namely samples M12, M26) indeed in this case restoration intervention take into account the consolidation of all the sides of the mock-ups. These preliminary results highlights the need of further formulation of the mortar to allow to the mortar to fill the internal voids, thus further consideration about the viscosity are needed. However, the restoration process can be considered good thanks to its ability to reattach the detached *tesserae* and to fill the superficial cracks visible in the specimens.

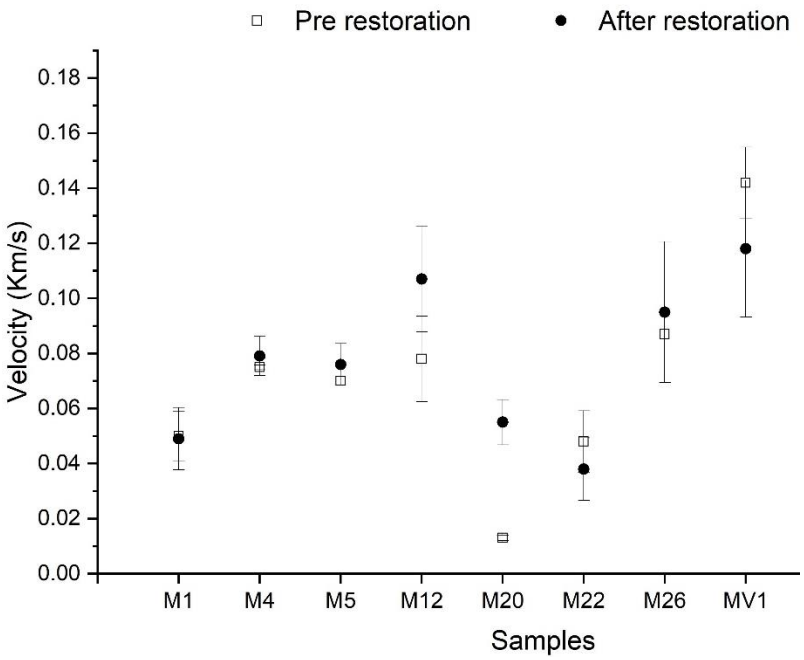

Figure 93 Graph with UPV results for each sample, before and after the restoration process.

6 Conclusions and future perspectives

This study presents a methodological approach aimed at developing a new mortar for mosaic restoration. To achieve this objective, a multidisciplinary approach was employed, integrating archaeometric analysis, geological data, and material science. In the mix design project, two key standpoints were considered: the compatibility of the designed material with the ancient substrate and the sustainability of the material in both its production and application phases. The designed product is the result of ancient recipes adapted to meet modern restoration needs.

The first phase of this research was focused on the acquisition of information about the geological and chemical composition of samples of ancient mosaics, including both *tesserae* and mortar.
The archaeometric study identified the petrographic nature of the 153 *tesserae* of a mosaic from the archaeological site of Aquileia. For the majority of these specimens, it was possible to determine the specific region of sourcing of the stone and marble used. A combination of petrographic analysis and colorimetric assessments revealed that *tesserae* with visually identical colours were crafted from various lithotypes. This suggests that, local artisans had access to materials from different locations.
The majority of the *tesserae* are white or light-coloured, primarily composed of grainstone, wackestone, mudstone, and packstone from the Trieste Karst region. In contrast, the dark-coloured *tesserae* are mostly made of laminated mudstone to wackestone, although identifying their precise origin remains challenging due to limited references in the literature. However, similar lithotypes have been documented in the Aurisina quarrying district. The coloured *tesserae* examined were found to be crafted possibly from materials coming from more distant locations. For example a dark green tessera made of *porfido verde antico*, a dark grey tessera made of *cipollino verde* or *bigio*, coming from Greece and a pink tessera made of *giallo antico marble* sourced in North Africa. This highlights the diverse array of materials that reached Aquileia through various trade routes during specific periods. However, the demand for coloured materials was not always satisfied with natural lithotypes due to their rarity and high value, leading to the use of ceramic tiles as substitutes for red, yellow, and sometimes even white *tesserae*, as observed in this study. The archaeometric investigation reveals significant details about the raw materials used in mosaics, enhancing our understanding of mosaic components and the variety of lithic materials brought to the ancient city.

The presence of mortar in some of the selected fragments and specimens of mosaics allowed its analysis. The identification of distinct mortar layers was meticulously conducted, with each layer's composition extensively analysed across a broad range of samples. The results demonstrated that the majority of the specimens adhere to Roman recipes for mortar production and Vitruvian layering compositions.

The composition of mortars from specific *stratum* was evaluated. As a result the mortars showed different compositions mainly corresponding to different type and concentration of aggregates used. The *tesserae setting bed stratum* was found to be composed of either pure lime or a mix of lime and sand. The *Nucleus stratum* primarily consisted of aerial lime mixed with sand and *cocciopesto* in different concentrations. The analysis highlighted the fundamental role of *cocciopesto* in enhancing the hydraulicity of the mortar. The presence of an additional *stratum* of mortar, indicated as coarse mortar *stratum*, in only 2 specimens, led to its extensive examination. It was composed similarly to the *Nucleus stratum* but contained visibly larger aggregates and absence of *cocciopesto*. The application of variations in the preparation of the layers was common at Roman time, because the recipes were changed on the basis of availability of material, technical knowledge and care used for the mosaic preparation. In this *stratum* presence of pieces of shells were identified in the aggregate composition. This discovery will be further investigated in the future, to assess the chemical contribution of shells to the characteristic composition of the mortar. The investigation of the composition of different layers also allowed for an assessment of stratification heterogeneity, indicating instances where the same mortar was used for both *Nucleus* and *tesserae* setting bed *strata* or where different mortars with varying aggregate compositions were employed. The majority of the specimens are characterised by high-quality stratification. The presence of *tesserae* setting bed stratification in most specimens further signifies the high quality of the mosaics. Evaluating the different stratifications enabled the identification of variability in artistic production, likely influenced by the availability of materials. These findings enhance our archaeological understanding of mortar composition, providing a more comprehensive insight into the construction techniques used in mosaic production. Most importantly, the results derived from this characterisation phase served as a foundation and inspiration for the development of innovative mortars. Additionally, the results achieved through characterisation allowed for the faithful reproduction of ancient mosaics system.

The produced mock-ups were used as specimens to explore the internal microstructure of mosaic systems using Synchrotron Radiation Computed Tomography (SX-CT). The use of mock-ups that replicate ancient mosaics is justified by the novelty of applying this type of analysis to evaluate fragile heritage materials like mosaics. This analysis overcomes challenges related to beam and glass interactions present when using X-ray Computed Tomography. The analysis allowed the acquisition of detailed spatial data and enabled 2D and 3D reconstructions of the specimens and the production of high-resolution images.

The results provide new insights into the internal structure, cracks, and pore networks within the mortar of mosaics, quantifying total internal porosity by accounting for both closed and micro-pores in the volumetric sum. The analysis reveals the absence of porosity in stone *tesserae*, while porosity is present in glass *tesserae*. The *Supra Nucleus* (*tesserae* setting bed) layer exhibits cracks and interconnected pores, which can lead to further damage. In comparison, specimens made with glass *tesserae* shows fewer and smaller cracks respect to stone ones. These results can suggest a possible greater adhesion of the mortar to the glass *tesserae* and, therefore, less deterioration.
The *Nucleus* layer contains both open and closed pores caused by trapped air during casting, with visible pores and vesicles, as well as smaller aggregates. The *Nucleus* layers exhibited the lowest porosity and the result is similar across all the specimens, reflecting the use of finer mortar. Conversely, despite using the same production technique, the *Rudus* layers, which is the most porous among all the *strata*, demonstrated variable porosity in different specimens possibly due to the use of large, irregular aggregates, which created large voids and cracks, with almost all pores interconnected.
These results enable a direct analysis of structural weaknesses, as porosity and cracks represent vulnerable points for the conservation of material integrity, advancing our understanding of mosaic structures. Overall, the results confirm the feasibility of SXCT analysis for studying archaeological materials, specifically ancient mosaic fragments. Future applications of this analysis could include the evaluation of the penetration depth of treatments, offering solutions for assessing consolidation.

The information obtained during the characterisation phase was used to inspire the mix design of the mortar. During my PhD, I successfully developed six different paleo-inspired mortars. Thanks to tests conducted at various curing times, it was possible to effectively assess the structural properties of the materials and their changes related to the hardening process. The combination of chemical analyses allowed for further consideration of the correlation between composition and structural properties.

Two mortars, referred to as X and Y, were designed based on the composition of *Nucleus*, using *cocciopesto* and sand as aggregates and two different binders: slaked lime and NHL 3.5, respectively. Their chemical analyses showed comparable compositions, with minor differences due to the different binders used. Mechanical evaluations indicated that mortar Y outperformed mortar X in several areas, including workability, flexural strength, and compressive resistance. It also demonstrated superior elasticity and indentation strength, making it a preferable choice for restoration due to its enhanced mechanical properties. These two mortars serve as the base recipes for producing other mortars with various additives.

Recent needs in restoration have emphasised the demand for new materials that are compatible with ancient mortars while also possessing enhanced properties, including sustainability and eco-friendliness. This has led to the study and development of two new additives.
A self-healing additive called CSMMA was synthesised and added to the two starting mortars producing mortars XCS and YCS. The additive consists of an active binding core encapsulated within a polymeric shell. This material was added to the two initial mortars, which were then tested and compared to assess the additive's effect on the mortars' characteristics. Although the mortars demonstrated limited self-healing capabilities, mortar YCS exhibits a significant enhancement in strength and resistance compared to mortar Y.
The results of the self-healing tests indicated a sudden activation rather than a reactive response at the point of breakage, suggesting that the self-healing material had already reacted, possibly due to a weak covering of the polymeric capsule. Consequently, further research is needed to determine the best method for encapsulating the binding core.

As noted by Pliny the Elder, Romans often added various organic and inorganic materials to their mortars to improve properties during application and enhance their longevity. This ancient practice has been renewed in the current interest in producing green and sustainable materials. *Opuntia ficus indica* gel has been produced and tested for the purpose of research. Indeed, its positive effects are supported by ancient accounts, such as those from Mesoamerican construction methods, as well as modern analyses on cements addittivated with *Opuntia ficus indica* mucilage.
This gel was added to the two initial mortars, resulting in mortars XN and YN. Testing these mortars in their fresh state showed that the gel positively affected their rheological and workability properties compared to formulations made with standard water, thus influencing the mortar's maturation process. This result, coupled with the flexural and compressive strength tests, demonstrates an enhancement in strength. Therefore, it is reasonable to suggest an increase in the formation of calcium silicate hydrate (CSH) mineral forms, a phase that improves mortar strength. Additionally, this mortar exhibits the lowest water absorption among all the designed mortars, indicating a higher density, possibly due to the addition of the gel facilitating the formation of a more organised microstructure.
The water retention capability of the gel may be responsible for delaying the drying of the mortar. Specifically, for mortars with slaked lime, a reduction in drying was observed. This reduction in hardening time can promote the formation of a more organised microstructure, contributing to enhanced strength and reduced water absorption.

For restoration purposes, the compatibility of mortars with ancient substrates, represented by a sample of historical mortar, was also assessed. Mortars Y and YN were found to be the most compatible in terms of mechanical properties and chemical analysis. These findings suggest that these mortars can mimic the elastic behaviour of the original material, responding similarly to

time-induced or degradation-related movements. It is possible that the ancient mortar contained additional substances not detectable by the techniques used in this study, which could account for the slight differences in behaviour compared to the other formulated mortars. However, the addition of *Opuntia ficus indica* gel and NHL 3.5 as a binder addressed these differences effectively.

Due to the absence of feasible methods in literature for evaluating the adhesive properties of mortar *tesserae* system, a new pull-out test was designed. Unlike currently available tests, this test was designed considering the small dimensions and the depth of nesting of *tesserae* of an original mosaic. It allows the measurement of the maximum force each sample can withstand before the *tesserae* detach from the mortar, an information that can be correlated to the adhesive properties of the mortar. Multiple tests were conducted on different mortar types, and the results showed that mortars containing *Opuntia ficus indica* gel (XN and YN) withstood greater forces than those without. Mortar YN exhibited the highest resistance to *tesserae* detachment.

A comprehensive evaluation of all the results achieved underscores that YN generally demonstrates the greatest performance in all the tests. Thus, this mortar, produced using *Opuntia ficus indica* gel and NHL 3.5 as binders, was considered the best and was used for simulating restoration interventions. The restoration process was applied to degraded mock-ups of mosaics to simulate the actual state of the art of archaeological material. The restoration involved the use of mortar YN to consolidate the edges and underside of degraded mosaics, fill cracks, and reattach detached *tesserae*. To assess the effectiveness of the restoration in filling internal cracks, the presence of air within the mortar and the relative voids were evaluated using Ultrasonic Pulse Velocity (UPV) analysis. The results showed a decrease in velocity for all specimens after degradation, indicating an increase in porosity. However, after restoration, most specimens maintained their velocity, suggesting that internal porosity was not filled. Some specimens showed improved velocity results, indicating a reduction in cracks and porosity due to effective consolidation. Nevertheless, some results before and after the restoration did not change, suggesting a need for further mortar formulation to enhance the filling of internal voids. Nonetheless, the restoration process successfully reattached detached *tesserae* and filled superficial cracks, demonstrating applicability of mortar YN for restoration purposes.

Mortar YN, offers a valuable alternative to current conservation materials. The confirmation of compatibility between the newly developed mortars and the original materials highlights the importance of “reverse engineering” in designing restoration materials that mimic the properties of the original support. Inspired by ancient Roman recipes, this research provides a strong foundation for developing compatible materials for future restoration work. Additionally, the use of *Opuntia ficus indica* gel in substitution to water represent a green sustainable choice as additive that can effectively improve mortar properties.

This study emerged at the intersection of history and science in the production of mortar. The strength of this research lies in its comprehensiveness and evolution. Every aspect of the conservation of ancient Roman mosaics has been carefully evaluated, with all elements interconnected and serving the final purpose of the study. From the macro to the micro level, the composition of the mosaics has been thoroughly investigated offering fundamental information useful for mortar mix design phase.

Moreover, the research outlines a clear pathway for the design, production, analysis, and testing of mortars, ensuring that all steps are rooted in historical recipes, with full respect for the archaeological surfaces. This comprehensive research represents a valuable strategy for designing conservation mortars, positioning itself as a significant contribution to the field of novel materials for conservation. The key strength of this work lies in the rich historical context that supports each step, offering a complete narrative that connects the past to cutting-edge scientific advancements in conservation.

7 Annex

Annex_A Characterisation of archaeological material

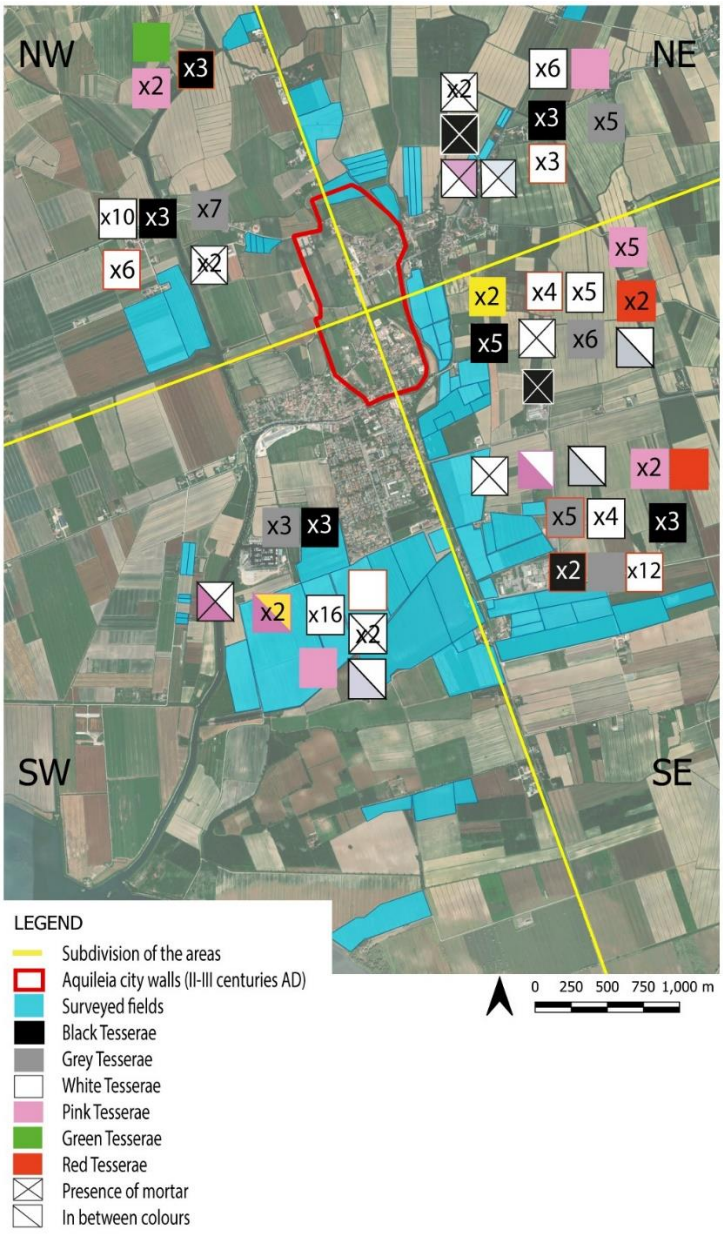

Figure 1S Map of the area of provenance of the selected samples. The map report the distribution of the materials across different geographical regions (NW, NE, SW, SE), each divided by yellow lines. The collected materials are represented by squares of various colours, corresponding to the colour of the *tesserae*. The label "xN." found on some squares indicates the number of specimens of that specific colour acquired in each geographical area, in cases where more than one specimen was selected.

Additional materials of §3.1 Characterisation of *tesserae*

Table 1S Summary of the information acquired for each specimen. In the first column, we indicate the sub area of provenance of the materials labelled as NW for Northwest, NE for Northeast, SW for Southwest, SE for Southeast. In the following columns are reported: the name of the sample, the morphological description made with naked eye, the colorimetric group (W for white, B for black, G for grey, P for pink, Y for yellow, R for red and Ge for green), petrographic characterisation of the material of composition.

Area	Sample	Description of the specimens	Group	Characterisation of the material
NO	**1A**	White single tessera	W	Wackestone; Aurisina marble, from Karst area
	1B	4 white *tesserae* nested in mortar	W	Wackestone; Aurisina marble, from Karst area
NE	**2A**	3 whitish-pinkish *tesserae* nested in mortar	W	Packestone; from Karst area
	2B	3 whitish-greyish *tesserae* nested in mortar	W	Packestone; from Karst area
SE	**3**	4 white *tesserae* nested in mortar	W	Mudstone; Aurisina marble, from Karst area
SO	**4**	4 whitish-pinkish *tesserae* nested in mortar	W	Grainstone; Aurisina marble, from Karst area
SE	**5A**	4 white *tesserae* nested in mortar	W	Wackestone; Aurisina marble, from Karst area
	5B	White single tessera	W	Grainstone; Aurisina marble, from Karst area
NO	**6A**	Black single tessera with external residues of mortar	B	Laminated wackestone, probably from the Karst area
	6B	White single tessera	W	Packestone; from Karst area
NE	**7A**	2 white *tesserae* nested in mortar	W	Mudstone; Aurisina marble, from Karst area
	7B	White single tessera with decay	W	Wackestone; Aurisina marble, from Karst area
NE	**8**	7 black *tesserae* nested in mortar	B	Laminated wackestone, probably from the Karst area
SE	**9**	6 black *tesserae* nested in mortar	B	Laminated wackestone, probably from the Karst area
SO	**10A**	Grey single tessera	G	Wackestone; Aurisina marble, from Karst area
	10B	Black single tessera	B	Laminated wackestone, probably from the Karst area
	10C	Black single tessera	B	Laminated wackestone, probably from the Karst area
SO	**11**	6 white *tesserae* nested in mortar	W	Mudstone; Aurisina marble, from Karst area
SE	**12A**	Whitish-pinkish single tessera	P	Mudstone; Aurisina marble, from Karst area
	12B	Whitish-pinkish single tessera	P	Mudstone; Aurisina marble, from Karst area
	12C	Black single tessera	B	Laminated wackestone, probably from the Karst area
	12D	Black single tessera	B	Laminated wackestone, probably from the Karst area

NO	**13**	6 white *tesserae* nested in mortar	W	Grainstone; Aurisina marble, from Karst area
NE	**14**	6 white *tesserae* nested in mortar	W	Wackestone; Aurisina marble, from Karst area
SE	**15A**	White single tessera	W	Mudstone; Aurisina marble, from Karst area
	15B	Whitish-grey single tessera	W	Grainstone; Aurisina marble, from Karst area
	15C	Black single tessera	B	Laminated wackestone, probably from the Karst area
SO	**16**	4 white *tesserae* nested in mortar	W	Packestone; from Karst area
SE	**17A**	Grey single tessera with patina of decay	G	Mudstone; Aurisina marble, from Karst area
	17B	Grey single tessera	G	Grainstone; Aurisina marble, from Karst area
	17C	White single tessera	W	Mudstone; Aurisina marble, from Karst area
	17D	White single tessera	W	Grainstone; Aurisina marble, from Karst area
NO	**18A**	Black single tessera	B	Chert, probably from the Karst area
	18B	White single tessera	W	Wackestone; Aurisina marble, from Karst area
	18C	Green-black single tessera	Green	Porphyry, *porfido verde antico*
NE	**19A**	Grey single tessera	G	Mudstone; Aurisina marble, from Karst area
	19B	Black single tessera nested in mortar	B	Laminated wackestone, probably from the Karst area
SE	**20A**	Grey single tessera	G	Laminated wackestone, probably from the Karst area
	20B	Grey single tessera	G	Grainstone; Aurisina marble, from Karst area
	20C	Pink single tessera	P	Mudstone; Aurisina marble, from Karst area
SO	**21A**	White single tessera with patina of decay	W	Grainstone; Aurisina marble, from Karst area
	21B	Grey single tessera with residues of mortar	G	Wackestone; Aurisina marble, from Karst area
SE	**22A**	Grey single tessera	G	Mudstone; Aurisina marble, from Karst area
	22B	Grey single tessera	G	Grainstone; Aurisina marble, from Karst area
	22C	Black single tessera	B	Laminated wackestone, probably from the Karst area
	22D	White single tessera	W	Grainstone; Aurisina marble, from Karst area
NO	**23A**	Black single tessera	B	Chert, probably from Karst area
	23B	White single tessera	W	Packestone; from Karst area
	23C	Pink single tessera	P	Grainstone; Aurisina marble, from Karst area
NE	**24A**	Black single tessera	B	Laminated wackestone, probably from the Karst area

	24B	Black single tessera	B	Laminated wackestone, probably from the Karst area
	24C	White single tessera	W	Chert, probably from the Karst area
SE	**25A**	White single tessera with residues of mortar	W	Packestone; from Karst area
	25B	White single tessera	W	Wackestone; Aurisina marble, from Karst area
	25C	Black single tessera with residues of mortar	B	Grainstone; Aurisina marble, from Karst area
SO	**26A**	Grey single tessera	G	Laminated wackestone, probably from the Karst area
	26B	Grey single tessera	G	Mudstone; Aurisina marble, from Karst area
	26C	Black single tessera	B	Laminated wackestone, probably from the Karst area
	26D	White single tessera, possibly cotto material	W	Ceramic material
NO	**27A**	Grey single tessera	G	Wackestone; Aurisina marble, from Karst area
	27B	Grey single tessera	G	Wackestone; Aurisina marble, from Karst area
NO	**28A**	Grey single tessera	G	Mudstone; Aurisina marble, from Karst area
	28B	Grey single tessera	G	Grainstone; Aurisina marble, from Karst area
NE	**29A**	Grey single tessera	G	Grainstone; Aurisina marble, from Karst area
	29B	Grey single tessera	G	Wackestone; Aurisina marble, from Karst area
	29C	Black single tessera	B	Laminated wackestone, probably from the Karst area
SE	**30A**	Yellow single tessera	Y	Ceramic material
	30B	Yellow single tessera	Y	Ceramic material
	30C	Red single tessera	R	Laminated wackestone; probably from the Karst area
	30D	Red single tessera	R	Hardground with ferruginous and clay-rich ooids, unknown provenance
SE	**31A**	Pink single tessera	P	Wackestone; Aurisina marble, from Karst area
	31B	Pink single tessera	P	Fine-grained crystalline limestone, *Giallo Antico marble*
	31C	Pink single tessera	P	Wackestone; Aurisina marble, from Karst area
SO	**32A**	Yellow-pinkish single tessera	Y	Mudstone; Aurisina marble, from Karst area
	32B	Yellow-pinkish single tessera	Y	Grainstone; Aurisina marble, from Karst area
	32C	White single tessera	W	Mudstone; Aurisina marble, from Karst area
NO	**33A**	White single tessera	W	Grainstone; Aurisina marble, from Karst area
	33B	Pink single tessera	P	Grainstone; Aurisina marble, from Karst area

	33C	Black single tessera with oxidation patina	B	Laminated wackestone, probably from the Karst area
NE	**34A**	White single tessera	W	Wackestone; Aurisina marble, from Karst area
	34B	Grey single tessera	G	Grainstone; Aurisina marble, from Karst area
	34C	Grey single tessera	G	Mudstone; Aurisina marble, from Karst area
SE	**35A**	White single tessera	W	Packestone; from Karst area
	35B	Grey single tessera	G	Wackestone; Aurisina marble, from Karst area
	35C	White single tessera, possibly cotto material	W	Ceramic material
SO	**36A**	White-greyish single tessera with residues of mortar	W	Packestone; from Karst area
	36B	White single tessera with residues of mortar	W	Grainstone; Aurisina marble, from Karst area
SE	**37A**	Grey single tessera with residues of mortar	G	Grainstone; Aurisina marble, from Karst area
	37B	Black single tessera with residues of mortar	B	Laminated wackestone, probably from the Karst area
	37C	Black single tessera	B	Impure calcite marble, cipollino bigio; from Karystos
	37D	Red single tessera	R	Ceramic material
NO	**38A**	White single tessera with residues of mortar and patina of decay	W	Grainstone; Aurisina marble, from Karst area
	38B	White single tessera with residues of mortar	W	Grainstone; Aurisina marble, from Karst area
NE	**39A**	White large single tessera with residues of mortar	W	Wackestone; Aurisina marble, from Karst area
	39B	Pink single tessera	P	Wackestone; Aurisina marble, from Karst area
SE	**40A**	Grey single tessera	G	Wackestone; Aurisina marble, from Karst area
	40B	Grey single tessera	G	Wackestone; Aurisina marble, from Karst area
	40C	Grey single tessera with residues of mortar	G	Laminated wackestone, probably from the Karst area
SO	**41A**	White single tessera	W	Grainstone; Aurisina marble, from Karst area
	41B	White single tessera	W	Medium-grained crystalline limestone, unknown provenance
	41C	White-pinkish single tessera	P	Wackestone; Aurisina marble, from Karst area
SE	**42A**	Pink single tessera with patina of decay	P	Wackestone; Aurisina marble, from Karst area
	42B	White single tessera with patina of decay	W	Wackestone; Aurisina marble, from Karst area
NO	**43A**	White single tessera	W	Grainstone; Aurisina marble, from Karst area
	43B	White single tessera	W	Wackestone; Aurisina marble, from Karst area

	43C	White single tessera	W	Mudstone; Aurisina marble, from Karst area
	43D	Black single tessera	B	Laminated wackestone, probably from the Karst area
NE	**44A**	White single tessera with patina of decay	W	Mudstone; Aurisina marble, from Karst area
	44B	White single tessera	W	Wackestone; Aurisina marble, from Karst area
SE	**45A**	White single tessera with patina of decay	W	Wackestone; Aurisina marble, from Karst area
	45B	Grey single tessera with residues of mortar	G	Silicified grainstone; unknown provenance
SO	**46A**	White single tessera with patina of decay	W	Grainstone; Aurisina marble, from Karst area
	46B	White single tessera	W	Wackestone; Aurisina marble, from Karst area
	46C	White single tessera similar to gypsum	W	Mudstone; Aurisina marble, from Karst area
SE	**47A**	White single tessera	W	Grainstone; Aurisina marble, from Karst area
	47B	Grey single tessera	G	Grainstone; Aurisina marble, from Karst area
NO	**48A**	White single tessera with patina of decay	W	Wackestone, unknown provenance
	48B	White single tessera	W	Packestone; from Karst area
	48C	White single tessera	W	Mudstone; Aurisina marble, from Karst area
NE	**49A**	Grey single tessera	G	Grainstone; Aurisina marble, from Karst area
	49B	White single tessera	W	Grainstone; Aurisina marble, from Karst area
	49C	White single tessera	W	Wackestone; Aurisina marble, from Karst area
SE	**50A**	Grey single tessera	G	Chert, probably from the Karst area
	50B	Black single tessera	B	Laminated wackestone, probably from the Karst area
	50C	Black single tessera	B	Laminated wackestone, probably from the Karst area
SO	**51A**	White single tessera	W	Grainstone; Aurisina marble, from Karst area
	51B	White single tessera	W	Wackestone; Aurisina marble, from Karst area
	51C	White single tessera	W	Packestone; from Karst area
SE	**52A**	White-pinkish single tessera	P	Mudstone; Aurisina marble, from Karst area
	52B	White single tessera	W	Grainstone; Aurisina marble, from Karst area
SE	**52C**	White single tessera	W	Packestone; from Karst area
	52D	White single tessera	W	Grainstone; Aurisina marble, from Karst area
	52E	White single tessera	W	Packestone; from Karst area

NO	**53A**	Grey single tessera	G	Grainstone; Aurisina marble, from Karst area
	53B	Grey single tessera	G	Packestone; from Karst area
	53C	Grey single tessera	G	Chert, probably from Karst area
	53D	Black single tessera with patina of decay	B	Laminated wackestone, probably from the Karst area
SE	**54A**	White-pinkish single tessera	W	Mudstone; Aurisina marble, from Karst area
	54B	White single tessera	W	Grainstone; Aurisina marble, from Karst area
	54C	White single tessera possible cotto material	W	Ceramic material
SO	**55A**	White single tessera	W	Wackestone; Aurisina marble, from Karst area
	55B	White single tessera	W	Grainstone; Aurisina marble, from Karst area
SO	**55C**	White single tessera	W	Packestone; from Karst area
	55D	White single tessera	W	Grainstone; Aurisina marble, from Karst area
SE	**56A**	White single tessera	W	Mudstone; Aurisina marble, from Karst area
	56B	White single tessera	W	Mudstone, unknown provenance
	56C	White single tessera	W	Packestone; from Karst area
SE	**57A**	White single tessera	W	Grainstone; Aurisina marble, from Karst area
	57B	White single tessera	W	Packestone; from Karst area
	57C	White single tessera	W	Packestone; from Karst area
NE	**58A**	6 white *tesserae* nested in mortar	W	Wackestone; Aurisina marble, from Karst area
	58B	5 white *tesserae* nested in mortar	W	Grainstone; Aurisina marble, from Karst area
	58C	2 white and 1 black *tesserae* nested in mortar	W	Wackestone and Laminated wackestone; Aurisina marble, from Karst area

Table 2S Polarised optical microscopic analysis of thin sections, acquired with 2.5x of magnification. For each colorimetric group is reported one micrograph for each type of material individuated. For each material, are reported the petrographic name, the quantity of specimens recognized of each specific material and the corresponding sample name depicted in the image as an example.

WHITE			
GRAINSTONE 24 Sample 43A	**WACKESTONE** 20 Sample 1B	**PACKSTONE** 16 Sample 16	**MUDSTONE** 13 Sample 43C
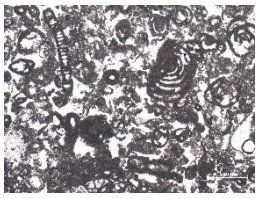	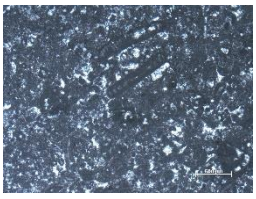	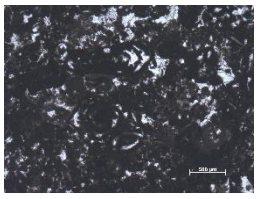	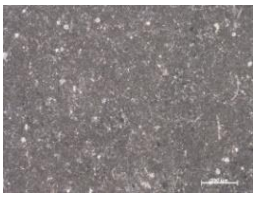

CERAMIC MATERIAL 3 Sample 26D	**CHERT** 1 Sample 24C	**MEDIUM GRAINED CRYSTALLINE LIMESTONE** 1 Sample 41B	
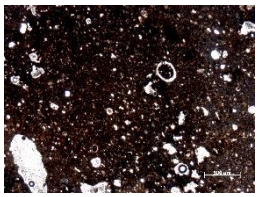	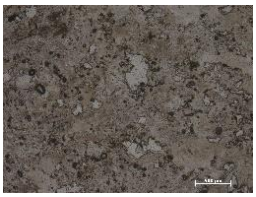	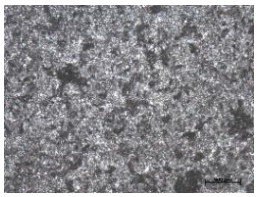	
GREY			
GRAINSTONE 10 Sample 22B	**WACKESTONE** 8 Sample 10A	**MUDSTONE** 6 Sample 26B	**LAMINATED WACKESTONE** 3 Sample 40C
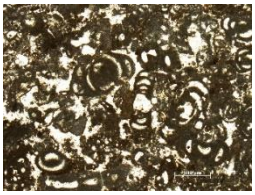	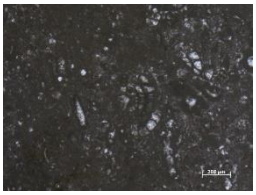	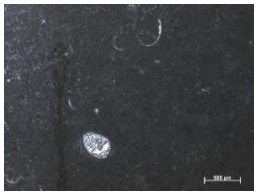	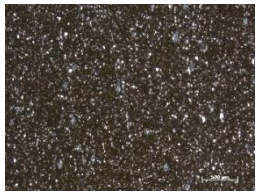
CHERT 2 Sample 50A	**PACKSTONE** 1 Sample 53B	**SILICIFIED GRAINSTONE** 1 Sample 45B	
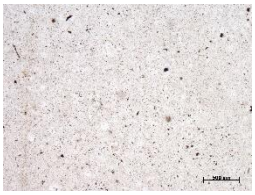	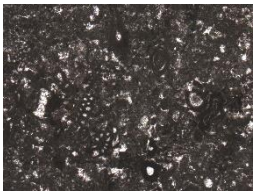	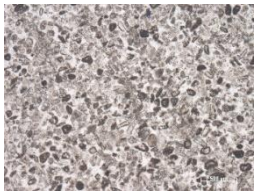	
BLACK			
LAMINATED WACKESTONE 20 Sample 12C	**CHERT** 2 Sample 23A	**GRAINSTONE** 1 Sample 25C	**IMPURE CALCITIC MARBLE** 1 Sample 37C
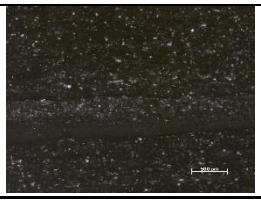	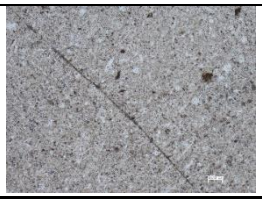	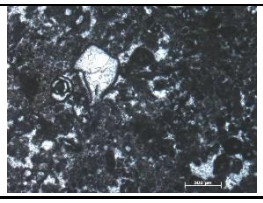	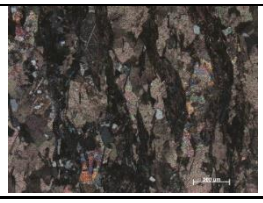

PINK			
WACKESTONE 5 Sample 41C	**MUDSTONE** 4 Sample 12B	**GRAINSTONE** 2 Sample 23C	**FINE GRAINED CRYSTALLINE LIMESTONE** 1 Sample 31B
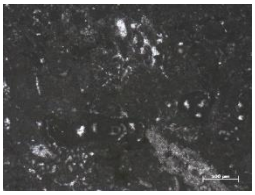	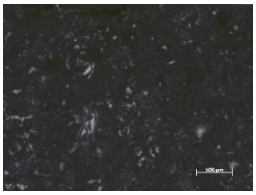	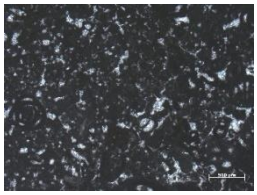	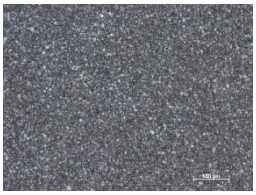
YELLOW			
CERAMIC MATERIAL 2 Sample 30A	**MUDSTONE** 1 Sample 32A	**GRAINSTONE** 1 Sample 32B	
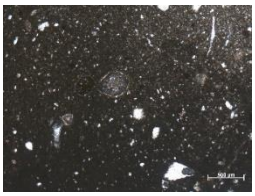	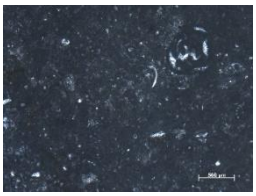	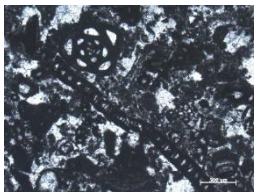	
RED			
LAMINATED WACKESTONE 1 Sample 30C	**HARDGROUND** 1 Sample 30D	**CERAMIC MATERIAL** 1 Sample 37D	
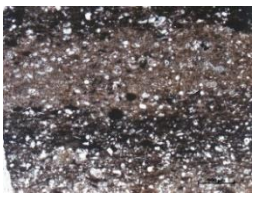	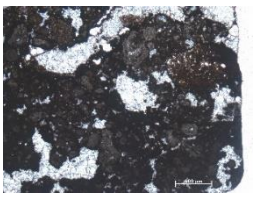	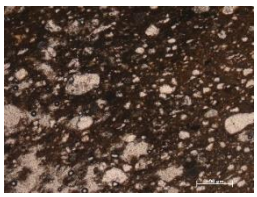	
GREEN			
PORPHYRY 1 Sample 18C			
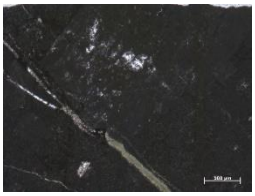			

Additional materials of §3.2 Characterisation of mortars

Table 3S Additional XRD diffractogram of specimens which present also additional minerals in their composition: A) Sample 14, B) Sample 4, C) Sample 16.

Sample name	Composition
14	Calcium Carbonate, Montmorillonite 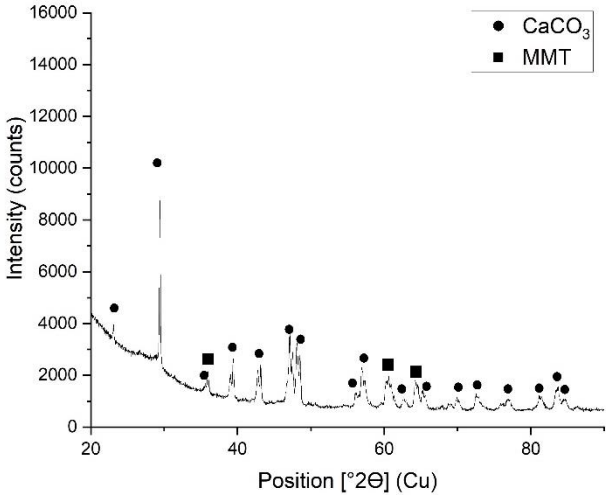
4	Calcium Carbonate, Quartz 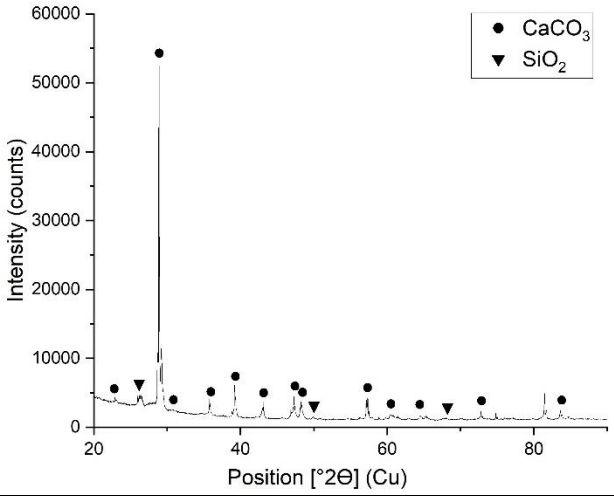
16	Calcium Carbonate, Quartz, Dolomite, Diopside

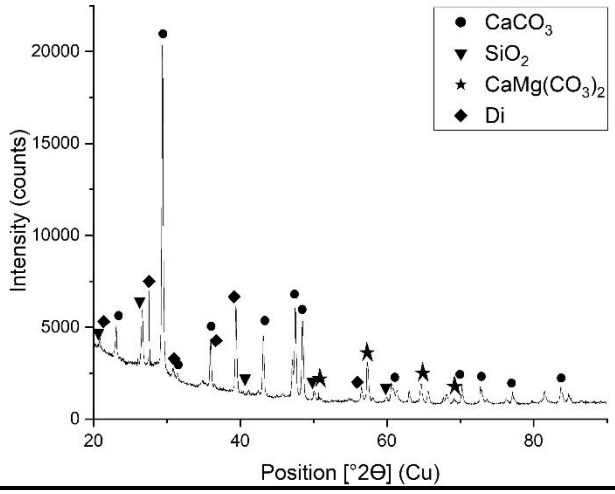

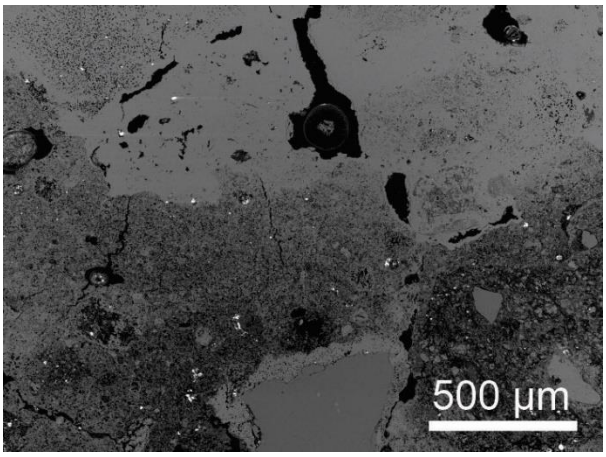

Figure 2S SEM analysis of Sample 8.

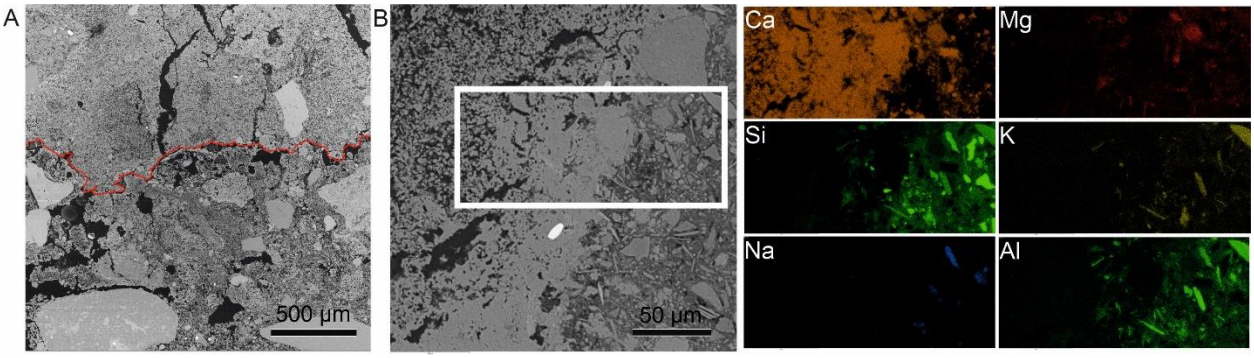

Figure 3S SEM analysis of sample 58B: A) point of interface between *Nucleus* and coarse mortar *stratum* is marked with red line; B) in the white square is indicated the area analysed with EDS, elemental maps with the relative elements investigated are reported nearby.

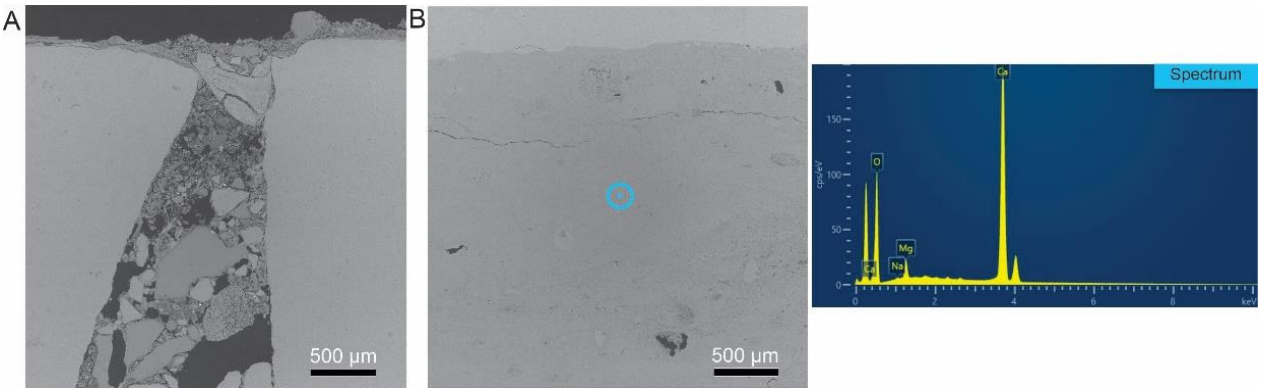

Figure 4S SEM analysis of sample 58C: A) Tessera setting bed *stratum*, characterised by a mix of lime and sand; B) *Nucleus stratum* the blue spot indicate the point of analyses conducted with EDS, the relative spectrum is reported nearby. µ

Table 4S Summary of the results achieved by process of characterisation of mortars. For each specimen is reported the name, a brief comment of the nature of each recorded *stratum*, with the number of the type of mortar recorded with XRD analysis.

Tot.	Specimen	Setting bed	*Nucleus*	*Coarse mortar*
29	**1B**	lime (2)	lime (2)	
	2A	lime with sand (1)		
	2B	lime with sand	aerial (2)	
	3	lime with sand (2)		
	4	lime with sand	lime (2)	
	5A	lime with sand (3)		
	6A	lime (1)	lime (1)	
	7A	lime with sand (2)		
	8	lime with sand	lime with visible *cocciopesto*, hydraulic (2)	
	9	lime with sand	lime with voids of big aggregates missing, aerial	
	11	lime with sand (2)		
	14	lime with sand	lime with visible *cocciopesto*, hydraulic (1)	
	16	lime with sand (3)		
	19C		lime	
	21B	lime with sand		
	25A		lime	
	36B		lime (1)	
	37A	lime with sand		
	37B		lime	
	38B	lime with sand	lime with sand	
	39A	lime (2)		

44A		lime with sand	
45B	lime with sand (2)		
49A	lime with sand		
51A	lime with sand (2)		
57A	lime with sand		
58A	lime with sand	lime with visible *cocciopesto* (3)	lime with big aggregates (2)
58B	lime	lime with visible *cocciopesto* (1)	lime with big aggregates (2)
58C	lime with sand (2)	lime, aerial (2)	

Additional materials of §3.3 Analysis of mosaic system

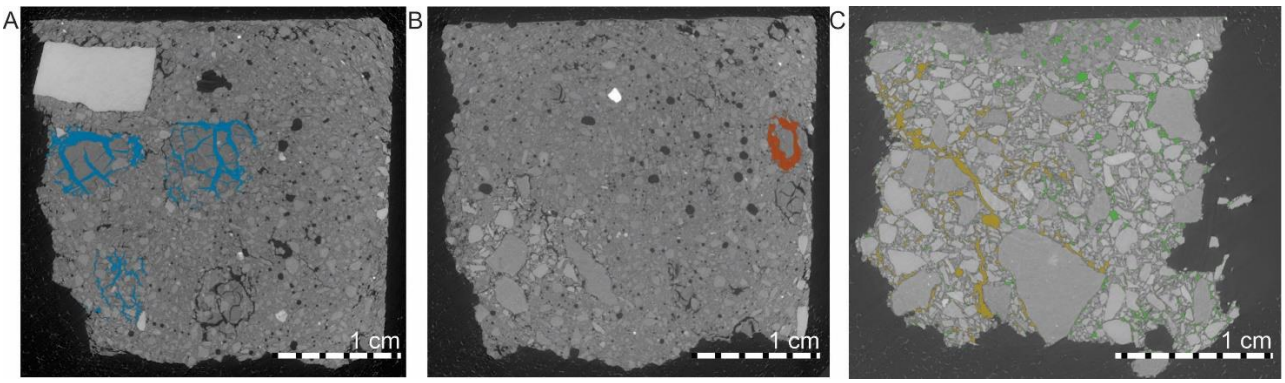

Figure 5S Large interconnected pore of Petra specimen: A) *Supra Nucleus*; B) *Nucleus*; C) *Rudus*.

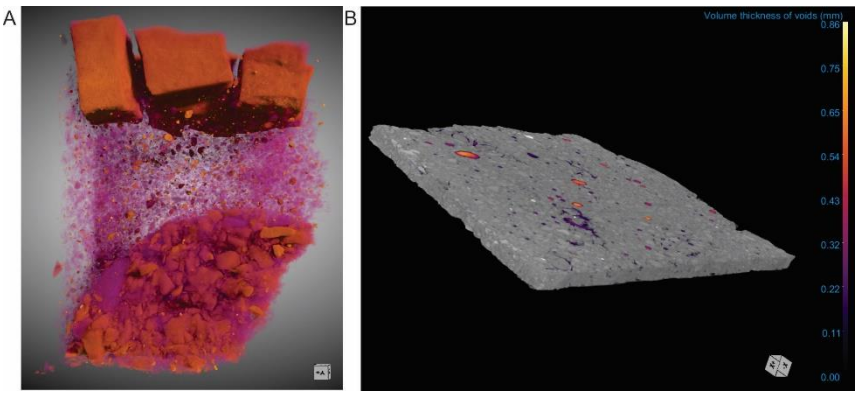

Figure 6S 3D image of Petra specimen: A) 3D render of the specimen where only bright voxels are displayed (image intensities below a defined threshold are hidden). Bright voxels correspond to elements with greater density; B) volume thickness of voids (i.e. local void size) within the *Nucleus stratum*.

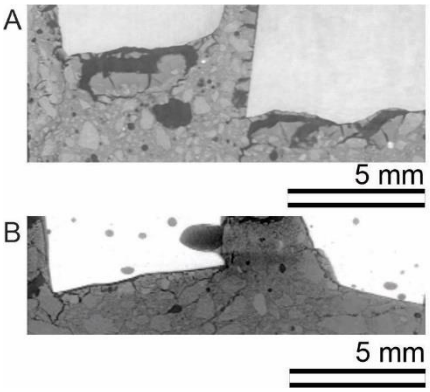

Figure 7S *Supra Nucleus* analysis of the internal cracks: A) Petra; B) Venezia.

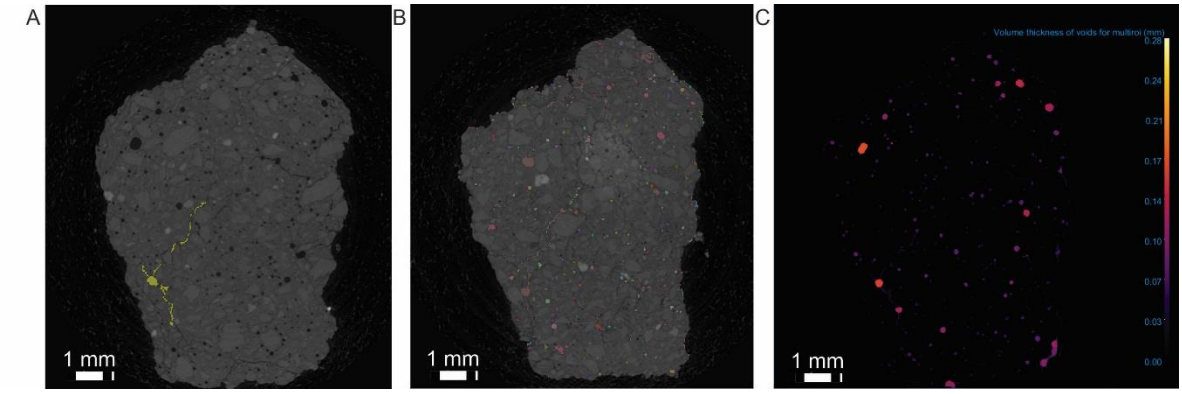

Figure 8S *Nucleus* analysis of M_01 specimen: A) Large interconnected pore; B) porosity; C) Volume thickness of voids.

Annex_B Definition of the composition of the aggregates ratio

Additional material of §4.1. Preliminary test for self-healing mortar production

Mortars without additives were prepared as benchmarks to evaluate the effects of different aggregate compositions. Three formulations, labelled A, B, and C, were created based on varying ratios of sand and *cocciopesto*. All mortars were prepared with a consistent binder-to-aggregate ratio of 1:3. The specific aggregate compositions for each mortar are detailed in Table 5S. Mortar A was made using only *cocciopesto*, mixed with slaked lime and water, while Mortars B and C were formulated with different ratios of sand and *cocciopesto*.

Table 5S Composition of mortars A, B and C.

Mortar	**Binder** 1	**Aggregate** 3	
		Sand	*Cocciopesto*
A		-	All
B	Slaked lime	1	4
C		1	2

Compressive strength test at various curing times was performed for the evaluation of the change of mechanical properties of the mortars prepared with different recipes. Compressive strength test has been conducted in triplicate at 14, 28, 56 days of hardening, the results are reported in table 6S.

Table 6S Compressive strength results at different days

Mortar	**Rc [N/mm^2]**		
	14 days	**28 days**	**56 days**
A	1,42	0,93	0,92
B	0,92	1,33	1,09
C	0,92	1,04	0,87

Mortar A developed high resistance at 14 days, which decreased over time, stabilizing between 28 and 56 days of curing. In contrast, Mortars B and C followed a similar trend, with an initial increase in resistance that peaked at 28 days, followed by a decrease from 28 to 56 days. Mortar C generally showed the lowest compression strength due to the high sand content in its formulation, making it

more friable and, therefore, less suitable for practical applications. When comparing Mortars A and B, the latter proved to be the most effective. The high initial strength recorded for Mortar A suggests a faster curing process, likely due to the greater amount of *cocciopesto* present. However, for research purposes, a mortar that hardens more gradually, in line with the conventional 28-day curing period, is preferable. In this case, Mortar B meets that requirement.

Annex_C Further investigation of characterisation of Nopal gel

Additional material of §4.2.1. Evaluation of the biological growth on natural gels

The potential growth of microorganisms in the gel was tested by storing 100 mL of the compound at room temperature (23°C, 60% relative humidity). Images of gel growth are shown in Figure 9S. Visible growth can be observed after one week of storage, as indicated by the presence of white spots on the gel, that growth continuously along the time of observation. To address this, the gel was treated with an antifungal additive, and mould growth was monitored through a series of photographic observations.

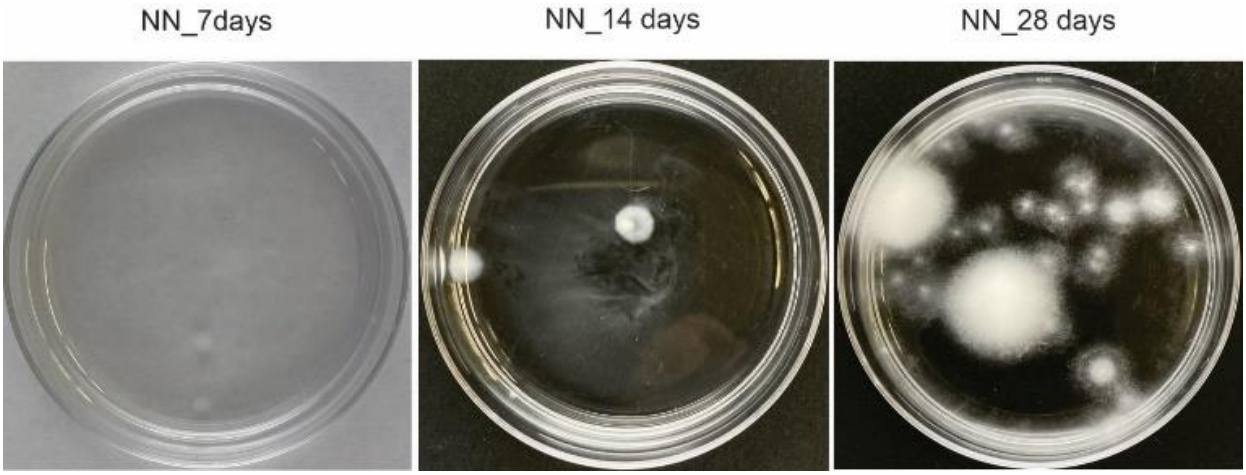

Figure 9S Evaluation of the growth of mould on gel.

Six samples were prepared by placing 50 ml of gel in petri dishes. Sodium benzoate and nipagine were tested as anti micotic by adding them at different concentrations (0.5 mg/ml, 1 mg/ml, 2 mg/ml). The systems were kept in the same ambient conditions and biological growth was observed over time, images are reported in Figure 10S and Figure 11S, respectively.

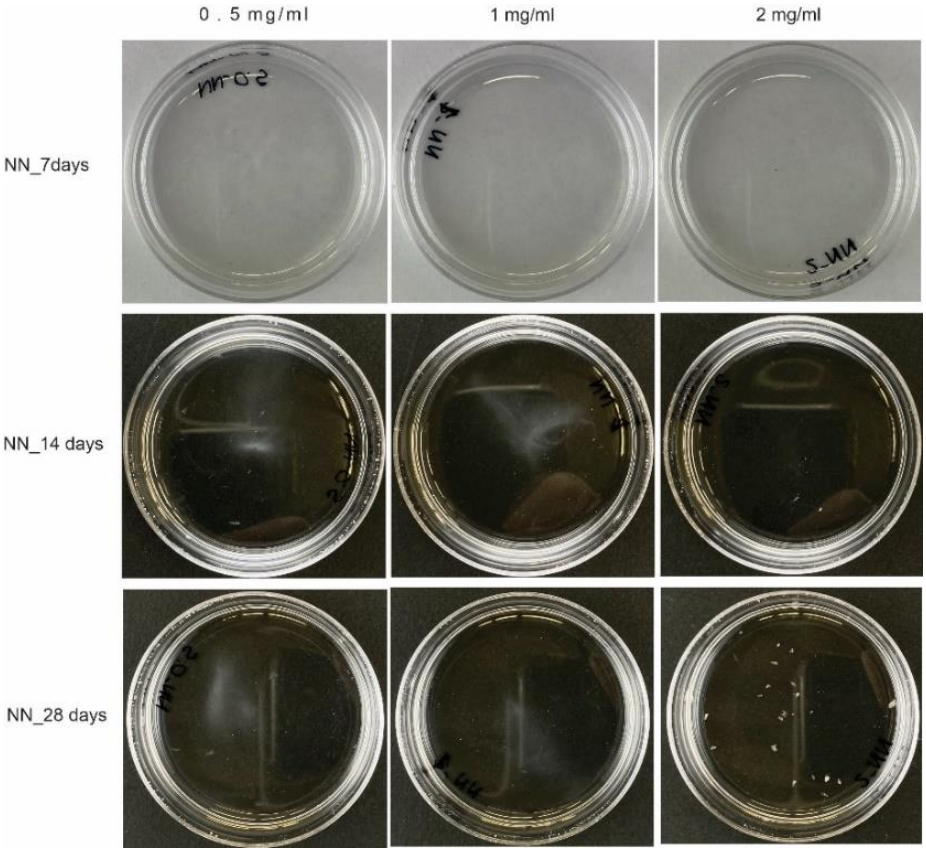

Figure 10S Evaluation of the growth of mould on gel with the addition of nipagine.

Addition of nipagine demonstrates a good reduction of mould growth. However, since the 14 days gel addittivated with concentrations of nipagine of 0.5 and 1 mg/ml show the presence of a white mould not recorded with a concentration of 2 mg/ml. Nevertheless, after 28 days also this gel shows the presence of mould spots on the surface.

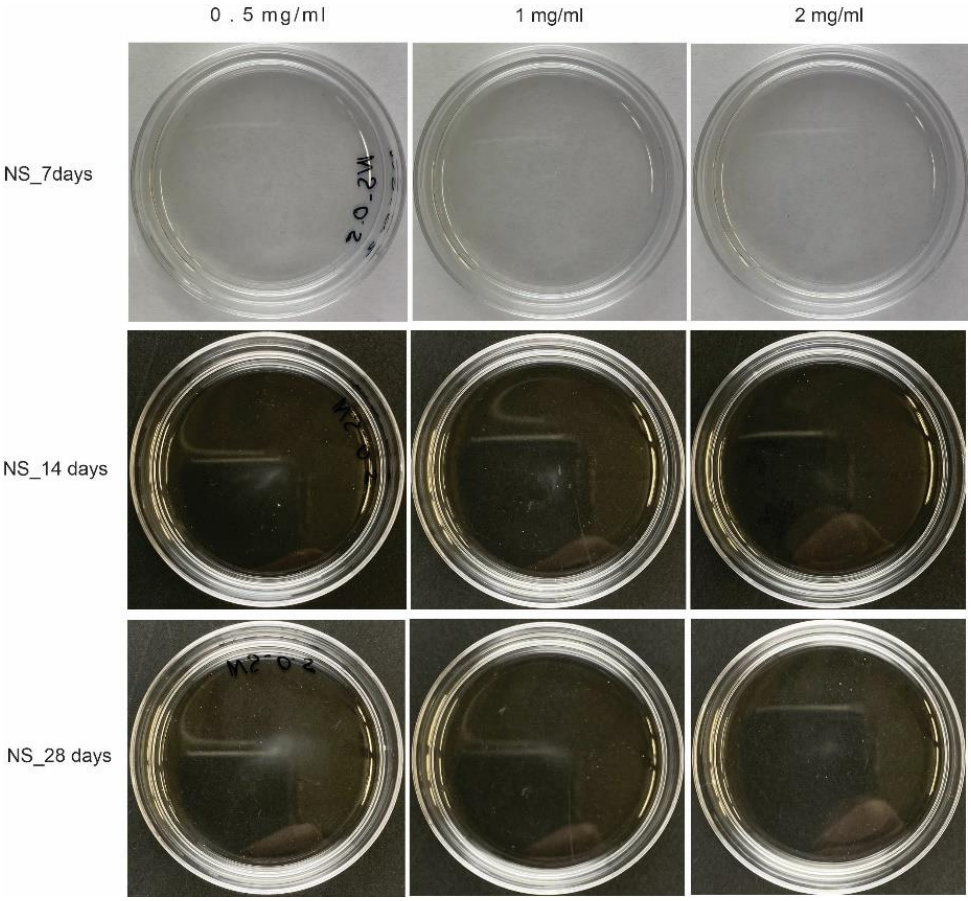

Figure 11S Evaluation of the growth of mould on gel with the addition of Sodium Benzoate.

From the observation of the samples of gel addittivated with sodium benzoate it is possible to assess the presence of mould growth at 28 days for the gel addittivated with the 0.5 mg/ml of additive. Absence of mould growth was recorded at 28 days on the gel addittivated with a concentration of Sodium Benzoate of 1 mg/ml and also of 2 mg/ml. Thus, the concentration of 1 mg7ml was considered enough in order to inhibit mould growth.

Additional analysis of §4.2.2 *Opuntia ficus indica* gel composition

Additional FTIR and DSC-TGA analyses were conducted on gel samples produced by immersing *Opuntia ficus indica* for varying durations. The goal of the analyses was to assess whether differences in the immersion time affected the gel's composition. Figure 12S presents the stacked FTIR spectra of gel produced by time of immersion of 2, 5 and 8 weeks, revealing no significant differences. Similarly, the DSC-TGA analysis (Figure 13S) also showed no notable changes. These results confirm that an immersion time of 24 hours is sufficient to produce the hydrogel, and extending the immersion period has no impact on the gel's composition.

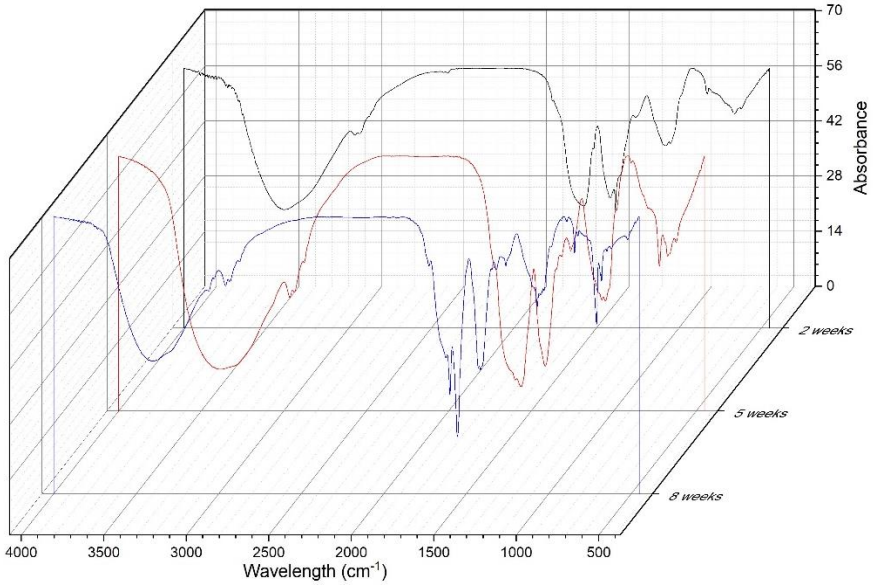

Figure 12S FTIR spectra of Nopal gel at different times of immersion.

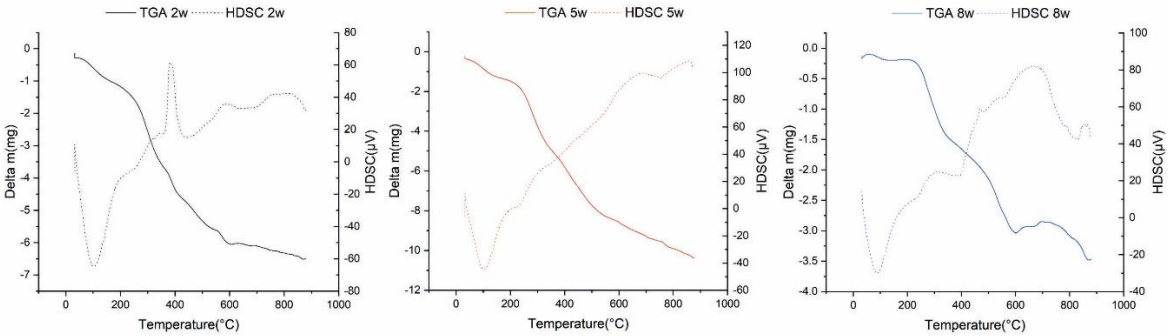

Figure 13S DSC-TGA of Nopal gel at different times of immersion.

Annex_D Further investigation of characterisation and use of self-healing material

Additional analysis of §4.3.2 Evaluation of the composition of CSMMA

FTIR analysis

In Figure 14S is reported the FTIR of pure PMMA taken from literature (Namouchi et al. 2009) and used as reference for the evaluation of FTIR of mortar with CSMMA.

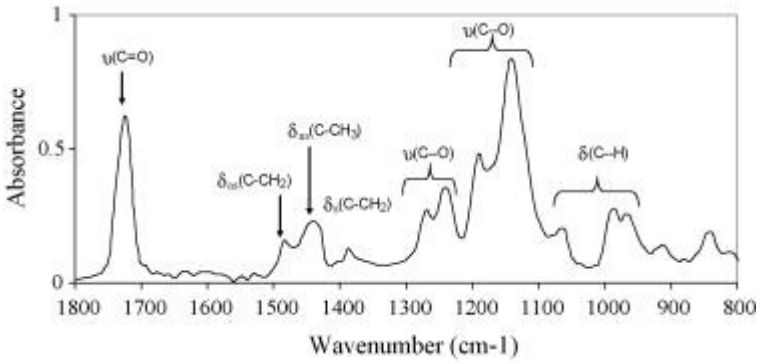

Figure 14S FTIR of PMMA.

Evaluation of the quantity of self-heling material to add

In order to define the quantity of self-healing additive CSMMA to add to the mortars, Slump test was performed to assess the change in viscosity to parity of different concentration of self-healing. In Table 7S are reported information about the composition of the tested mortars.

Table 7S Composition of the mortars.

Formulation	**Binder**	**Aggregate**		**Additives**
	1	3		CSMMA
	Slaked lime	Sand	*Cocciopesto*	
B				-
BCS1		1	4	1%
BCS3				3%

In Figure 16S is reported the graph with the results of the slump test. It is clear that to parity of greater concentration of additive the diameter of the slump test decrease. The fresh mortar is less workable because of the increment in viscosity. The decrement recorded for mortar with 1% of additive is still acceptable reducing the workability of the 17 % respect to mortar with the CSMMA, making this concentration the best to use for the purpose of research.

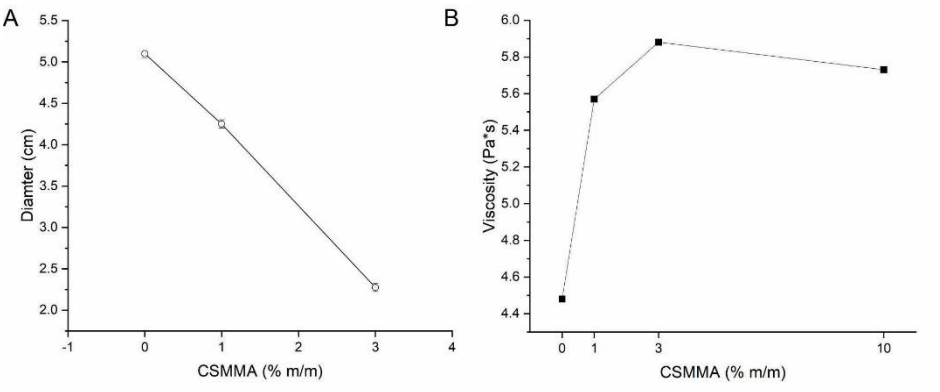

Figure 16S Results of rheological test: A) Slump test results; B) Results of viscosity.

In addition to Slump test, also rheological analysis has been performed on pure slaked lime (with 0.5% of water cement ratio) and slaked lime with CSMMA at three different concentrations 1%, 3%, 10%. The results are reported in Figure SB, it is evident the increment of viscosity of the mortar to parity of the increment of CSMMA concentration from 1% to 3%. The value obtained to 10% is lower respect to 3% but it can be considered stable or results of an experimental error.

Annex_E Further characterisation of prepared mortars

XRD analysis

In Table 8S are reported the results of XRD analysis conducted on all the designed mortars. No significant differences in composition can be assessed and the results are in line with what expected considering the nature of the binder, aggregates and additives used for mortars production.

Table 8S XRD analysis of mortars

Mineral Name	X	XN	XCS	Y	YN	YCS
Quartz	71	75	71	62	62	69
Calcite	16	7	14	22	14	9
Albite	9	5	5	7	7	6
Portlandite		7	5	9	15	10
Brucite	4	6				6

List of figures

Bibliography

[1] H. Lavagne, Il mosaico attraverso i secoli, Longo Editore, Ravenna, 1988.

[2] S. Dilaria, M. Secco, J. Bonetto, G. Ricci, G. Artioli, Making ancient mortars Hydraulic. How to Parametrize Type and Crystallinity of Reaction Products in Different Recipes, in: Conservation and Restoration of Historic Mortars and Masonry Structures, n.d.: pp. 36–52.

[3] L.M. Seymour, J. Maragh, P. Sabatini, M. Di Tommaso, J.C. Weaver, A. Masic, Hot mixing: Mechanistic insights into the durability of ancient Roman concrete, Sci. Adv. 9 (2023) eadd1602. https://doi.org/10.1126/sciadv.add1602.

[4] S. Pavía, S. Caro, An investigation of Roman mortar technology through the petrographic analysis of archaeological material, Construction and Building Materials 22 (2008) 1807–1811. https://doi.org/10.1016/j.conbuildmat.2007.05.003.

[5] G. Artioli, M. Secco, A. Addis, The Vitruvian legacy: Mortars and binders before and after the Roman world, in: The Contribution of Mineralogy to Cultural Heritage, Mineralogical Society of Great Britain and Ireland, 2019: pp. 151–202. https://doi.org/10.1180/EMU-notes.20.4.

[6] Pliny the Elder, Naturalis Historia, Liber XXXVI, n.d.

[7] P. Pasqualucci, Da un riesame delle fonti e dall'analisi dei mosaici di Privernum una nuova lettura della tecnica di esecuzione pavimentale romana, in: Atti X Coll. AISCOM, 2004: pp. 527–538.

[8] C. Fiori, M. Vandini, Teorie e tecniche per la conservazione del mosaico, Collana i Talenti, il prato, Padova, 2002.

[9] I. Pennati, Storia e teoria del restauro dei mosaici. Un itinerario dall'antichità al XX secolo., Edifir, Firenze, 2019.

[10] Moropoulou A., Diagnostic and protection of Hagia Sophia mosaics, Journal of Cultural Heritage (2013) 133–139.

[11] T. Roby, The conservation of mosaics in situ: preserving context and integrity, in: Stories in Stone: Conserving Mosaics of Roman Africa, 2011: pp. 101–114.

[12] R. Albini, C. Zizola, Zippori. In situ conservation of a floor mosaic in polychrome stones and glass paste, in: Vlth International Conference of the International Committee for the Conservation of Mosaics, 1996: pp. 235–247.

[13] D. Chelazzi, G. Poggi, Y. Jaidar, N. Toccafondi, R. Giorgi, P. Baglioni, Hydroxide nanoparticles for cultural heritage: Consolidation and protection of wall paintings and carbonate materials, Journal of Colloid and Interface Science 392 (2013) 42–49. https://doi.org/10.1016/j.jcis.2012.09.069.

[14] A.P. Ferreira Pinto, J. Delgado Rodrigues, Consolidation of carbonate stones: Influence of treatment procedures on the strengthening action of consolidants, Journal of Cultural Heritage 13 (2012) 154–166. https://doi.org/10.1016/j.culher.2011.07.003.

[15] J. Stewart, The Conservation of Mosaics on Archaeological Sites, in: Conservation of Cultural Heritage in the Arab Region. Issues in the Conservation and Management of Heritage Sites, 2016.

[16] V. Pachta, P. Marinou, M. Stefanidou, Development and testing of repair mortars for floor mosaic substrates, Journal of Building Engineering 20 (2018) 501–509. https://doi.org/10.1016/j.jobe.2018.08.019.

[17] J. Lanas, J.I. Alvarez-Galindo, Masonry repair lime-based mortars: factors affecting the mechanical behavior, Cement and Concrete Research 33 (2003) 1867–1876. https://doi.org/10.1016/S0008-8846(03)00210-2.
[18] R.M. Lawrence, T.J. Mays, S.P. Rigby, P. Walker, D. D'Ayala, Effects of carbonation on the pore structure of non-hydraulic lime mortars, Cement and Concrete Research 37 (2007) 1059–1069. https://doi.org/10.1016/j.cemconres.2007.04.011.
[19] 2017_Bertrand - Paleo-inspired Systems.pdf, (n.d.).
[20] A. Moropoulou, A. Bakolas, P. Moundoulas, E. Aggelakopoulou, REVERSE ENGINEERING: A PROPER METHODOLOGY FOR COMPATIBLE RESTORATION MORTARS, (2005).
[21] C.G. Hernández Carrillo, J.A. Gómez-Cuaspud, C.E. Martínez Suarez, Compositional, thermal and microstructural characterization of the Nopal (*opuntia ficus indica*), for addition in commercial cement mixtures, J. Phys.: Conf. Ser. 935 (2017) 012045. https://doi.org/10.1088/1742-6596/935/1/012045.
[22] A.A. Torres-Acosta, L. Alejandra Díaz-Cruz, Concrete durability enhancement from nopal (opuntia ficus-indica) additions, Construction and Building Materials 243 (2020) 118170. https://doi.org/10.1016/j.conbuildmat.2020.118170.
[23] M.T. Barbosa, C.D.R. Innocencio, L.O. Salzani, T.D.S. Pereira, N.L.G.D. De Souza, L.F.C. De Oliveira, Lime-based mortars with added silica fume and bioproducts for restoration and preservation of heritage buildings, J Build Rehabil 8 (2023) 37. https://doi.org/10.1007/s41024-023-00283-5.
[24] B. Park, Y.C. Choi, Effect of healing products on the self-healing performance of cementitious materials with crystalline admixtures, Construction and Building Materials 270 (2021) 121389. https://doi.org/10.1016/j.conbuildmat.2020.121389.
[25] K. Vijay, M. Murmu, S.V. Deo, Bacteria based self healing concrete – A review, Construction and Building Materials 152 (2017) 1008–1014. https://doi.org/10.1016/j.conbuildmat.2017.07.040.
[26] S.K. Ghosh, Self-Healing Materials: Fundamentals, Design Strategies, and Applications, in: Self-Healing Materials, John Wiley & Sons, Ltd, 2008: pp. 1–28. https://doi.org/10.1002/9783527625376.ch1.
[27] K.M.D. Dunbabin, MOSAICS OF THE GREEK AND ROMAN WORLD, Cambridge University Press, 1999.
[28] I. Fiorentini-Rancuzzi, Il mosaico. Materiali e tecniche dalle origni a oggi, Ravenna, 1984.
[29] G. Bovini, G.C. Argan, P. Portoghesi, P. Ficher, MOSAICI D'ARTISTI CONTEMPORANEI, Longo Editore, Ravenna, 1986.
[30] F. Guidobaldi, M. Grandi, Proposta di classificazione dei cementizi e mosaici omogenei ed eterogenei, in: Ancona, 2006.
[31] F. Ghedini, M. Bueno, M. Novello, F. Rinaldi, I pavimenti romani di Aquileia, Antenor Quaderni, Padova University, 2017.
[32] J.T. Bakker, Detail of the floor of room D., The Buildings in Ostia (Topographical Dictionary) (n.d.). https://www.ostia-antica.org/regio3/6/6-1.htm.
[33] Vatican Museums, Asàrotos òikos mosaic, Musei Vaticani (n.d.). https://www.museivaticani.va/content/museivaticani/en/collezioni/musei/museo-gregoriano-profano/Mosaico-dell-asarotos-oikos.html.
[34] Darius and Alexander battle., MANN-Museo Archeologico Nazionale Di Napoli (n.d.). https://mann-napoli.it/en/mosaici-2/.

[35] L. Vlad Borelli, Musivaria Mosaico e opus sectile in età antica: storia, tecniche, conservazione, Rome, 2016.
[36] Musei Capitolini, Mosaic of the Doves, Musei Capitolini (n.d.). https://www.museicapitolini.org/en/percorsi/percorsi_per_sale/palazzo_nuovo/sala_delle_colombe/mosaico_delle_colombe.
[37] A. Haug, Villa of Mysteries, Pompeii. November 2017. Room 47, looking east through window across flooring., Pompeii in Pictures (n.d.). https://www.pompeiiinpictures.com/pompeiiinpictures/RV/villa%20mysteries%20p03.htm.
[38] R. Hanson, VI.1/7, Herculaneum, August 2021. Looking north across flooring of segmented black, grey and white marble., Herculaneum in Pictures (n.d.). https://herculaneum.uk/Ins%206/Herculaneum%206%2001%20p1.htm.
[39] M. Grandi Carletti, Opus signinum e cocciopesto: alcune osservazioni terminologiche, in: Atti Del VII Colloquio Dell'Associazione Italiana per Lo Studio e La Conservazione Del Mosaico (Pompei, 22-25/03/2000), Ravenna, 2001: pp. 183–197.
[40] M.L. Morricone Matini, Roma, edifici repubblicani sottostanti alla Domus Aurea., Tess-Sistema per La Catalogazione Informatizzata Dei Pavimenti Antichi (n.d.). https://tess.beniculturali.unipd.it/web/terminologia-e-definizioni/classi-pavimentali/cementizio/.
[41] Cato the Elder, Liber De Agri Cultura, n.d.
[42] Vitruvius, The ten Books of Architecture, Translated by Morgan M.H., Dover Publications INC, New York, 1960.
[43] R.E.M. Moore, A Newly Observed Stratum in Roman Floor Mosaics, AJA 72 (1968) 57–68.
[44] I. Papayianni, V. Pachta, M. Stefanidou, Analysis of ancient mortars and design of compatible repair mortars: The case study of Odeion of the archaeological site of Dion, Construction and Building Materials 40 (2013) 84–92. https://doi.org/10.1016/j.conbuildmat.2012.09.086.
[45] S. Fabio, B. Massimo, C. Stefano, L. Carla, M. Catarina, M. José, Ancient restoration and production technologies of Roman mortars from monuments placed in hydrogeological risk areas: a case study, Archaeol Anthropol Sci 12 (2020) 147. https://doi.org/10.1007/s12520-020-01080-8.
[46] C. Rispoli, G. Montesano, M. Verde, G. Balassone, S. Columbu, A. De Bonis, C. Di Benedetto, F. D'Uva, R. Esposito, S.F. Graziano, M. Mercurio, V. Morra, P. Cappelletti, The key to ancient Roman mortars hydraulicity: ceramic fragments or volcanic materials? A lesson from the Phlegrean archaeological area (southern Italy), Construction and Building Materials 411 (2024) 134408. https://doi.org/10.1016/j.conbuildmat.2023.134408.
[47] M. Farneti, Technical-Historical Glossary of Mosaic Art, Longo Editore, Ravenna, 1993.
[48] V. Pachta, M. Stefanidou, Technology of multilayer mortars applied in ancient floor mosaic substrates, Journal of Archaeological Science: Reports 20 (2018) 683–691. https://doi.org/10.1016/j.jasrep.2018.06.018.
[49] G. Galli, Il mosaico nella Tradizione di Ravenna, Storia, Materiali, Techniche, Collana:Atelier-Che cosa con che, Ulisse Edizioni, Torino, 1989.
[50] S. Dilaria, M. Secco, J. Bonetto, G. Artioli, Technical analysis on materials and characteristics of mortar-based compounds in Roman and Late antique Aquileia (Udine,

Italy). A preliminary report of the results, in: 5th Historic Mortars Conference, Pamplona, Spain, 2019.
[51] M. Secco, L. Valentini, A. Addis, Ancient and Modern Binders, in: Nanotechnologies and Nanomaterials for Diagnostic, Conservation and Restoration of Cultural Heritage, Elsevier, 2019: pp. 205–237. https://doi.org/10.1016/B978-0-12-813910-3.00010-0.
[52] P. Pineda, S. Medina-Carrasco, A. Iranzo, L. Borau, I. García-Jiménez, Pore structure and interdisciplinary analyses in Roman mortars: Building techniques and durability factors identification, Construction and Building Materials 317 (2022) 125821. https://doi.org/10.1016/j.conbuildmat.2021.125821.
[53] M.D. Jackson, E.N. Landis, P.F. Brune, M. Vitti, H. Chen, Q. Li, M. Kunz, H.-R. Wenk, P.J.M. Monteiro, A.R. Ingraffea, Mechanical resilience and cementitious processes in Imperial Roman architectural mortar, Proc. Natl. Acad. Sci. U.S.A. 111 (2014) 18484–18489. https://doi.org/10.1073/pnas.1417456111.
[54] C.M. Stolz, A.B. Masuero, D.T. Pagnussat, A.P. Kirchheim, Influence of substrate texture on the tensile and shear bond strength of rendering mortars, Construction and Building Materials 128 (2016) 298–307. https://doi.org/10.1016/j.conbuildmat.2016.10.097.
[55] M. Gomez Serrito, I materiali lapidei naturali della domus dei putti danzanti: marmi bianchi e colorati, in: L'architettura Privata Ad Aquileia in Età Romana, 2011: pp. 309–316.
[56] M. Secco, S. Dilaria, A. Addis, J. Bonetto, G. Artioli, M. Salvadori, The Evolution of the Vitruvian Recipes over 500 Years of Floor-Making Techniques: The Case Studies of the *Domus delle Bestie Ferite* and the *Domus di Tito Macro* (Aquileia, Italy): Evolution of Vitruvian recipes over 500 years of floor-making, Archaeometry 60 (2018) 185–206. https://doi.org/10.1111/arcm.12305.
[57] C. Previato, Aquileia. Materiali, forme e sistemi costruttivi dall'età repubblicana alla tarda età imperiale, Antenor quaderni, Padova University Press, 2015.
[58] S. Dilaria, Archeologia e archeometria delle miscele leganti di Aquileia romana e tardoantica, Quasar, Rome, 2024.
[59] C. Boschetti, et al., Making Roman Mosaics in Aquileia (I BC – IV AD): Technology, Materials, Style and Workshop Practices. Two Case Studies from the insula della Casa delle Bestie Ferite, in: Local Styles or Common Pattern Books in Roman Wall., 2021: pp. 91–111.
[60] M. Salvadori, Edilizia privata e apparati decorativi ad Aquileia: lo stato della ricerca, in: L'architettura Privata Ad Aquileia in Età Romana, Padova, 2011: pp. 181–194.
[61] M. Bueno, M. Novello, F. Rinaldi, Per un corpus dei mosaici di Aquileia: status quo e prosepttive future, in: L'architettura Privata Ad Aquileia in Età Romana, Antenor Quaderni, Padova, 2011: pp. 195–220.
[62] J. Lux, S. Kramar, I mosaici bianco-neri scoperti nella villa rustica presso Mosnje, in: Mozaiki Severnega Jadrana. I Mosaici Dell'alto Adriatico, 2010: pp. 122–125.
[63] S. Dilaria, M. Secco, M. Rubinich, J. Bonetto, D. Miriello, D. Barca, G. Artioli, High-performing mortar-based materials from the late imperial baths of Aquileia: an outstanding example of Roman building tradition in Northern Italy, Geoarcheology 37 (2022) 637–657.
[64] C. Previato, Tra monti, fiume e mare: l'estrazione e il commercio della pietra nella regio X-Venetia et Histria, in: I Pascoli, i Campi, Il Mare. Paesaggi d'altura e Di Pianura in Italia Dall'Età Del Bronzo al Medioevo, Edipuglia, 2015: pp. 31–49.
[65] J. Bonetto, C. Previato, Trasformazioni del paesaggio e trasformazioni della città: le cave di pietra per Aquileia, in: Le modificazioni del paesaggio nell'altoadriatico tra pre-protostoria

ed altomedioevo, Antichità altoadriatiche, EUT Edizioni Università di Trieste, Trieste, 2013: pp. 141–162.
[66] L. Maritan, C. Mazzoli, E. Melis, A multidisciplinary approach to the characterization of roman gravestone from Aquileia (Udine, Italy), Archaeometry 45 (2003) 363–374.
[67] R.M. Ion, B.A. Bakirov, S.E. Kichanov, D.P. Kozlenko, A.V. Belushkin, C. Radulescu, I.D. Dulama, I.A. Bucurica, A.I. Gheboianu, R.M. Stirbescu, S. Teodorescu, L. Iancu, M.E. David, R.M. Grigorescu, Non-Destructive and Micro-Invasive Techniques for Characterizing the Ancient Roman Mosaic Fragments, Applied Sciences 10 (2020) 3781. https://doi.org/10.3390/app10113781.
[68] M. Verità, L. Lazzarini, E. Tesser, F. Antonelli, Villa del Casale (Piazza Armerina, Sicily): stone and glass tesserae in the baths floor mosaics, Archaeol Anthropol Sci 11 (2019) 373–385. https://doi.org/10.1007/s12520-017-0559-5.
[69] D. Barca, E. Fiorenza, M. D'Andrea, E. Le Pera, M. Musella, F. Sudano, A. Taliano Grasso, Chemical and Petrographic Characterization of Stone and Glass Tesserae in the Nereid and Geometric Mosaics from the S. Aloe Quarter in Vibo Valentia–Calabria, Italy, Minerals 9 (2019) 729. https://doi.org/10.3390/min9120729.
[70] S. Miletić, S. Kramar, J. Lux, A. Šmuc, N. Zupančič, Provenience analysis of Roman stone artefacts from sedimentary rocks from the archaeological site near Mošnje, NW Slovenia, Geologija 59 (2016) 35–54.
[71] EN12407- Natural stone test methods. Petrographic examination, (2019).
[72] S. Miletić, A. Šmuc, M. Dolenec, M. Miler, A. Mladenovič, M. Gutman Levstik, S. Dolenec, Identification and provenance determination of stone tesserae used in mosaics from Roman Celeia, Slovenia, Archaeometry 64 (2022) 561–577.
[73] O. Gomez-Laserna, A. Irto, P. Irizar, G. Lando, C. Bretti, I. Martinez-Arkarazo, L. Campagna, P. Cardiano, Non-Invasive Approach to Investigate the Mineralogy and Production Technology of the Mosaic Tesserae from the Roman Domus of Villa San Pancrazio (Taormina, Italy), Crystals 11 (2021) 1423. https://doi.org/10.3390/cryst11111423.
[74] UNI EN 16572:2015-Conservazione dei beni culturali - Glossario dei termini tecnici relativi alle malte di allettamento e gli intonaci utilizzati nel patrimonio culturale, (2015).
[75] M. Stefanidou, V. Pachta, S. Konopissi, F. Karkadelidou, I. Papayianni, Analysis and characterization of hydraulic mortars from ancient cisterns and baths in Greece, Mater Struct 47 (2014) 571–580. https://doi.org/10.1617/s11527-013-0080-y.
[76] F. Izzo, A. Arizzi, P. Cappelletti, G. Cultrone, A. De Bonis, C. Germinario, S.F. Graziano, C. Grifa, V. Guarino, M. Mercurio, V. Morra, A. Langella, The art of building in the Roman period (89 B.C. – 79 A.D.): Mortars, plasters and mosaic floors from ancient Stabiae (Naples, Italy), Construction and Building Materials 117 (2016) 129–143. https://doi.org/10.1016/j.conbuildmat.2016.04.101.
[77] UNI EN 17187, Conservazione del patrimonio culturale - Caratterizzazione delle malte utilizzate nel patrimonio culturale, (2020).
[78] UNI EN 16085:2012-Conservazione dei beni culturali - Metodologia per il campionamento dei materiali costituenti i beni culturali - Regole generali, (2012).
[79] EN 15886:2010 – Conservation of cultural property. Test methods. Colour measurement of surfaces, 2010.
[80] E. Pecchioni, F. Fratini, E. Cantisani, Atlas of the ancient mortars in thin section under optical microscope, Nardini, 2014.

[81] S. Pavía, S. Caro, An investigation of Roman mortar technology through the petrographic analysis of archaeological material, Construction and Building Materials 22 (2008) 1807–1811. https://doi.org/10.1016/j.conbuildmat.2007.05.003.
[82] M. Elzafraney, P. Soroushian, Assessment of microcrack development in concrete materials of different strengths, Materials and Structures 37 (2004).
[83] Z. Owsiak, Microscopic methods for analysis of mortars from historical masonry structures, Bulletin of the Polish Academy of Sciences Technical Sciences (2020) 136042–136042. https://doi.org/10.24425/bpasts.2021.136042.
[84] G. Montesano, M. Verde, S. Columbu, S.F. Graziano, L. Guerriero, M.L. Iadanza, A. Manna, C. Rispoli, P. Cappelletti, Ancient Roman Mortars from Anfiteatro Flavio (Pozzuoli, Southern Italy): A Mineralogical, Petrographic and Chemical Study, Coatings 12 (2022) 1712. https://doi.org/10.3390/coatings12111712.
[85] G. Borsoi, A. Santos Silva, P. Menezes, A. Candeias, J. Mirão, Analytical characterization of ancient mortars from the archaeological roman site of Pisões (Beja, Portugal), Construction and Building Materials 204 (2019) 597–608. https://doi.org/10.1016/j.conbuildmat.2019.01.233.
[86] R.J. Ball, M.P. Ansell, T.B. Su-Cadirci, V.A. Baki, P.J. Fletcher, A. Lichtenberger, R. Raja, W. Wootton, Analysis of mosaic mortars from the Roman, Byzantine and Early Islamic periods sourced from Gerasa's Northwest Quarter, Herit Sci 12 (2024) 168. https://doi.org/10.1186/s40494-024-01277-3.
[87] C. Manganelli Del Fà, La porosità nei materiali lapidei naturali e artificiali. Problematiche di determinazione della porosità. Correlazione tra caratteristiche fisiche dei materiali, porosità, dinamica dei fluidi, degrado e trattamenti conservativi, Modena, 2002.
[88] C. Fiori, Macchiarola, M., Studio e confronti fra la composizione chimica di vetri del II-I sec. a.C. provenienti da Delos (Grecia) e vetri provenienti dalla Capitanata (FG): Herdonia, I-II sec. d.C., Arpi e Ascoli Satriano, II sec. a.C., in: Atti 2e Giornate Naz. Di Stud. AIHV-Com. Naz. Ital., 1998: pp. 139–146.
[89] P.L. Cosentino, P. Capizzi, G. Fiandaca, R. Martorana, P. Messina, Advances in microgeophysics for engineering and cultural heritage, J. Earth Sci. 20 (2009) 626–639. https://doi.org/10.1007/s12583-009-0052-x.
[90] S. Hong, P. Liu, J. Zhang, F. Xing, B. Dong, Visual & quantitative identification of cracking in mortar subjected to loads using X-ray computed tomography method, Cement and Concrete Composites 100 (2019) 15–24. https://doi.org/10.1016/j.cemconcomp.2019.03.010.
[91] S. Divya Rani, A.V. Rahul, M. Santhanam, A multi-analytical approach for pore structure assessment in historic lime mortars, Construction and Building Materials 272 (2021) 121905. https://doi.org/10.1016/j.conbuildmat.2020.121905.
[92] G. Sokhansefat, M. Moradian, M. Finnell, A. Behravan, M.T. Ley, C. Lucero, J. Weiss, Using X-ray computed tomography to investigate mortar subjected to freeze-thaw cycles, Cement and Concrete Composites 108 (2020) 103520. https://doi.org/10.1016/j.cemconcomp.2020.103520.
[93] M. Pateryon-Salome, F. Peryin, A. Laval-Jeantet, P.O. Spanne, P. Cloetens, G. Peix, 3D microtomography of cancellous bone samples using synchrotron radiation, in: Medical Imaging 1996: Physics of Medical Imaging, Newport Beach, CA, United States, 1996.

[94] A. Snigirev, I. Snigireva, V. Kohn, S. Kuznetsov, I. Schelokov, On the possibilities of x-ray phase contrast microimaging by coherent high-energy synchrotron radiation, Review of Scientific Instruments 66 (1995) 5486–5492.
[95] O. Rozenbaum, 3-D characterization of weathered building limestones by high resolution synchrotron X-ray microtomography, Science of The Total Environment 409 (2011) 1959–1966. https://doi.org/10.1016/j.scitotenv.2011.02.014.
[96] E. Possenti, C. Conti, G.D. Gatta, M. Merlini, M. Realini, C. Colombo, Synchrotron radiation μ X-ray diffraction in transmission geometry for investigating the penetration depth of conservation treatments on cultural heritage stone materials, Anal. Methods 12 (2020) 1587–1594. https://doi.org/10.1039/D0AY00010H.
[97] G. Massinelli, E. Possenti, C. Colombo, G.D. Gatta, M. Realini, N. Marinoni, 4D imaging and quantification of the effect of a Phosphate-Based treatment on building materials by means of synchrotron X-ray Microtomography: New insights into the dynamic of the consolidation process, Construction and Building Materials 397 (2023) 132348. https://doi.org/10.1016/j.conbuildmat.2023.132348.
[98] C. Colantonio, P. Baldassarri, P. Avino, M.L. Astolfi, G. Visco, Visual and Physical Degradation of the Black and White Mosaic of a Roman Domus under Palazzo Valentini in Rome: A Preliminary Study, Molecules 27 (2022) 7765. https://doi.org/10.3390/molecules27227765.
[99] C. Fiori, La conservazione dei mosaici, Progetto Restauro 10 (2004) 2–14.
[100] Á. Török, B. Szemerey-Kiss, Freeze-thaw durability of repair mortars and porous limestone: compatibility issues, Prog Earth Planet Sci 6 (2019) 42. https://doi.org/10.1186/s40645-019-0282-1.
[101] C. Saiz-Jimenez, J. Garcia-Rowe, J.M. Rodriguez-Hidalgo, Biodeterioration of polychrome Roman mosaics, International Biodeterioration 28 (1991) 65–79. https://doi.org/10.1016/0265-3036(91)90034-O.
[102] A. Altieri, D. Poggi, S. Ricci, Mosaic pavements from the Thermae of Caracalla (Rome): biodeterioration and methods of control, in: Mosaics Make a Site: The Conservation in Situ of Mosaics on Archaeological Sites. Proceedings of the VIth Conference of the International Committee for the Conservation of Mosaics, Nicosia, Cyprus, 1996, 2003: pp. 249–260.
[103] Y.M. Elgohary, M.M.A. Mansour, M.Z.M. Salem, Assessment of the potential effects of plants with their secreted biochemicals on the biodeterioration of archaeological stones, Biomass Conv. Bioref. 14 (2024) 12069–12083. https://doi.org/10.1007/s13399-022-03300-8.
[104] PIQUÉ F., BURCH R., ROBY T., DEMAS M., Learning from the literature : a review of published works on mosaic deterioration and conservation treatments, in: Lessons Learned : Reflecting on the Theory and Practice of Mosaic Conservation = Leçons Retenues : Les Enseignements Tirés Des Expériences Passées Dans Le Domaine de La Conservation Des Mosaïques, Getty Conservation Institute, Hammamet, 2005: pp. 33–45.
[105] A. Varone, Un nuovo pavimento musivo pompeiano in corso di restauro al momento dell'eruzione del Vesuvio nel 79 d.C., in: Atti Del III Colloquio AISCOM, Bordighiera, 1996: pp. 681–694.
[106] C. Brandi, Cosa debba intendersi per restauro preventivo, in Bollettino dell'ICR, 1956.
[107] C. Muscolino, I mosaici dell'arcone di S. Vitale a Ravenna. Osservazioni e scelte metodologiche per un restauro, in: Mosaici a S. Vitale Ed Altri Restauri, Longo Editore, Ravenna, 1992: pp. 55–67.

[108] A. Melucco-Vaccaro, Il restauro del mosaico paritale in situ. Tradizioni, tendenze in atto, professionalità, in: Mosaici a S. Vitale Ed Altri Restauri, Longo Editore, Ravenna, 1992: pp. 81–83.
[109] P. Pensabene, E. Gallocchio, V. Bruni, VECCHI E NUOVI MOSAICI DEI FONDI EX CAL E RIZZ I DI AQUILEIA: IPOTESI DI RICONTESTUALIZZAZIONE, in: Atti Del XX Colloquio Dell'associazione Italiana per Lo Studio e La Conservazione Del Mosaico, Tivoli, 2015: pp. 437–444.
[110] Madrigali E., Esperienze di restauro e valorizzazione di Aquileia: L'esempio dei fondi ex Cossar, in: L'architettura Privata Ad Aquileia in Età Romana, Padova, 2011.
[111] B. Županek, M.L. Kikelj, K. Žagar, S. Kramar, A new lightweight support for the restoration and presentation of a large Roman mosaic, Journal of Cultural Heritage 19 (2016) 477–485. https://doi.org/10.1016/j.culher.2016.01.005.
[112] G. Beccati, Mosaici e pavimenti marmorei , Scavi di Ostia, Roma, 1962.
[113] D. Nikhil Kumar, P. Rathish Kumar, Investigations on alternate lime-pozzolana based mortars for repair of heritage structures, Construction and Building Materials 341 (2022) 127776. https://doi.org/10.1016/j.conbuildmat.2022.127776.
[114] R. Veiga, Air lime mortars: What else do we need to know to apply them in conservation and rehabilitation interventions? A review, Construction and Building Materials 157 (2017) 132–140. https://doi.org/10.1016/j.conbuildmat.2017.09.080.
[115] Macchiarola, M., Conservazione musiva in Italia:luci ed ombre, in: I Mosaici Dell'alto Adriatico, 2010: pp. 37–44.
[116] UNI 10924:2001 Beni culturali - Malte per elementi costruttivi e decorativi - Classificazione e terminologia, (2001).
[117] M. Stefanidou, I. Papayianni, The role of aggregates on the structure and properties of lime mortars, Cement and Concrete Composites 27 (2005) 914–919. https://doi.org/10.1016/j.cemconcomp.2005.05.001.
[118] V. Nezˇerka, M. Somr, J. Zeman, MICROMECHANICS-BASED MODELS OF COCCIOPESTO MORTARS, Engineering Mechanics (2012).
[119] V.S. Athira, S. Manohar, Carbonation of air lime mortars under natural and accelerated conditions – A systematic review, Materials Today: Proceedings (2023) S2214785323019806. https://doi.org/10.1016/j.matpr.2023.04.082.
[120] L. Medeghini, L. Calzolari, M. Botticelli, M. Di Fazio, C. De Vito, I. Pettiti, F. Bardelli, S. Mignardi, The secret of ancient Roman hydraulic mortar: the lesson learnt from the past for future cements, Cement and Concrete Composites 148 (2024) 105484. https://doi.org/10.1016/j.cemconcomp.2024.105484.
[121] D. Ergenç, L.S. Gómez-Villalba, R. Fort, Crystal development during carbonation of lime-based mortars in different environmental conditions, Materials Characterization 142 (2018) 276–288. https://doi.org/10.1016/j.matchar.2018.05.043.
[122] M. Thiery, G. Villain, P. Dangla, G. Platret, Investigation of the carbonation front shape on cementitious materials: Effects of the chemical kinetics, Cement and Concrete Research 37 (2007) 1047–1058. https://doi.org/10.1016/j.cemconres.2007.04.002.
[123] A. Moropoulou, A. Bakolas, K. Bisbikou, Investigation of the technology of historic mortars, Journal of Cultural Heritage 1 (2000) 45–58. https://doi.org/10.1016/S1296-2074(99)00118-1.
[124] L. Schueremans, Ö. Cizer, E. Janssens, G. Serré, K.V. Balen, Characterization of repair mortars for the assessment of their compatibility in restoration projects: Research and

practice, Construction and Building Materials 25 (2011) 4338–4350. https://doi.org/10.1016/j.conbuildmat.2011.01.008.
[125] M.E. Loke, K. Pallav, G. Cultrone, C. Di Filippo, Investigating the standard design and production procedure of heritage mortars for compatible and durable masonry restoration, Journal of Building Engineering 94 (2024) 110012. https://doi.org/10.1016/j.jobe.2024.110012.
[126] S. Botas, R. Veiga, A. Velosa, Air lime mortars for conservation of historic tiles: Bond strength of new mortars to old tiles, Construction and Building Materials 145 (2017) 426–434. https://doi.org/10.1016/j.conbuildmat.2017.04.027.
[127] A. Moropoulou, A. Bakolas, P. Moundoulas, E. Aggelakopoulou, S. Anagnostopoulou, Optimization of compatible restoration mortars for the earthquake protection of Hagia Sophia, Journal of Cultural Heritage 14 (2013) e147–e152. https://doi.org/10.1016/j.culher.2013.01.008.
[128] P. Faria, F. Henriques, V. Rato, Comparative evaluation of lime mortars for architectural conservation, Journal of Cultural Heritage 9 (2008) 338–346. https://doi.org/10.1016/j.culher.2008.03.003.
[129] L. Bertrand, C. Gervais, A. Masic, L. Robbiola, Paleo-inspired Systems: Durability, Sustainability, and Remarkable Properties, Angewandte Chemie 57 (2018) 7288–7295. https://doi.org/10.1002/anie.201709303.
[130] R.R. Gallegos-Villela, F.D. Larrea-Zambrano, C.E. Goyes-Lopez, J.F. Perez-Sanchez, E.J. Suarez-Dominguez, A. Palacio-Perez, Effect of natural additives on concrete mechanical properties, Cogent Engineering 8 (2021) 1870790. https://doi.org/10.1080/23311916.2020.1870790.
[131] C. James, G. Sivasankarapillai, Assessment of Natural Additives Modified Lime Mortars for Repair of Historic Structures with Strength, Durability and Microstructural Parameters, Period. Polytech. Civil Eng. (2022). https://doi.org/10.3311/PPci.21135.
[132] C. Alisi, L. Bacchetta, E. Bojorquez, M. Falconieri, S. Gagliardi, M. Insaurralde, M.F.F. Martinez, A.M. Orozco, F. Persia, A.R. Sprocati, S. Procacci, A. Tatì, Mucilages from Different Plant Species Affect the Characteristics of Bio-Mortars for Restoration, Coatings 11 (2021) 75. https://doi.org/10.3390/coatings11010075.
[133] F.M. León-Martínez, P.F. de J. Cano-Barrita, L. Lagunez-Rivera, L. Medina-Torres, Study of nopal mucilage and marine brown algae extract as viscosity-enhancing admixtures for cement based materials, Construction and Building Materials 53 (2014) 190–202. https://doi.org/10.1016/j.conbuildmat.2013.11.068.
[134] A. Aquilina, R.P. Borg, J. Buhagiar, The application of Natural Organic Additives in Concrete: Opuntia ficus-indica., IOP Conf. Ser.: Mater. Sci. Eng. 442 (2018) 012016. https://doi.org/10.1088/1757-899X/442/1/012016.
[135] R. Ravi, T. Selvaraj, S.K. Sekar, Characterization of Hydraulic Lime Mortar Containing *Opuntia ficus-indica* as a Bio-Admixture for Restoration Applications, International Journal of Architectural Heritage 10 (2016) 714–725. https://doi.org/10.1080/15583058.2015.1109735.
[136] N. Nuzhyna, Anatomically distinct representatives of Cactaceae Juss. family have different response to acute heat shock stress, (2018).
[137] L. Bacchetta, S. Procacci, V. Martina, S. Gagliardi, E. Bojorquez-Quintal, O. Maccioni, M. Falconieri, M. Moreno, F. Zaza, G. Platamone, C. Alisi, Estrazione e caratterizzazione di mucillagine da cladodi di Opuntia ficus-indica e di capsaicinoidi da frutti di Capsicum spp.,

in: Da OPuntia Ficus Indica e Capsicum Spp. Prodotti Sostenibili per i Beni Culturali, ENEA Agenzia nazionale per le nuove tecnologie, L'energia e lo sviluppo economico sostenibile, 2021.
[138] Los Murales de la Batalla y del Pórtico "A", Cacaxtla, Tlaxcala, Mediateca Inah (n.d.). https://mediateca.inah.gob.mx/islandora_74/.
[139] E. Mazzetto, Le pitture murali di Cacaxtla e le influenze maya nel Messico centrale, La Ricerca Folklorica (2010) 111–125.
[140] C. Brittenham, Los pintores del Mural de la Batalla de Cacaxtla, in: Memorias Del Primer Coloquio Internacional: Cacaxtla a Sus Treinta Anos de Investigacion, México, Instituto Nacional de Antropologia e Historia - Consejo Nacional para la Cultura y las Artes, 2006: pp. 503–521.
[141] D. Rivera, F. Flynn Paine, Diego Rivera, Museum of Modern Art, Norton, 1931.
[142] A. Kettenmann, Diego Rivera,1887-1957: A Revolutionary Spirit in Modern Art, Taschen, 2003.
[143] Diego Rivera, first and second floor murals of the Secretaría de Educación Pública, Smarthistory (n.d.). https://smarthistory.org/rivera-murals-ministry-public-education/.
[144] M.L. Cardenas, S. Serna, J. Velasco de la Garza, Effect of raw and cooked nopal (Opuntia ficus indica) ingestion on growth and total cholesterol, lipoproteins and blood glucose in rats., Archivos Latinoamericanos de Nutricion 48 (4) (1998) 316–323.
[145] C. Sáenz, E. Sepúlveda, B. Matsuhiro, Opuntia spp mucilage's: a functional component with industrial perspectives, Journal of Arid Environments 57 (2004) 275–290. https://doi.org/10.1016/S0140-1963(03)00106-X.
[146] A.R. Sprocati, C. Alisi, G. Migliore, P. Marconi, F. Tasso, Sustainable Restoration Through Biotechnological Processes: A Proof of Concept, in: E. Joseph (Ed.), Microorganisms in the Deterioration and Preservation of Cultural Heritage, Springer International Publishing, Cham, 2021: pp. 235–261. https://doi.org/10.1007/978-3-030-69411-1_11.
[147] S.V. Vargas-Solano, F. Rodríguez-González, R. Martínez-Velarde, R. Campos-Mendiola, M.A. Hurtado-Salgado, J. Muthuswamy Ponniah, Composicion quimica del mucilago de Nopal en diferentes etapas de madurez., Agro (2022). https://doi.org/10.47163/agrociencia.v56i2.2726.
[148] F. Rodríguez-González, J. Pérez-González, C.N. Muñoz-López, S.V. Vargas-Solano, B.M. Marín-Santibáñez, Influence of age on molecular characteristics and rheological behavior of nopal mucilage, Food Science & Nutrition 9 (2021) 6776–6785. https://doi.org/10.1002/fsn3.2629.
[149] M. Martins, M.H. Ribeiro, C.M.M. Almeida, Physicochemical, Nutritional, and Medicinal Properties of Opuntia ficus-indica (L.) Mill. and Its Main Agro-Industrial Use: A Review, Plants 12 (2023) 1512. https://doi.org/10.3390/plants12071512.
[150] M. Contreras-Padilla, M.E. Rodríguez-García, E. Gutiérrez-Cortez, M. del C. Valderrama-Bravo, J.I. Rojas-Molina, E.M. Rivera-Muñoz, Physicochemical and rheological characterization of Opuntia ficus mucilage at three different maturity stages of cladode, European Polymer Journal 78 (2016) 226–234. https://doi.org/10.1016/j.eurpolymj.2016.03.024.
[151] M. Contreras-Padilla, E.M. Rivera-Muñoz, E. Gutiérrez-Cortez, A.R. Del López, M.E. Rodríguez-García, Characterization of crystalline structures in Opuntia ficus-indica, J Biol Phys 41 (2015) 99–112. https://doi.org/10.1007/s10867-014-9368-6.

[152] A. Cárdenas, F.M. Goycoolea, M. Rinaudo, On the gelling behaviour of 'nopal' (Opuntia ficus indica) low methoxyl pectin, Carbohydrate Polymers 73 (2008) 212–222. https://doi.org/10.1016/j.carbpol.2007.11.017.
[153] A.F. Rivera Cañón, C.G. Hernández Carrillo, J.A. Gómez Cuaspud, Evaluation of physicochemical properties of Nopal (Opuntia Ficus-Indica) as bio coagulant-flocculant for water treatment, J. Phys.: Conf. Ser. 2046 (2021) 012057. https://doi.org/10.1088/1742-6596/2046/1/012057.
[154] Y. Kita, The functions of vegetable mucilage in lime and earth mortars - A Review, (n.d.) 7.
[155] F.M. León-Martínez, P.F.D.J. Cano-Barrita, F. Castellanos, K.B. Luna-Vicente, S. Ramírez-Arellanes, C. Gómez-Yáñez, Carbonation of high-calcium lime mortars containing cactus mucilage as additive: a spectroscopic approach, J Mater Sci 56 (2021) 3778–3789. https://doi.org/10.1007/s10853-020-05514-5.
[156] C. Rodriguez-Navarro, E. Ruiz-Agudo, A. Burgos-Cara, K. Elert, E.F. Hansen, Crystallization and Colloidal Stabilization of Ca(OH) $_2$ in the Presence of Nopal Juice (*Opuntia ficus indica*): Implications in Architectural Heritage Conservation, Langmuir 33 (2017) 10936–10950. https://doi.org/10.1021/acs.langmuir.7b02423.
[157] A. Cárdenas, W.M. Arguelles, F.M. Goycoolea, On the Possible Role of Opuntia ficus-indica Mucilage, (n.d.).
[158] L. Ventolà, M. Vendrell, P. Giraldez, L. Merino, Traditional organic additives improve lime mortars: New old materials for restoration and building natural stone fabrics, Construction and Building Materials 25 (2011) 3313–3318. https://doi.org/10.1016/j.conbuildmat.2011.03.020.
[159] R. Ciriminna, N. Chavarría-Hernández, A.I. Rodríguez-Hernández, Toward unfolding the bioeconomy of nopal (Opuntia spp.), (2019).
[160] G. Di Bella, G.L. Vecchio, A. Albergamo, V. Nava, G. Bartolomeo, A. Macrì, L. Bacchetta, V. Lo Turco, A.G. Potortì, Chemical characterization of Sicilian dried nopal [Opuntia ficus-indica (L.) Mill.], Journal of Food Composition and Analysis 106 (2022) 104307. https://doi.org/10.1016/j.jfca.2021.104307.
[161] G. Timpanaro, V.T. Foti, The structural characteristics, Economic performance and prospects for the italian cactus pear industry, Journal of the Professional Association for Cactus Development 16 (2014) 32–50.
[162] L. Bacchetta, R. Balducchi, Il fico d'India dagli scarti alla bioeconomia, in: Informatore Agrario, 2019: pp. 38–41.
[163] F.G. Giordano, N. Boon, N. De Belie, Influence of Hydrated Lime on the Self-Healing Capacity of Cement Mortars, MATEC Web Conf. 378 (2023) 02021. https://doi.org/10.1051/matecconf/202337802021.
[164] H. Mihashi, T. Nishiwaki, Development of Engineered Self-Healing and Self-Repairing Concrete-State-of-the-Art Report, ACT 10 (2012) 170–184. https://doi.org/10.3151/jact.10.170.
[165] M. Rajczakowska, K. Habermehl-Cwirzen, H. Hedlund, A. Cwirzen, The Effect of Exposure on the Autogenous Self-Healing of Ordinary Portland Cement Mortars, Materials 12 (2019) 3926. https://doi.org/10.3390/ma12233926.
[166] T.S. Qureshi, A. Kanellopoulos, A. Al-Tabbaa, Encapsulation of expansive powder minerals within a concentric glass capsule system for self-healing concrete, Construction

and Building Materials 121 (2016) 629–643. https://doi.org/10.1016/j.conbuildmat.2016.06.030.
[167] B. Lubelli, T.G. Nijland, Self-healing of lime based mortars: microscopy observations on case studies, (n.d.).
[168] A. Izaguirre, J. Lanas, J.I. Álvarez, Characterization of aerial lime-based mortars modified by the addition of two different water-retaining agents, Cement and Concrete Composites 33 (2011) 309–318. https://doi.org/10.1016/j.cemconcomp.2010.09.008.
[169] C. De Nardi, A. Cecchi, L. Ferrara, A. Benedetti, D. Cristofori, Effect of age and level of damage on the autogenous healing of lime mortars, Composites Part B: Engineering 124 (2017) 144–157. https://doi.org/10.1016/j.compositesb.2017.05.041.
[170] W. Zhang, Q. Zheng, A. Ashour, B. Han, Self-healing cement concrete composites for resilient infrastructures: A review, Composites Part B: Engineering 189 (2020) 107892. https://doi.org/10.1016/j.compositesb.2020.107892.
[171] G.T.D.S. Lima, L. Silvestro, L.U.D. Tambara Júnior, M. Cheriaf, J.C. Rocha, Autonomous Self-Healing Agents in Cementitious Materials: Parameters and Impacts on Mortar Properties, Buildings 14 (2024) 2000. https://doi.org/10.3390/buildings14072000.
[172] B. Šavija, J. Feiteira, M. Araújo, S. Chatrabhuti, J.-M. Raquez, K. Van Tittelboom, E. Gruyaert, N. De Belie, E. Schlangen, Simulation-Aided Design of Tubular Polymeric Capsules for Self-Healing Concrete, Materials 10 (2017) 10. https://doi.org/10.3390/ma10010010.
[173] K. Van Tittelboom, N. De Belie, Self-Healing in Cementitious Materials—A Review, Materials 6 (2013) 2182–2217. https://doi.org/10.3390/ma6062182.
[174] R.A. Khushnood, Z.A. Qureshi, N. Shaheen, S. Ali, Bio-mineralized self-healing recycled aggregate concrete for sustainable infrastructure, Science of The Total Environment 703 (2020) 135007. https://doi.org/10.1016/j.scitotenv.2019.135007.
[175] Y. Javeed, Y. Goh, K.H. Mo, S.P. Yap, B.F. Leo, Microbial self-healing in concrete: A comprehensive exploration of bacterial viability, implementation techniques, and mechanical properties, Journal of Materials Research and Technology 29 (2024) 2376–2395. https://doi.org/10.1016/j.jmrt.2024.01.261.
[176] C. De Nardi, S. Bullo, L. Ferrara, L. Ronchin, A. Vavasori, Effectiveness of crystalline admixtures and lime/cement coated granules in engineered self-healing capacity of lime mortars, Mater Struct 50 (2017) 191. https://doi.org/10.1617/s11527-017-1053-3.
[177] L. Lazzarini, Poikiloi lithoi, versiculores maculae: i marmi colorati della Grecia antica. Storia, uso, diffusione, cave, geologia, caratterizzazione scientifica, archeometria., Gentili editori e stampatori in Pisa, 2007.
[178] R.J. Dunham, Classification of Carbonate Rocks According to Depositional Textures, in: Classification of Carbonate Rocks. A Symposium, American Association of Petroleum Geologists, 1962.
[179] A. Šmuc, M. Dolenec, M. Lesar-Kikelj, J. Lux, M. Pflaum, B. Šeme, B. Županek, L. Gale, S. Kramar, Variety of Black and White Limestone Tesserae Used in Ancient Mosaics in Slovenia, Archaeometry 59 (2017) 205–221.
[180] M. Brilli, F. Antonelli, F. Giustini, L. Lazzarini, P. Pensabene, Black limestones used in antiquity: the petrographic, isotopic and EPR database for provenance determination, Journal of Archaeological Science 37 (2010) 994–1005.
[181] L. Consorti, D. Arbulla, L. Bonini, S. Fabbi, F. Fanti, M. Franceschi, G. Frijia, G.A. Pini, The Mesozoic palaeoenvironmental richness of the Trieste Karst, GFT 13 (2021) 1–40.

[182] A. Tarlao, M. Tentor, G. Tunis, S. Venturini, Evidenze di una fase tettonica nel Senoniano Inferiore dell'area del villaggio del pescatore (Trieste), in: Gortania - Atti Museo Friuli Storia Naturale, Udine, 1993: pp. 23–34.
[183] A.A. Chiarenza, M. Fabbri, L. Consorti, M. Muscioni, D.C. Evans, J.L. Cantalapiedra, F. Fanti, An Italian dinosaur Lagerstätte reveals the tempo and mode of hadrosauriform body size evolution, Sci Rep 11 (2021).
[184] F. Cucchi, S. Biolchi, L. Zini, B. Jurkovšek, T. Kolar-Jurkovšek, Geologia e geomorfologia del Carso Classico, in: Le Acque Del Carso Classico, EUT Edizioni Università di Trieste, 2015: pp. 23–38.
[185] B. Otoničar, Upper Cretaceous to Paleogene Forbulge Unconformity Associated With Foreland Basin Evolution (Kras, Matarsko Podolje and Istria; SW Slovenia and NW Croatia), Acta Carsologica 36 (2007) 101–120.
[186] B. Jurkovšek, S. Biolchi, S. Furlani, T. Kolar-Jurkovšek, L. Zini, J. Jež, G. Tunis, M. Bavec, F. Cucchi, Geology of the Classical Karst Region (SW Slovenia–NE Italy), Journal of Maps 12 (2016) 352–362.
[187] I.K. Whitbread, The Characterisation of Argillaceous Inclusions in Ceramic Thin Sections, Archaeometry 28 (1986) 79–88.
[188] I.K. Whitbread, A proposal for the systematic description of thin sections towards the study of ancient ceramic technology., in: 25th International Symposium on Archaeometry, Elsevier, Amsterdam, 1989: pp. 127–138.
[189] I.K. Whitbread, Greek transport amphorae: a petrological and archaeological study, School at Athens, The British. Athens: Fitch Laboratory Occasional Paper (1995).
[190] C.N. Arnoldi, E. Azzar, M. Barbieri, P. Tucci, Petrographic and geochemical features of the «Cipollino Verde» marble from the Apuan Alps (northern Tuscany, Italy) and archaeometric implications, Mineralogy, Crystallography, Geochemistry, Ore Deposits, Petrology, Volcanology 68 (1999) 145–162.
[191] G. Massa, D. Pieruccioni, Geological Characterization of the Marble Commercial Varieties Outcropping in the Frigido Valley (Apuan Alps, Italy), Geoheritage 12 (2020) 60.
[192] V. Rubinetto, L. Appolonia, S. De Leo, M. Serra, A. Borghi, A Petrographic Study of the Anthropomorphic Stelae from the Megalithic Area of Saint-Martin-De-Corléans (Aosta, Northern Italy), Archaeometry 56 (2014) 927–950.
[193] F. Antonelli, L. Lazzarini, S. Cancelliere, L. Buffone, The coloured stones and marbles decorating the Odeion of Pompeii, in: 2020, IMEKO TC-4 International Conference on Metrology for Archaeology and Cultural Heritage, Trento, Italy, 2020: pp. 425–430.
[194] I. Badouna, P. Koutsovitis, C. Karkalis, K. Laskaridis, N. Koukouzas, P. Tyrologou, M. Patronis, C. Papatrechas, P. Petrounias, Petrological and Geochemical Properties of Greek Carbonate Stones, Associated with Their Physico-Mechanical and Aesthetic Characteristics, Minerals 10 (2020) 507. https://doi.org/10.3390/min10060507.
[195] L.N. Warr, IMA–CNMNC approved mineral symbols, MinMag 85 (2021) 291–320. https://doi.org/10.1180/mgm.2021.43.
[196] M. Tentor, G. Tunis, S. Venturini, Fenomeni di silicizzazione nel Cenomaniano del Carso monfalconese., in: Natura Nascosta, Monfalcone, 1993: pp. 1–18.
[197] G. Tunis, N. Pugliese, B. Jurkovšek, B. Ogorelec, K. Drobne, R. Riccamboni, V.C. Tewari, Microbialites as Markers of Biotic and Abiotic Events in the Karst District, Slovenia and Italy, in: V. Tewari, J. Seckbach (Eds.), STROMATOLITES: Interaction of Microbes with Sediments, Springer Netherlands, Dordrecht, 2011: pp. 251–272.

[198] W. Chen, H. Honghui, T. Bai, S. Jiang, Geochemistry of Monazite within Carbonatite Related REE Deposits, Resources 6 (2017) 51. https://doi.org/10.3390/resources6040051.
[199] O. von Knorring, T.N. Clifford, On a skarn monazite occurrence from the Namib desert near Usakos, South-West Africa, Mineralogical Magazine and Journal of the Mineralogical Society 32 (1960) 650–653. https://doi.org/10.1180/minmag.1960.032.251.06.
[200] A. Tentor, Osservazioni stratigrafiche sul monte Brestovi (Carso goriziano), in: Natura Nascosta, 2007: pp. 1–23.
[201] A. Šmuc, M. Dolenec, M. Lesar-Kikelj, J. Lux, M. Pflaum, B. Šeme, B. Županek, L. Gale, S. Kramar, Variety of Black and White Limestone Tesserae Used in Ancient Mosaics in Slovenia: Limestone tesserae used in ancient mosaics in Slovenia, Archaeometry 59 (2017) 205–221. https://doi.org/10.1111/arcm.12250.
[202] I. Badouna, P. Koutsovitis, C. Karkalis, K. Laskaridis, N. Koukouzas, P. Tyrologou, M. Patronis, C. Papatrechas, P. Petrounias, Petrological and Geochemical Properties of Greek Carbonate Stones, Associated with Their Physico-Mechanical and Aesthetic Characteristics, Minerals 10 (2020) 507.
[203] S. Capedri, G. Venturelli, S. De Maria, M.P.M. Uguzzoni, G. Pancotti, Characterisation and provenance of stones used in the mosaics of the domus dei Coiedii at Roman Suasa (Ancona, Italy), Journal of Cultural Heritage 2 (2001) 7–22.
[204] L.J. Vicat, Practical and scientific treatise on calcareous mortars and cements, artificial and natural., Architectural library, London, 1837.
[205] L. Paama, I. Pitkänen, H. Rönkkömäki, P. Perämäki, Thermal and infrared spectroscopic characterization of historical mortars, Thermochimica Acta 320 (1998) 127–133. https://doi.org/10.1016/S0040-6031(98)00421-3.
[206] P.J.P. Gleize, E.V. Motta, D.A. Silva, H.R. Roman, Characterization of historical mortars from Santa Catarina (Brazil), Cement and Concrete Composites 31 (2009) 342–346. https://doi.org/10.1016/j.cemconcomp.2009.02.013.
[207] Portulano B., et al., Caratteri stratigrafici dei mosaici di Aquileia, in: Scienza e Beni Culturali XVIII, 2002: pp. 637–646.
[208] G. Iori, M. Alzu'bi, A. Abbadi, et al., BEATS: BEAmline for synchrotron X-ray microTomography at SESAME, JOURNAL OF SYNCHROTRON RADIATION 31 (2024) 1358–1372.
[209] G. Weitkamp, A. Bregt, R. Van Lammeren, Measuring Visible Space to Assess Landscape Openness, Landscape Research 36 (2011) 127–150. https://doi.org/10.1080/01426397.2010.549219.
[210] D. Gürsoy, F. De Carlo, X. Xiao, C. Jacobsen, TomoPy: a framework for the analysis of synchrotron tomographic data, Journal of Synchrotron Radiation 21 (2014) 1188–1193. https://doi.org/10.1107/S1600577514013939.
[211] G. Iori, P. Hans, I. Foudeh, M. Alzu'bi, M. Al Mohammad, S. Matalgah, Alrecon: computed tomography reconstruction web application based on Solara, ORE 4 (2024). https://doi.org/10.12688/openreseurope.16863.2.
[212] N.T. Vo, R.C. Atwood, M. Drakopoulos, Superior techniques for eliminating ring artifacts in X-ray micro-tomography, Opt. Express 26 (2018) 28396. https://doi.org/10.1364/OE.26.028396.
[213] D. Paganin, S.C. Mayo, T.E. Gureyev, P.R. Miller, S.W. Wilkins, Simultaneous phase and amplitude extraction from a single defocused image of a homogeneous object, Journal of Microscopy 206 (2002) 33–40. https://doi.org/10.1046/j.1365-2818.2002.01010.x.

[214] J. Schindelin, I. Arganda-Carreras, E. Frise, V. Kaynig, M. Longair, T. Pietzsch, S. Preibisch, C. Rueden, S. Saalfeld, B. Schmid, J.-Y. Tinevez, D.J. White, V. Hartenstein, K. Eliceiri, P. Tomancak, A. Cardona, Fiji: an open-source platform for biological-image analysis, Nature Methods 9 (2012) 676–682. https://doi.org/10.1038/nmeth.2019.

[215] E. Uğurlu Sağın, H.E. Duran, H. Böke, Archaeometric study of Roman bricks and cocciopesto aggregates from the ancient city of Nysa, Western Anatolia, Journal of Archaeological Science: Reports 57 (2024) 104594. https://doi.org/10.1016/j.jasrep.2024.104594.

[216] G. Eramo, M. Clausi, G. Fioretti, D. Pinto, The Use of Lime over the Centuries: The Complexity of the Apulian Built Heritage, Minerals 14 (2024) 91. https://doi.org/10.3390/min14010091.

[217] E.A. Laycock, D. Pirrie, F. Clegg, A.M.T. Bell, P. Bidwell, An investigation to establish the source of the Roman lime mortars used in Wallsend, UK, Construction and Building Materials 196 (2019) 611–625. https://doi.org/10.1016/j.conbuildmat.2018.11.108.

[218] B.A. Silva, A.P. Ferreira Pinto, A. Gomes, Natural hydraulic lime versus cement for blended lime mortars for restoration works, Construction and Building Materials 94 (2015) 346–360. https://doi.org/10.1016/j.conbuildmat.2015.06.058.

[219] L. Rampazzi, M.P. Colombini, C. Conti, C. Corti, A. Lluveras-Tenorio, A. Sansonetti, M. Zanaboni, Technology of Medieval Mortars: An Investigation into the Use of Organic Additives: Technology of medieval mortars, Archaeometry 58 (2016) 115–130. https://doi.org/10.1111/arcm.12155.

[220] P. Brzozowski, E. Horszczaruk, K. Hrabiuk, The Influence of Natural and Nano-additives on Early Strength of Cement Mortars, Procedia Engineering 172 (2017) 127–134. https://doi.org/10.1016/j.proeng.2017.02.034.

[221] A. Manoharan, C. Umarani, Properties of Air Lime Mortar with Bio-Additives, Sustainability 14 (2022) 8355. https://doi.org/10.3390/su14148355.

[222] M. Kumar, R. Bala, V.S. Gondil, S.K. Pandey, S. Chhibber, D.V.S. Jain, R.K. Sharma, N. Wangoo, Combating food pathogens using sodium benzoate functionalized silver nanoparticles: synthesis, characterization and antimicrobial evaluation, J Mater Sci 52 (2017) 8568–8575. https://doi.org/10.1007/s10853-017-1072-z.

[223] M.C. Otálora, A. Wilches-Torres, J.A.G. Castaño, Extraction and Physicochemical Characterization of Dried Powder Mucilage from Opuntia ficus-indica Cladodes and Aloe Vera Leaves: A Comparative Study, Polymers 13 (2021) 1689. https://doi.org/10.3390/polym13111689.

[224] M.C. Otálora, J.G. Carriazo, L. Iturriaga, M.A. Nazareno, C. Osorio, Microencapsulation of betalains obtained from cactus fruit (Opuntia ficus-indica) by spray drying using cactus cladode mucilage and maltodextrin as encapsulating agents, Food Chemistry 187 (2015) 174–181. https://doi.org/10.1016/j.foodchem.2015.04.090.

[225] M. Beltrá, L. Andreu-Coll, E. Roche, A. Médico, D. López-Lluch, Á.A. Carbonell-Barrachina, F. Hernández-García, E. Garcia-García, Mineral content of a lyophilized extract from the fruit Opuntia ficus indica (L.) Mill, Eur Food Res Technol 250 (2024) 821–827. https://doi.org/10.1007/s00217-023-04431-6.

[226] R. Aparicio-Ortuño, J.D. Lozada-Ramírez, C.A. De Parrodi, T.S. Silva-Pereira, K. Villaseñor-López, M.M. Ramírez-Rodrigues, A.E. Ortega-Regules, Characterization of mexican Opuntia ficus indica cladode and bioactive compound profile. Oxidative stress

resistance and anti-adipogenic effect in Caenorhabditis elegans, Food Measure (2024). https://doi.org/10.1007/s11694-024-02602-x.
[227] Z. Tan, S.A. Bernal, J.L. Provis, Reproducible mini-slump test procedure for measuring the yield stress of cementitious pastes, Mater Struct 50 (2017) 235. https://doi.org/10.1617/s11527-017-1103-x.
[228] C. Bressaglia, A. Vavasori, L. Ronchin, N.M.E. Stucchi, Studio e formulazione di malte per il restauro con additivi autoriparanti. Bachelor degree thesis., Università Ca'Foscari Venezia, 2023.
[229] I.S. Yahia, S.M.A.S. Keshk, S. AlFaify, A.M. El-Naggar, M.M. Abutalib, Synthesis and characterization of wide-scale UV–vis CUT-OFF laser filter using methyl violet-6B/PMMA polymeric composite films, Sensors and Actuators A: Physical 269 (2018) 388–393. https://doi.org/10.1016/j.sna.2017.11.048.
[230] K. Baltakys, R. Jauberthie, R. Siauciunas, R. Kaminskas, Influence of modification of SiO2 on the formation of calcium silicate hydrate, (n.d.).
[231] Y.-S. Wang, H.-S. Lee, R.-S. Lin, X.-Y. Wang, Effect of silicate-modified calcium oxide-based expansive agent on engineering properties and self-healing of ultra-high-strength concrete, Journal of Building Engineering 50 (2022) 104230. https://doi.org/10.1016/j.jobe.2022.104230.
[232] F. Namouchi, H. Smaoui, N. Fourati, C. Zerrouki, H. Guermazi, J.J. Bonnet, Investigation on electrical properties of thermally aged PMMA by combined use of FTIR and impedance spectroscopies, Journal of Alloys and Compounds 469 (2009) 197–202. https://doi.org/10.1016/j.jallcom.2008.01.148.
[233] E.G. Navarro-Mendoza, E.M. Alonso-Guzman, A. Sanchez-Calvillo, J.A. Bedolla-Arroyo, H. Becerra-Santacruz, A. Navarro-Ezquerra, B. Gonzalez-Sanchez, W. Martinez-Molina, Physical and Mechanical Characterization of Lime Pastes and Mortars for Use in Restoration, Heritage 6 (2023) 2582–2600. https://doi.org/10.3390/heritage6030136.
[234] ASTM C230/C230M-20: Standard Specification for Flow Table for Use in Tests of Hydraulic Cement, (2021).
[235] NORMAL 43/93, Misure colorimetriche di superfici opache., (1994).
[236] R.T. Marcus, The measurement of colour, in: Color for Sciece, Art and Technology, 1998: pp. 2–11.
[237] M. Chalaris, Theories and Trends in Porosimetry, AMMS 10 (2023). https://doi.org/10.31031/AMMS.2023.10.000740.
[238] E.W. Washburn, The dynamics of capillary flow, Physical Review 17 (1921) 115–116.
[239] S. Brunauer, P.H. Emmett, E. Teller, Adsorption of gases in multimolecular layers, American Chemical Society 60 (1938) 309–319.
[240] E.P. Barrett, B.G. Joyner, P.P. Halenda, The detrmination of pore volume and area distributions in porous substances. i. computations from nitrogen isotherms., Journal of the American Chemical Society 73 (1951) 373–380.
[241] NORMAL 4/80. Distribuzione del volume dei pori in funzione del loro diametro. Porosimtria a mercurio., (1980).
[242] S. Maria, Methods for porosity measurement in lime-based mortars, Construction and Building Materials 24 (2010) 2572–2578. https://doi.org/10.1016/j.conbuildmat.2010.05.019.

[243] UNI EN 1015-11:2019 - Metodi di prova per malte per opere murarie - Parte 11: Determinazione della resistenza a flessione e a compressione della malta indurita, (2020). https://store.uni.com/uni-en-1015-11-2019 (accessed February 20, 2024).
[244] W.C. Oliver, G.M. Pharr, An improved technique for determining hardness and elastic modulus using load and displacement sensing indentation experiments, J. Mater. Res. 7 (1992) 1564–1583. https://doi.org/10.1557/JMR.1992.1564.
[245] J.T. Morgan, D.T. Gordon, Influence of Pore Geometry on Water-Oil Relative Permeability, Journal of Petroleum Technology 22 (1970) 1199–1208. https://doi.org/10.2118/2588-PA.
[246] UNI EN 12371:2010 - UNI Ente Italiano di Normazione, (n.d.). https://store.uni.com/uni-en-12371-2010 (accessed August 11, 2024).
[247] UNI EN 14579:2005 Metodi di prova per pietre naturali - Determinazione della velocità di propagazione del suono, (2005).

Acknowledgments

This doctoral thesis has been prepared at the Centre for Cultural Heritage technology (CCHT@CaFoscari) and at the Department of Molecular Science and Nanosystem at Università Ca'Foscari Venezia.

I would like to thank my supervisor, Professor Vavasori, for all the valuable advices and discussions, as well as for granting me the freedom I needed to pursue the research I believe in.

I would also like to thank the PI, Dr. Arianna Traviglia, and all my colleagues in the CCHT group for their help and support. I am grateful to everyone who contributed positively and actively to my daily work and research.

I would like to thank Dr. Cristina de Nardi and the Department of Civil Engineering of Cardiff University for hosting me during my secondment, which allowed me to conduct fundamental analyses and tests on the designed mortars. This phase of research was crucial for the outcomes of this thesis.

The characterisation analysis of ancient materials was performed at the Università degli Studi di Padova. I am deeply grateful to Prof. Claudio Mazzoli and Dr. Chiara Coletti, who generously shared their knowledge of geology and archaeological materials with me.

A big thank you goes to Dr. Gianluca Iori, the SESAME laboratory, and its technicians. Thank you for the enthusiasm you demonstrated in your work, for your interest in my research, and for giving thoughtful attention to all of my questions.

I would like to thank the Scuola Mosaicisti del Friuli for the warm welcome I received, where the passion for mosaics inspires everyone who enters. Special thanks to Francesco Anchora for sharing his expertise in mosaic production and for accommodating all the requests of my research.

Thank you to Lythos srl for supplying the stones and marble and thanks to Vetreria Orsoni for providing the glass *tesserae*, materials used for the production of specimens.

A very special thank you to Massimo Pallida of Nopal Vet srl for providing *Opuntia ficus-indica* cladodes, without which this research might never have even begun.

Thanks to Museo Archeologico di Aquileia for allowing me to study and analyze samples of archaeological material.

Finally, I would like to thank the IIT facilities technicians, who, despite my numerous requests, performed all the necessary analyses for this research and provided training when needed: Lea Pasquale, Simone Lauciello, Luca Ceseracciu, Filippo Drago, Marco Leoncini, Luca Leoncino, and Sergio Bocchini.

Venezia

31/10/2024

Neva M. E. Stucchi